

UNCLASSIFIED

AD NUMBER

AD781810

LIMITATION CHANGES

TO:

Approved for public release; distribution is unlimited.

FROM:

Distribution authorized to U.S. Gov't. agencies only; Test and Evaluation; 18 APR 1973. Other requests shall be referred to Air Force Flight Dynamics Laboratory, ATTN: FBA, Wright-Patterson AFB, OH 45433.

AUTHORITY

AFFDL ltr dtd 13 Oct 1975

THIS PAGE IS UNCLASSIFIED

AD 0781810

AFFDL-TR-73-52  
VOLUME I

**ADVANCED METALLIC STRUCTURE:  
AIR SUPERIORITY FIGHTER WING  
DESIGN FOR IMPROVED COST, WEIGHT AND INTEGRITY**

F.A. FIGGE, et al  
NORTHROP CORPORATION  
AIRCRAFT DIVISION

TECHNICAL REPORT AFFDL-TR-73-52  
VOLUME I  
JUNE 1973

20080818 022

DISTRI  
STATEN  
REFER  
AIR FO

APPROVED FOR PUBLIC RELEASE;  
DISTRIBUTION UNLIMITED

EVALUATION;  
MUST BE  
ATTERSON

AIR FORCE FLIGHT DYNAMICS LABORATORY  
AIR FORCE SYSTEMS COMMAND  
WRIGHT-PATTERSON AIR FORCE BASE, OHIO



## NOTICE

When Government drawings, specifications, or other data are used for any purpose other than in connection with a definitely related Government procurement operation, the United States Government thereby incurs no responsibility nor any obligation whatsoever; and the fact that the government may have formulated, furnished, or in any way supplied the said drawings, specifications, or other data, is not to be regarded by implication or otherwise as in any manner licensing the holder or any other person or corporation, or conveying any rights or permission to manufacture, use or sell any patented invention that may in any way be related thereto.

Copies of this report should not be returned unless return is required by security considerations, contractual obligations, or notice on a specific document.

AD 781810

**ADVANCED METALLIC STRUCTURE:  
AIR SUPERIORITY FIGHTER WING DESIGN  
FOR IMPROVED COST, WEIGHT AND INTEGRITY**

**Volume I**

*F. A. FIGGE, ET AL*  
*NORTHROP CORPORATION*  
*AIRCRAFT DIVISION*

Distribution limited to U. S. Government agencies only; test and evaluation; statement applied 18 April 1973. Other requests for this document must be referred to Air Force Flight Dynamics Laboratory (FBA), Wright-Patterson Air Force Base, Ohio 45433.

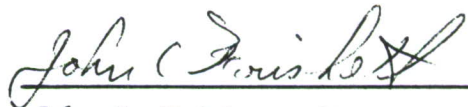
## FOREWORD

This technical report was prepared by the Northrop Corporation, Aircraft Division, under Contract AF33615-72-C-1891 (Project 486U). This work was sponsored by the Air Force Flight Dynamics Laboratory (AFFDL), under the joint management and technical direction of the AFFDL and the Air Force Materials Laboratory, Wright-Patterson Air Force Base, Ohio. Mr. Clark Beck, AFFDL, was the Air Force Project Engineer. The effort described in this report was performed between June 1972 and June 1973.

Listed below are the primary participants together with their areas of participation:

F. A. Figge	-	Program Management
L. Bernhardt	-	Design
W. Hilker	-	Stress Analysis and Weights
V. Frost	-	Stress Analysis
L. Jeans	-	Damage Tolerance and Fatigue Analysis
R. Wells	-	Materials and Processes
J. Hill	-	Manufacturing
J. Bennett	-	Cost Analysis
R. Clemens	-	Quality Control and NDI
W. Sturrock	-	Quality Control and NDI

This Technical Report has been reviewed and is approved:



John C. Frishett, Major, USAF  
Program Manager, AMS Program Office  
Structures Division

## ABSTRACT

The objective of this program was to reduce the weight of a fighter wing and carrythrough structure while maintaining its cost and life approximately equivalent to the baseline. Innovations in design concepts and application of new materials, manufacturing methods, and analysis techniques were to be expected.

General tasks of the program were to provide for concept formulation, first iteration preliminary design, material property testing to support preliminary design, and preliminary planning and cost estimation of a separate follow-on program. An additional task, initiated several months after the basic go-ahead, was to consider the new Damage Tolerance criteria sensitivity and trade studies, utilizing the baseline structure, materials and spectra, and by imposing "USAF Damage Tolerance Criteria," MIL-A-008866, dated 18 August 1972.

The report is divided into three volumes: Volume I contains the basic report, Volume II contains the damage tolerance criteria sensitivity study, and Volume III contains the results of the materials test program.

The structural wing box of the Northrop F-5E Air-Superiority Fighter was selected as the baseline structure to provide realistic structural and functional constraints and requirements for the study. It is a dry wing, all-aluminum, multi-spar design. It can carry a large variety of external stores and weighs approximately 1,000 pounds.

From a large variety of initial concepts, three designs emerged as having potential for further study and evaluation in a follow-on program. These are: (1) A full depth honeycomb design, featuring titanium skins and aluminum core, (2) a six-spar design featuring aluminum upper skin, titanium lower skin and substructure, with extensive use of welding between the lower skin and substructure, and (3) a six-spar all-aluminum design, somewhat similar to the baseline, but utilizing sine-wave spars, titanium tip and landing gear ribs, and some newer aluminum alloys.



# TABLE OF CONTENTS

<u>Section</u>		<u>Page</u>
I	INTRODUCTION . . . . .	1
II	BASELINE . . . . .	5
	1. Description . . . . .	5
	2. Update . . . . .	18
III	TECHNICAL ACCOMPLISHMENTS . . . . .	21
	1. Structural Design . . . . .	21
	2. Stress Analysis . . . . .	87
	3. Aeroelastic Analysis . . . . .	127
	4. Damage Tolerance Analysis . . . . .	137
	5. Fatigue Analysis . . . . .	150
	6. Materials Engineering . . . . .	161
	7. Manufacturing R&D . . . . .	168
	8. Quality Control and NDI . . . . .	173
	9. Cost Analysis . . . . .	177
	10. Weights Analysis . . . . .	200
IV	RANKING OF CONCEPTS . . . . .	211
V	CONCLUSIONS . . . . .	215
VI	PAYOFFS . . . . .	217
	1. Cost . . . . .	217
	2. Weight . . . . .	221
VII	RECOMMENDATIONS FOR TECHNOLOGY DEVELOPMENT . . . . .	225
APPENDIX I	CORRUGATED WEB SPAR STIFFNESS REQUIREMENTS . . . . .	227
APPENDIX II	CALCULATION OF PERFORATED PLATE AVERAGE ELASTIC CONSTANTS AND STIFFNESSES . . . . .	241
APPENDIX III	WEIGHT AND COST SAVINGS IN CONCEPTS . . . . .	251
APPENDIX IV	SKIN THICKNESS DATA . . . . .	261
REFERENCES	. . . . .	293

# LIST OF FIGURES

<u>Figure</u>		<u>Page</u>
1	F-5E Three View . . . . .	9
2	F-5E Wing Panel Structural Arrangement . . . . .	13
3	F-5E Main Wing Box Structure . . . . .	15
4	Baseline Internal Spar and Lower Skin Failure Analysis . . . . .	20
5	Concept Formulation and Evaluation Flow Chart . . . . .	22
6	Spar Spacing Limits . . . . .	25
7	Wing Skin Concepts . . . . .	27
8	Constant Height Interior Spar Concepts . . . . .	33
9	Tapered Interior Spar Concepts . . . . .	35
10	Concept No. 1 Full Depth Honeycomb Wing . . . . .	39
11	Concept No. 2 Warren Truss Spar Wing . . . . .	45
12	Concept No. 2 Warren Truss Spar Wing (Continued) . . . . .	47
13	Concept No. 2 Warren Truss Spar Wing (Continued) . . . . .	49
14	Concept No. 2 Warren Truss Spar Wing (Continued) . . . . .	51
15	Concept No. 3 Aluminum Titanium 6-Spar Wing . . . . .	55
16	Concept No. 3A Welded Titanium 6-Spar Wing . . . . .	59
17	Concept No. 4 Honeycomb Panel Stiffened 5-Spar Wing . . . . .	63
18	Concept No. 5 Honeycomb Panel Stiffened 4-Spar Wing . . . . .	65
19	Concept 6/7 Ti-Borsic/Geodesic Wing Structure . . . . .	69
20	Concept 6/7 Ti-Borsic Upper Skin Panel Details . . . . .	71
21	Concept 6/7 Ti-Borsic Upper Skin Weld Assembly . . . . .	73
22	Concept 6/7 Geodesic Lower Skin . . . . .	77
23	Concept No. 8 Aluminum Precision Forged Substructure 6-Spar Wing . . . . .	81
24	F-5E Ultimate Design Shear Moment and Torque Envelopes . . . . .	90
25	Ultimate Wing Load Envelope . . . . .	91

# LIST OF FIGURES (Continued)

<u>Figure</u>		<u>Page</u>
26	Upper Surface Maximum Spanwise Load Intensity (Lb/In Ult) . . . . .	94
27	Lower Surface Maximum Spanwise Load Intensity (Lb/In Ult) . . . . .	95
28	Summary of Maximum Ultimate Shear Flows, Trunnion Reactions and Rib Loads . . . . .	96
29	Wing Finite Element Grid . . . . .	97
30	Skin Stresses at Root Rib (Section A-A) . . . . .	98
31	Typical Honeycomb Panel . . . . .	103
32	Truss Spar Gridwork With 6 Diagonal Spars . . . . .	108
33	Conventional Spar Gridwork With 5 Interior Spars . . . . .	108
34	Elastic Tension and Compression Modulus of Ti-Borsic Laminates at R. T. . . . .	112
35	Estimated Allowable Tension Strength of Ti-Borsic Laminates at R. T. . . . .	113
36	Estimated Allowable In-Plane Shear Strength of Ti-Borsic Laminates at R. T. . . . .	113
37	Geodesic Skin with 45-Degree Diagonal Members . . . . .	115
38	Percent of Area Removed Versus ( $b_L/h$ ) for the Geodesic Skin Design . . . . .	118
39	Ratio of Longitudinal Member Stress in Geodesic Skin Over Stress in Plain Skin of Same Weight . . . . .	118
40	Finite-Element Model of the Repeating Geodesic Pattern Under Axial Loads and Sherar Loads . . . . .	119
41	Finite-Element Model for Lower Geodesic Skin Representative of W.S. 73 . . . . .	122
42	Typical Beaded Compression Panel . . . . .	126
43	Predicted Aileron Reversal Speeds . . . . .	128
44	Wing Twist Per Degree of Aileron Travel . . . . .	130
45	Wing Bending Stiffnesses for Baseline F-5E . . . . .	133
46	Wing Torsional Stiffnesses for Baseline F-5E, and For Concepts 1, 5 and 8 . . . . .	134
47	F-5E Damage Tolerant Critical Wing Structure . . . . .	138
48	Internal Spar and Lower Skin Failure Analysis . . . . .	145

# LIST OF FIGURES (Continued)

<u>Figure</u>		<u>Page</u>
49	T76 Plate Crack Growth Rate Comparison, Test Versus Design . . . . .	146
50	Ti-6Al-4V $\beta$ MA Plate Crack Growth Rate Comparison, Test Versus Design . . . . .	147
51	Crack Growth Rate Comparison of Aluminum Alloys . . . . .	149
52	Fatigue Critical Areas . . . . .	152
53	Axial Load Fatigue Behavior of Selected Aluminum Alloys . . . . .	156
54	Axial Load Fatigue Behavior of Ti-6Al-4V Annealed Sheet . . .	157
55	Fatigue Design Stress for Ti-6Al-4V $\beta$ MA Plate . . . . .	160
56	Full Depth Honeycomb . . . . .	170
57	Aluminum/Ti Welded . . . . .	171
58	Aluminum, 6 Spar . . . . .	172
59	Cost Element Structure for Part Cost Estimation in a Production Environment . . . . .	179
60	Normalized Costs for Spar Designs . . . . .	186
61	Normalized Costs for Spar Designs (Continued) . . . . .	186
62	Normalized Costs for Spar Designs (Continued) . . . . .	187
63	Normalized Costs for Spar Designs (Concluded) . . . . .	187
64	Cost-Quantity Relationship & Comparison . . . . .	188
65	Summary of Relative Cost for Various Wing Box Concepts . . . .	190
66	Sensitivity Analysis Assuming Change in Labor Hours . . . . .	198
67	Sensitivity Analysis Assuming Change in Production Material Cost . . . . .	199
68	Effect of Wing Structure Weight Reduction on F-5E Flyaway Costs . . . . .	219
69	Effect of Wing Structure Weight Reduction on F-5E Life Cycle Costs . . . . .	220
70	Effect of Weight Reduction on F-5E Turn Capability . . . . .	222
71	Effects of Weight Reduction on Air-to-Air Combat Combat Maneuvering . . . . .	223
72	Schematic of Corrugated Web Spar . . . . .	229
73	Idealized Prismatic Channel Section . . . . .	229
74	Plate Subjected to Harmonically Varying Edge Moment . . . . .	231



# LIST OF FIGURES (Continued)

<u>Figure</u>		<u>Page</u>
75	Variation of Web Torsional Restraint Parameter With Wave Length . . . . .	236
76	Variation with Buckle Wave Length of Minimum Extensional Stiffness Parameter Required to Produce Nodes at the Supports for Long Plates . . . . .	238
77	Possible Stiffness Variations . . . . .	239
78	Repeating Triangular Hole Pattern . . . . .	243
79	Problem to be Analyzed for Biaxial Normal Stress Distribution . . . . .	243
80	Shear and Normal Stress Distribution . . . . .	246
81	Rotated Stress Distribution . . . . .	246
82	Problem to be Analyzed for Shear Stiffness . . . . .	247
83	Tapers - Upper Wing Skin F-5E Baseline . . . . .	261
84	Taper Areas Lower Wing Outer Surface F-5E Baseline . . . . .	262
85	Taper Areas Wing Inner Surface F-5E Baseline . . . . .	263
86	Skin Thicknesses, Concept 1 . . . . .	265
87	Skin Thicknesses, Concept 1 . . . . .	267
88	Skin Thicknesses, Concept 1 . . . . .	269
89	Skin Thicknesses, Concept 1 . . . . .	271
90	Skin Thicknesses, Concept 1 . . . . .	273
91	Skin Thicknesses, Concept 3 . . . . .	275
92	Skin Thicknesses, Concept 4 . . . . .	277
93	Skin Thicknesses, Concept 4 . . . . .	279
94	Skin Thicknesses, Concepts 4 and 5 . . . . .	281
95	Skin Thicknesses, Concept 5 . . . . .	283
96	Skin Thicknesses, Concept 5 . . . . .	285
97	Skin Thicknesses, Concept 6 . . . . .	287
98	Skin Thicknesses, Concept 8 . . . . .	289
99	Skin Thicknesses, Concept 8 . . . . .	291

# LIST OF TABLES

<u>Table</u>		<u>Page</u>
I	F-5E Characteristics . . . . .	7
II	External Stores Capability . . . . .	11
III	Material Matrix . . . . .	31
IV	Summary and Description of Critical F-5E Wing Load Conditions . . . . .	89
V	Mechanical Properties Used in Design - Titanium Alloys . . . . .	100
VI	Mechanical Properties Used in Design - Aluminum Alloys . . . . .	100
VII	Summary of Allowable Ultimate Design Stresses (KSI) for Titanium Lower Structure (Concepts 1, 3, 3A, 4, 5) . . . . .	101
VIII	Summary of Allowable Ultimate Design Stresses (KSI) for Aluminum Lower Structure (Concepts 1A, 8, 8A). . . . .	102
IX	Estimated Elastic and Strength Properties of Unidirectional Ti-Borsic . . . . .	111
X	Skin Weight Ratios for a Ti-Borsic 4-Spar Upper Wing Skin . . . . .	114
XI	Comparison of Equal Weight Plain Aluminum, Plain Titanium and Geodesic Titanium Skins . . . . .	121
XII	Comparison of Equal Weight Plain Aluminum, Plain Titanium and Geodesic Titanium With 20% Cover Skins. . . . .	124
XIII	Condensed Bending Moment Spectrum - Wing Sta. 29.50 . . . . .	154
XIV	Materials Comparison . . . . .	163
XV	Titanium Design Values Based on Limited Test Program . . . . .	165
XVI	Aluminum Design Values Based on Limited Test Program . . . . .	166
XVII	NDI Methods . . . . .	175
XVIII	Computer Printed Cost Sheet for Concept 1 - Ribs . . . . .	184
XIX	Cost/Unit for 300 Units (1977 Dollars) . . . . .	191
XX	Detailed Cost Breakdown of Baseline and Concepts . . . . .	193

LIST OF TABLES (Continued)

<u>Table</u>		<u>Page</u>
XXI	Major Differences in Wing Box Concepts . . . . .	195
XXII	Summary of Wing Structural Weights for 8 Concepts . . . .	201
XXIII	Detailed Structural Weight Breakdown for 8 Concepts . . .	202
XXIV	Concept Ranking . . . . .	212

## SECTION I

### INTRODUCTION

The objective of the preliminary design study was to evolve, evaluate, and compare new structural concepts in order to reduce the weight of a fighter wing and carrythrough structure while maintaining its cost and life approximately equivalent to a representative advanced lightweight fighter system. To achieve this objective, advantage was to be taken of (a) innovative design concepts and applications, and (b) new and improved materials, processes, and manufacturing methods which generally have had sufficient development to show near-term potential for possible application to next generation systems--operational in about the latter 1970's or early 1980's. It was also necessary that all of the advanced structural design concepts comply with the damage tolerance requirements of MIL-A-008866, Revision D, dated August, 1972.

The Northrop F-5E Air Superiority Fighter (fifteen to twenty thousand pound gross weight) was selected as the baseline to provide realistic functional, structural, and operational requirements and constraints for the study. The specific component examined was the main wing box and carry-through structure. The baseline aircraft structural box is "dry," continuous from tip to tip (25.2 feet), has maximum depth of 5.8 inches, and is designed for a maximum load intensity of 24,000 lb/in. The structural box is essentially all-aluminum alloy, has external stores provisions at the tips and two other stations per panel, is designed to the MIL-A-8860 series of structural design criteria specifications, and weighs approximately 1,000 pounds.

The design concepts considered in this study were partially based on recommendations arising out of work performed by Northrop under Contract AF33615-72-C-1451, "Advanced Lightweight Fighter Structural Concept Study", and partially on suggestions arising out of brainstorming sessions early in the program.

A variety of configurations studied included features and combinations, such as: full depth honeycomb; integrally stiffened, thick-skin, and



sandwich panel covers; various arrangements and constructions of spars; mechanically attached, welded, and adhesive bonded assemblies; and aluminum and titanium alloys. Weight and cost comparisons were obtained.

From the studies, three design concepts were evolved for further study. The concepts are:

1. Full-depth adhesive bonded honeycomb with titanium upper and lower covers
2. 6-spar with aluminum upper covers, titanium lower covers, titanium substructure and extensive use of welding of the titanium.
3. 6-spar aluminum design utilizing sine-wave spars and advanced aluminum alloys

It was found necessary to either add advanced composites to the covers of the various concepts, or increase skin gages slightly to increase torsional rigidity for aeroelastic requirements.

Substructure studies focused largely on design and manufacturing/material processes in an attempt to reduce costs, as it was found that those components contributed to costs in a significant way. Specifically, a trade study was conducted amongst twenty-one different spar concepts, the results of which showed that a sine-wave type spar, either formed or forged, was the most cost effective. Precision aluminum forgings continue to show considerable promise, and some advantage appears to be gained by using titanium castings, although not as great as originally thought.

New and advanced metallic materials were tested considering primarily static and fatigue strengths, corrosion and stress-corrosion, toughness and crack-growth rates. Promising materials identified for specific application are:

1. Titanium: Ti-6-4  $\beta$ MA Plate and Sheet  
Ti-6-4  $\beta$ MA Forging  
Ti-6-4A Casting  
Ti-6-22-22 STA Plate  
Ti-6-22-22 STA Forging
2. Aluminum: X2048-T851 Plate  
7050-T736 Forging

7050-T7651 Plate  
7175-T736 Forging  
7475-T7651 Plate

Steel, beryllium, and magnesium alloys were found to have very little potential for the wing concepts investigated in this program.

Allowable design stresses were determined for the various elements of the wing box. Fatigue analyses were used to develop allowables to meet safe-life requirements. Fracture mechanics analyses were used to find the damage tolerance allowables for several materials and design concepts primarily for the inspectable and non-inspectable safe crack growth conditions.

Detail weight estimates were made for the various design concepts--each satisfying all of the strength, fatigue, damage tolerance, and aeroelastic requirements. The lightest advanced concept structural wing box (full depth honeycomb construction with titanium upper and lower covers) weighs approximately 870 pounds. The heaviest concept, using multispar construction with aluminum upper covers and titanium lower cover weighs approximately 933 pounds. These values compare to approximately 981 pounds for the F-5E production wing box. Weight penalties incurred by the various concepts for the addition of either advanced composites or increased skin gages to restore torsional stiffness to the F-5E requirements range from 0 to 18 pounds. These are included in the weights quoted above.

Cost estimates were developed for each basic design concept. Estimates were based upon projected 1977 material and labor costs, the average cost of a 300 lot procurement, and the assumption that advanced materials, processes, and manufacturing development costs would be borne by separate development programs.

Costs of the various concepts varied from 1.6 to 0.75 times the baseline cost. The most expensive design was a 5-spar design which employed titanium honeycomb stiffened skins. The least expensive design was a 6-spar aluminum concept employing sine-wave spars and some newer aluminum alloys.

Recommendations are made for areas where further technology development work should be done.

## SECTION II

### BASELINE

#### 1. DESCRIPTION

To provide a realistic set of requirements and parameters upon which to focus the studies conducted under this program, it was necessary to select a suitable baseline airplane and wing component. These requirements and parameters were to set such factors as:

1. General geometry and size of the wing.
2. Loading intensities (static and fatigue).
3. Operational performance boundaries (load factors, speeds, store requirements).
4. Other various typical functional requirements such as:
  - a. Hardpoints for external stores, landing gear, and control surfaces.
  - b. Provisions for electrical, hydraulic, and mechanical control systems.

It was desired that the structure to be studied be derived from a modern, lightweight fighter type of aircraft in about the 15,000 to 25,000 pound gross weight class. This generally corresponds to a system designed primarily for the air-superiority mission role.

The Northrop F-5E air superiority fighter is the baseline aircraft designated for this program. The F-5E is the latest member of the F-5 series of supersonic fighters designed for high performance, low initial and operating costs, and minimum logistics requirements. Fuselage and wing structures have been redesigned, and the airplane is currently in production at Northrop. First flight took place in the summer of 1972. The F-5E is just entering



service, but the basic design has been proven by more than 1000 F-5A's and F-5B's in worldwide operational service.

The F-5E is a single place, twin turbojet, supersonic fighter. The configuration includes a low wing, all-movable horizontal tail, and conventional vertical fin and rudder. General configuration (three-view) is shown in Figure 1. Numerous service-proven features are retained from previous F-5 models. These features are essentially a consolidation of the special items provided separately for various nations operating earlier F-5's. Some of these features are:

1. Two-position nose gear, to raise the aircraft nose to increase angle of attack for shorter takeoff capability under heavy load (Canadian CF-5's and the Netherlands NF-5's currently use this system).
2. Electrically heated anti-ice windshield for cold weather environments (originally developed for Norwegian F-5).
3. Jet-assisted takeoff provisions and tail arresting hook for use on short runways (Norwegian F-5's).

Emphasis on maneuverability and air combat capabilities in F-5E design is a departure from earlier F-5's, which were designed more as general-purpose attack aircraft. However, earlier F-5's were very agile aircraft, enabling them to consistently defeat other high performance aircraft in simulated air combat maneuvers. To improve maneuverability, the F-5E has a maneuvering flap system that can be deployed instantaneously and continuously to increase turn rate. The flap system is similar to the one currently in use on the CF-5's and NF-5's. This system employs both leading edge and trailing edge flaps. Although the primary emphasis is on maneuverability, F-5E power, speed and climb performance have been increased by use of two new 5000-pound thrust J85-GE-21 engines with enlarged ducts and auxiliary inlet doors. Additional F-5E characteristics are presented in Table I.



TABLE I. F-5E CHARACTERISTICS

<b>BASIC WING (Excluding L. E. Extension)</b>	
Span . . . . .	26.7 ft
Area . . . . .	186.3 ft <sup>2</sup>
Taper Ratio . . . . .	0.19
Aspect Ratio . . . . .	3.82
Sweepback of 25% chord . . . . .	24°
Airfoil Section . . . . .	NACA 65A-004.8 modified
<b>POWER PLANT</b>	
Engine . . . . .	2 J85-GE-21 Turbojet with afterburners
Maximum Power Rating (with afterburners). . . . .	10,000 lb. sea level static thrust.
<b>WEIGHTS</b>	
Empty . . . . .	9588 lb
T. O. Weight	
Launcher Rail Configuration. . . . .	15,400 lb
AIM-9 Configuration . . . . .	15,745 lb
Maximum Gross Weight. . . . .	21,834 lb
<b>DESIGN LOAD FACTORS</b>	
Air-to-air configuration. . . . .	7.33g and -3.0g
Air-to-ground configuration . . . . .	6.5g and -2.0g
<b>PERFORMANCE</b>	
Time to climb - sea level to 40,000 ft . . . . .	3.6 min
with afterburners	
Combat radius	
Subsonic intercept (no external tank) . . . . .	400 nmi
Supersonic intercept ( 275 gal tank) . . . . .	190 nmi
Combat Ceiling . . . . .	53,500 ft
Maximum Speed at 36,000 ft:	
Launcher Rail Configuration . . . . .	Mach 1.6
AIM Configuration . . . . .	Mach 1.5
Takeoff distance (AIM-9 configuration). . . . .	1900 ft

The F-5E has two M-39 20 mm nose cannons, providing a combined firing capability of 3000 rounds per minute (about 11 seconds of continuous fire). In addition seven external stores stations are provided (five jettisonable pylons and two wing tips). External stores capability is shown in Table II.





TABLE II. EXTERNAL STORES CAPABILITY

STORE STATION CAPACITY - LB

450

2100

1000

3000

M-39 20MM GUNS

	STORE	TIP	STORE STATION CAPACITY - LB					TIP
			WS 123.0	WS 93.5	WS 0	WS 93.5	WS 123.0	
QUALIFIED ITEMS	275-GAL TANK				●			
	AIM-9B, AIM-9E, AIM-9J SIDEWINDER	●						●
	TDU-11/B TARGET ROCKET							●
	M129E2 LEAFLET BOMB		●	●	●	●	●	
	MK-36 DESTRUCTOR (MK-825SE & MOD KIT)		●	●	●	●	●	
	MK-82 GP & SNAKEYE 500-LB BOMB		●	●	●	●	●	
	MK-84GP 2000-LB BOMB				●			
	BLU-1B, BLU-1B/B, BLU-1C/B, 27/B, 27A/B, 27B/B FINNED AND UNFINNED NAPALM		●	●	●	●	●	
	BLU-32A/B, BLU-32B/B FINNED AND UNFINNED NAPALM		●	●	●	●	●	
	CBU-24B/B, CBU-49B/B, CBU-52A/B, CBU-58/B CLUSTER BOMB UNIT		●	●	●	●	●	
	LAU-68A/A (7) 2.75-INCH ROCKETS		●	●		●	●	
	LAU-3/A, LAU-3A/A (19) 2.75-INCH ROCKETS TO MAP REQMTS		●	●		●	●	
	SUU-20/A, SUU-20/A(M), SUU-20A/A, SUU-20B/A BOMB AND ROCKET PACK				●			
	SUU-25A/A, SUU-25C/A FLARE DISPENSER		●				●	
	TDU-10/B TOW TARGET (DART W/CARRIER)						●	
	RMU-10/A REEL (DART)				●			
GROWTH ITEMS	50-GAL TIP TANK	●						●
	275-GAL TANK			●		●		
	150-GAL TANK			●	●	●		
	M117, 750-LB BOMB		●	●	●	●	●	
	ROCKEYE II (MK-20 MOD 2) CLUSTER BOMB		●	●	●	●	●	
	MK-81 GP & SNAKEYE 250-LB BOMB		●	●	●	●	●	
	MK-83GP 1000-LB BOMB		●	●	●	●	●	
	CBU-2A/A, CBU-9/A		●				●	
	LAU-60/A (19) 2.75-INCH ROCKETS TO MAP REQMTS		●	●		●	●	
	LAU-10/A (4) 5-INCH ROCKETS TO MAP REQMTS		●				●	
	TRIPLE EJECTOR RACK (TER) W/MK-81 GP AND SNAKEYE		●	●	●	●	●	
	MULTIPLE EJECTOR RACK (MER) (5) MK-81 GP AND SNAKEYE				●			
	MER (5) MK-82 GP AND SNAKEYE				●			
	TER/MK-82 GP AND SNAKEYE			●	●	●		

Current structures and manufacturing technologies are utilized in air-frame design. Structural configuration, materials, manufacturing methods, and analysis techniques used are based on experience accumulated over 10 years of design, production and service of the F-5's. The structural design criteria are based on MIL-A-8860 series specifications. The F-5E structural integrity program is in accordance with applicable portions of ASD-TR-66-57.

The F-5E is representative of present day operational high performance air superiority fighters. The availability of design, manufacturing, ground test, performance, and cost data of earlier F-5's provides a good reference to measure efficiencies, integrity and reliability. The use of current structures and manufacturing technologies assures that the baseline weights and costs represent a valid reference from which to measure technology advances developed in the proposed program.

a. General Description

The F-5E wing panel, as shown in Figure 2, consists of the main box structure including carrythrough, leading and trailing edge flaps, ailerons, leading edge extensions, and trailing edge panels. The main landing gear is in the inboard portion of the wing and attached to the rib at Wing Station (W.S.) 73.3 and inboard portion of the 44% spar. External store capabilities are provided at the wing tips and by jettisonable pylons at W.S. 93.5 and W.S. 123.0. The wing panel is a single piece structure extending continuously from tip to tip with no cover splices. The wing attaches to the fuselage at six points: two each at the 15%, 44%, and 66.6% spars -- the former two locations being the primary attachments and the latter (66.6%) being a "secondary" shear tie attachment. Basic wing dimensional data are contained in Figures 2 and 3 and in Table I.

b. Main Wing Structural Box

The main wing structural box (including carrythrough structure), the focal point for the present study, is shown in Figure 3.

The main wing box is a thick-skin, multispar, all-aluminum structure except for steel ribs supporting the landing gear and wing tip stores. As



noted above, the wing is attached to the fuselage through six shear-type fittings. The fittings at the 15% and 44% spars are integral parts of two canted, forged ribs located at the wing-fuselage intersection line.

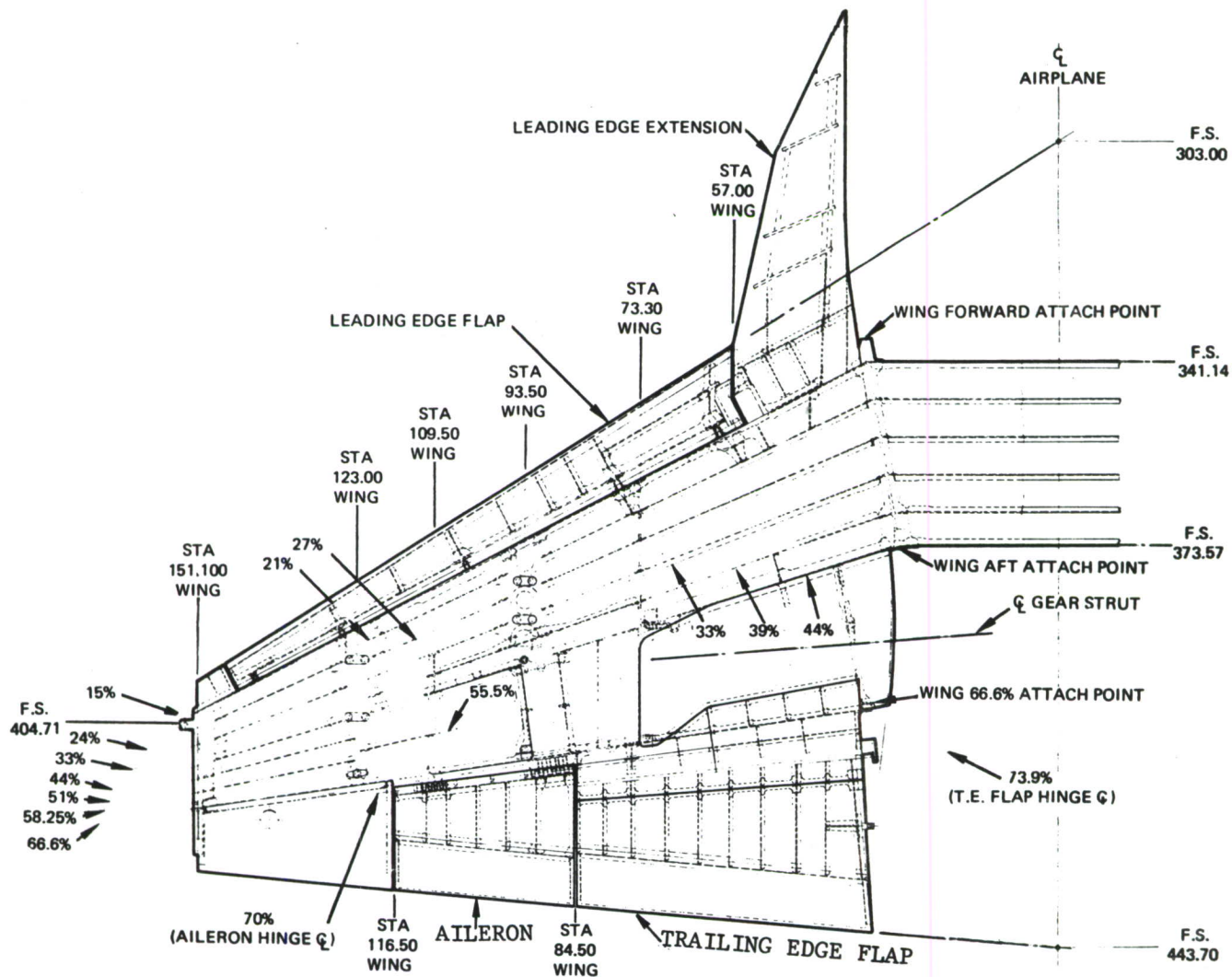


FIGURE 2. F-5E WING PANEL STRUCTURAL ARRANGEMENT

Pylon attach ribs are incorporated in the wing structure at Wing Stations 93.50 and 123.00. The pylon at W.S. 93.50 is attached with five bolts and two shear pins and the outboard pylon with four bolts and two shear pins. Each wing tip has a structural attachment for either an AIM-9 missile launcher or a 50-gallon fuel tank.

The main landing gear strut well is bounded by the W.S. 73.30 rib, the 44% and 66.6% spars and the side of the fuselage.

Inboard of W.S. 73.30, the torque box structure extends from the 15% to the 44% spars and Fuselage Stations 341.14 and 373.57 in the carrythrough region across the fuselage. Between W.S. 73.30 and 116, the torque box extends back to the 66.6% spar, and outboard of W.S. 116 it extends back to the trailing edge. The large majority of the bending structure is between the 15% and 44% spars.

Various systems are contained in the main box structure. Fuel line, air vent line and electrical conduits extend from the root to tip. Hydraulic actuators for the ailerons are in the aft portion of the box at approximately W.S. 93.5. No internal fuel is contained in the main box because of its small volume and the need to provide space for the functional systems.

#### (1) Main Skins

The upper and lower skins are machined from aluminum alloy plate extending across the entire wing span terminating at W.S. 151.0. Of significance are the skin "lands" which provide a common plane for the spars and ribs and also provide load paths for the axial loads in the spars where they end abruptly at a rib. Flaring of the skin lands at spar and rib intersection points assures gradual load pickup to the skins thus reducing load concentrations. The upper skin is made from 7075-T651 aluminum alloy, and the lower skin is made from 7075-T7351 aluminum alloy.

#### (2) Spars

All spars are channel sections except the 66.6% spar, which is an I-section. They are machined from 7075-T73 and -T76 aluminum alloy extrusions and 7049-T73 (44%) and 7175-T736 (66%) forgings. All spars are discontinuous at each rib with the exception of 15% and 66.6% spars. Integral



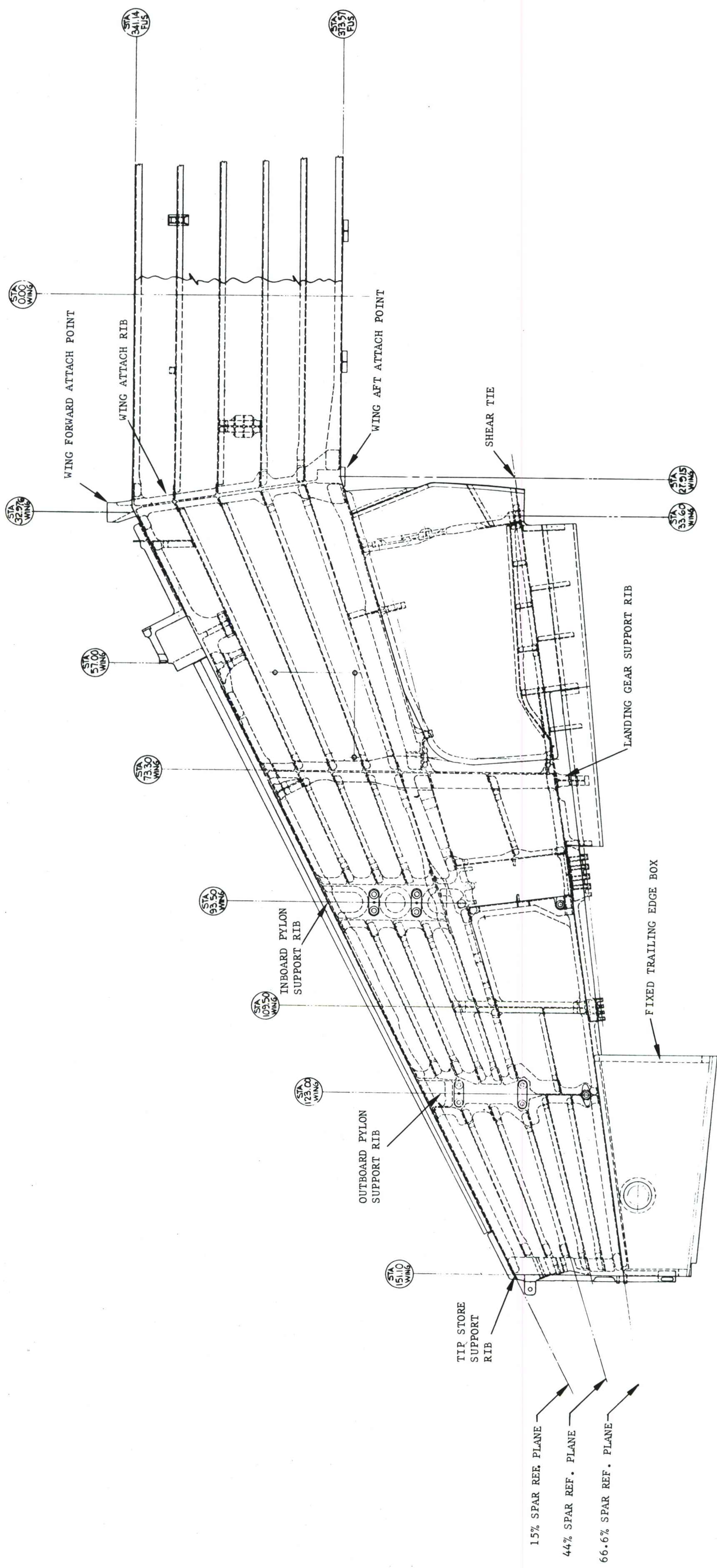


FIGURE 3. F-5E MAIN WING BOX STRUCTURE

rib tabs or angle clips provide the necessary shear ties between the spars and ribs.

### (3) Ribs

The root rib is located between W.S. 32.976 at the forward end to W.S. 27.915 at the aft end. The rib ends are integral fittings which provide the shear ties to the mating fuselage fittings. The rib is machined from a 7075-T7352 aluminum alloy forging.

The rib at W.S. 73.30 is continuous from the 15% to the 66.6% spar. The rib is an I section machined from a Hy-Tuf steel forging. Lugs positioned at the 44% and the 66.6% spars provide trunnion supports for the main landing gear. The inboard end of the forward trunnion lug ties directly to the 44% spar, thus acting as a shear web in this area.

The rib at W.S. 93.5 is machined from a 7175-T736 hand forged billet and is continuous from the 15% to the 39% chord, providing an integral four-point socket fitting for support of the inboard pylon structure. The rib is spliced at the 39% chord to an aileron actuator support rib which extends aft beyond the 44% chord line providing backup support for the aileron actuator as well as additional shear and bearing support for the pylon. Auxiliary ribs extend aft to the 66.6% spar.

The rib at W.S. 109.5 extends aft from the 33% to the 66.6% spar plane. The rib is an I-section machined from a 7075-T73 forging and serves as a backup for the outboard aileron hinge fitting.

The rib at W.S. 123.00 is machined from a 7175-T736 hand forged billet and is continuous from the 15% to the 66.6% spar providing an integral four-point socket fitting to support the outboard pylon structure. The rib portion aft of the 44% spar is an unsymmetrical I-section serving as load redistribution member for the secondary box skin panels.

The rib at W.S. 151.10 is continuous from the 15% spar to the trailing edge. It is a solid rib forward of the 44% spar narrowing to an I-section thin web rib aft of the 66.6% spar plane. The rib is machined from a 4140 steel die forging with integral lugs providing attach points for the tip launcher and fuel tank.



#### (4) Upper Skin Panels

The upper wing skin cover between the 44% and 66.6% spars and bounded by the root rib and the rib at W.S. 73.3 consists of an aluminum honeycomb panel with 7075-T6 facing sheets. This panel is the upper aerodynamic surface of the main landing gear bay. The upper wing skin cover between the 44% and 66% spars extending from Wing Cant Station (W.C.S.) 91.7 to W.S. 109.5 consists of an aluminum honeycomb panel with 7075-T6 facings. This panel is the upper aerodynamic surface of the aileron mechanism bay.

#### (5) Lower Removable Panels

The lower skin cover between the 44% and 66.6% spars extending from W.C.S. 85.2 to W.S. 123.0 consists, in part, of aluminum honeycomb panels with 7075-T6 facings, and a machined skin panel. These panels are completely removable and permit access to the aileron mechanism bay.

#### (6) Trailing Edge

The trailing edge structure between W.S. 151.1 and W.S. 116.0 consists of a full depth honeycomb panel with 2024-T4 and closing ribs.

### 2. UPDATE

The baseline F-5E wing structure was designed prior to the existence of the current USAF damage tolerant criteria (Volume II, Appendix II). This criteria was applied to applicable portions of the baseline wing structure to "up-date" this structure to these requirements. The objective of this study was to estimate the weight and cost of a production state-of-the-art wing which would be directly comparable, criteria-wise, to the advanced concepts studied in this program.

Definitions of critical damage tolerant structure and the basic method of analysis are outlined in Section III. 4. This analysis includes an assumed sequence of failures taking into account the crack growth life of the interior spar flange and load distribution into the skin subsequent to

spar flange failure. Additional necessary assumptions included in this section that are pertinent to the baseline study are summarized below:

1. Plane stress plastic zone condition in spar flange and plane strain in the skin panel.
2. Crack growth retardation prediction due to overloads based on average of Willenborg, et al, method<sup>(1)</sup> and linear cumulative growth.
3. Spar flange not critical to flight safety (no damage tolerant service life requirements).
4. Multiple 0.05 flaws at fastener hole common to flange/skin.
5. 0.05 fatigue induced flaw in skin at hole adjacent to above at time of flange failure. This flaw location was the most critical.

The last assumption, while not required by the criteria for monolithic structure, meets the "intent" of the criteria in the area of in-service flaws.

Since the baseline lower skin is a monolithic structural arrangement, the service life requirement would be two lifetimes or 8,000 hours for non-inspectability. An analysis completed at the fatigue flawed fastener hole demonstrated that the crack growth life exceeds the 8,000 hour requirement (Figure 4). Thus, the wing meets the damage tolerance requirements and no weight penalty is incurred in "updating" the baseline.

---

(1) Willenborg, J., Engle, R. M., and Wood, H. A., "A Crack Growth Retardation Model Using an Effective Stress Concept," AFFDL-TM-71-1-FBR, January 1971.

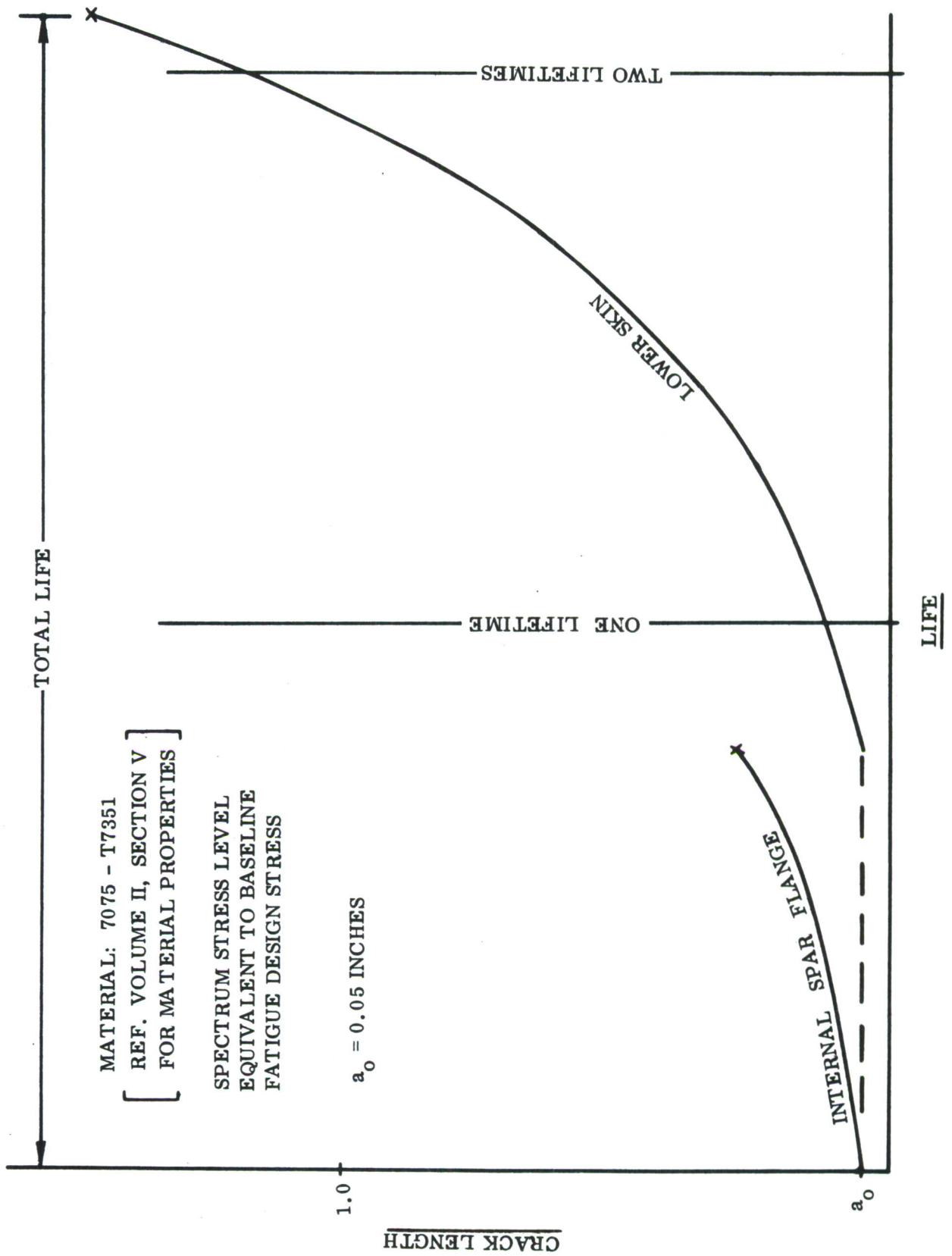


FIGURE 4. BASELINE INTERNAL SPAR AND LOWER SKIN FAILURE ANALYSIS

### SECTION III

#### TECHNICAL ACCOMPLISHMENTS

##### 1. STRUCTURAL DESIGN

###### a. Introduction

###### (1) Preliminary Effort

At the program's outset, some general design precepts were formulated either in addition to, or as a result of, the supplied program definition. It was generally conceded that the most propitious material for the conversion of pre-production technology into production techniques was titanium. While the principal advantage of titanium alloys (i.e., high strength at temperature) was not required for the performance regime of the selected F-5E baseline aircraft, it was felt that the exercising of titanium technology in this program would provide the greatest benefits for future generation aircraft of the air superiority class.

The second area of technological advancement deemed most likely to produce the greatest return for effort expended was in material fabrication techniques. The goal set forth was to reduce the material buy-fly ratio to as low as possible. Inherent in all this is the assumption that all the available advanced materials, be they aluminum, titanium or whatever, will be given primary consideration.

With these precepts in mind, several brainstorming sessions were held. The ideas put forth at these meetings ranged in scope from entire wing structural concepts to methods of reducing the effects of through flaws at holes in detail attachments. The end result of the brainstorming was a multitude of detail and system concepts which combined geometrically into such a vast number of possible wing designs that to investigate each combination as a separate entity would exhaust all the time allotted for concept selections and still not complete the task.

It was obvious that some sort of "game plan" was necessary to reduce the complexity of the concept formulation task to manageable proportions. Figure 5 depicts this concept formulation plan in flow chart form. A brief explanation of its derivation follows.



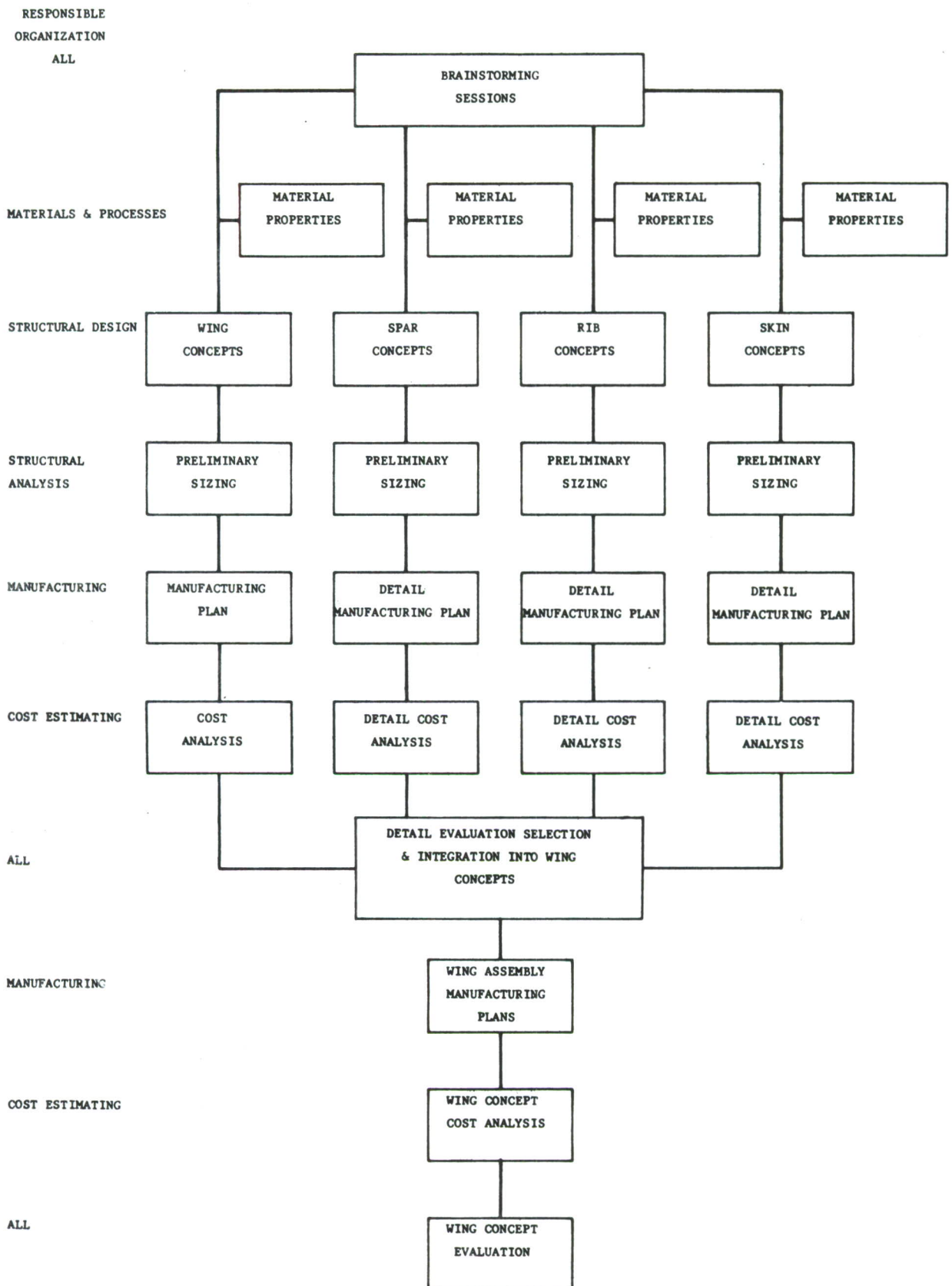


FIGURE 5. CONCEPT FORMULATION AND EVALUATION FLOW CHART

The "Quick Look" program <sup>(1)</sup> showed that a significant portion of both the cost and weight of any of the wing designs proposed was contained in the substructure. It was also apparent that wings constructed of titanium, while the lightest, were much more costly than wings constructed of aluminum. The utilization of higher specific strength materials was influenced by the attendant reductions in torsional stiffness of the wing and reduced compressive allowables of the thinner gages employed, unless additional stiffening methods were employed. This problem was compounded by the extreme thinness of the F-5E baseline wing.

With this in mind, it was felt that a detail component optimization program was in order, in which each detail concept was fully evaluated and ranked. The flow chart shows the principal milestones in this procedure. In this diagram, a column for complete wing system concepts is also shown. This column's inclusion recognized that in some wing design approaches the component parts are so wholly interdependent that they do not lend themselves to separate detail analysis. The full depth honeycomb stiffened and truss spar designs are prime examples of this.

The initial design effort concentrated on two principal areas. The first was an in-depth cost-weight tradeoff of eight differing methods of spar construction. These were expanded to twenty-one spar concepts when the additional variable of material was introduced. (See Figures 8 and 9 in Subsection III.1.a.(3).) An illustration of the limits of spar spacing under consideration and its attendant effect on systems plumbing in the wing is shown in Figure 6. It will be noted that when more than six spars are used, it becomes impossible to install the fuel and vent lines in the wing. The chordwise distance between spars is less than the fuel and vent line connector fitting's length. This fitting would have to be redesigned, separating the fuel line and vent line into separate wing bays, thus altering the inboard wing pylon interface, which is contrary to this program's ground rules. Therefore, no wing design with more than six spars was considered in this program.

---

(1) C. Rosenkranz, et al, Advanced Lightweight Fighter Structural Concept Study, AFFDL TR-72-98, dated July 1972.

While the possible combinations resulting from the combining of the two studies was formidable, once design allowables, load distribution, and stiffness and strain compatibility criteria were determined, a significant reduction in the viable approaches was realized.

The second study was of wing cover construction approaches. Multi-member, single member, external stiffening, integral stiffening, spar spacing and material were the variables considered in this study. An illustration of the initial wing skin concepts contemplated in this program is shown in Figure 7.

With the knowledge gained from the "Quick Look" study<sup>(1)</sup>, some general constraints were applied to the aforementioned studies. These are:

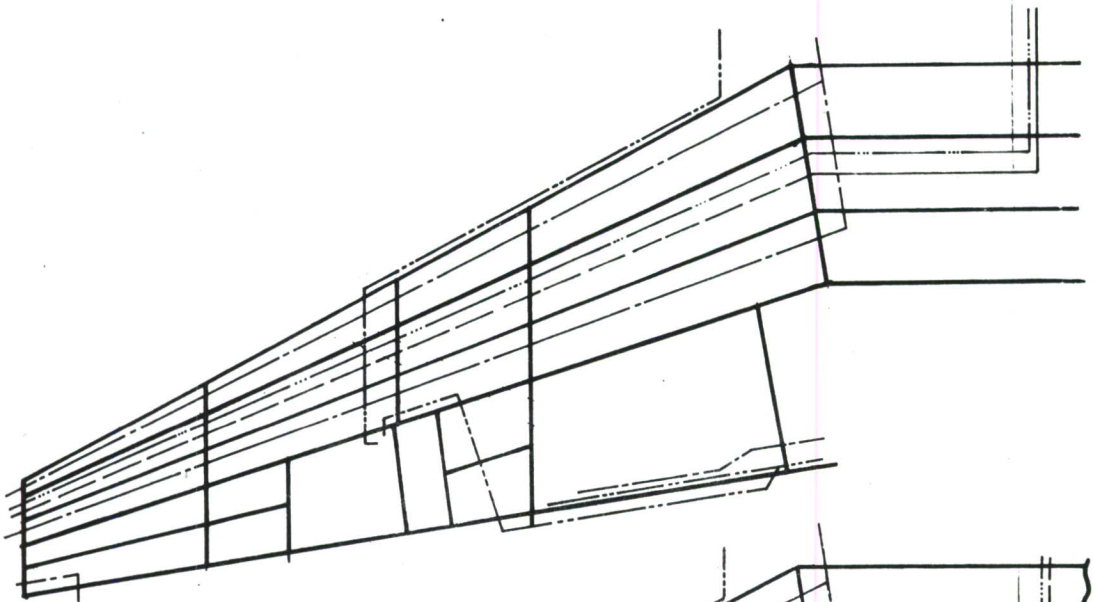
1. All complex and or heavy section substructural members will be precision forged or cast as their geometric complexity precludes applying the other spar construction techniques. (Note: The expense of 100% machining has been amply demonstrated in "Quick Look" and further cost analysis conducted later on in this program substantiated this position).
2. When titanium or other high cost materials are used as wing covers with integrally machined stiffeners, such stiffeners shall not cause a material thickness increase.
3. There appears to be no method to manufacture a laminated or lamelated fail-safe lower skin and avoid the extreme stress concentrations demanded by the multiple flaw requirement of the service life criteria under which this program must operate. While this does not necessarily preclude fail-safe multiple load path design, it does eliminate the conventional laminated or lamelated approach.

---

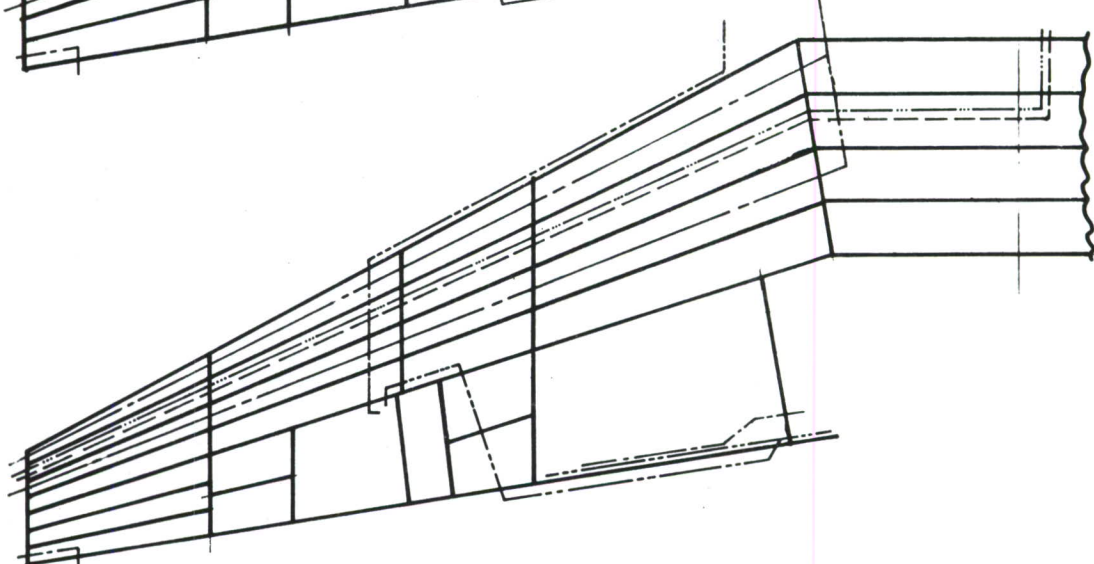
(1) C. Rosenkranz, et al, Advanced Lightweight Fighter Structural Concept Study, AFFDL TR-72-98, dated July 1972.



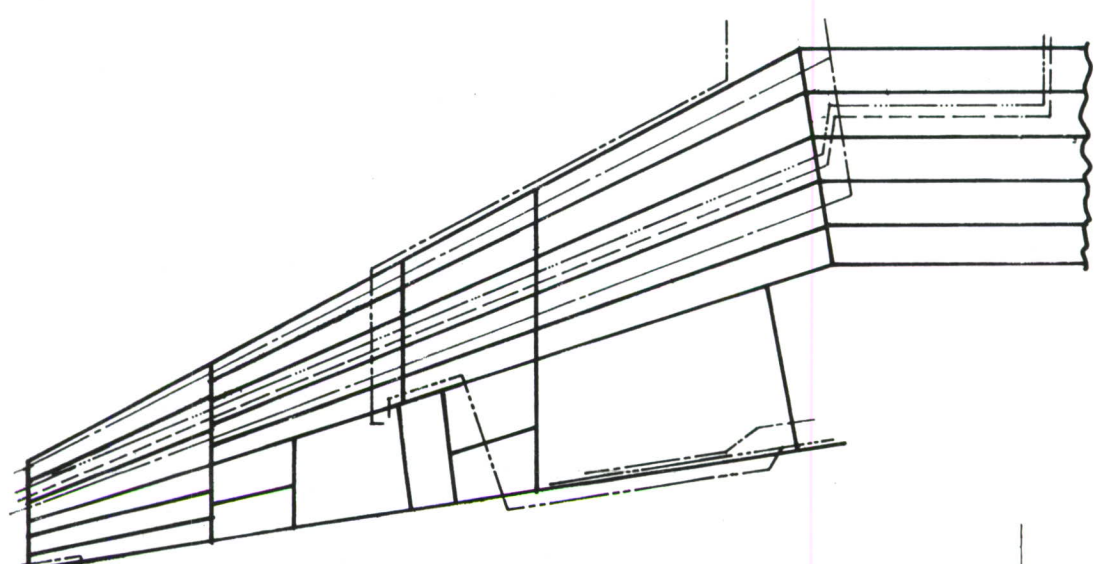
4 SPAR



5 SPAR

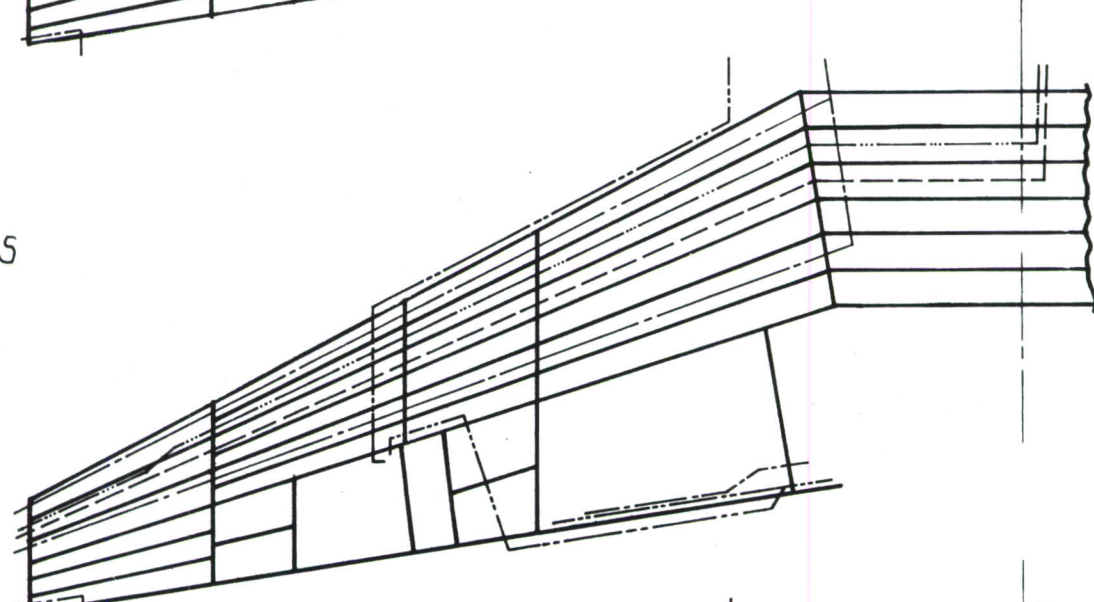


6 SPAR



----- ELECTRICAL CONDUITS  
----- HYDRAULIC LINES  
----- FUEL LINE  
----- VENT LINE

7 SPAR



8 SPAR

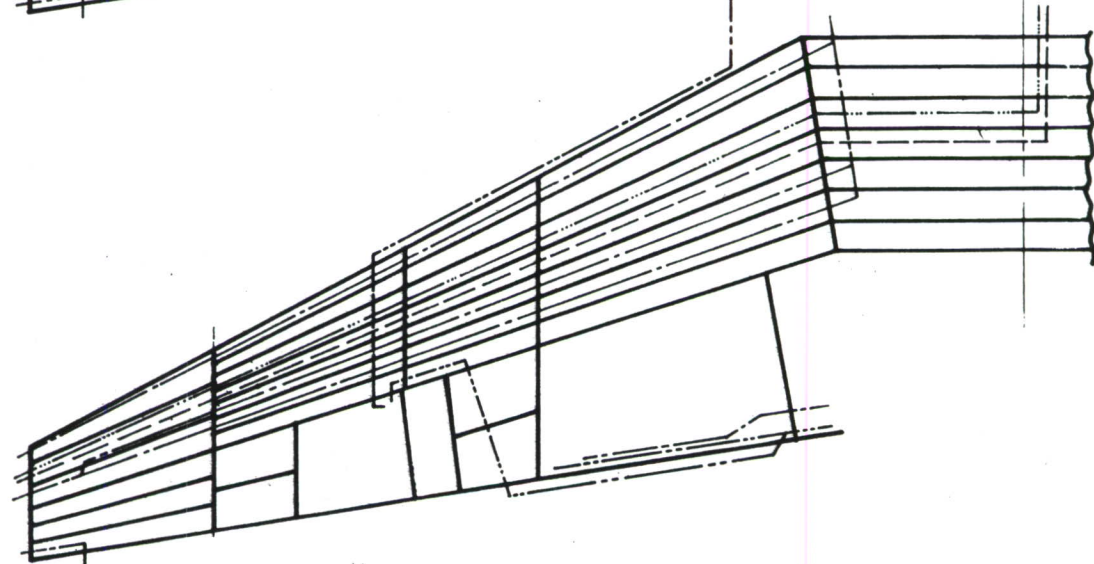


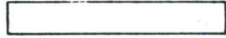
FIGURE 6. SPAR SPACING LIMITS



## SKIN CONCEPTS

### UPPER SKINS

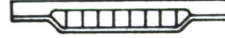
#### ALUMINUM OR TITANIUM



PLAIN PANEL



INTEGRAL STIFFENED



HONEYCOMB PANEL  
STIFFENED



BEADED PANEL  
STIFFENED

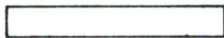
#### BORSIC REINFORCED AL OR Ti



PLAIN PANEL

### LOWER SKINS

#### ALUMINUM OR TITANIUM MONOLITHIC



PLAIN PANEL



INTEGRAL STIFFENED



HONEYCOMB PANEL  
STIFFENED



BEADED PANEL  
STIFFENED

#### BORSIC REINFORCED AL OR Ti



PLAIN PANEL



ADHESIVE BONDED  
LAMINATED



LAMELATED  
MECHANICALLY FASTENED



LAMELATED  
BORSIC/METAL MATRIX  
COMPOSITE  
MECHANICALLY FASTENED

FIGURE 7. WING SKIN CONCEPTS

## (2) Material Selection

Table III presents the material matrix for the final design concepts produced in this program. While a more detailed account of the material selection process is contained elsewhere in this report, a few anomalies and contra-indicated (with respect to the "Quick Look Program") material selections seem to exist. The following remarks are intended to clarify these substitutions.

While Ti-6Al-4V STA casting published data indicates significant mechanical property improvement over the annealed condition, its low ductility, substantiated by this contract's materials test program, caused its exclusion from the program. Since a certain degree of plastic deformation under load is an underlying assumption of any structural analysis and the ability of Ti-6Al-4V STA castings to conform to this assumed behavior is questionable, it was felt that the use of such a brittle material for airframe primary structure entails too great a risk.

When the pylon ribs are changed to annealed Ti-6Al-4V, a weight increase over the STA castings is incurred. These castings were only marginally cost/weight effective with the higher strength material and fail at being so in the annealed condition. Their use is now confined to those designs where compatibility of thermal expansion rates or their weldability is required.

The aluminum spars and skins of the concept No. 3 wing tip are in accord with least risk original design premise of that concept. The only other cost/weight effective alternative is the adhesively bonded titanium wing tip which fails to qualify in this instance.

## (3) Wing Interior Spar Concepts

Figures 8 and 9 depict eleven spar configurations, made of both 6Al-4V annealed titanium and 2024-T3 aluminum, which have been evaluated on a basis of manufacturing complexity, cost and weight.

While the number of designs under consideration may appear at first glance excessive, it must be born in mind the height and thickness variations will limit the applicability of many of these designs in some

or all of the wing configurations under study in this program. It is for this reason that so many spar variations are being studied.

This study consists of six spar designs for the center box between canted wing station 38.926 ribs along the 38% plane. Spar No. 1, Figure 8, is of one piece titanium sheet with a vertically corrugated hot formed channel web. This design is also being considered in aluminum alloy. A test specimen of this corrugated spar has been successfully formed from 0.063 thick 6Al-4V titanium sheet.

Spar No. 2 consists of both spar caps welded to a sine wave vertical web. The caps are tungsten arc (GTA) burn-through weldments. The welding of the spar is accomplished by the GTA process which uses infrared sensors in a closed loop control system, which provides automatic centering of the weld on the web. This feature, by virtue of its eliminating the necessity for specific welding fixtures for each spar configuration and high quality welds, is considered the most economical for this particular spar design.

The third spar design is fabricated from a one piece titanium extrusion, the web ends being slotted horizontally at the wing reference plane to allow for the joggling of each spar cap flange. The slotted web is then plasma arc welded to form the finished spar.

Spar No. 4 is a one piece extrusion of either titanium or aluminum alloys. The upper and lower spar caps are step machined at each end instead of being joggled as in spar No. 3.

It should be noted that only the titanium extrusions are finish machined all over as the quality of the stock extruded surface is too rough to be acceptable for finished parts. This will also hold true for all subsequent extruded titanium spar design in this discussion.

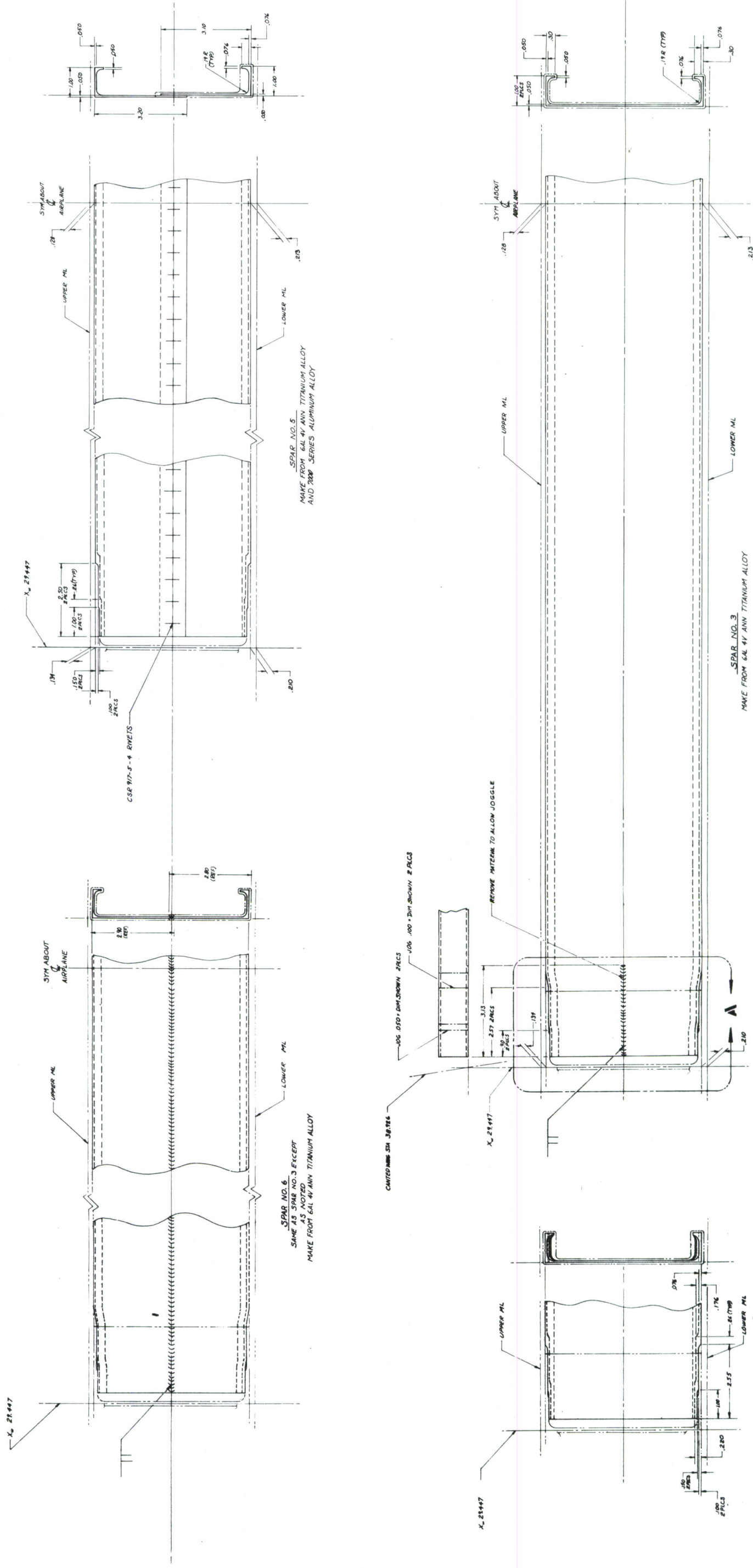
Spar No. 5 will be made from two "L" shaped extrusions with machined spar cap flanges as in configuration No. 4. The upper and lower halves are riveted together, upon installation, along the center of the spar web to form the complete spar. Spar material is either 6Al-4V annealed titanium or aluminum alloy. This two-piece approach eliminates much of the shimming required on final assembly.



TABLE III.  
ADVANCED METALLIC  
STRUCTURAL  
CONCEPT/MATERIAL  
MATRIX

	Concept No. 1 Ti. Full Depth H.C. Core	Concept No. 1A Al. Full Depth H.C. Core	Concept No. 3 Al/Ti 6-Spar	Concept No. 3A Al/Ti Welded 6-Spar	Concept No. 4 H.C. Panel 5-Spar	Concept No. 5 H.C. Panel 4-Spar	Concept No. 6/7 Ti-Borsic/Geodesic	Concept No. 8 Al Prec. Forged 6-Spar	Concept No. 8A Al Integral Web 6-Spar	Concept No's 1, 4, 5, and 6/7 Wing Tip	Wing Tip Concept No. 1A	Wing Tip Concept No. 3	Wing Tip Concept No. 3A	Wing Tip Concept No. 8	Wing Tip Concept No. 8A
Upper Skin	Ti-6-22-22 STA Plate	7050-T7651 Plate	7050-T7651 Plate	Ti-6-22-22 STA Plate	Ti-6-22-22 STA Plate	Ti-Borsic	7050-T7651 Plate	7050-T7651 Plate	7050-T7651 Plate	Ti-6-22-22 STA SH	7050-T7651 Plate	7050-T7651 Plate	7050-T7651 Plate	7050-T7651 Plate	7050-T7651 Plate
Lower Skin	Ti-6Al-4V BMA Plate	7475-T7651 Plate	Ti-6Al-4V BMA Plate	Ti-6Al-4V BMA Plate	Ti-6Al-4V BMA Plate	Ti-6Al-4V BMA Lam Sh	7475-T7651 Plate	X2 048-T736 Plate	Ti-6-22-22 STA SH	7475-T7651 Sheet	Ti-6Al-4V BMA Plate	7475-T7651 Sheet	7475-T7651 Sheet	X2048-T851 Plate	7050-T7651 Plate
15% Spar	Ti-6Al-4V BMA P.F.	7050-T736 P.F.	Ti-6Al-4V BMA P.F.	7050-T736 P.F.	7050-T736 P.F.	Ti-6Al-4V BMA P.F.	7050-T736 P.F.	7050-T736 P.F.	Ti-6Al-4V BMA P.F.	7050-T736 P.F.	Ti-6Al-4V BMA P.F.	7050-T736 P.F.	7050-T736 P.F.	7050-T736 P.F.	7050-T736 P.F.
44% Spar	Ti-6Al-4V BMA P.F.	7050-T736 P.F.	Ti-6Al-4V BMA P.F.	7050-T736 P.F.	7050-T736 P.F.	Ti-6Al-4V BMA P.F.	7050-T736 P.F.	7050-T736 P.F.	N/A	N/A	Ti-6Al-4V BMA Sheet	7075-T736 Sheet	7075-T736 Sheet	7075-T736 Sheet	7075-T736 Sheet
66% Spar	Ti-6Al-4V BMA P.F.	7050-T736 P.F.	Ti-6Al-4V BMA P.F.	7050-T736 P.F.	7050-T736 P.F.	Ti-6Al-4V BMA P.F.	7050-T736 P.F.	7050-T736 P.F.	Ti-6Al-4V BMA P.F.	7050-T736 P.F.	Ti-6Al-4V BMA P.F.	7050-T736 P.F.	7050-T736 P.F.	7050-T736 P.F.	7050-T736 P.F.
Interior Spars	N/A	N/A	Ti-6Al-4V BMA Sheet	7050-T736 P.F.	7050-T736 P.F.	Ti-6Al-4V BMA Sheet	7050-T736 P.F.	7050-T736 P.F.	N/A	N/A	Ti-6Al-4V BMA Sheet	7075-T736 Sheet	N/A	N/A	N/A
Root Rib	Ti-6-22-22 STA P.F.	7050-T736 P.F.	Ti-6-22-22 STA P.F.	7050-T736 P.F.	7050-T736 P.F.	Ti-6-22-22 STA P.F.	7050-T736 P.F.	7050-T736 P.F.	N/A	N/A	7050-T736 P.F.	7050-T736 P.F.	7050-T736 P.F.	7050-T736 P.F.	N/A
Gear Rib (W.S. 73.3)	Ti-6-22-22 STA P.F.	7050-T736 P.F.	Ti-6-22-22 STA P.F.	7050-T736 P.F.	7050-T736 P.F.	Ti-6-22-22 STA P.F.	7050-T736 P.F.	7050-T736 P.F.	Ti-6-22-22 STA P.F.	N/A	7050-T736 P.F.	7050-T736 P.F.	7050-T736 P.F.	7050-T736 P.F.	N/A
Inboard Pylon Rib (W.S. 93.5)	Ti-6Al-4V ANN Cstg	7175-T736 H.F.	Ti-6Al-4V ANN Cstg	7175-T736 H.F.	7175-T736 H.F.	Ti-6Al-4V ANN Cstg	7175-T736 H.F.	7175-T736 H.F.	7175-T736 H.F.	N/A	Ti-6Al-4V ANN Cstg	7175-T736 H.F.	7175-T736 H.F.	7175-T736 H.F.	N/A
Outboard Pylon Rib (W.S. 123.0)	Ti-6Al-4V ANN Cstg	7175-T736 H.F.	Ti-6Al-4V ANN Cstg	7175-T736 H.F.	7175-T736 H.F.	Ti-6Al-4V ANN Cstg	7175-T736 H.F.	7175-T736 H.F.	Ti-6Al-4V ANN Cstg	7175-T736 H.F.	Ti-6Al-4V ANN Cstg	7175-T736 H.F.	7175-T736 H.F.	7175-T736 H.F.	7175-T736 H.F.
Tip Rib	Ti-6Al-4V ANN Cstg	7175-T736 H.F.	Ti-6Al-4V ANN Cstg	7175-T736 H.F.	7175-T736 H.F.	Ti-6Al-4V ANN Cstg	7175-T736 H.F.	7175-T736 H.F.	Ti-6Al-4V ANN Cstg	7175-T736 H.F.	Ti-6Al-4V ANN Cstg	7175-T736 H.F.	7175-T736 H.F.	Ti-6Al-4V ANN Cstg	Ti-6Al-4V ANN Cstg
Honeycomb Core Upper	N/A	7175-T736 H.F.	Ti-6Al-4V ANN Cstg	7175-T736 H.F.	7175-T736 H.F.	Ti-6Al-4V ANN Cstg	7175-T736 H.F.	7175-T736 H.F.	Ti-6Al-4V ANN Cstg	7175-T736 H.F.	Ti-6Al-4V ANN Cstg	7175-T736 H.F.	7175-T736 H.F.	Ti-6Al-4V ANN Cstg	N/A
Honeycomb Core Lower	N/A	7175-T736 H.F.	Ti-6Al-4V ANN Cstg	7175-T736 H.F.	7175-T736 H.F.	Ti-6Al-4V ANN Cstg	7175-T736 H.F.	7175-T736 H.F.	Ti-6Al-4V ANN Cstg	7175-T736 H.F.	Ti-6Al-4V ANN Cstg	7175-T736 H.F.	7175-T736 H.F.	Ti-6Al-4V ANN Cstg	N/A
Honeycomb Core Full Depth	5056 Al <sup>3</sup> 3.1 #/Ft	5056 Al <sup>3</sup> 3.1 #/Ft	5056 Al <sup>3</sup> 3.1 #/Ft	5056 Al <sup>3</sup> 3.1 #/Ft	5056 Al <sup>3</sup> 3.1 #/Ft	5056 Al <sup>3</sup> 3.1 #/Ft	5056 Al <sup>3</sup> 3.1 #/Ft	5056 Al <sup>3</sup> 3.1 #/Ft	5056 Al <sup>3</sup> 3.1 #/Ft	5056 Al <sup>3</sup> 3.1 #/Ft	5056 Al <sup>3</sup> 3.1 #/Ft	5056 Al <sup>3</sup> 3.1 #/Ft	5056 Al <sup>3</sup> 3.1 #/Ft	5056 Al <sup>3</sup> 3.1 #/Ft	5056 Al <sup>3</sup> 3.1 #/Ft









WING STA 73.30

CANTED WING STA 38.966

38 1/2 PLANE

BURN THROUGH WELD

K

UPPER ML

0.030 STOCK

WARD

LOWER ML

SPAR NO. 8  
MAKE FROM 6AL 4V 8MM TITANIUM

K-K

BURN THROUGH WELD

CANTED WING STA 38.926

38 1/2 PLANE

X-27447  
(TRACE)

J

UPPER ML

0.0451.002

40

0.0321.002

40

0.080 STOCK

J-J

LOWER ML

SPAR NO. 7  
MAKE FROM 6AL 4V 8MM TITANIUM ALLOY  
AND 7000 SERIES ALUMINUM ALLOY

REVISION NOTES		REVISIONS		DATE APPROVED	
REV	NOTE	DATE	DESCRIPTION	DATE	APPROVED
1	REFER TO USAGE LIST FOR EFF				
2	SEE REF EO FOR EFF				

REV	SH

NORTHROP GRUMMAN		SIZE	CODE
A DIVISION OF		J	J
NORTHROP CORPORATION		76623	
MEMPHIS, TENN.		SCALE	

Sheet





Spar No. 6 will be made from two extrusions of 6Al-4V annealed titanium. The upper and lower spar caps are joggled at each end and each half is welded together in the center of the spar web. The plasma-arc welding process is again employed for this spar design.

Spars No. 7 through 11, Figure 9, are typical, tapered outboard wing spars. It will be noted that one piece extruded titanium spars are excluded from this discussion as the excessive flange stock required for machining the taper makes this approach uneconomical.

Spar No. 8 is a tapered planform version of spar design No. 2.

The No. 9 spar is a three element, fail-safe spar consisting of a corrugated web of rectangular cross-section which is riveted to hat shaped spar caps at both the vertical flanges and inner mold line; the latter attachment being effected through tabs formed on the upper and lower edges of the corrugated spar web.

Spar No. 10 is the tapered version of spar No. 5.

Spar No. 11 is the same as spar No. 10, except the upper and lower halves of the spar are welded together to form a lighter unit. This approach is applicable for 6Al-4V annealed titanium only.

The results of this study are shown in detail in subsection III.9.c. From these results, it is readily apparent that the formed sheet metal sine wave spar is the most cost effective design both in aluminum and titanium. The stress analysis allows for the use of the titanium version in all interior spar applications as the maximum thicknesses required do not exceed .125, the maximum gage capable of being formed to this configuration. The maximum aluminum sheet gage of the interior spars can not exceed .125.

b. Concept No. 1 - Full-Depth Honeycomb Wing (Figure 10)

This design concept is one of the "Quick Look" designs selected for further and more detailed study in this program, since it was the lightest and most torsionally rigid design in the "Quick Look" Study.

This concept consists of nine full-depth aluminum honeycomb core bays (bounded by peripheral spars and ribs) adhesively bonded to machine-tapered titanium plate skins. These skins are procured in one piece, rough cut to



shape, resulting in substantial material cost savings over the purchase of rectangular plate stock.

The substructure is made entirely of titanium to eliminate the presence of any bond preloading caused by bonding the materials at differing rates of thermal expansion.

To reduce the problems of bonding the entire wing structure at one time, the wing tip structure (bounded by the Wing Sta. 123.0 pylon rib, the 15% spar, the 66.6% spar, and the Wing Sta. 151.1 tip rib) is a separate bonded assembly. The pylon rib is used to splice the upper and lower wing skins at its outboard moldline flanges. This approach splices the panels in a low-load area, utilizing existing rib attach fasteners and rib material to effect the splice. Splice weight and cost increases are minimized. The outer wing panels can now be fabricated from standard sheet gages rather than the thick premium stock required for the main wing skin panels, which will significantly reduce the material to be removed from these panels during machining. This approach to the wing outermost section will be used in all subsequent design studies which use both upper and lower titanium wing skins.

The primary wing interior structure comprises three main spars (the 15%, 44%, and 66.6% spars) and five ribs at Wing Sta. 38.93 cant., 73.3, 93.5, 123.0, and 151.1.

These structural members will all be designed to slow crack growth criteria.

The complexity and increased load levels in the peripheral spars preclude the use of formed sheet metal for their construction. As the spars possess natural draft and are long, rather flexible parts, they are ideally suited to precision forging. Lack of inherent stiffness in a part poses many difficulties for casting and weld assembly techniques. Because of greater tolerances, additional machining, and supplementary straightening operations, manufacturing costs of cast or welded spars are increased to the point where they can no longer compete with precision forgings, even though forging non-recurring costs are much greater. The wing attach rib and landing gear rib, by the same reasoning, will also be precision forged in titanium.

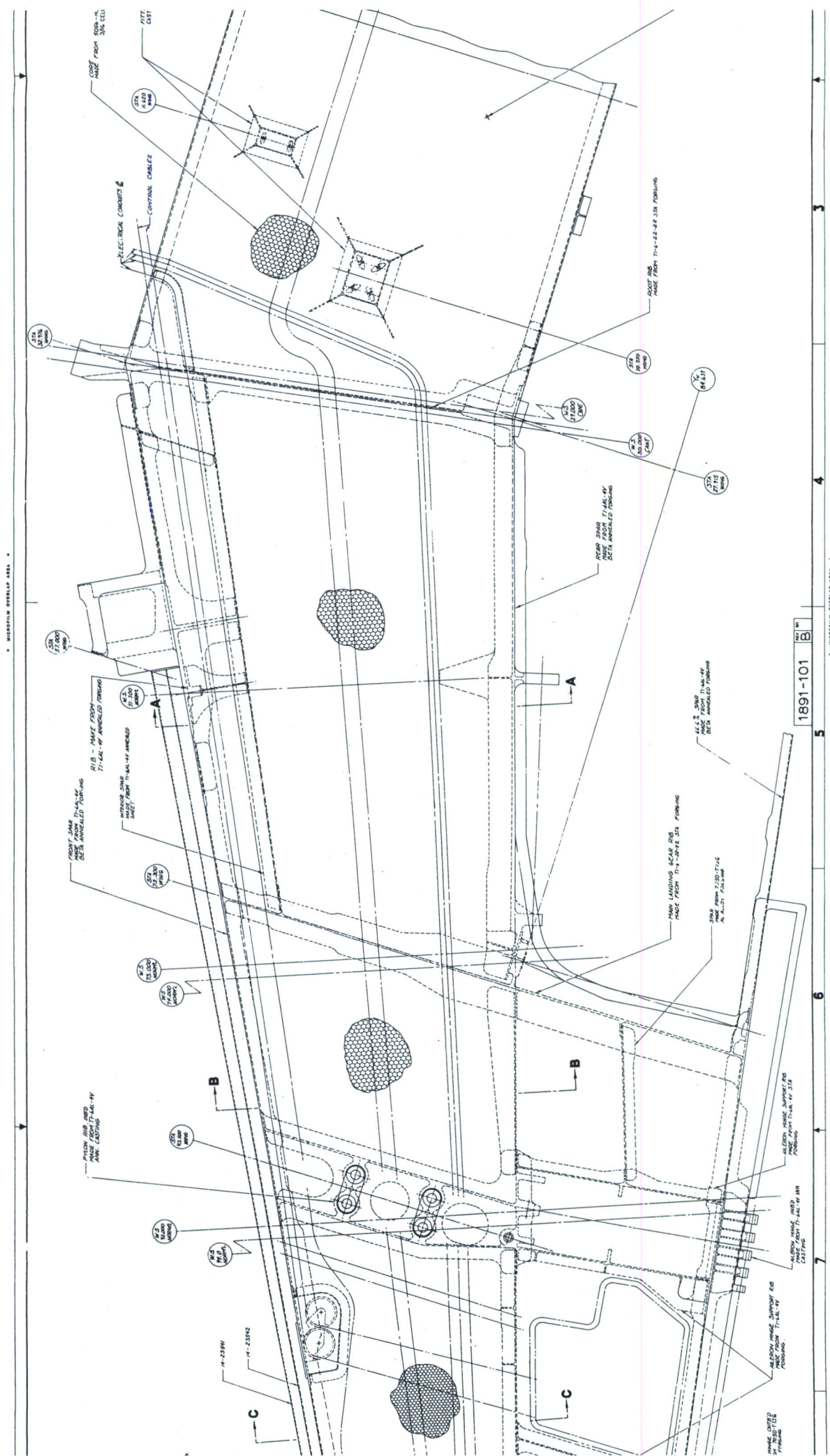
The most complex ribs are the pylon ribs at Wing Sta. 93.5 and 123.0. Machining titanium parts out of billet stock is rarely shown to be cost



FIGURE 10. CONCEPT NO. 1 FULL DEPTH HONEYCOMB WING







2





effective. Only if the parts are very simple and machining is limited, or the parts are of such size or shape that existing methods of preforming (i.e., forging, casting or extruding) cannot be used, can complete machining from billet stock be considered. As these ribs are highly complex configurations, the forging process does not result in sufficiently finished parts to justify the high nonrecurring costs attendant with that process. Casting is the most economical approach to their fabrication. Titanium castings also do not exhibit the large reductions in mechanical properties, as compared to wrought material, that is experienced with aluminum castings. Precision investment castings are called for in all cases. The casting of these ribs in sand was investigated but the minimum allowable wall thickness of 0.250 inch required by this process results in parts that require 100% machining and the additional cost of this machining more than offsets the reduced casting piece price of the sand castings. As investment castings, the material that must be subsequently removed from the ribs by machining is reduced by 80 percent (compared to forging), as only the moldline and interior faying surfaces need be machined. In all cases, only 0.060 inch of material need be removed. The pylon ribs are within the size capability of existing equipment.

The Wing Sta. 93.5 pylon rib casting could possibly be extended to include the two parallel aileron actuator support ribs immediately to its rear. These aileron actuator ribs are shown as separate parts. Combining these three parts so increases the size and complexity of the rib casting that its cost exceeds the combined piece price of the smaller cast pylon rib and the two aileron ribs.

The Wing Sta. 151 tip rib is also investment cast in titanium. To make this rib as a precision forging would require a four-piece segmented die in a double-action press. The attendant high nonrecurring cost of this approach cannot be offset by the decreased weight and improved strength inherent in the forging process.

The speed brake attach fittings being deep hollow boxes like the pylon ribs and part of the bonded wing assembly are titanium investment castings. The inboard aileron hinge fitting is a titanium investment casting which is lighter than the 17-4PH steel investment casting it replaces.

In the leading edge area of the wing box several ribs and a spar at approximately 21% are shown. The outboard rib supports the inboard leading edge flap hinge. The central rib mounts the leading edge flap actuator and the inboard rib distributes the point load induced by the wing leading edge extension structure. These details are titanium precision forgings requiring no finish machining. The 21% spar is of formed titanium sheet and functions as both a honeycomb close out member and the aft attachment for the aforementioned ribs. This leading edge area is not filled with honeycomb core. The high density of systems routing here precludes the installation of sufficient core material to be weight effective.

The seven bays inboard of Wing Sta. 123.0 and aft of the 44% spar contain the aileron actuation mechanism and the main landing gear strut, which precludes the application of full-depth honeycomb core construction. It therefore is necessary to select an alternative method of stiffening the upper and lower covers in those areas. Two methods of accomplishing this necessary stiffening were investigated. The first approach considered was to machine a waffle pattern of integral stiffeners in the wing skins. Unfortunately when this is done with a titanium skin the stiffener size necessary to produce adequate panel support either is too wide, resulting in excessive panel weight, or too high which increases the stock panel thickness thereby increasing the wing skin material cost to the point where this approach is no longer cost effective.

The second approach was to employ adhesively bonded aluminum honeycomb panels with titanium inner pans to the fixed upper wing skin panels in a manner similar to the wing skin stiffening employed in Concepts No. 4 and No. 5. The wing bond assembly sequence calls for the upper wing skin to be bonded to the substructure in one bonding operation followed by the fitting of the core to the lower skin and then bonding the lower skin to the wing assembly in a second bonding operation. This sequence of operations allows the honeycomb panel stiffening to be assembled and bonded to the upper skin during the first bonding cycle.

The upper wing skin area inboard of the gear rib and aft of the 44% spar is composed of a honeycomb sandwich panel with equal thickness graphite/epoxy



face sheets similar in arrangements to the baseline aluminum honeycomb structure. The aileron actuator bay access doors on the lower wing surface outboard of Wing Sta. 85.2 cant. is of similar construction. The application of non-metallic composites in these specific panels results in a 12.6 pound per shipset weight savings. As all of these panels are separate from their respective wing skins and are replacable in service it is felt their utilization would not adversely affect the reliability or repairability of any of the concepts under study in this program. These graphite/epoxy panels therefore are used in this design and all the other subsequent designs described in this report.

The three aileron hinge support ribs are titanium precision forgings. The two stub spars in this area may be made from aluminum precision forgings as they are installed after the bonding of the wing is complete. These spars are also located in a shear lag area where the strain incompatibility of aluminum spars and titanium skins poses no problems or weight penalties.

The wing skins are both bonded and mechanically fastened to the ribs and spars in the full-depth honeycomb areas. This is done as an economy measure to avoid the expense of masking the details to be bonded and to eliminate the possibility of disbonds being initiated at the edge of the glue line. While the bonding of riveted joints improves the fatigue and damage tolerant behavior of the wing structure, lack of reliable quantitative data on this type of joint precluded its utilization in both the safe life and damage tolerant life analyses.

The results of this second iteration produced an interesting variation to the "Quick Look" results. This design has increased in weight and decreased in cost over the previous study results. The weight increase results largely from the additional adhesives potting and ancillary core closeout members required when various internal conduits, control cables and other aircraft systems are installed in the wing.

The reduced cost is achieved by reduced material cost of the wing skins as these are to be purchased in the form of rough sawn plate thereby decreasing the amount of raw stock purchased by some 40%. All titanium plate raw stock for all subsequent wing concepts shall be purchased in this manner.

c. Concept No. 1A - Full-Depth Honeycomb Wing - Aluminum Skins and Substructure

This concept is the same as Concept No. 1 except that aluminum has been substituted for titanium in all detail parts with the exception of the gear rib and tip rib. These ribs are made from steel forgings on the baseline wing and will be made from a titanium precision forging and titanium casting, respectively, in this design. The pylon ribs will be hogged out from 7175-T736 aluminum hand forged billet as in the baseline aircraft as sufficient detail cannot be obtained from the forging process to justify the die costs involved. The speed brake attach fittings are of similar manufacture for the same reason. All other aluminum substructure is precision forged.

The investigation of this variation of Concept No. 1 was undertaken in an attempt to marry the significant weight savings of the full depth honeycomb configuration with the low cost of aluminum construction. While a 34 percent reduction in cost was realized, a 6 percent weight increase over Concept No. 1 was incurred. This weight increase was mainly a result of the lower specific design allowables of the aluminum skins. A small additional weight penalty was incurred through the use of longer titanium fasteners through the necessarily thicker aluminum skins.

d. Concept No. 2 - Warren Truss Spar Wing (Figures 11 through 14)

The following is a description of a titanium wing design with the interior spars arranged to form a Warren truss. The principal objectives being sought are increased torsional rigidity, partial elimination of wing ribs and the attainment of multiple load path spars.

The interior structure is a series of one-piece formed sheet titanium spars with sine wave beaded webs with nesting semi-circular, cross-sectioned caps, supported in cradle filler blocks at the wing skin attach fasteners. It is readily apparent from the drawings that this method of attaching the truss web junctures to the wing skin precludes loading the truss webs eccentrically. Shims installed between the wing skin and its mating "cradle" block take care of vertical tolerance accumulation. The spar webs are symmetrically beaded for stiffness.

As this design progressed a major handicap to its successful employment in this program became apparent. The baseline wing envelope with its

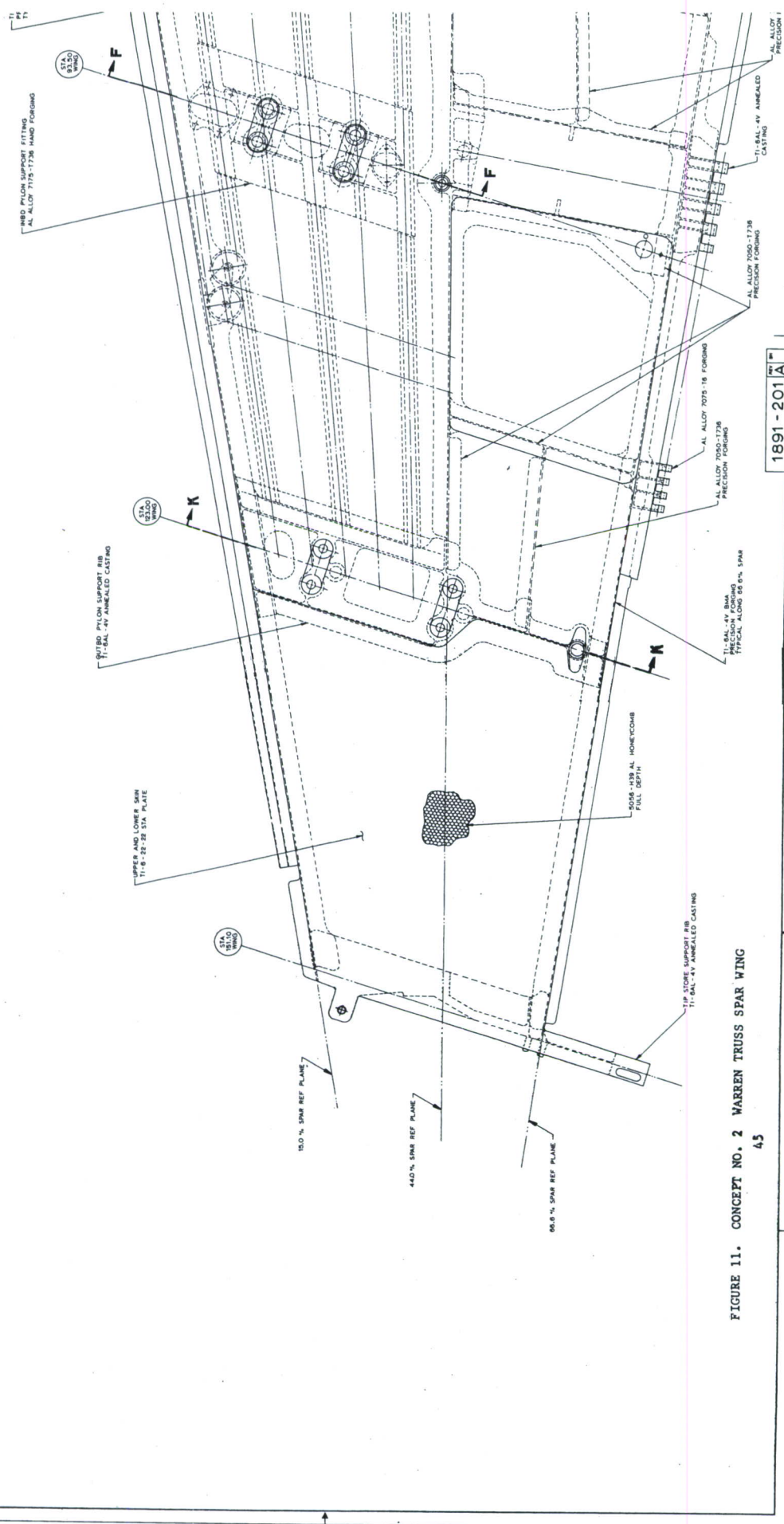
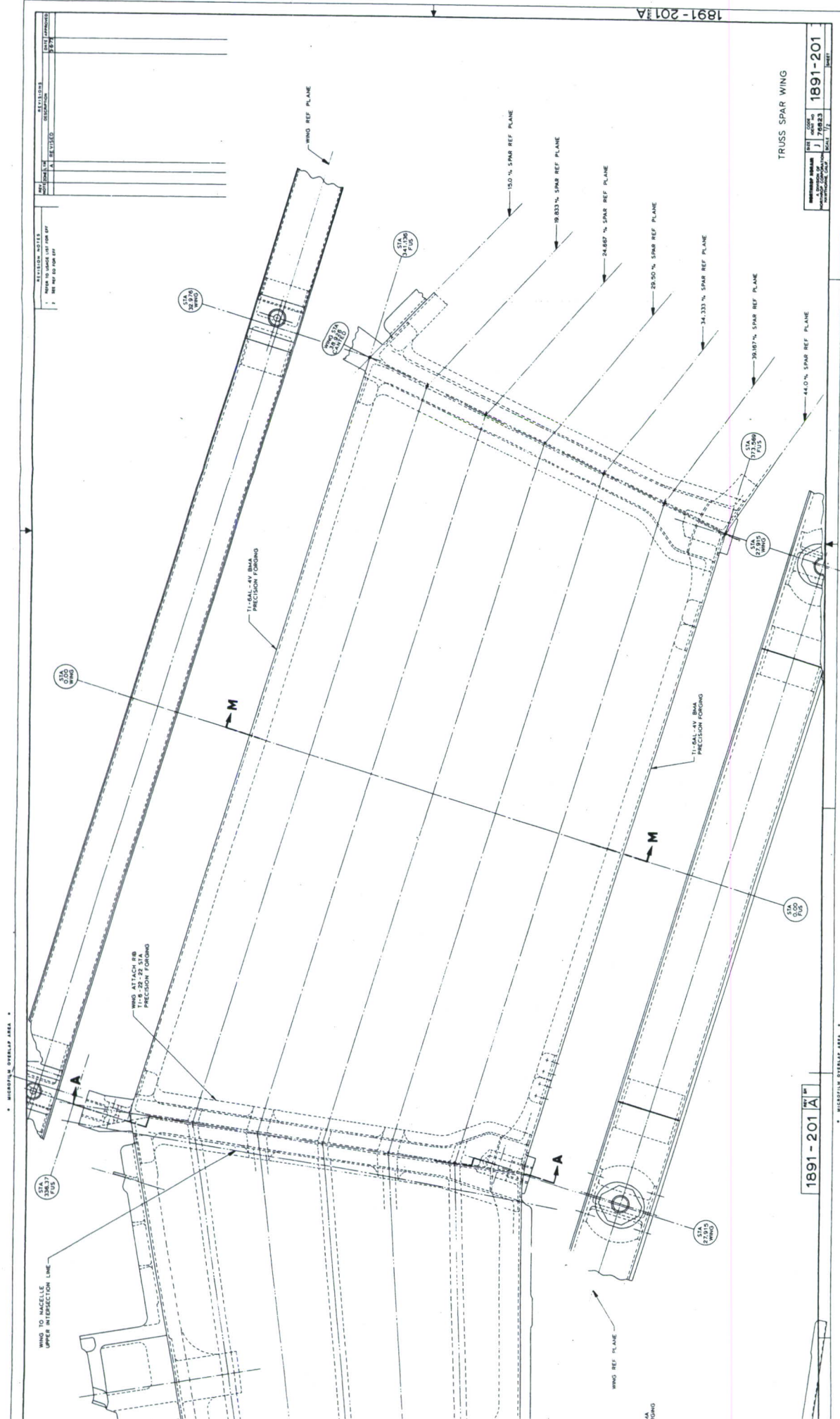


FIGURE 11. CONCEPT NO. 2 WARREN TRUSS SPAR WING













1891-202	REV	SA
	A	

1891-202	REV	SA
	A	

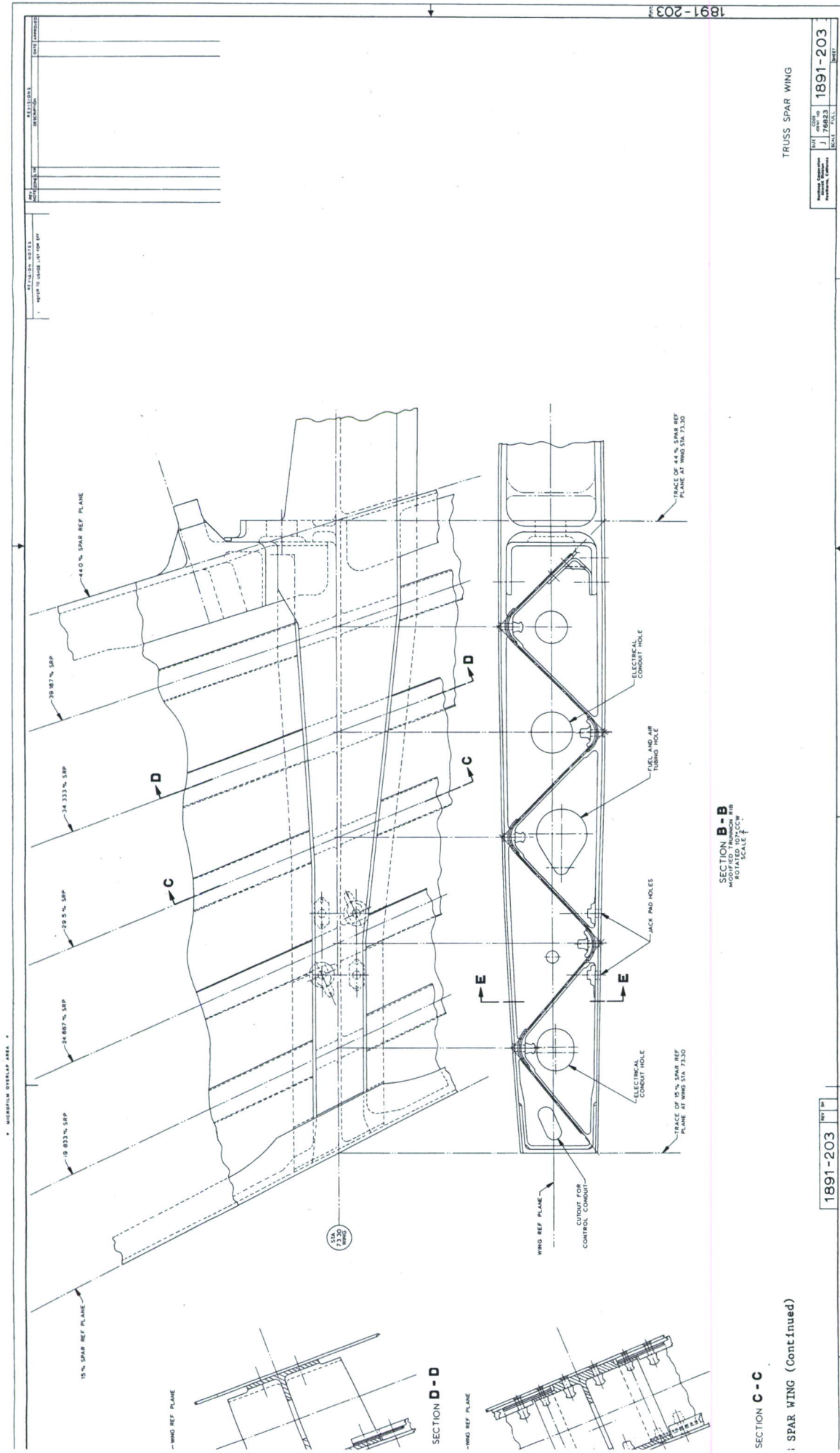


SECTION A - A  
SECTION AT CANTED WING STA 38.926

FIGURE 13. CONCEPT NO. 2 WARREN TRUSS SPAR WING (Continued)



2



SECTION C-C

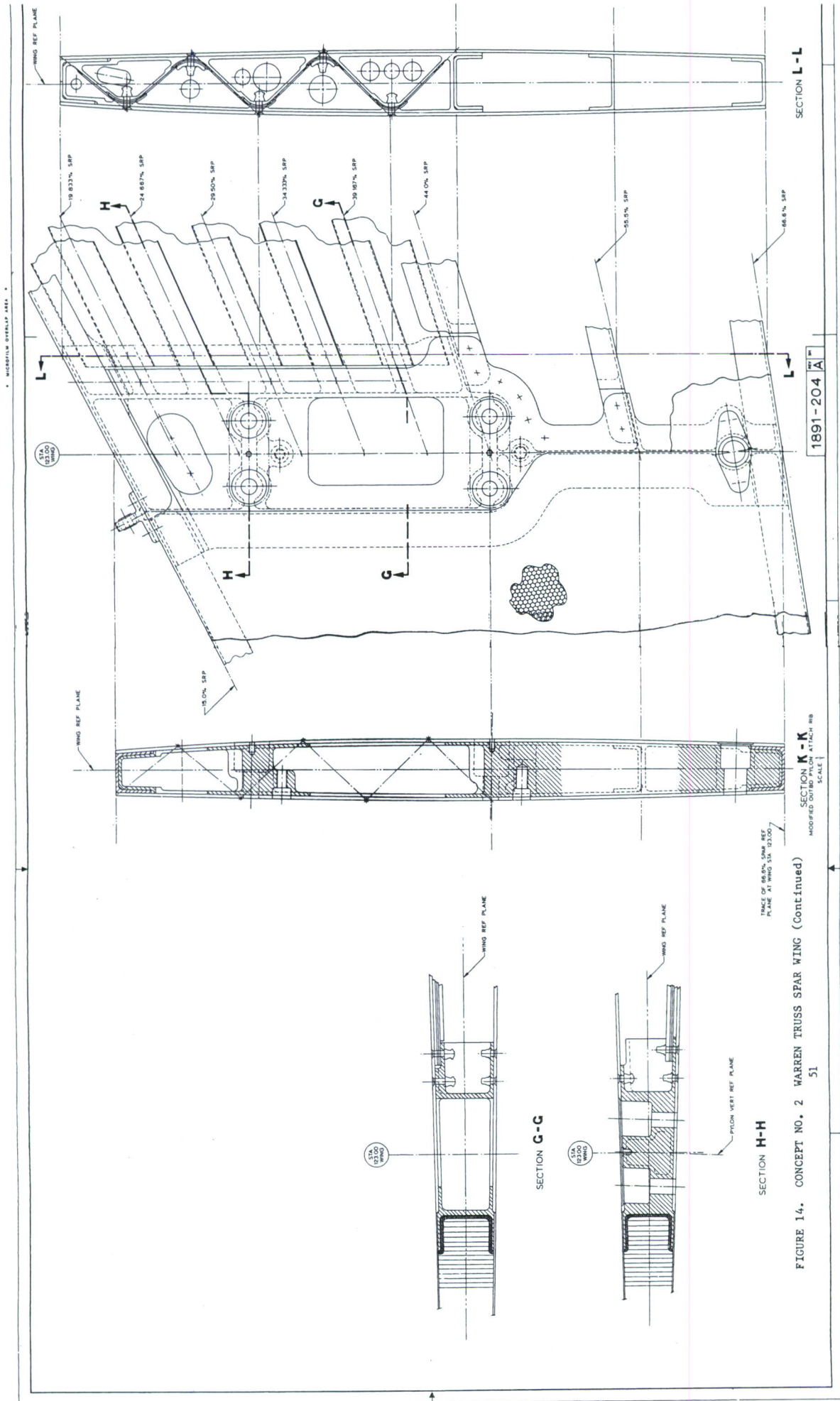
SPAR WING (Continued)

TRUSS SPAR WING

REV	DATE	BY	CHKD	APP'D	1891-203	SHEET
1	7/28/83	J	J	J	1891-203	1

1891-203

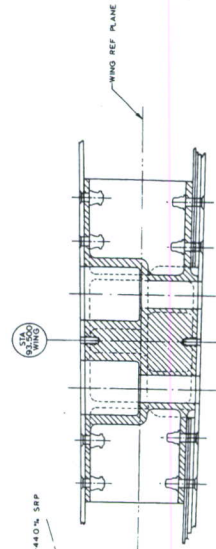
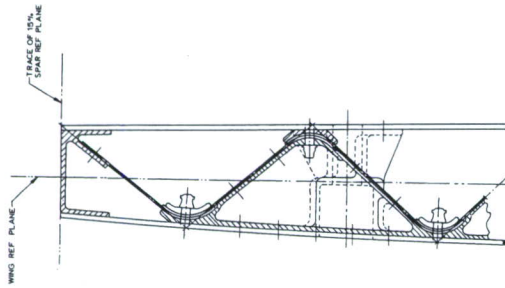
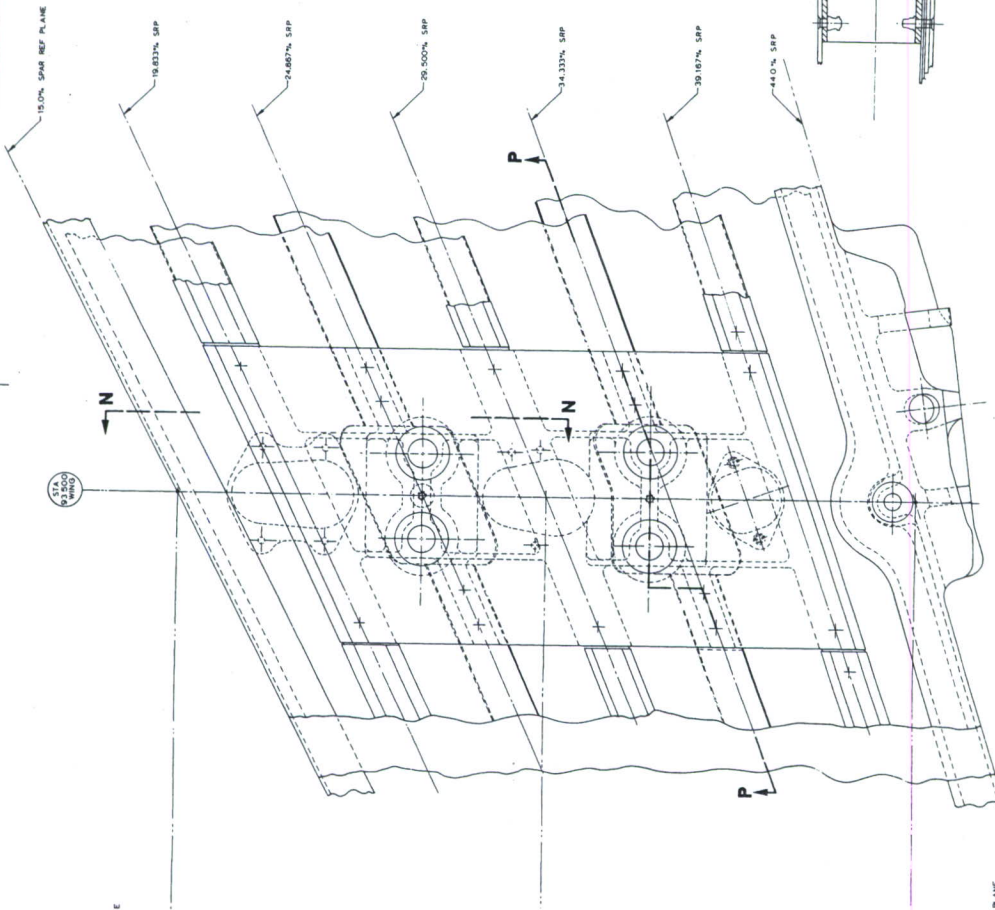
1891-203







5. MICROFILM OVERLAP AREA



TRUSS SPAR WING

EXCLUDED NOTES

1. Refer to standard left rib set
2. Rib set up to rib set

REV	DESCRIPTION	DATE
1	1891-204 1A	1891

1891-204 1A

1891-204

3

sweep and taper, both starting at the root rib, and the wing pylon attach bolt patterns, mitigate against the successful application of this structural arrangement. The Warren Truss substructure is a relatively inflexible structural arrangement. While it may be viable in a new design, it has inherent geometric constraints which preclude its efficiently replacing a prior structural arrangement where no envelope or interface revisions are permissible. This constraint of required baseline geometry prevented the elimination of the root rib. Some portions of the inboard pylon rib were successfully eliminated. Lack of sufficient wing depth prohibited the continuation of this structural arrangement beyond the outboard pylon rib. The wing tip from the outboard pylon rib outboard and the substructure aft of the 44% spar remains the same as for the full depth honeycomb wing design described previously.

The full main landing gear trunnion rib is retained. The chordwise bending moments, in this area, are of such magnitude that even minor reductions in chordwise bending material cannot be tolerated.

The nesting feature of the interior spars and the joining of the forward and aft interior spars did indeed give multiple load path spar caps, but the amount the design allowable stress increase realized when damage tolerance is no longer a factor (i.e., the wing design is now either safe life or static strength critical) was minimal. An in-depth discussion of this subject is contained in Subsection III-2d. of this report with the respective design allowables summarized in Tables VII and VIII of that section.

A comparative finite element program was also undertaken to determine the torsional rigidity of this concept as opposed to the more conventional multisparred designs in this study. The results of this study indicate no apparent increase in torsional rigidity for the Warren Truss Spar configuration. (See subsection III.2.d for a description of this program). Having thus failed to achieve to any significant degree any of the design objectives originally ascribed to it, the Warren Truss Spar concept was abandoned as a viable design approach for this program.

e. Concept No. 3 - Aluminum/Titanium 6-Spar Wing (Figure 15)

This concept was originally formulated to take advantage of the increased specific fatigue strength and fracture toughness of titanium in the wing areas where these design aspects are most critical. Additionally, this concept as conceived was to represent the lowest cost and least risk utilization of titanium in the concepts under study in this program.

This concept initially consisted of a titanium lower wing skin with spanwise beaded panels bonded to its inner surface. It was thought that this method of stiffening a titanium lower skin, though rather inflexible in application, would be the most cost effective method of utilizing applied stiffening to a titanium wing skin. Because of the limited applicability of this type of stiffening its employment was limited to the lower skin of a six spar wing.

The resulting wing is similar in planform to the baseline wing. As the upper wing skin was not critical from a crack growth standpoint, and the wing possesses the spar spacing necessary for adequate upper skin support a 7050-T7651 aluminum alloy plate was used for the upper skin of this configuration. The use of titanium in this design is confined to the area where fracture toughness is of prime importance. It became evident during the second iteration of the stress analysis that if the quantity of material used for the beaded inner pans is added instead to the outer wing skin thickness, the compressive stability of these thicker panels is greater than the beaded panels originally considered. Therefore a plain machined Ti-6Al-4V  $\beta$ MA plate lower skin replaced the beaded stiffened skin.

The interior spars are of formed Ti-6Al-4V  $\beta$ MA sheet and are employed outboard to the outboard pylon rib. The interior wing spars outboard of the outboard pylon rib are 7075-T73 formed sheet aluminum without web corrugations. The wing is so thin at this point that corrugating the spar webs only saves .6 pounds. This insignificant weight savings cannot justify the increase in tooling costs necessary to produce the corrugations.

The bonded tip assembly was not considered for this design to remain consistent with the least risk premise mentioned in the opening paragraph of this concept description. The lower tip skin is of 7050-T7651 machine



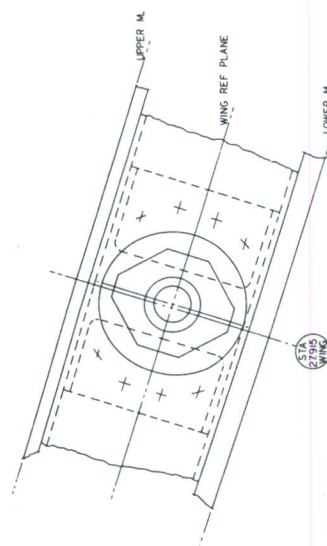
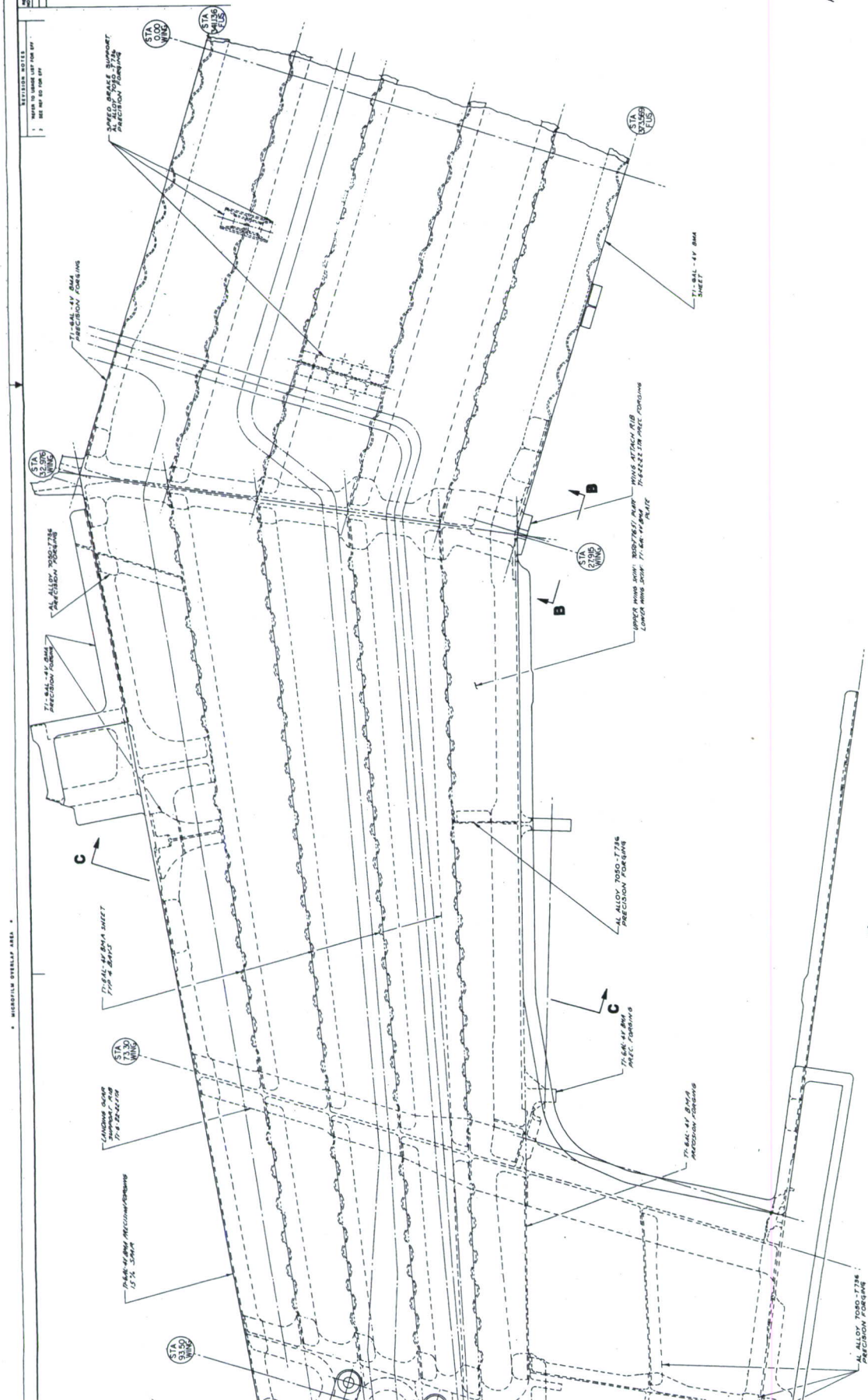


FIGURE 15. CONCEPT NO. 3 ALUMINUM/TITANIUM 6-SPAR WING







tapered aluminum plate spliced at the outboard pylon rib. The peripheral spars (i.e., the 15% and 66%) are precision forged 7050-T736 aluminum in the tip region only.

The peripheral spars inboard of the wing Sta. 123 are all Ti-6Al-4V  $\beta$ MA precision forgings. The landing gear rib is precision forged Ti-6-22-22 STA.

The inboard pylon ribs are made from 7175-T736 hand forged billet as in the baseline. The strain compatibility of aluminum with titanium is not a pacing criteria for chordwise structure so the use of an aluminum rib with a titanium lower skin imposes no weight penalty on that account. The resulting rib shows a one pound weight penalty over a cast titanium rib similar to the one used in configuration No. 1. With only a one pound weight differential between the cast titanium rib and the machined aluminum rib the latter proves to be the most cost effective design.

It may be argued that the wing attach rib should also be of aluminum for the same reasons. While the cost effectiveness of such a design approach is without question, this rib is one of the most critical of wing structural elements and lower mould line fastener hole quality is of paramount importance. It is felt that the deleterious effect of pulling of chips from the titanium spars through the aluminum rib flanges would tend to produce flawed holes in the rib flanges. A precision forged Ti6-22-22 STA rib precludes this problem and is therefore the most prudent design approach for this highly fatigue critical area. The remainder of the stub ribs and speed brake attach fittings being freed from the thermal expansion constraints of a bonding cycle may be made from precision forged 7050-T736 aluminum alloy.

A 5 percent weight saving was realized with this design, but at a 37 percent cost increase. This cost increase is directly attributable to the high material cost of the titanium lower skin, the high spar piece count, the increased rib complexity necessary to splice these spars, and the increased cost to assemble this large number of titanium spars.

f. Concept No. 3A - Welded Titanium 6-Spar Wing (Figure 16)

This design attempts to exploit to advantage the weldability of titanium alloys in the one design concept where titanium is used extensively without adhesive bonding. The principal advantages sought are improved fatigue and crack growth allowables through the elimination of all fasteners through the lower skin in the critical areas, and increasing the efficiency of the lower wing bending material by placing it as close to the lower wing outer mold line as possible.

This concept is basically Concept No. 3, except the substructure is T.I.G. weld assembled and then the lower wing skin is electron beam welded to this substructure. When the X-ray inspection, stress relieving and straightening have been completed, the upper 7050-T7651 aluminum skin is attached to the welded structure with blind fasteners. The lower skin is welded to the substructure from root to tip. While there is no design allowable advantage gained in welding the tip structure it is felt that a transition from welded to mechanically fastened structure will most certainly cause local stress concentrations at the termination of the welds if a one piece lower skin is maintained to the wing tip. The only other alternative is to splice the tip skin at the pylon rib. Since the additional welding required for the tip section does not represent a significant increase in weld time or difficulty, eliminates a splice, and will not adversely affect the structural integrity of the structure, the wing tip structure will be welded in the same manner as the inboard portions of the wing.

Assembly of the substructure and lower wing skin by welding considerably alters the substructure cost. This alteration manifests itself principally in the decreased complexity of the Ti-forgings and castings that constitute the bulk of the substructure. These details which were formerly channels or "I" beams with both inner mold lines contained on the part are now "Tees" or angle cross-sectioned parts containing only the upper inner mold line of the wing. This eliminates the major close tolerance dimension on these parts reducing the risk factor in procuring these parts as well as lowering their cost and reducing the amount of subsequent machining required (die lock is eliminated). However, there may no longer be any aluminum substructure

WING ATTACH AREA

WING ATTACH RIB  
PRECISION FORMING

WING ATTACH RIB  
PRECISION FORMING

SPEED BRAKE SUPPORT  
PRECISION FORMING

LOWER SKIN  
T1-BAL-47 BMA PLANE

10% SPAR REF PLANE

21% SPAR REF PLANE

27% SPAR REF PLANE

33% SPAR REF PLANE

39% SPAR REF PLANE

44% SPAR REF PLANE

LOWER IN

WING REF PLANE

UPPER IN

E.B. WELD  
TYPICAL

UPPER SKIN

AL ALLOY 7050-T7651 PLATE

SECTION B-B  
ROTATED 73° CCW

TRACE 88.8% SSP

LOWER IN

WING REF PLANE

UPPER IN

E.B. WELD  
TYPICAL

FWD  
UP

SECTION A-A  
ROTATED 90° CCW

FIGURE 16. CONCEPT NO. 3A WELDED TITANIUM 6-SPAR WING

1891-A301

SECTION C-C

WING ATTACH AREA

E.B. WELD  
TYPICAL FOR ALL SPARS AND  
INTERIOR SPARS EXCEPT AS SHOWN

INTERIOR SPAR

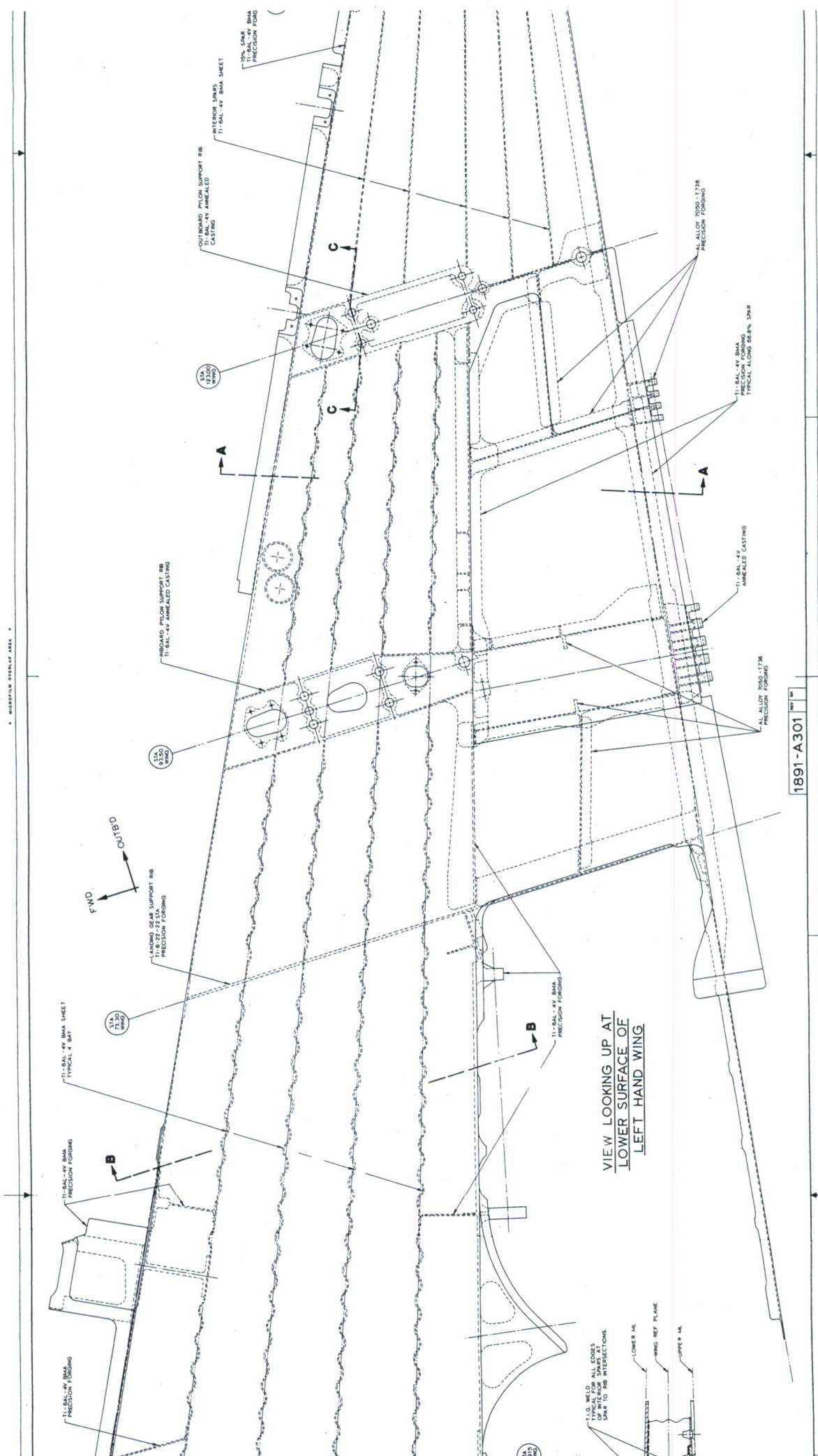
T1-BAL-47 BMA SHEET

PYLON VERT REF PLANE

T1-BAL-47 BMA SHEET

E.B. WELD  
TYPICAL FOR ALL SPARS AND  
INTERIOR SPARS EXCEPT AS SHOWN







details as all these interior members are welded to the lower skin. The cost increases incurred in converting aluminum parts to titanium counteract the dollars saved through simplification of the relatively uncomplicated spar details and the total spar cost shows a slight rise. The converse is true when the highly complex ribs are examined. Here the simplification of the details is of a higher order and the net result is a reduction in rib detail costs.

The increased assembly costs incurred in the welding process further negate these savings resulting in a slight cost increase over Concept No. 3. The increased efficiency of the wing's lower bending material is evident as the weight of this concept is 12 pounds less than that of Concept No. 3.

g. Concept No. 4 - Honeycomb Panel Stiffened 5-Spar Wing (Figure 17)

This skin design is one of several approaches to the wing skin stiffening vs. interior spars trade-off studies being conducted in this program wherein the cost and/or weight of applied wing skin stiffening is traded off against the savings available from reduced substructure piece count and complexity made possible by the increased wing skin stiffness.

The wing skins of this design are constructed of taper machined and pocketed titanium outer wing skins adhesively bonded to thin sheet titanium inner pans filled with aluminum honeycomb core. All the skin bays will have honeycomb panel stiffening.

The inner pans will be formed in one piece from 15% spar to 44% spar in the chordwise direction. To reduce the pan size they will be butt spliced at each rib station using the existing rib flanges for splice material.

The substructure differs from Concept No. 3 in that one whole span-wise spar location is deleted. The remaining interior spars are then re-located being equally spaced front to rear between the 15% and 44% spars. This spar reduction reduces wing rib complexity by eliminating one set of spar web attach flanges. It also slightly reduces the assembly cost as fastener count is reduced. There is one side effect to this approach, however, which should be noted. The stub ribs, speed brake attach fittings now increase somewhat in length adding to their cost.



The alloys from which the wing components are made are unchanged from their counterparts in Concept No. 3. The one obvious exception is the upper wing skin. In an attempt to keep the upper bending material as close to the wing outer mold line as possible, thereby maximizing its efficiency, the thicker aluminum skin has been discarded in favor of the titanium wing skin shown. The tip assembly being only 1.1 inches high at wing station 151.1, the inner pans of the honeycomb stiffening panels intrude upon the available interior space so as to prevent the electrical and fuel line routing to the tip store. It is then of necessity that the tip assembly from the wing station 123 pylon rib outboard be the full depth bonded honeycomb assembly described in Concept No. 1.

This again requires the outboard pylon rib to be a Ti-6Al-4V annealed casting to remain thermally compatible with the tip assembly.

It is readily deduced from the weight and cost summary tables that though the weight decrease from that of Concept 3 is significant, the wing skin cost increases are of such magnitude that this weight saving is not cost effective.

#### h. Concept No. 5 - Honeycomb Panel Stiffened 4-Spar Wing (Figure 18)

The general trend of reduced weight with reduced substructure evident in Concept No. 4 was pursued further to ascertain whether this downward weight trend would continue and if further reductions in substructure count and wing skin assembly complexity could reduce the total wing cost to produce as cost/weight effective a design as Concept No. 1 or No. 3.

A three spar design was first considered. As spars are eliminated the stub rib lengths and panel widths increase in a harmonic progression. From a six-to five-spar wing this amounts to a 25% length increase. From a five-spar wing to a four-spar wing the increase is 33% and from a four-spar wing to a three-spar wing the length increase is 50%. In a three-spar wing this increases the combined length of the stub ribs to where they have a total length equal to a spar running from landing gear rib to landing gear rib.

The effect of the increased spar spacing is most seriously felt in that portion of the 15% spar immediately outboard of the wing attach rib where the increased length of the integral rib represents too deep a draw to forge in a direction parallel to the wing reference plane. This spar's forging direction

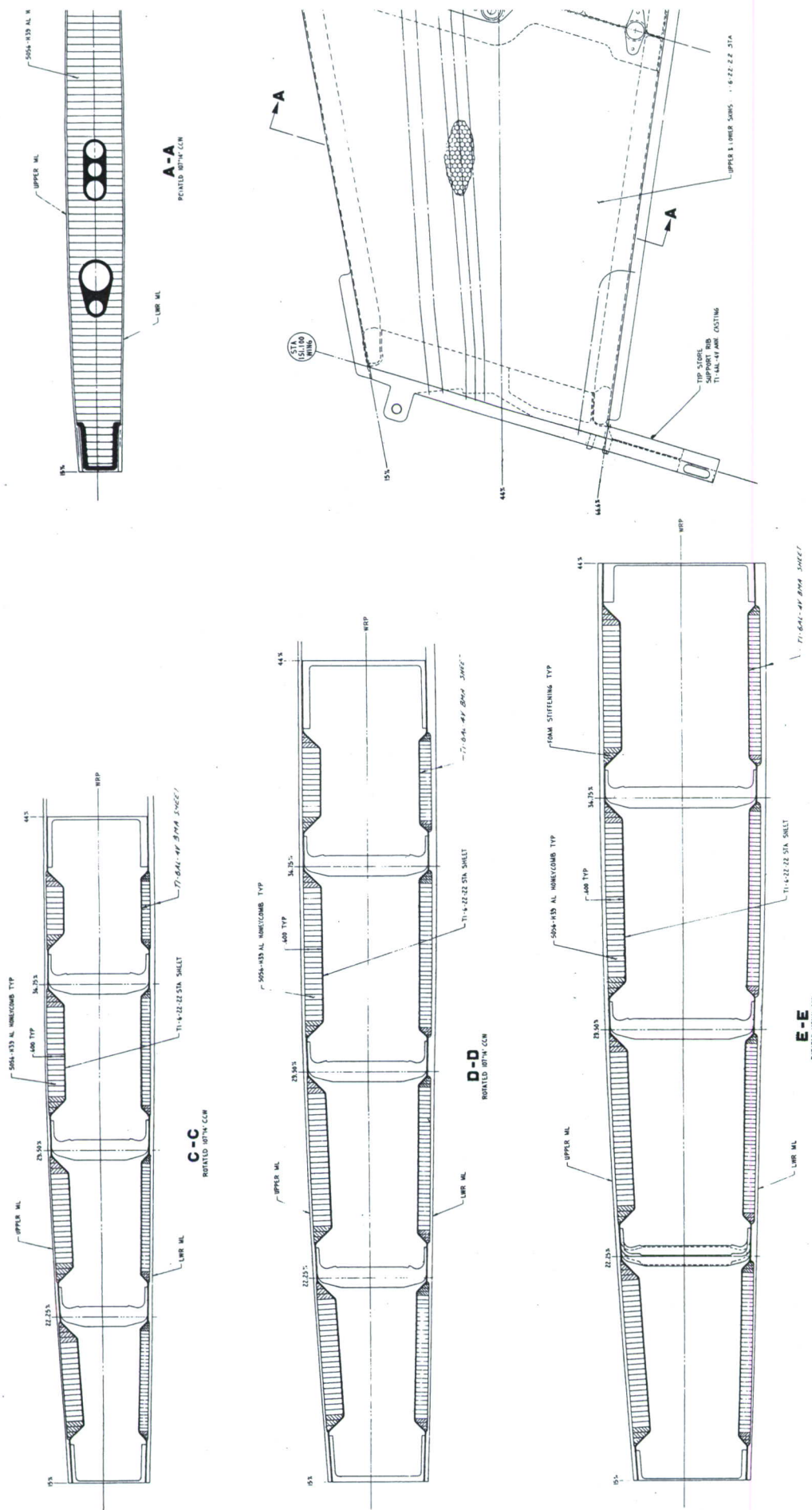
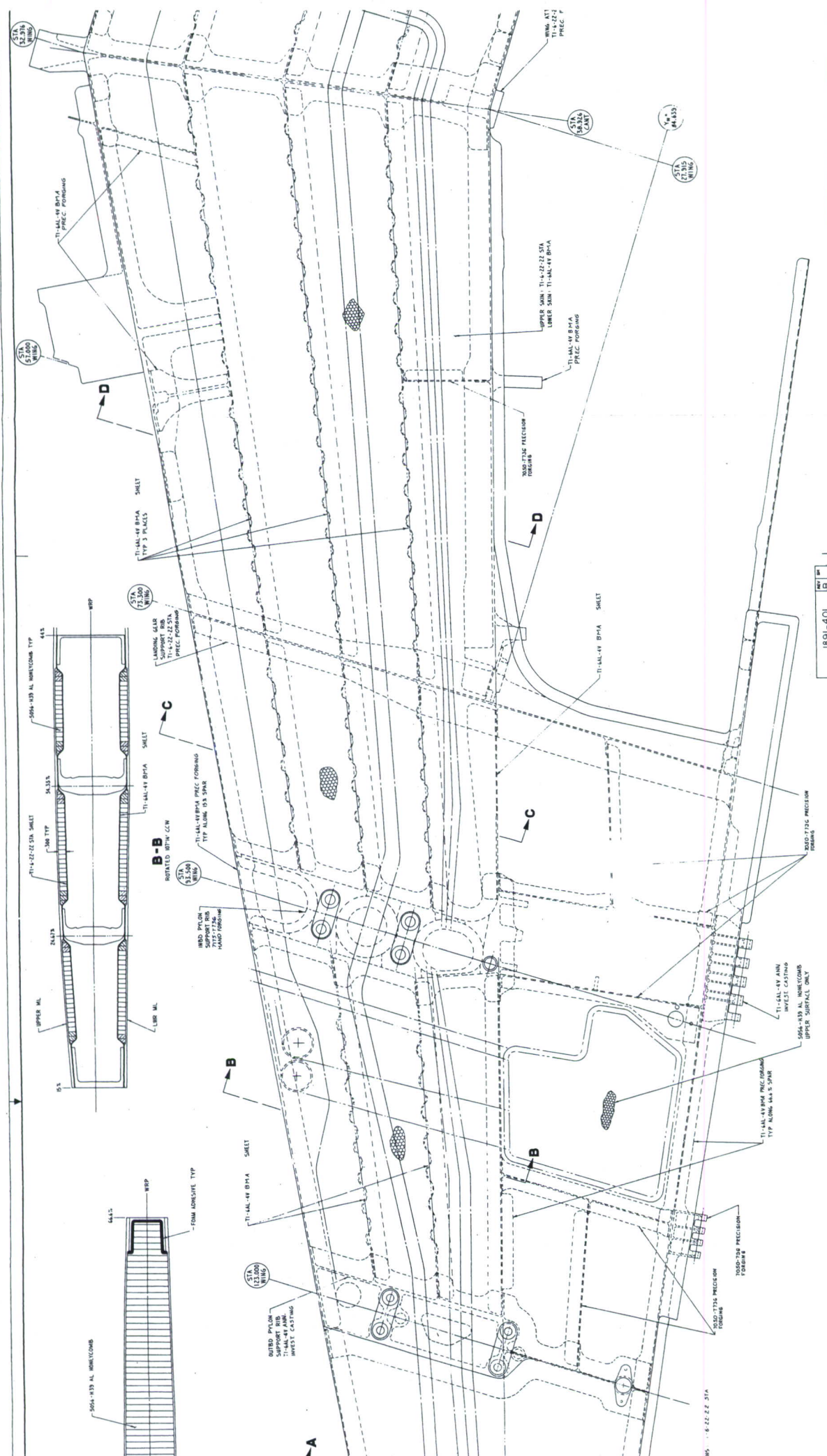
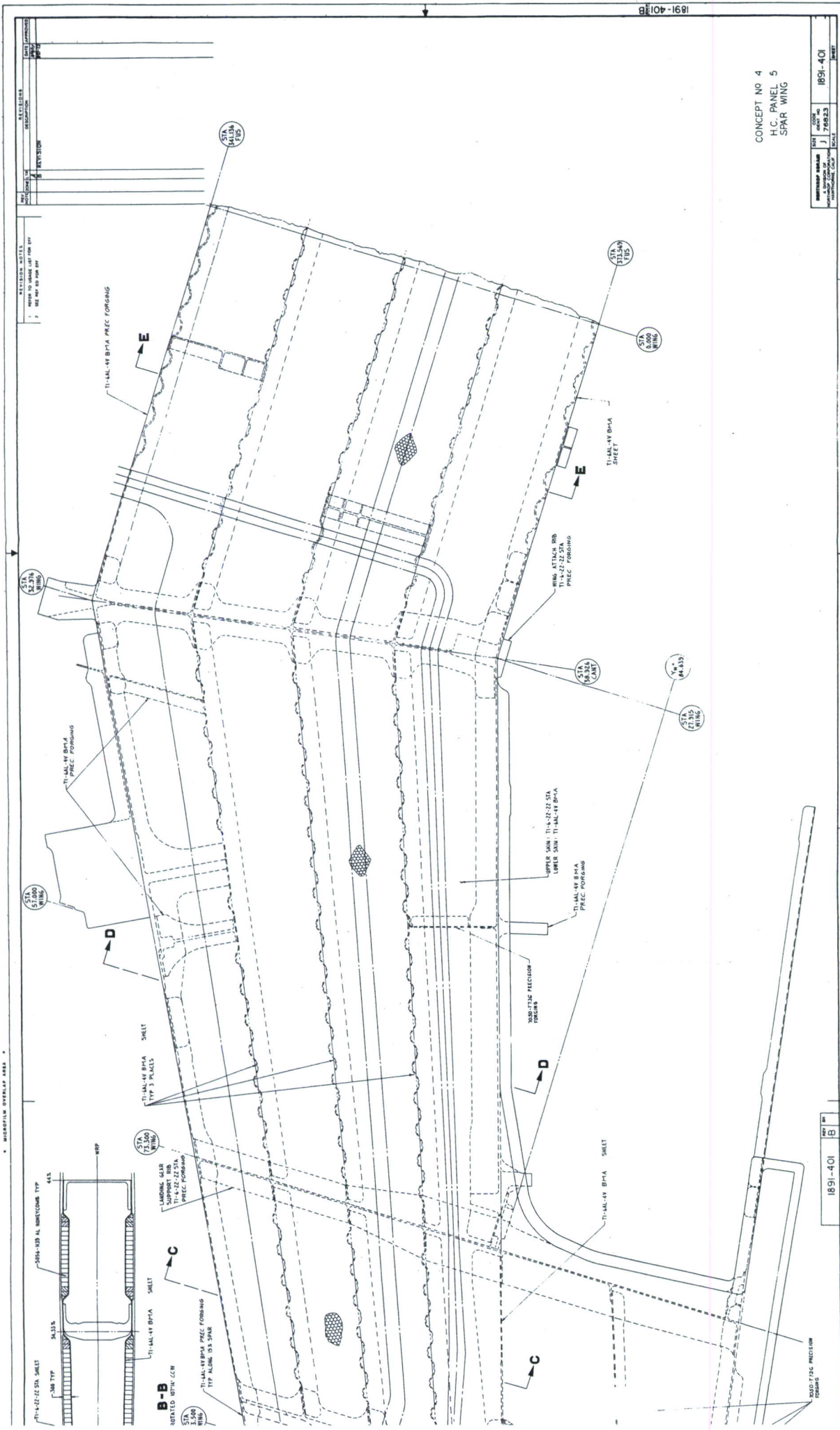


FIGURE 17. CONCEPT NO. 4 HONEYCOMB PANEL STIFFENED 5-SPAR WING







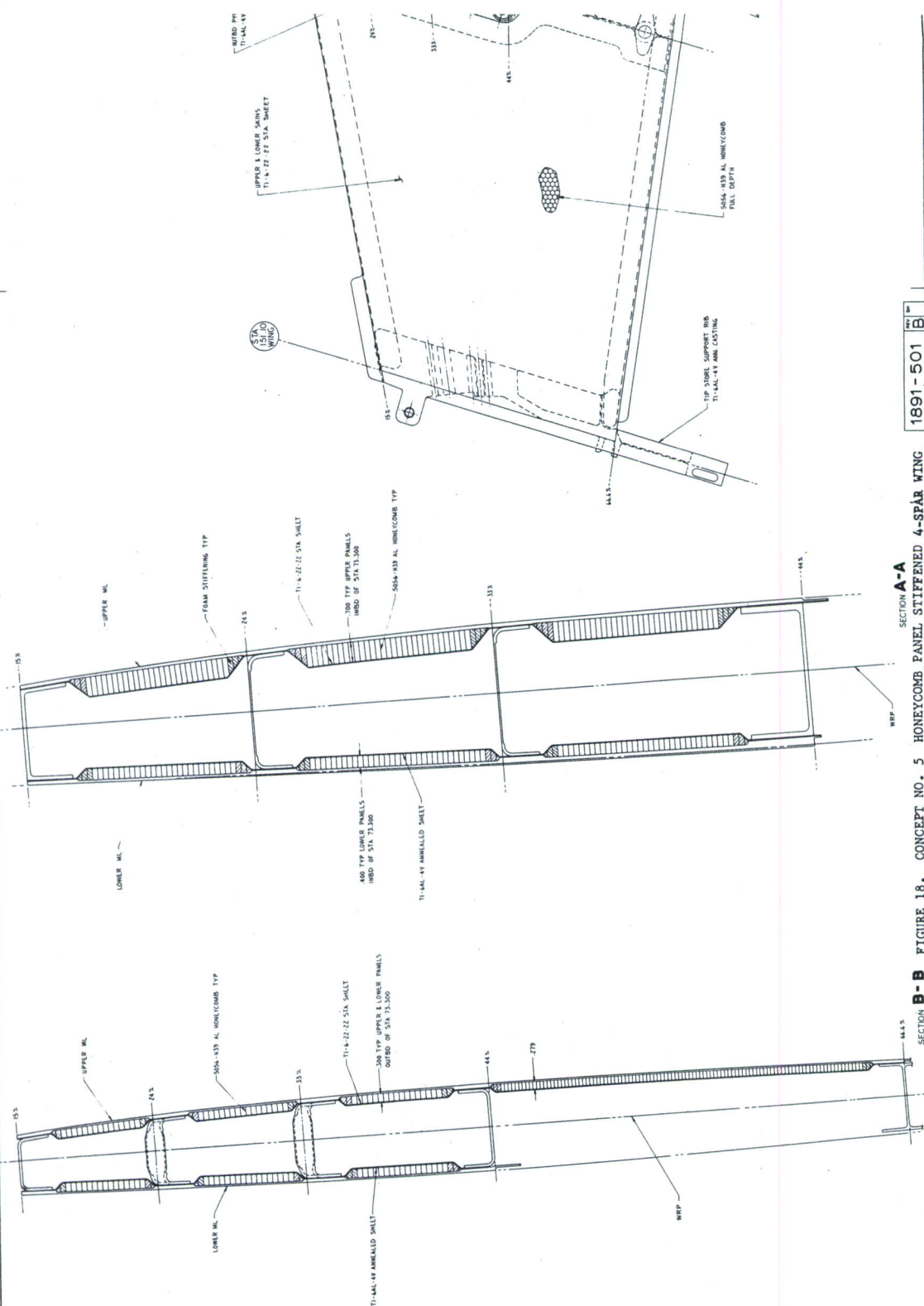


CONCEPT NO 4  
H.C. PANEL 5  
SPAR WING

1891-401

1891-401

10	10
----	----



44.6.5

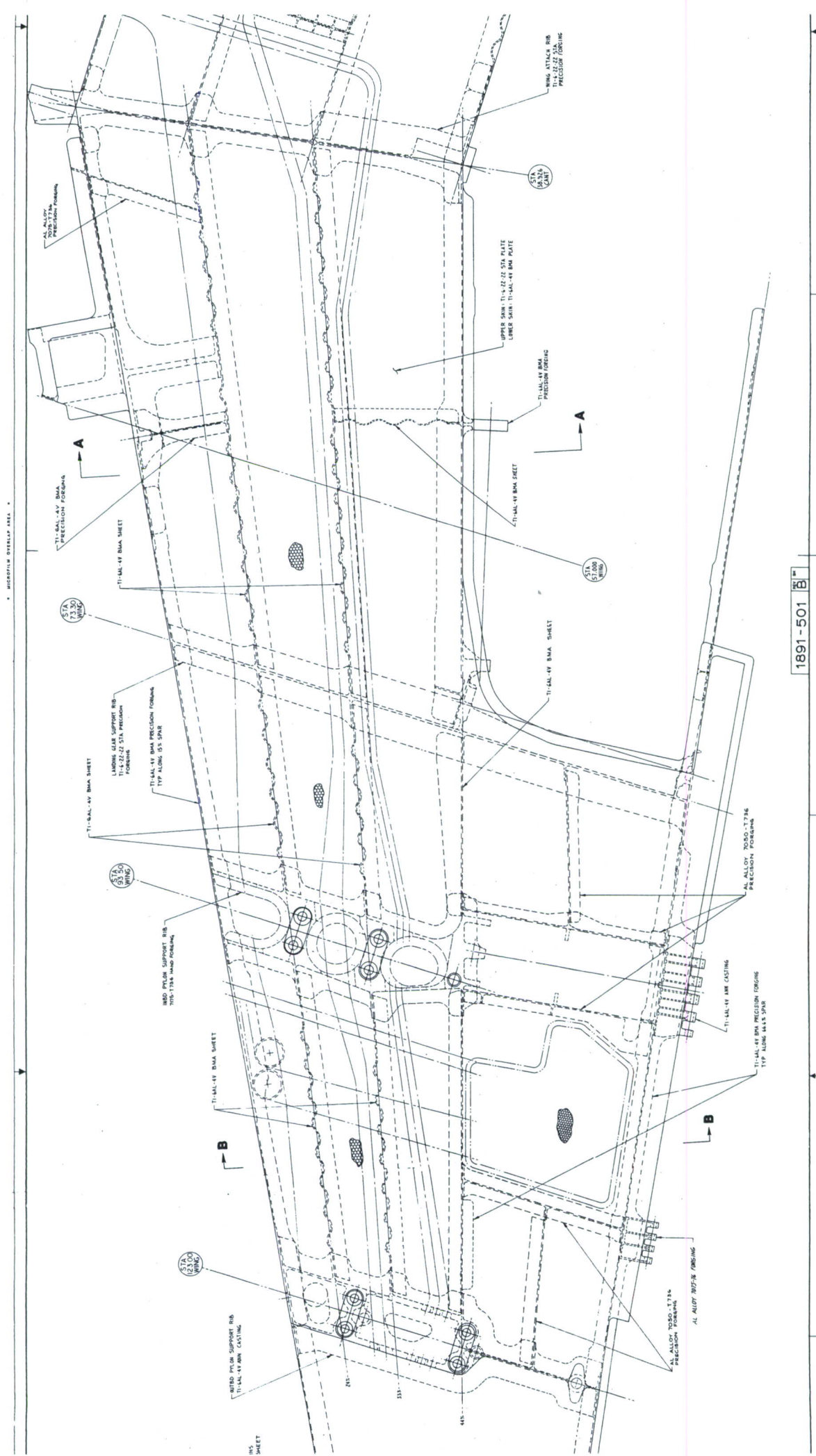
SECTION **B-B**

FIGURE 18. CONCEPT NO. 5 HONEYCOMB PANEL STIFFENED 4-SPAR WING

SECTION **A-A**

WRP

1891-501	REV	B
----------	-----	---



1891-501	Alt	B	mm
----------	-----	---	----

MICROFILM OVERLAP AREA %







must now be normal to the wing reference plane and the resulting part is little more than a conventional forging requiring much more machining to produce a finished part.

In order to supply adequate edge support for the now wider panels, the remaining interior spars must exceed 0.125 inch thick, the upper limit for forming these spars in titanium sheet. Additionally, the 44% spar segment in the wing carrythrough structure would also exceed this limit and become a precision forging.

The substitution of titanium precision forged spars definitely reverses the downward trend of spar costs. The increased rib length likewise reverses a similar trend in rib cost plus halting the downward course of the assembly costs. The only area where this cost reversal does not occur is in the wing skin cost. The reduced number of panels on these skins in a three-spar design does reduce the complexity and thus their expense. This reduction cannot, however, offset the increased spar and rib costs. For these reasons a three-spar wing study was not continued into the layout stage.

When a four-spar wing is contemplated, however, the interior spars are still within the forming limits of titanium sheet. The quantity of spar-skin attachments is reduced as the loss of one complete spar vis-a-vis a 33% length increase in rib-skin attachments results in a net loss. Wing skin complexity and cost is also reduced. The deletion of the spar attach web in the ribs reduces their complexity and required machining to such an extent that a rib cost reduction is still realized, rib length increases notwithstanding.

The four-spar wing shown in Figure 18 is identical to the Concept No. 4 wing except the spar count is reduced and the honeycomb core height is somewhat thicker in the regions inboard of the landing gear rib. This concept representing as it does, the practical minimum of spared substructure still does not approach the efficiency of the full-depth honeycomb design previously described.

i. Concept No. 6/7 - Ti-Borsic/Geodesic 4-Spar Wing (Figures 19 through 21)

(1) Ti-Borsic Upper Skin (Figures 20 and 21)

This concept study was undertaken in an attempt to utilize the higher specific stiffness of composite materials within the basic design limitation of a metallic wing structure. Little was known of the mechanical properties of Ti-Borsic composite material when this investigation was initiated. Even less was known about the fatigue and crack growth behavior of this material. For a fuller discussion of the method used to arrive at a working set of material allowables, see subsection III.2.e.

The basic raw material (i.e., Ti-Borsic) consists of a flat tape, up to 12 inches wide, composed of a unidirectional layer of silicon carbide coated boron fibers pressure diffusion bonded between two sheets of Ti-6Al-4V foil forming a sandwich some 6 mils thick. This "mono-tape" is subsequently laid up to the desired thickness with the appropriate fiber orientation and diffusion bonded into a single panel.

Since improved stiffness was a proven attribute of this composite material and no fatigue and crack growth data was or became available, this material's use was confined to the upper wing skin. Again, because of the unknown fatigue and crack growth behavior and the known difficulty of drilling through the Borsic filaments, it was decided to limit the composite material application to the center of the skin panel bays between the spars and ribs. The area directly above the substructure flanges was composed of matrix material only through which the wing skin attach fasteners are installed.

The wing is composed of 38 discrete panels. Each of these panels is constructed from a Ti-6Al-4V inner and outer cover panel, in between which many mono-tape laminations are placed. This stack of tapes is feathered at its edges to avoid the delamination which might occur if the stack were blunt edged and better effect the transition from composite to 100% matrix at the tape stack edges. This tape stack is also surrounded by a "picture frame" of matrix material, in this case Ti-6Al-4V, which fills the void between the titanium panel covers and the composite interiors.



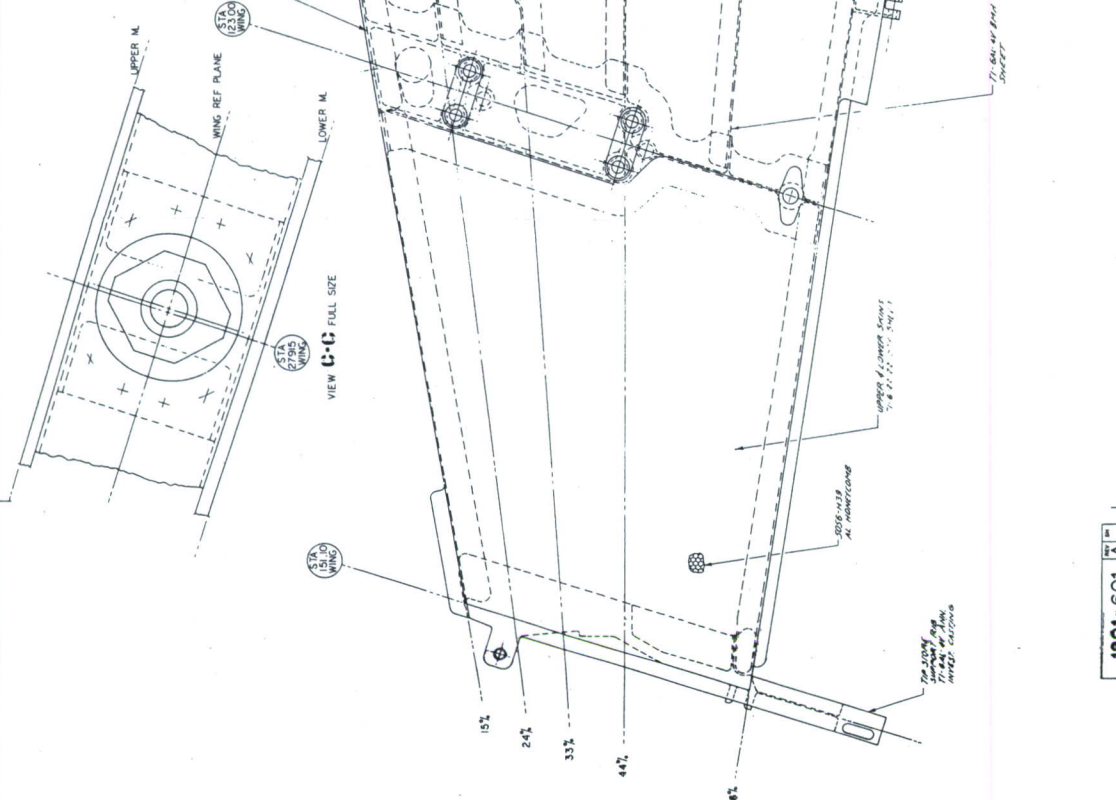
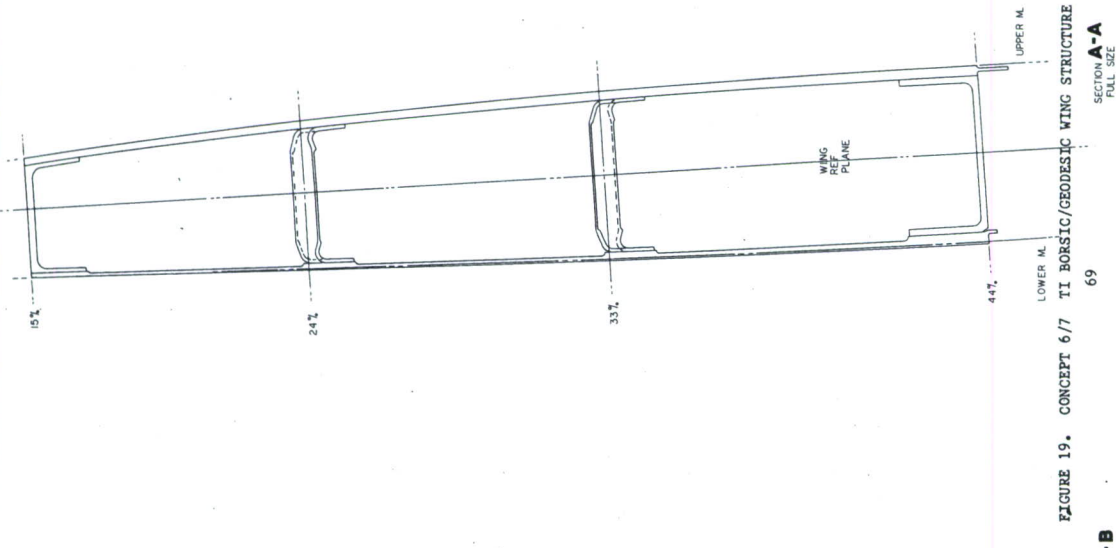
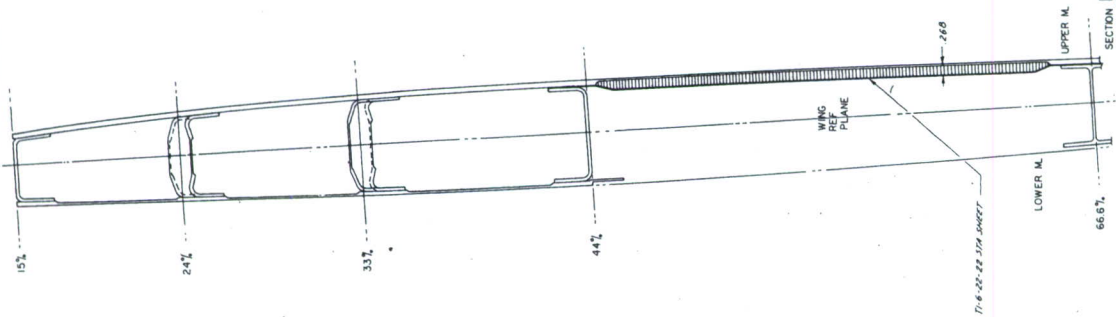
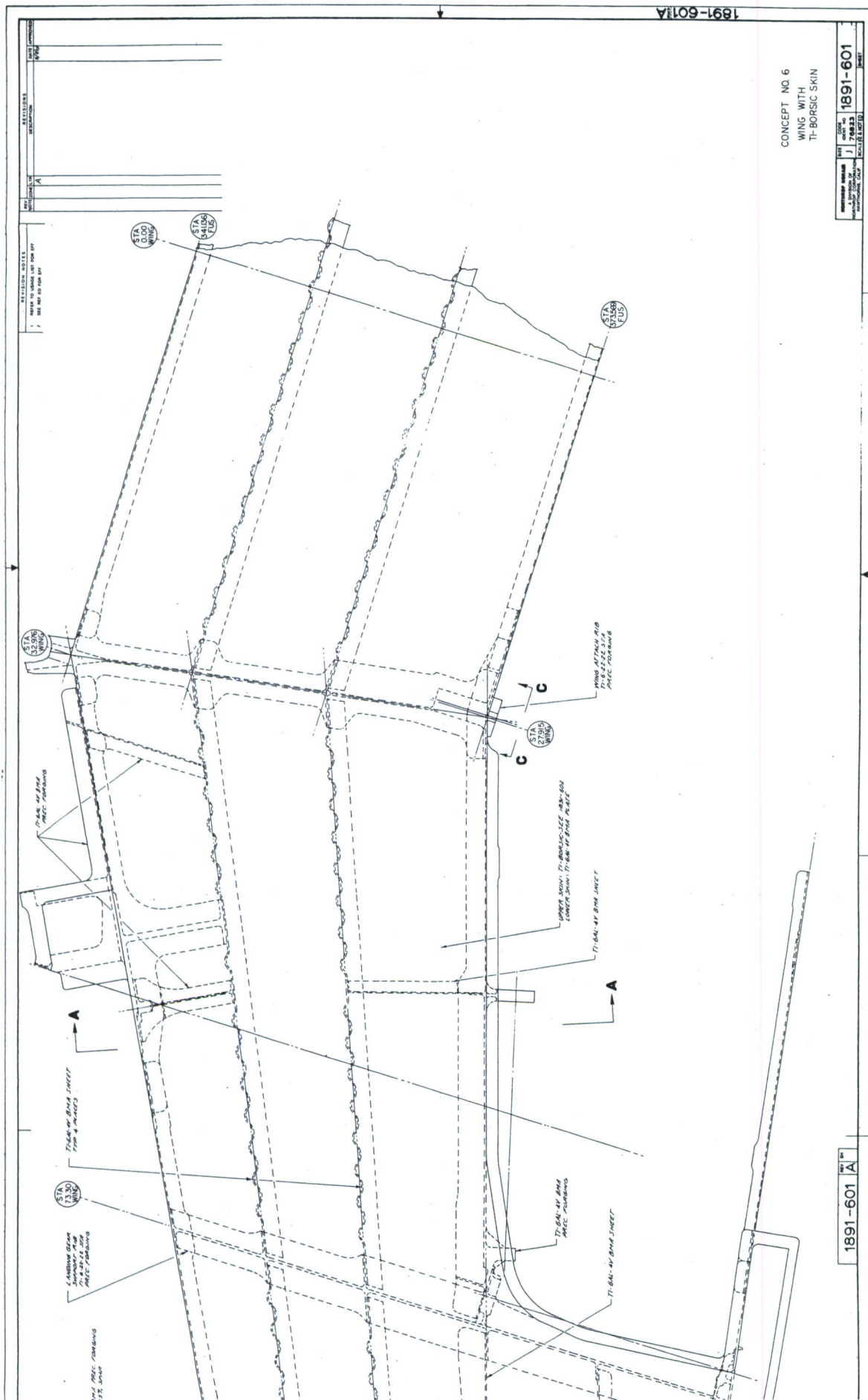


FIGURE 19. CONCEPT 6/7 TI BORSIC/GEODESIC WING STRUCTURE







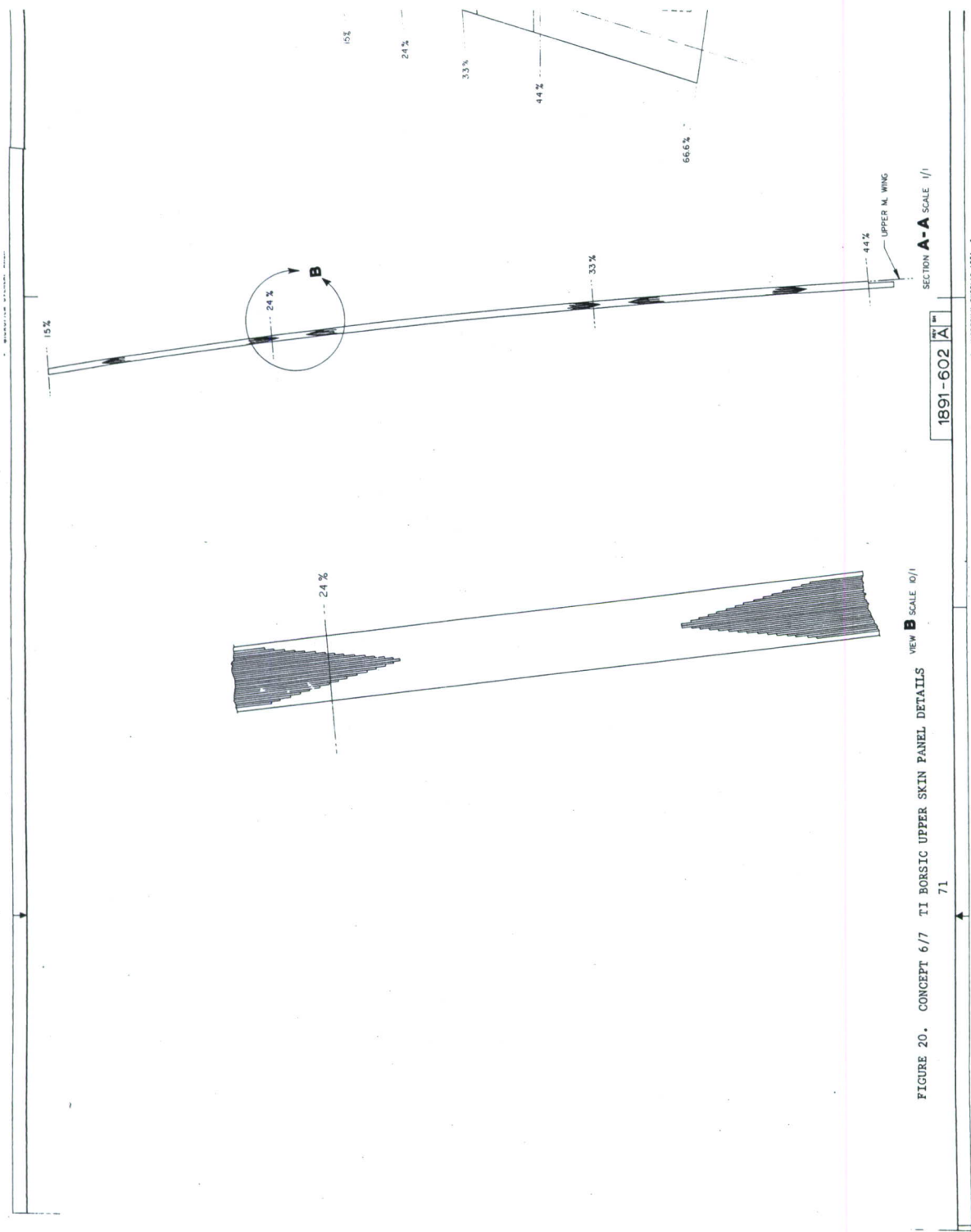
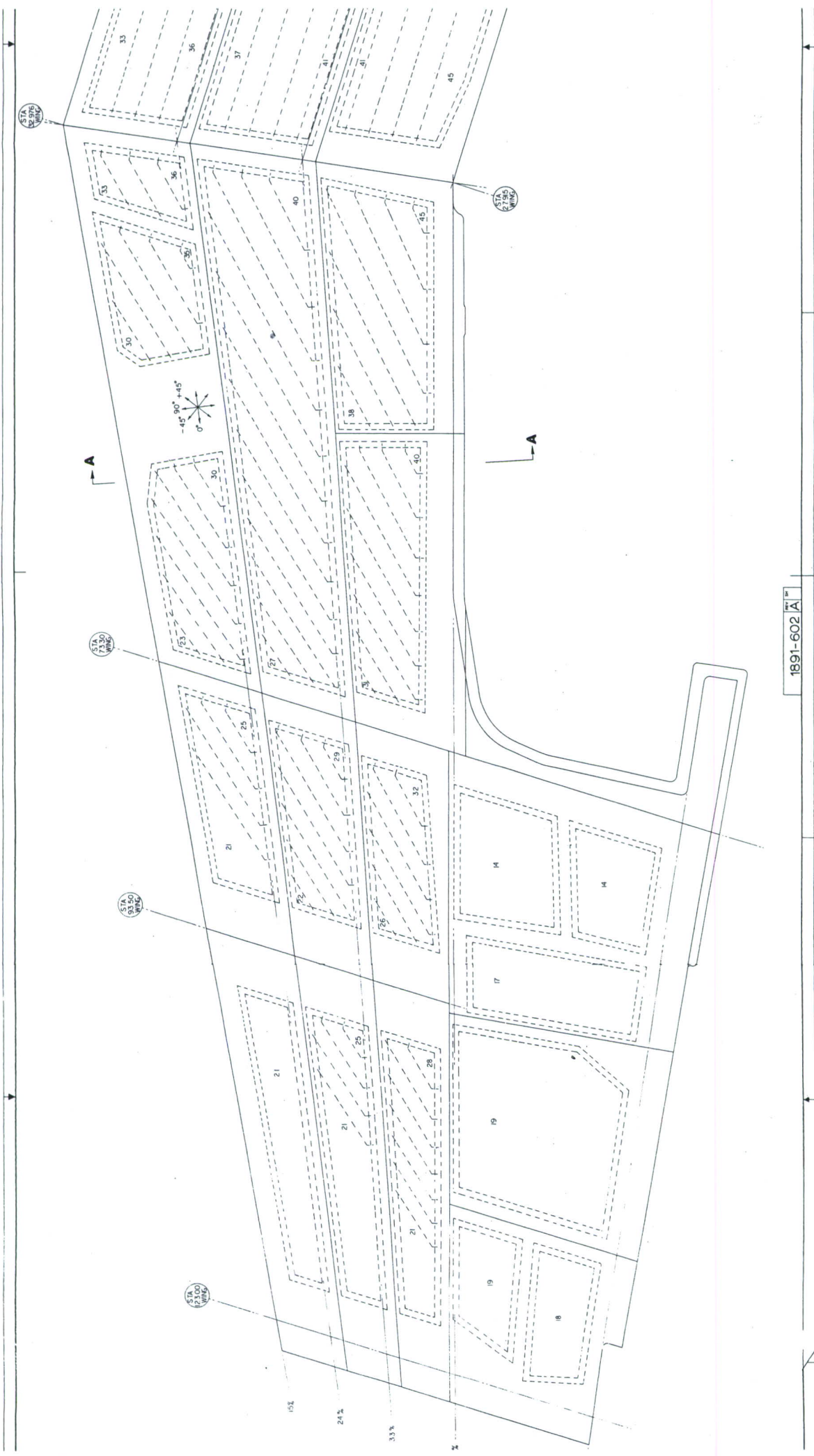
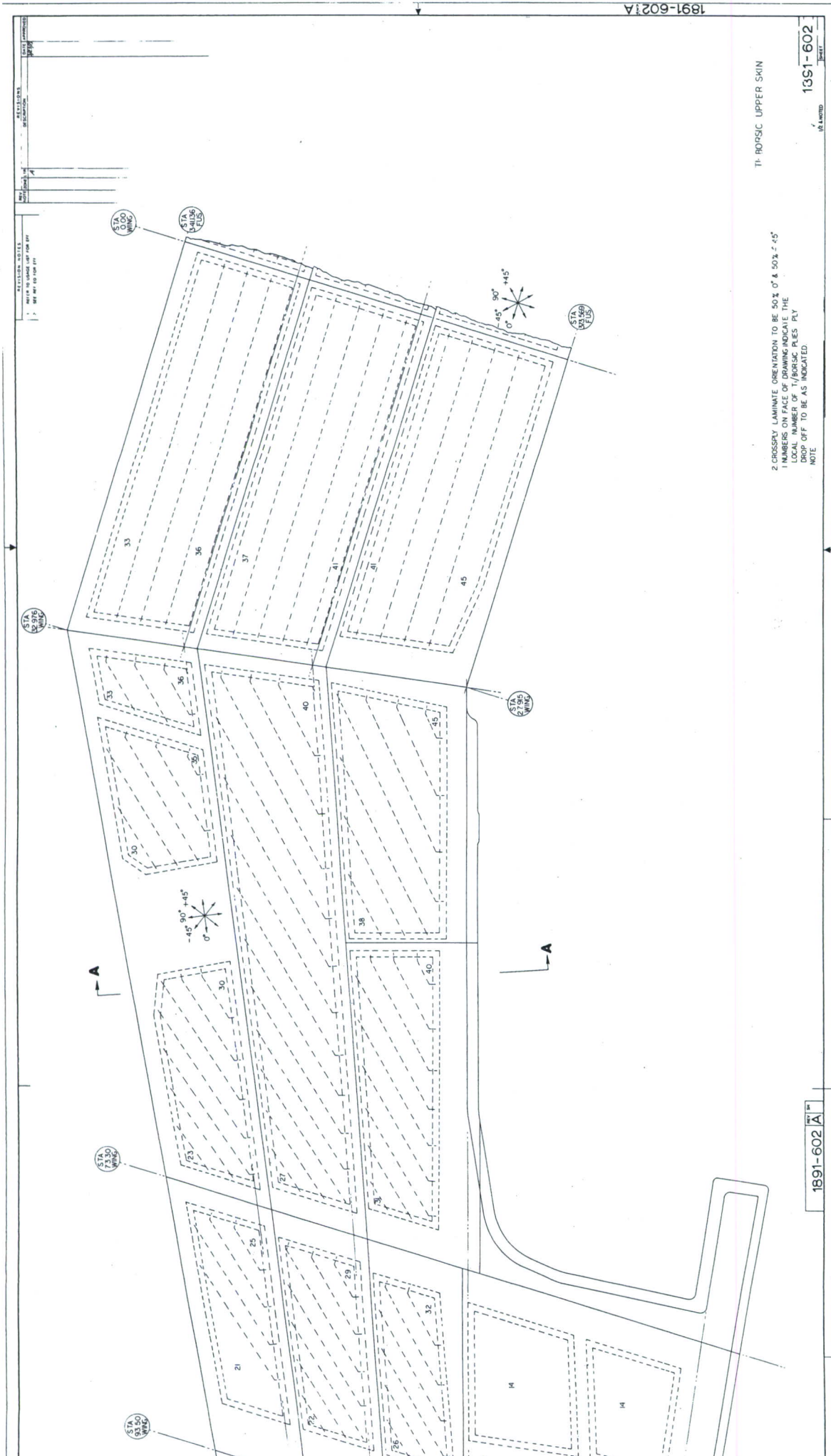


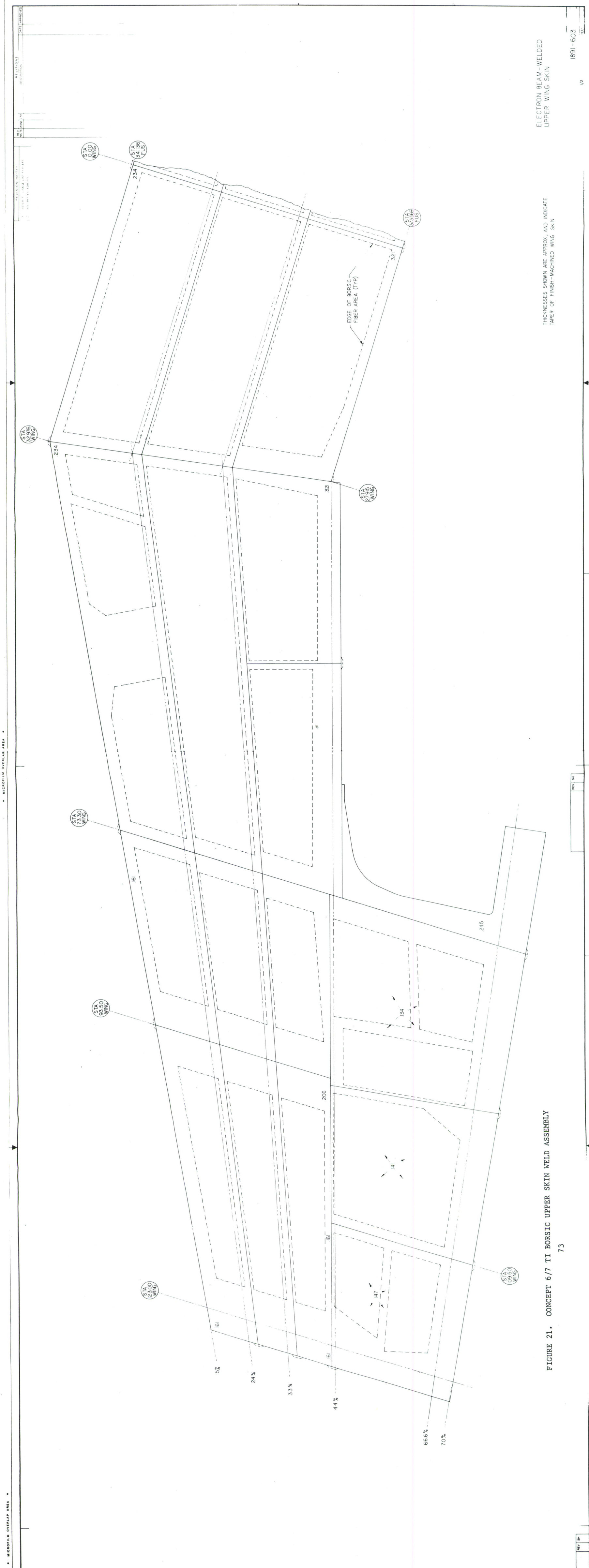
FIGURE 20. CONCEPT 6/7 TI BORSIC UPPER SKIN PANEL DETAILS

2









THICKNESSES SHOWN ARE APPROX. AND INDICATE  
TAPER OF FINISH-MACHINED WING SKIN

ELECTRON BEAM-WELDED  
UPPER WING SKIN

FIGURE 21. CONCEPT 6/7 TI BORSIC UPPER SKIN WELD ASSEMBLY

This assembly is then pressure diffusion bonded together. These panel assemblies will then be machine tapered, the inner panel cover being thick enough to allow machining, have their edges trimmed to size and electron beam welded into a complete wing skin.

The four-spar substructure was selected for this skin as it was felt that the skin's high cost would make a six-spar wing design too costly. It was also felt that the great stiffness possessed by this material would provide sufficiently stable wing skin panels at this reduced spar spacing. This substructure is shown in Figure 19.

Unfortunately, with the fiber orientation required to provide adequate shear stiffness and bending stiffness (i.e.,  $50^\circ$   $0^\circ$ ,  $-50^\circ \pm 45^\circ$ ) so lowers the allowable operating stress of the completed wing skin that a weight penalty was incurred. It is possible to negate this penalty by adding spars, but as an estimated cost of this skin panel exceeded the cost of the least expensive of the proposed wing concepts, further study of this skin concept was halted.

It may be of interest to note that at the beginning of the program, both Ti-Borsic and Aluminum-Borsic composites were considered. While the data available on this latter composite was more extensive, crack growth and fatigue behavior of the material was still insufficient. This lack of data required the same interrupted panel configuration to be employed as in the Ti-Borsic design. The Aluminum-Borsic matrix of 6061 aluminum alloy, however, has such low mechanical properties that the quantity of matrix material required to resist the high chordwise bending moments at the landing gear rib was prohibitive and it was no longer considered a viable material candidate.

## (2) Geodesic Lower Skin (Figure 22)

Faced with severe compressive stability problems when employing high strength materials for wing skin, a completely different approach to wing skin design was explored. An open geodesic truss work was used in place of the plain machine tapered skins heretofore considered. The configuration shown was achieved by removing approximately 50% of the chordwise area of a plain skin, via the triangular cutouts shown, and this area then was added to the remaining truss members proportionally to maintain the same



wing bending material distribution. The resulting truss skin was roughly twice the thickness at any given point, and the same weight of the plain skin it replaced. This truss was then covered by a minimum gage cover skin adhesively bonded in place, its thickness being sufficient only to preclude buckling of the unsupported triangular panels at limit load.

The advantages foreseen for this method of construction were twofold. First, increased wing stiffness, by virtue of its increased thickness, allows the use of fewer interior spars. Its second advantage is that it provides both the practical maximum number of discrete and independent failsafe members possible, with no increase in flaw initiation sites (i.e., fastener holes), and crack arrest capability with respect to the cover skins. It was assumed that since a single failed member represents so small a portion of the gross wing skin area, and even when failed it was completely framed by the remaining truss members, the resulting stress increases, both locally and overall, would be minimized.

At this point, a finite element analysis program was initiated to determine the specific behavior of this skin concept. The detailed account of this program is found in subsection III.2.f of this report.

The program results were somewhat mixed. The presumed fail-safe behavior of this concept was indeed a fact. Additionally, the load redistribution area was not localized around the failed member but diffuse in nature and the stress increases resulting from member failure are held to reasonable levels.

Unfortunately, the underlying cause for this favorable load redistribution is this concept's innate lack of extensional stiffness. To overcome this, the cover skins were increased in thickness and now represent 20% of the wing skin cross sectional area. This reduces the geodesic core height, and when skin weight is held constant, compressive stability problems are encountered. When additional material is added to regain this stiffness, a weight penalty is incurred. As with the previously discussed Ti-Borsic skin, the marrying of this wing skin to a six spar wing would reduce this weight penalty, but increase the total wing structure cost.



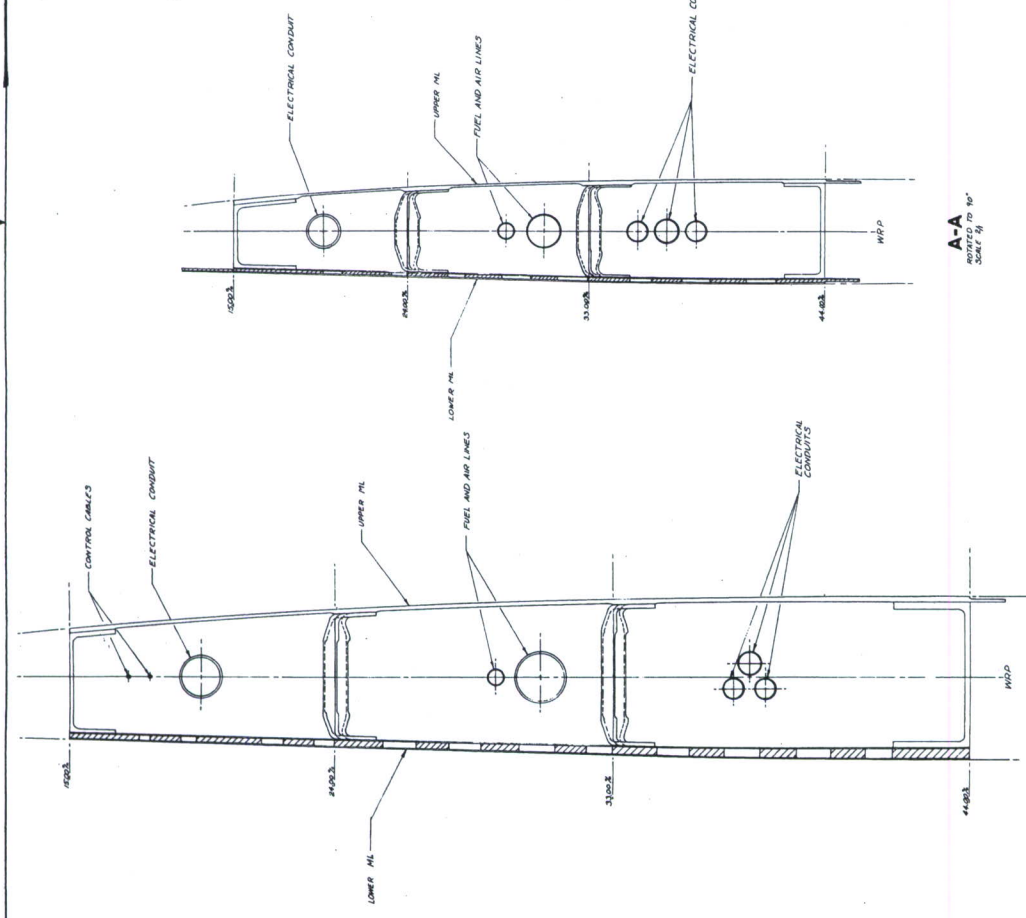
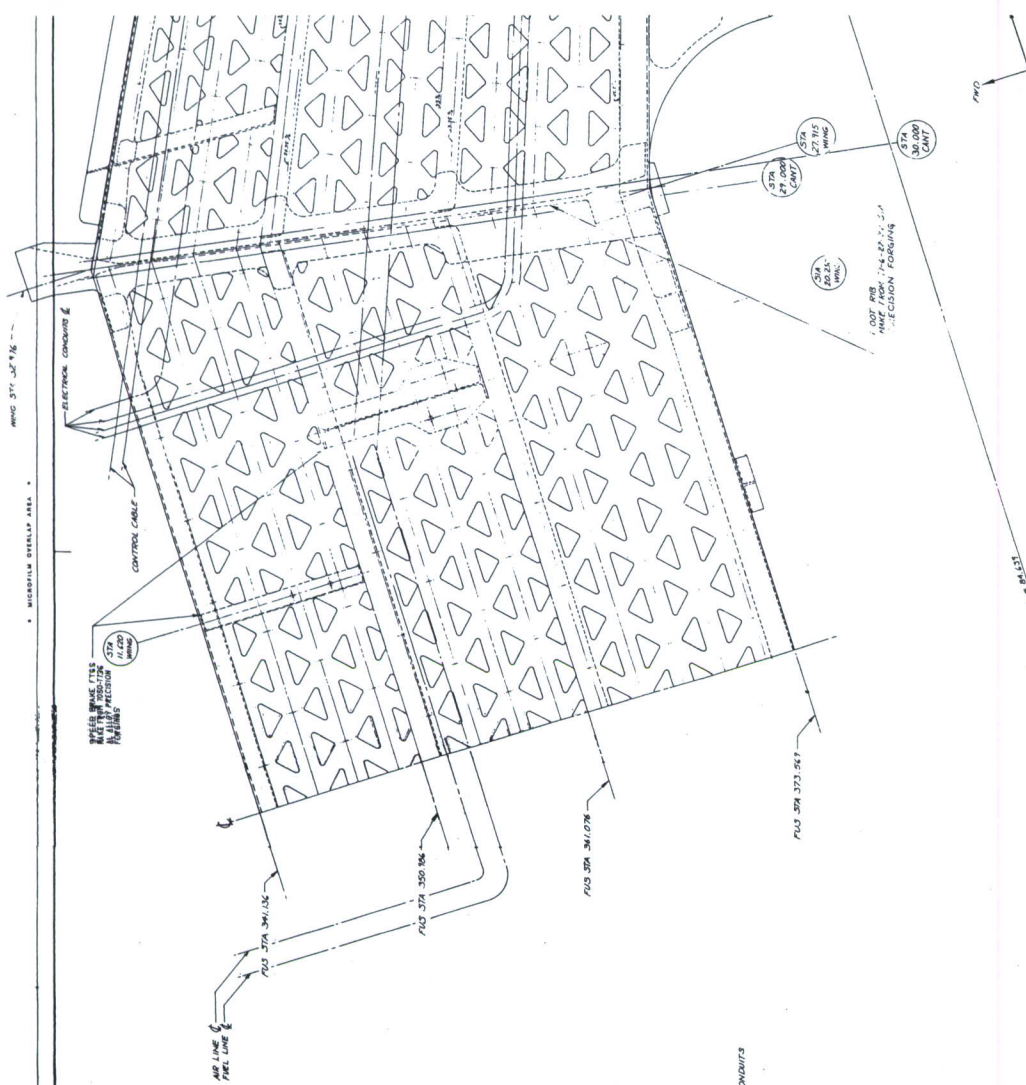


FIGURE 22. CONCEPT 6/7 GEODESIC LOWER SKIN









Figure 22 depicts the results of applying a geodesic pattern to a tapering wing planform with a four spar substructure. It will be noted that there are two distinct tapering triangular hole patterns employed. It is impossible to stay with one tapering pattern for the entire semi-span as the hole size in the outboard regions is reduced to below practicable manufacturing limits and the greater percentage of remaining material composed of fillets does not allow the removal of 50% of the chordwise area. The second hole pattern is started just outboard of the gear rib to minimize any weight penalties incurred from the misalignment of the spanwise elements of the skin.

The wing structure aft of the 44% spar with the exception of the wing skins outboard of Wing Station 73.3 is similar to the baseline wing.

The skin is constructed of 0.040 inch Ti-6Al-4V  $\beta$ MA sheet laminations NOR-Ti-Bonded together with adhesively bonded cover skins of the same material. The geodesic pattern ceases outboard of the inboard pylon rib. Both the diffusion bonding and brazing of the cover skins to the geodesic core was contemplated, but as no conclusive data exists on the crack arrest or retardation behavior of these joints, the adhesive bonding method was selected as the most reliable method of obtaining definite crack arrest behavior in the cover skins. Consistent with the above position, the laminated geodesic core was considered as monolithic plate in the crack growth analysis.

This wing skin, in preliminary cost analysis, cost in the neighborhood of \$30,000. This and its previously mentioned weight penalty and lack of extensional stiffness seriously prejudice this design. Conversely, because of its exemplary fail safe behavior, it was agreed upon that this design would not be abandoned without assessing its effect when included in a complete wing concept.

The first problem encountered when including this skin in a complete wing structure was its adverse effect on wing flutter and aileron reversal. To counteract this, the Ti-Borsic upper skin, with its great inherent stiffness, was included in this proposed wing system giving rise to the concept No. 6/7 appellation.

The wing so configured (i.e., Ti-Borsic upper skin, geodesic lower skin, and 4-spar wing substructure as in concept No. 5) is a functionally viable fail safe wing design. While not economically feasible and possessing large risk because of its Ti-Borsic upper skin, it is felt that on a thicker wing that is not as stiffness critical or when metal matrix composite technology advances sufficiently to provide the data now lacking, this geodesic wing skin may prove worthy of serious consideration. In fact, it is possible, given the data now lacking on Ti-Borsic fatigue and crack growth behavior, that Ti-Borsic cover skins could well overcome the lack of extensional stiffness of the geodesic configuration and these skins could be used on both the upper and lower wing surfaces. Advancement in lamination techniques, such as roll bonding could also reduce the cost of the geodesic core to a more realistic figure and result in a cost and weight effective fail-safe wing design. More developmental work needs to be done on this type of structure.

j. Concept No. 8 - Aluminum Precision Forged Substructure 6-Spar Wing  
(Figure 23)

This design is a further refinement of the lowest cost "Quick Look" design. It is similar in planform to the baseline aircraft. It differs in several major aspects, however. The first is the substitution of more advanced aluminum alloys in the various structural elements of the wing. Titanium has been used in place of steel for the landing gear rib and the tip rib. The latter is a Ti-6Al-4V annealed casting; the former being a Ti-6-22-22 STA forging. The second principal difference of this design is the precision forging of all the aluminum substructural elements. As can be seen in the Cost Summary Table (Table XX in Subsection 9) the substructure costs are about halved as a result of this low buy-fly ratio approach. Finally, corrugating the spar webs, the source of a 17-pound weight saving at a minimal increase in die cost, complete the specific variances from the baseline aircraft.

This design again proves to be the most economical of the concepts under investigation, realizing a 25 percent cost reduction. It also achieves an 11 percent weight saving. This concept also poses the least risk of all and is the most amenable to incorporation of its precepts into production design.









k. Concept 8A - Integral Web 6 Spar Aluminum Wing

This design bears roughly the same relationship to Concept No. 8 as Concept No. 3A does to No. 3, with the exception of a mechanically fastened lower skin in lieu of welding. This is due primarily to the mechanical properties of available weldable aluminum alloys being so low as to prohibit their use in this design.

The spars are attached to the lower skin through lap splices to stub webs machined integrally with the lower skin. This necessitates a switch from the 7475-T7651 alloy plate to X2048-T851 plate as the former is only available in thicknesses of less than one inch. This results in a lower skin with somewhat reduced mechanical properties.

The fit-up problems associated with lap splicing separate ribs and spars with integral-to-the-skin stub webs was deemed excessive and so the ribs remained as in the baseline. This requires a transition from an angle cross-section of the spars to the original channel configuration just prior to the rib spar juncture. Therefore, it becomes impossible to eliminate the lower skin to rib attach fasteners.

The cost of this concept is higher than Concept No. 8 by virtue of the tripled cost of the lower wing skin raw stock and increased assembly cost. The reduced lower skin allowables and the inability to eliminate all the lower mold line fasteners combine to produce a wing only 0.1 percent lighter and 3 percent more expensive than Concept No. 8 with no greater state-of-the-art advancement and no real increase in either safe life or damage tolerance. For these reasons investigation of this concept was halted short of the completed layout stage.

l. Conclusions and Recommendations

It is not surprising that all the design concepts which consist mostly of titanium are the most expensive. These concepts (i.e., 3, 1, 3A, 5, 4, and 6/7 in ascending order of cost) all cost more than 130 dollars per pound. The design concepts which are largely constructed from aluminum, on the other hand, all cost less than 91 dollars per pound.



While this divergence may be traced directly to the high material cost of titanium, it is significant to note that the greatest cost differentials from the baseline are produced by the titanium wing skins. These skins also represent the one area where the material buy-fly ratio is essentially unchanged from the baseline and is the underlying cause of these large cost differentials. Both current and anticipated titanium technology offers no relief in this area. If the skin raw stock could be roll tapered, for example, the material purchased could be reduced by 5 percent and 22 percent on the upper and lower skins respectively. From these figures it is obvious that even rudimentary presizing of titanium mill products will result in appreciable savings to the airframe manufacturer in both material cost and machining time. It is felt that the acquisition of the technology necessary to produce roll tapered titanium sheet and plate by the manufacturers of titanium mill products is of primary importance to the economic production of titanium wing structures. More work needs to be done in this area.

Proof of the economies available, when finished titanium products can be procured, is evident in the spar and rib columns of the cost summary Table of Section III.9. All the titanium spars and ribs, where practicable, are precision forged or investment cast parts that are approximately 80 percent complete as received from the vendor and the cost differentials to the equivalent baseline structure are relatively modest as compared to the wing skin costs which show titanium skins to range from 2.5 to 5 times the price of an equivalent aluminum skin.

In this program it was possible to show significant economies by substituting titanium castings and precision forgings for steel parts. It was also true that the substitution of a cast or precision forged part for a hogout of the same alloy was similarly beneficial. The titanium casting and forging technology is in its infancy when compared to aluminum and steel, for example, and it is felt that continued research and development effort in these spheres of activity will produce greater economies than comparative levels of effort in the more established technologies of steel and aluminum.

Inherent in all the designs under discussion is a substantially greater initial investment in tooling. To fully realize the economies presented in these design concepts, the quantity of units produced without revision to the specific structural items responsible for this high initial tooling



investment must remain as close to the initial quantity assumptions as possible. This is a much easier task in wing structure than in fuselage structure, but adequate growth assumptions must be made in the initial design stage to assure, as much as possible, that the majority of initial production hardware remaining unchanged for, in this specific instance, 300 units. It might well prove more advantageous to treat these aircraft modifications in a manner similar to the commercial aircraft industry's approach to so-called customer variables. These are all designed as options to be added to a basic aircraft. When handled in this manner, it is also possible, if desired, to retrofit existing fleets.

The use of Ti-Borsic metal matrix composite materials appears to be somewhat premature at this time. Too little is known of the mechanical properties of these materials, particularly in the fatigue and crack propagation areas so that efficient utilization of this class of material is greatly hampered. Also, enough is not known about the manufacturability aspects. While it is possible to use metal matrix composites in cost effective design of unidirectionally loaded simple parts, efficient design of parts subjected to a complex multidirectional load spectrum is more difficult to accomplish with the same degree of confidence given the paucity of existing data on the materials in question.

Conversely, the improvements in structural efficiency possible, when fully able to employ the superior strength and stiffness of these generally lower density materials, would truly advance the "state-of-the-art" with respect to aircraft structures. It is recommended that more developmental work be undertaken in this area.

It is not difficult to successfully employ an advanced high strength material in an area of high load intensity. It is only when attempting to achieve weight savings through the use of high strength materials in moderate load intensity environments does the real problem surface, namely that the specific stiffness of all isotropic metallic materials is relatively constant. On the other hand, one of the composite materials' principal advantage is their higher specific stiffness.

Early in the development of the titanium design concepts in this program, stiffness problems were encountered. It was readily apparent that when titanium was operated at its appropriate design allowable, local instability, wing flutter, and aileron reversal were encountered in varying degrees of severity. Additional material then had to be added back to the wing to regain the needed stiffness, thus reducing the weight savings to be realized.

While it was not possible to fully exploit the increased specific stiffness of the Ti-Borsic composite material for the reasons previously stated, it remains one of the promising structural materials available today. Only when metal matrix composite technology reaches a level of development equal to that of current non-metallic composite technology will the designer be able to take full advantage of its high specific stiffness. In recognition of the metal matrix's ability to withstand higher temperatures than the organic matrices currently in use, and its inherently greater ability to withstand in service abuse, it may eventually have a wider range of application than that of nonmetallic matrix composite material.

## 2. STRESS ANALYSIS

The stress analysis of the wing and carrythrough structure for each preliminary design study was based on the same external loads, fatigue spectrum, geometric constraints, and functional requirements as the baseline F-5E wing plus the additional RFP-specified requirements. The F-5E design is based on the MIL-A-8860 series specifications<sup>(1)</sup>, with applicability, revisions and additional requirements specified by the Air Force. The detailed structural design criteria used are the same as for the F-5E baseline<sup>(2)</sup>. These criteria plus the updated durability, damage tolerance, and fracture mechanics requirements contained in the RFQ Statement of Work<sup>(3)</sup> served as the program structural design criteria during the first five months of the program. At that time the damage tolerance requirements were completely revised and updated to include those contained in references (4) and (5).

This sub-section presents summary discussions of the loads and stress analyses performed during this program in each of the following major subject headings:

- a. External loads
- b. Internal loads
- c. Analysis of the eight selected overall structural concepts (1, 1A, 3, 3A, 4, 5, 8, 8A)
- d. Analysis of the Warren truss spar concept (Concept 2)
- e. Analysis of the Ti-Borsic upper skin concept
- f. Analysis of the geodesic Ti lower skin concept
- g. Analysis of beaded stiffening for Ti panels

---

(1) MIL-A-8860(ASG) through 8870(ASG) dated 18 May 1960.

(2) Northrop Report NOR 69-35B Structural Design Criteria for the F-5E Aircraft, April 1971.

(3) RFQ F33615-72-Q-1891 Attachment 1, "Service Life Requirements."

(4) Proposed MIL-STD-1530 (USAF), dated September 1972.

(5) "USAF Damage Tolerance Requirements," dated 18 August 1972.  
(see Volume II, Appendix II).



The stiffness characteristics of the various designs and any additional structural requirements imposed by flutter and aileron effectiveness considerations are discussed in sub-section III.3. The weights summary and detailed weight breakdowns are presented in sub-section III.10.

a. External Loads

The advanced structural concepts were analyzed to the same external loads as the baseline F-5E structure<sup>(1)</sup> including an allowance for the growth stores in the outboard wing area. This growth capability is provided by including the F-5A/B design loads<sup>(2)</sup> in the F-5E outer wing area. The F-5A/B loads include the effects of growth stores listed in Table II.

The critical F-5E design wing load conditions are described in Table IV. Subsonic maneuvering flight conditions predominate over supersonic conditions due to higher bending moments. In supersonic flight, aeroelastic effects move the wing airload center of pressure inboard, producing less wing bending moment than the subsonic conditions. The "clean" wing maneuvers and landing conditions produce the maximum loads inboard of the landing gear rib. The mid semi-span area is designed by both clean and underwing store maneuvers and by dynamic store ejections. The tip area is designed almost exclusively by dynamic gust, landing and store ejection conditions.

The resulting spanwise shear, moment and torque envelopes are plotted in Figure 24. Included are the "growth loads" in the outboard wing area and also increased wing torque between the root and the landing gear rib induced by wing structural twist and gear deflections during landing conditions. The moment versus torque envelope is shown for the most highly loaded root area in Figure 25 (undeflected gear).

In using these loads for the design of new wing structures concepts, it must be recognized that changes in wing mass and stiffness parameters can affect both the steady state aeroelastic loads and the loads arising from dynamic gust, landing, and store ejections. With respect to the aeroelastic loads, flexural stiffness reductions will decrease the wing angle

---

(1) Northrop Report NOR 71-118, F-5E Structural Design Loads, Feb. 1972.

(2) Northrop Report NOR 62-89, F-5 Structural Design Loads, Vol. I, Sept. 1965.

TABLE IV. SUMMARY AND DESCRIPTION OF CRITICAL F-5E WING LOAD CONDITIONS

CONDITION NUMBER	WEIGHT	C.G.	MACH	ALT.	N <sub>Z</sub>	CONFIGURATION			SPEED BRAKE	FLAP SETTING	REMARKS
						TIP	W.S. 123	W.S. 93.5			
SA10M000	15745	11.2	.80	S.L.	7.34	AIM-9J	---	---	C	0/0	MAX. L.E. FLAP LOAD @ 0° (100% FUEL)
SEP08005	↑	↑	↑	5000	7.33	↑	---	---	C	12/8	MAX. L.E. FLAP LOAD @ 12° (100% FUEL)
SC080024	18758	13.3	.85	24000	5.5	---	---	---	C	24/20	MAX. L.E. FLAP LOAD @ 24° (100% FUEL)
SE108505	18758	13.3	.85	5000	5.0	---	---	---	C	0/0	4 STORES PULL-UP (75% FUEL)
SE108505	17022	11.3	.88	5000	6.5	---	---	---	C	12/8	2 STORES PULL-UP (75% FUEL)
SEH08805	17022	11.3	.88	5000	6.5	---	---	---	C	0/0	2 STORES PULL-UP (75% FUEL)
SEI09008	15745	11.2	.90	8000	7.33	---	---	---	C	12/8	MAX N <sub>Z</sub> @ 100% FUEL AND MACH LIMIT
SEP09200	15745	11.2	.925	S.L.	7.25	---	---	---	C	12/8	SPEED BRAKE OPEN (100% FUEL)
SEA09509	13220	8.2	.95	9000	7.33	RAIL	---	---	C	0/0	FWD C.G. MAX. N <sub>Z</sub> @ MACH LIMIT (50% FUEL)
SEH09509	14800	12.0	.95	9000	6.50	AIM-9J	BLU-27(F)	---	C	12/8	2 STORES PULL-UP @ 25% FUEL
RPA09205	12895	19.7	.92	5000	7.33	RAIL	---	---	0	0/0	ROLLING PULL-OUT, AMMO OUT, AFT C.G.
-RBE09200	15745	11.2	.925	S.L.	-1.0	AIM-9J	---	---	0	0/0	ROLLING MAN. SPEED BRAKE OPEN (100% FUEL)
-SCH08024	15745	11.2	.80	24000	-3.00	AIM-9J	---	---	C	24/20	NEG. L.E. FLAP LOAD - 100% FUEL
-SAB08820	↑	↑	↑	20000	-3.00	↑	---	---	C	0/0	↑
-SEB09206	↑	↑	↑	6000	-3.00	↑	---	---	C	12/8	↑
L4AAA----	15000	1.3Vs	---	S.L.	1.0	RAIL	BLU-27(F)	---	C	0/0	STATIC LOC @ 10 FPS μ .55
TXN----	21818	---	---	S.L.	1.0	AIM-9J	---	MK-84	C	24/20	TAXI CONDITIONS @ MAX. T.O. WEIGHT
G-AAB----	15563	.935	---	S.L.	1.0	AIM-9J	---	---	C	0/0	DYN. CUST - G6000
G-AIA----	17300	.85	---	S.L.	1.0	RAIL	BLU-27(F)	---	C	0/0	DYN. CUST - G1200
G-AIB----	17645	.85	---	S.L.	1.0	AIM-9J	BLU-27(F)	---	C	0/0	DYN. CUST - G6200
G-ALA----	17208	.92	---	S.L.	1.0	RAIL	CHU-24	---	C	0/0	DYN. CUST - G1900
G-ALB----	17553	.85	---	S.L.	1.0	AIM-9J	CHU-24	---	C	0/0	DYN. CUST - G6900
E3ALB----	17553	---	---	---	2.0	AIM-9J	CHU-24	---	C	0/0	EJECT OUTR'D STORE 6E900
E3ALA----	17208	---	---	---	2.0	RAIL	CHU-24	---	C	0/0	EJECT OUTR'D STORE 1E900
E3LLA----	19092	---	---	---	2.0	RAIL	CHU-24	---	C	0/0	EJECT OUTR'D STORE 1E990
E3LLR----	19467	---	---	---	2.0	AIM-9J	CHU-24	---	C	0/0	EJECT OUTR'D STORE 6E990
E3ALA----	17300	---	---	---	1.5	RAIL	BLU-27(F)	---	C	0/0	EJECT OUTR'D STORE 1E200
E4LLB----	19467	---	---	---	2.0	AIM-9J	CHU-24	---	C	0/0	EJECT INB'D AND OUTB'D STORE 6E9E90
E711B----	20701	---	---	---	1.5	AIM-9J	BLU-27(F)	---	C	0/0	EJECT FUS. AND WING STORES 16222
E711B----	20476	---	---	---	1.5	AIM-9J	CHU-24	---	C	0/0	EJECT FUS. AND WING STORES 16999
L211B----	21589	.265	---	S.L.	1.0	AIM-9J	BLU-27(F)	MK-84	C	24/20	DYN. LDG. @ 6 FPS NL6228
L211B----	21405	.265	---	S.L.	1.0	AIM-9J	CHU-24	MK-84	C	24/20	DYN. LDG. @ 6 FPS NL6998
L1AAB----	15000	.221	---	S.L.	1.0	AIM-9J	CHU-24	---	C	24/20	DYN. LDG. @ 10 FPS NL6000



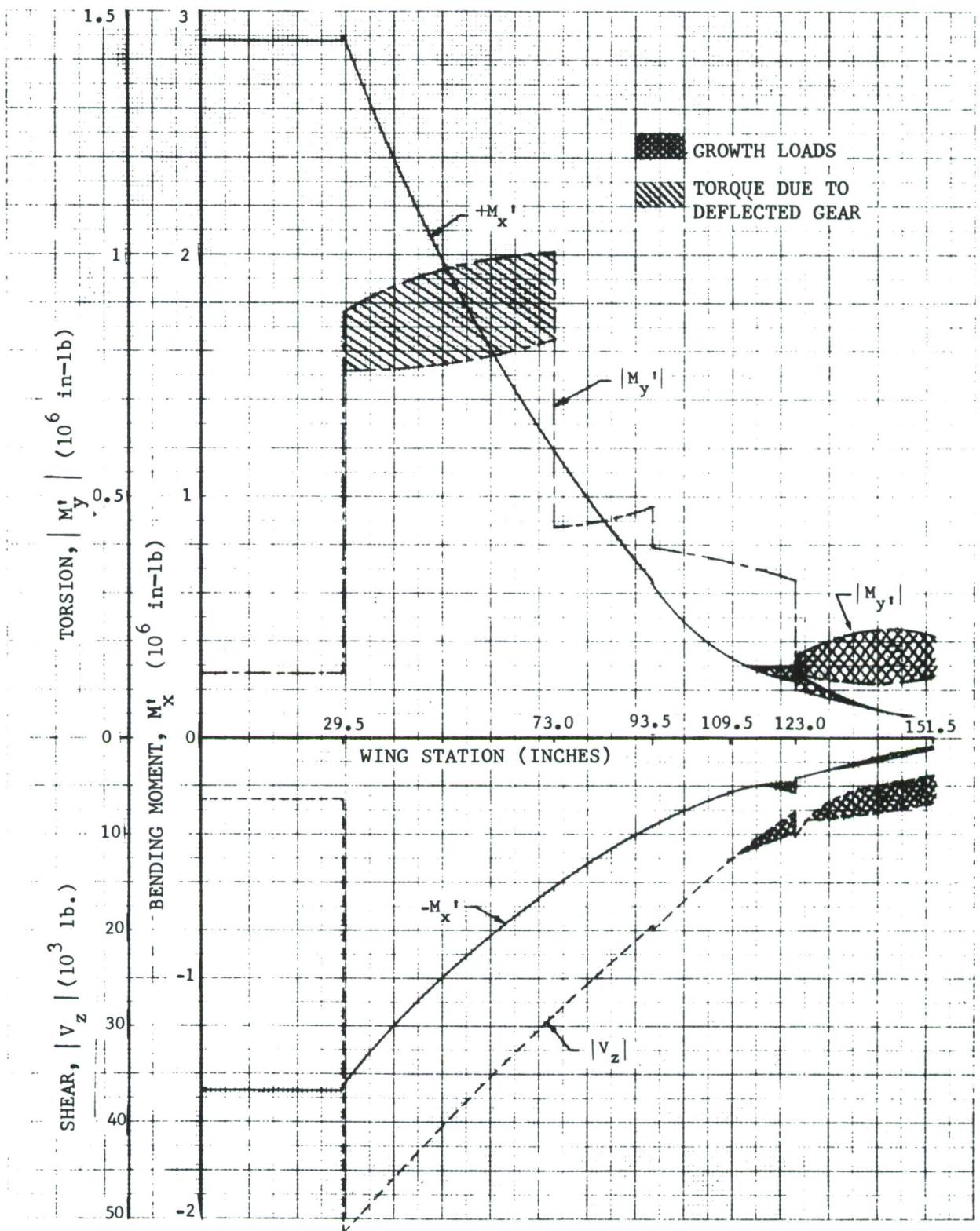


FIGURE 24. F-5E ULTIMATE DESIGN SHEAR MOMENT AND TORQUE ENVELOPES



WING LOAD AXIS AT 35 PC. CHORD

WING STA. 29.5 35 PCT. CHORD

BENDING (MX) VS TORSION (MY) SHEET

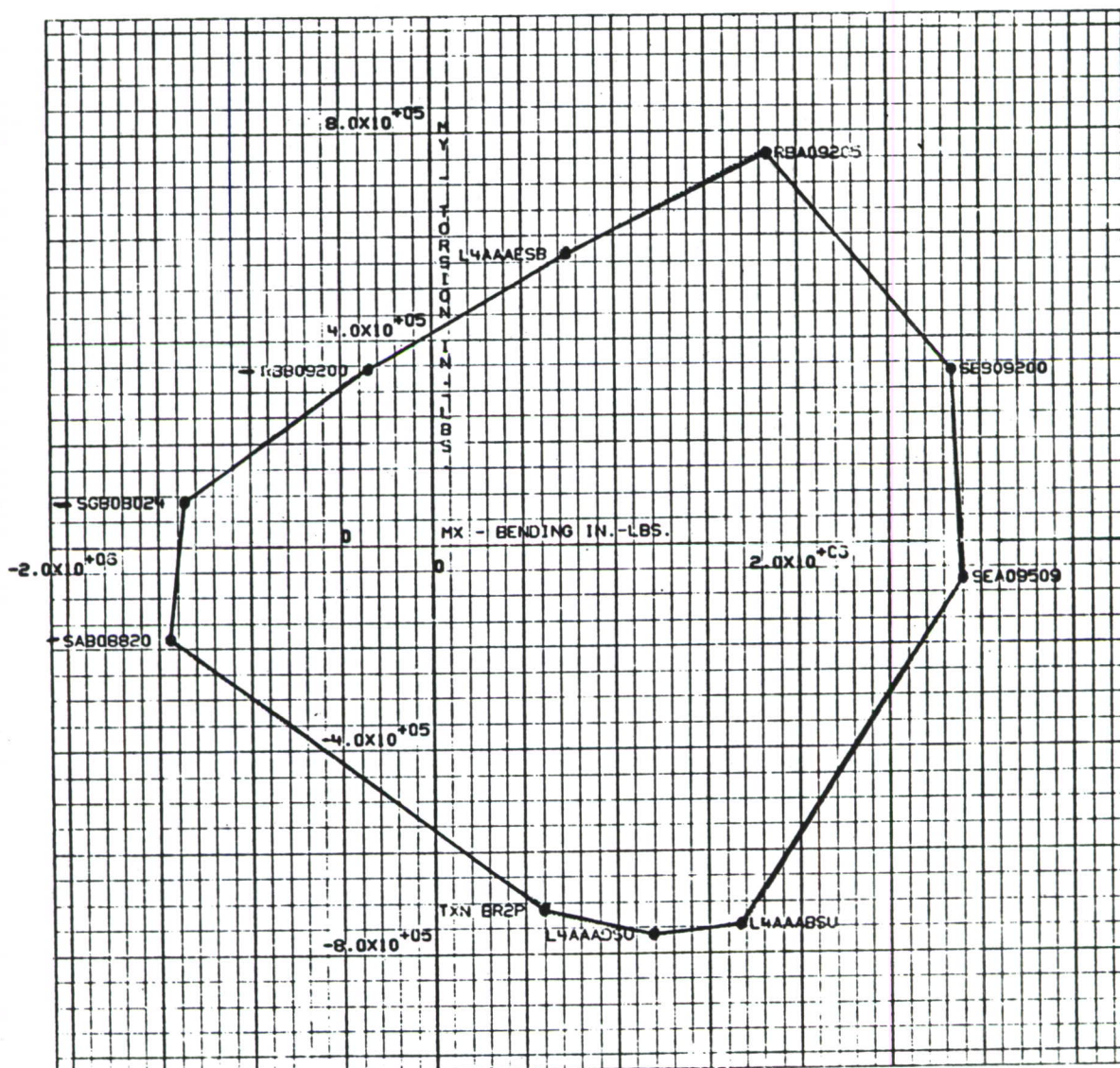


FIGURE 25. ULTIMATE WING LOAD ENVELOPE

of attack due to the swept configuration of the wing. This would cause a generally inboard shift of the wing c.p. and also increase the aerodynamic lift on the fuselage. The net tendency would be to decrease the wing shear, moments and torques. It is somewhat conservative, therefore, to use the present F-5E wing loads in the preliminary design of the advanced concepts.

It must be pointed out, however, that wing load changes may also affect the horizontal tail loads. The inboard c.p. shifts and the transfer of load to the fuselage (as described above) also has the net effect of shifting the c.p. forward. This has the tendency to increase the checked-manuever loads on the tail.

With respect to the dynamic loads, no clear cut conclusions can be made. Changes in wing stiffness characteristics can significantly affect the magnitude of these loads and nothing short of a full dynamic loads analysis for each suspected critical store configuration can predict these changes for any one wing design. However, certain situations do exist in the overall dynamics loads picture, which indicate that the risk of exceeding the present F-5E dynamic loads is less than might normally be expected. First, a review of the measured ejection and landing loads obtained during the F-5A/B flight test program showed comfortable margins relative to the analytically predicted values. This is attributed to the fact that aerodynamic damping was conservatively omitted from the analytical ejection and landing loads model and also due to the fact that store ejection forces were less than expected. As a result there is some margin available in the present loads envelopes to provide for some increases in actual dynamic landing and ejection loads should they occur.

Insofar as gust loads are concerned, however, no comparative flight test data exists. For the F-5E, gust loads are critical largely in the area outboard of W.S. 123. However, it is in this area that the "growth" loads (F-5A/B ejection conditions) exceed the E loads, so, again, some margin is available even for gust load increases. As a result of these observations, the present F-5E analytical loads plus the F-5A/B "growth" loads in the outer wing area were used "as is" for the purposes of this advanced structural design study.



## b. Internal Loads

The internal wing loads from the baseline F-5E project<sup>(1)</sup> served as the basis for the internal loads on this program. These loads include the spanwise and chordwise distributions of wing flexural loads and shear flows for each structural element for each load condition listed in Table IV. Also included are the chordwise distribution of wing rib shears and moments. An overview summary of these basic design loads is presented in Figures 26, 27, and 28. The first two illustrate the spanwise and chordwise variation of the wing cover loading in the more highly loaded inboard areas of the upper and lower surfaces, respectively. The third figure shows the maximum shear flows in the spar structure of the baseline 6-spar configuration. Also shown are the maximum wing-to-fuselage trunnion reactions and a tabular presentation of the maximum shears and moments in each principal wing rib.

It should be noted that the maximum bending moment in the landing gear rib is 917,000 in-lb. This is 76 percent of the maximum spanwise wing bending moment at this station (see Figure 24). These two requirements (i.e., a high spanwise load for maneuver conditions and a similarly high chordwise load for the critical landing condition) consistently posed one of the most severe design problems during this program. This situation is unique to thin wings with wing-mounted landing gears such as the F-5E.

In addition, a NASTRAN finite element model of the F-5E wing was run for the most critical root bending condition. The purpose of this NASTRAN run was to compare the internal loads from a relatively coarse preliminary design model (suitable in both this program and to the preliminary design phase of the follow-on 1B program) with the F-5E production design stresses for the same condition. The planform of this model is shown in Figure 29. It consisted of 283 nodes, 442 plates, and 534 bars. A comparison of skin stresses at the root is shown in Figure 30. Agreement with the F-5E design loads is good--only relatively minor differences are apparent. The model grid is, therefore, sufficiently fine for the advanced concepts to be compared on an equitable basis with the production F-5E design.

---

(1) Northrop Report NOR 71-172, F-5E Wing Internal Loads, Vol. II, May 1972.



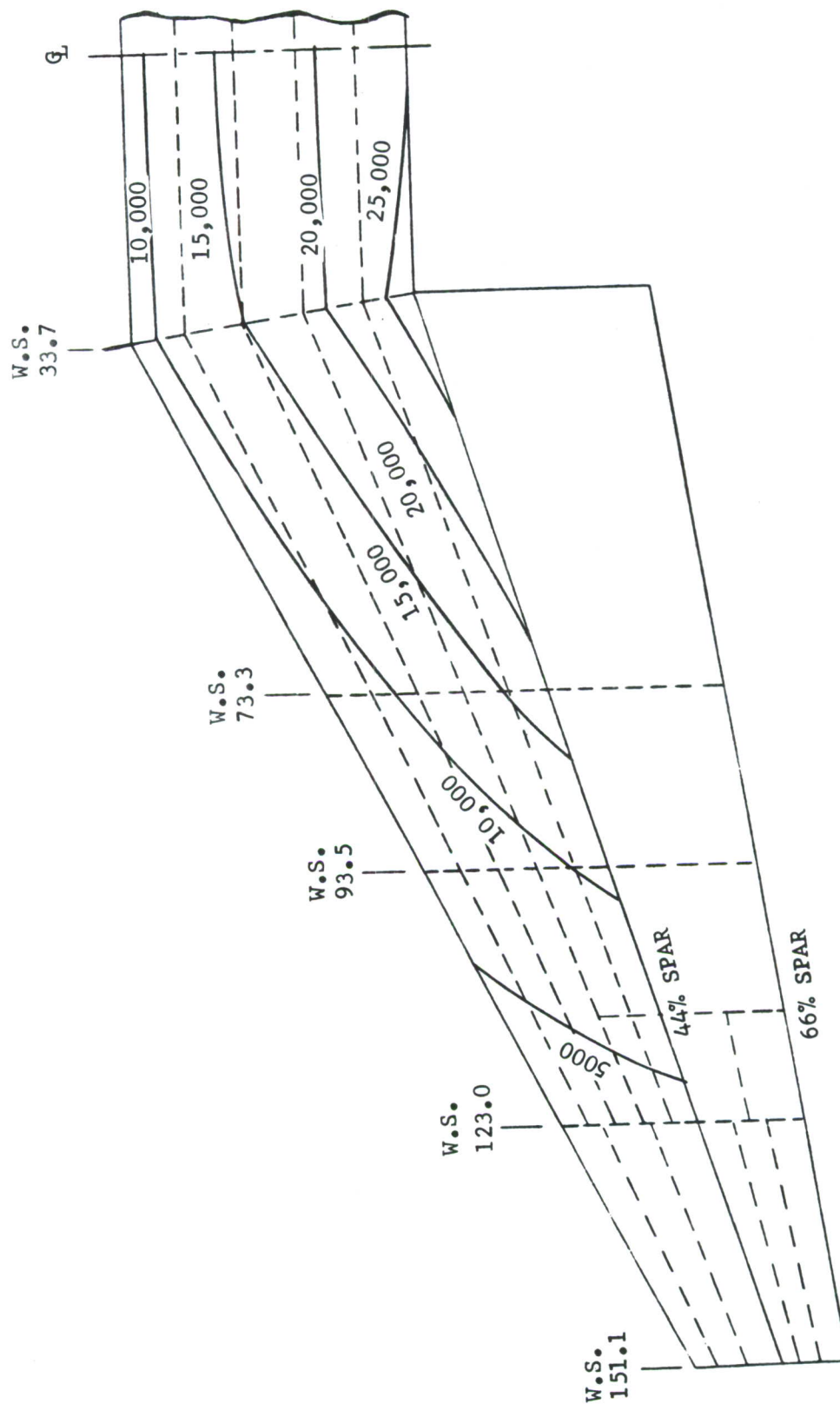


FIGURE 26. UPPER SURFACE MAXIMUM SPANWISE LOAD INTENSITY (LB/IN ULT)

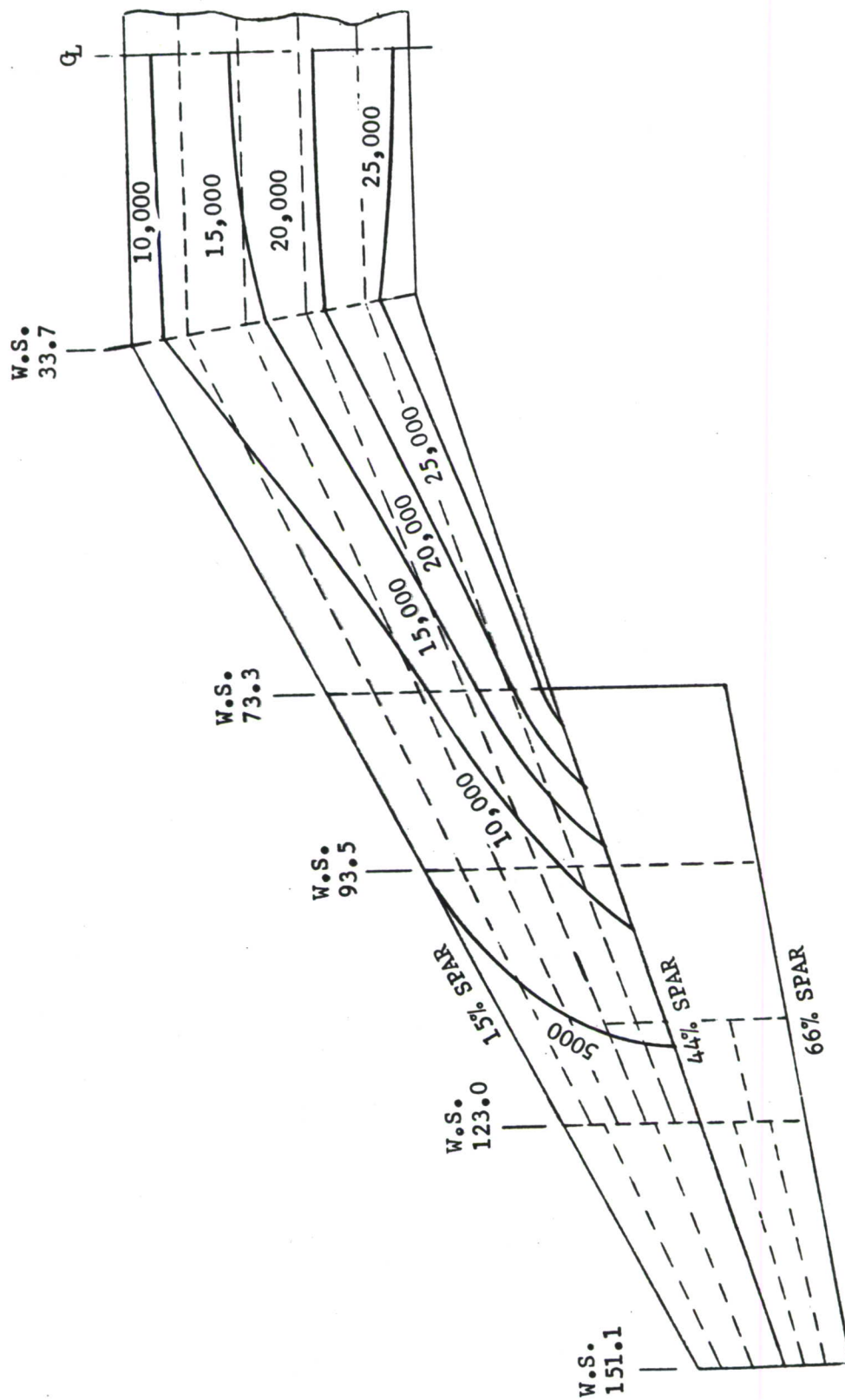


FIGURE 27. LOWER SURFACE MAXIMUM SPANWISE LOAD INTENSITY (LB/IN ULT)





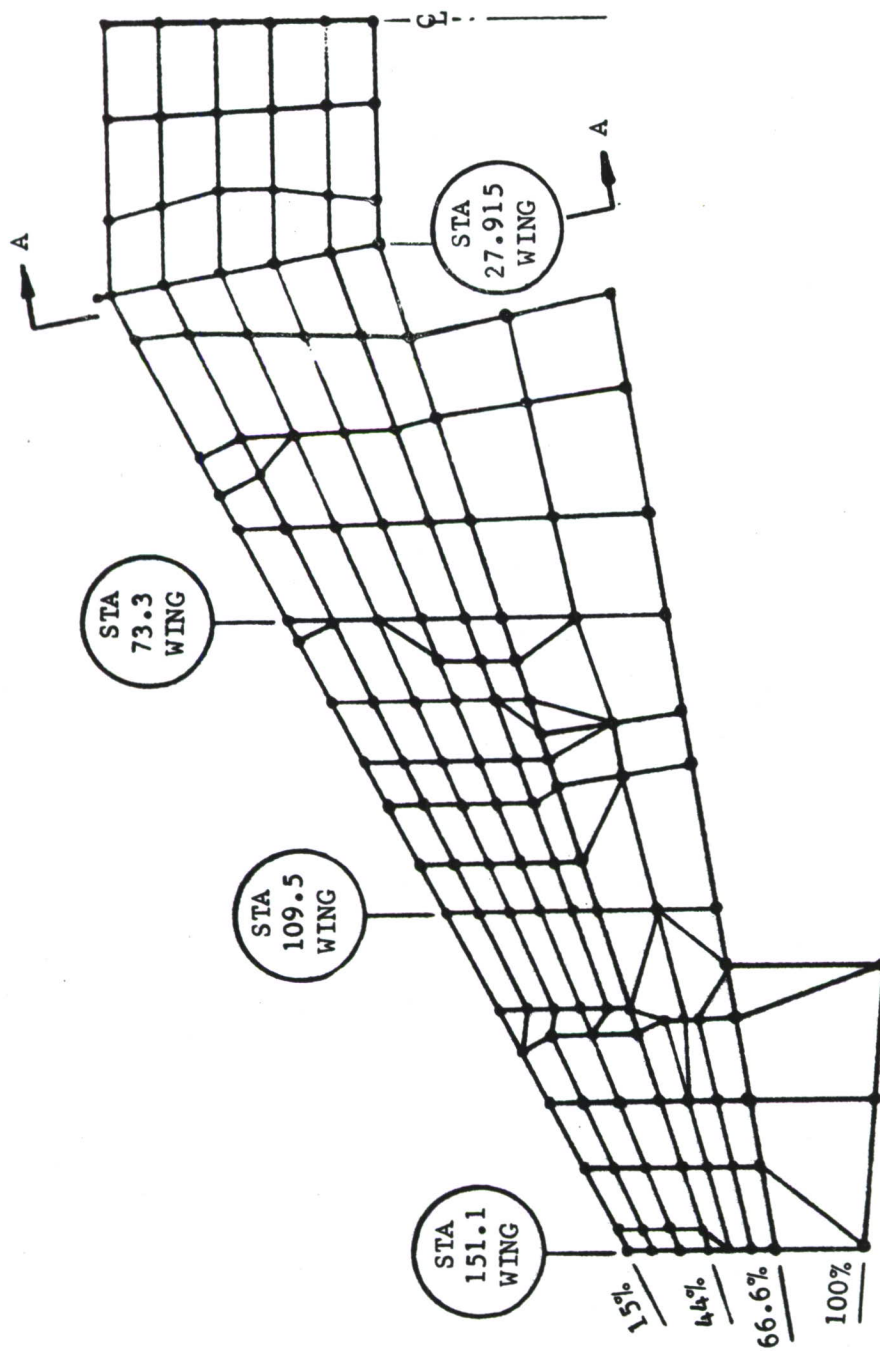


FIGURE 29. WING FINITE ELEMENT GRID

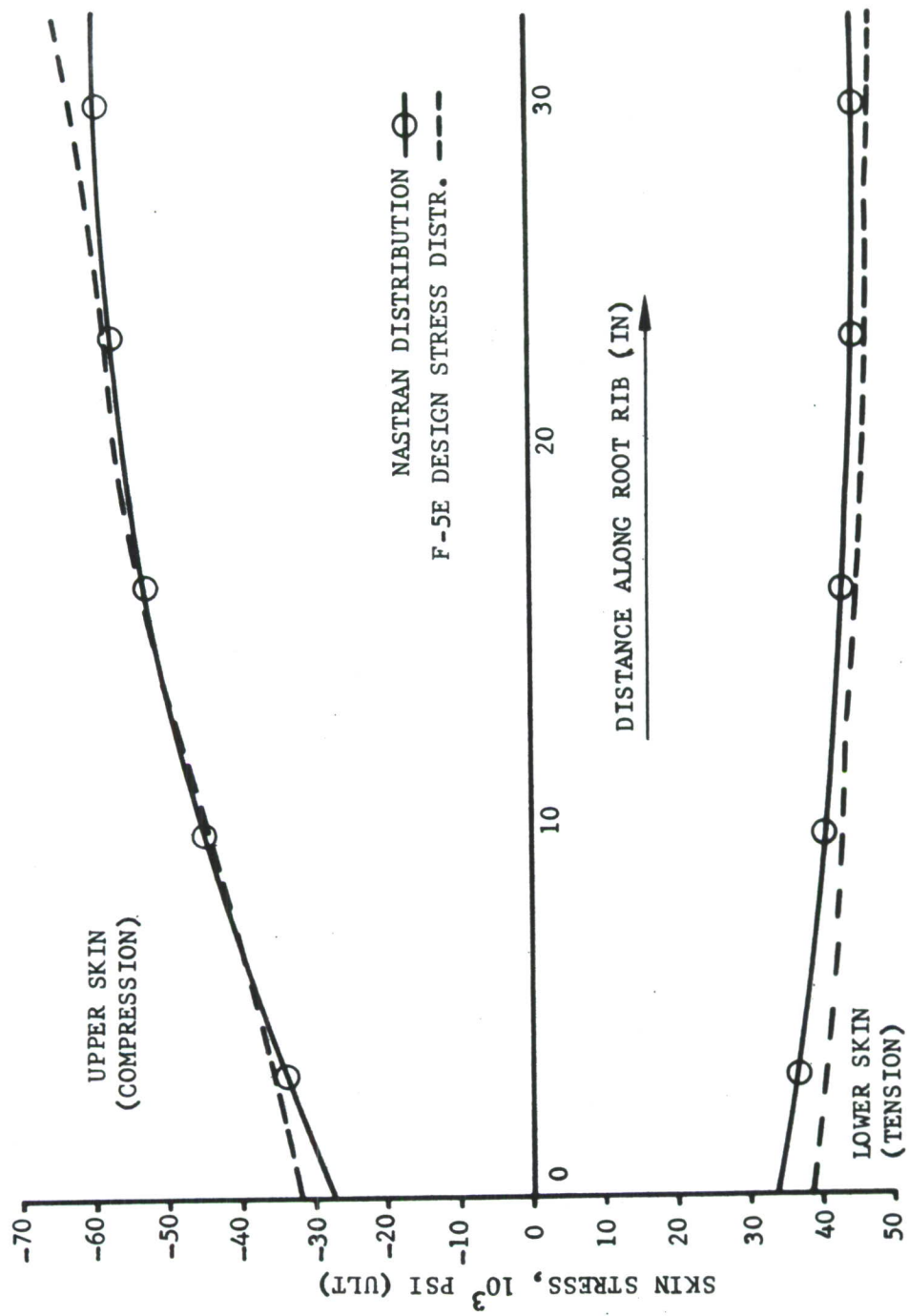


FIGURE 30. SKIN STRESSES AT ROOT RIB (SECTION A-A)

Adjustments were made to the F-5E design loads as dictated by the differing structural arrangements and details of each advanced concept. Predominant among these were:

- Spanwise axial loads from wing bending were re-distributed among wing skins, skin lands, and spar flanges as the relative proportion of these areas varied from concept to concept.
- Shear loads in the interior spars were adjusted as the number and stiffness of interior spars (or honeycomb core) varied from concept to concept. Shear loads in the peripheral spars (i.e., the boundary members of the main torque box) were found to be relatively insensitive to interior spar variations.

Most of the above load adjustments were minor enough to be accomplished manually by desk calculator. However, large computer data were generated as required to support the assumptions and general methodology.

#### c. Analysis of the Eight Selected Overall Structural Concepts

The eight selected design concepts (1, 1A, 3, 3A, 4, 5, 8 and 8A) were analyzed in sufficient detail to provide accurate component sizes for weight estimation. Most of this analysis was concerned with the upper and lower surfaces, the five major ribs, all spars, and the core used in both the honeycomb panels and full depth core designs.

For convenience the mechanical properties of the specific materials used in these concepts have been condensed from sub-sections III.4, III.5, and III.6. The static properties are tabulated in Tables V and VI. The tension allowables established by fatigue and slow crack growth, and a static tension value reduced to reflect the effect of holes are shown in Tables VII and VIII. The lesser of these values was used in the analysis of the tension critical structure.

Analytical methods, failure modes and major assumptions used in the stress analyses of each concept are described in the following paragraphs.

##### (1) Upper and Lower Surfaces

For Concepts 4 and 5 the upper and lower surfaces are titanium pan type honeycomb panels. This construction is illustrated in Figure 31. The gage of the inner face sheet was held to a minimum consistent with face wrinkling



TABLE V - MECHANICAL PROPERTIES USED IN DESIGN - TITANIUM ALLOYS

COMPONENT	SKINS		SPARS		RIBS		
	UPPER	LOWER					
MATERIAL	Ti-6-22 -22 STA	Ti-6-4 β MA	Ti-6-4 β MA	Ti-6-4 β MA	Ti-6-22 -22 STA	Ti-6-22 -22 STA	Ti-6-4 Annealed
FORM	Plate	Plate	Die Frg	Sheet	Die Frg	Die Frg	Casting
THICKNESS	0.50	0.50	2.00	0.249	0.50	1.00	--
$F_{tu}$ , ksi	161	128	135	134	161	149	130
$F_{ty}$ , ksi	148	116	120	126	148	139	120
$F_{cy}$ , ksi	160	121	126	132	160	147	126
$F_{su}$ , ksi	100	75	79	79	100	88	76
$E$ , $10^3$ ksi	17.2	16.0	16.0	16.0	17.2	16.0	16.0
$E_c$ , $10^3$ ksi	18.1	16.4	16.4	16.4	18.1	17.3	16.4
$G$ , $10^3$ ksi	6.6	6.2	6.2	6.2	6.6	6.2	6.2

Minimum Basis

TABLE VI - MECHANICAL PROPERTIES USED IN DESIGN - ALUMINUM ALLOYS

COMPONENT	UPPER SKIN	LOWER SKIN		SPARS		RIBS	
MATERIAL	7050-T7651	7475-T7651	X2048 T851	7050-T736	7075-T73	7050-T736	7175-T736
FORM	Plate	Plate	Plate	Die Frg	Sheet	Die Frg	Hd Frg
THICKNESS	1.00	1.00	3.00	3.00	.249	3.00	4.00
$F_{tu}$ , ksi	78	69	62	68	67	68	71
$F_{ty}$ , ksi	72	59	56	61	56	61	61
$F_{cy}$ , ksi	74	58	56	63	55	63	61
$F_{su}$ , ksi	44	40	35	39	38	39	43
$E$ $10^3$ ksi	10.2	10.2	10.2	10.2	10.3	10.2	10.0
$E_c$ $10^3$ ksi	10.6	10.6	11.3	10.6	10.6	10.6	10.4
$G$ $10^3$ ksi	3.9	3.9	3.9	3.9	3.9	3.9	3.9

Minimum Basis

TABLE VII - SUMMARY OF ALLOWABLE ULTIMATE DESIGN STRESSES (KSI)  
FOR TITANIUM LOWER STRUCTURE (CONCEPTS 1, 3, 3A, 4, 5)

SPANWISE STRUCTURE BETWEEN RIBS

Member	Failure Mode	Allow. In Member	W.S. 30			W.S. 73			W.S. 93		
			Corres. Skin Allow.	Crit./F Concept	Allow. In Member	Corres. Skin Allow.	Crit. F/ Concept	Allow. In Member	Corres. Skin Allow.	Crit. F/ Concept	
SKIN (6-4 $\beta$ MA) (Plate)	Static Tension		122(1)	3A		122(1)	ALL		122(1)	ALL	
	Safe Life		113(2)	I		130(2)			137(2)		
	Damage Tolerance		N.C.			N.C.			N.C.		
EDGE SPAR (6-4 $\beta$ MA) (Forging)	Static Tension	N.C.	N.C.		N.C.	N.C.		N.C.	N.C.		
	Safe Life	102(3)	120(4)		117(3)	130(4)		123(3)	136(4)		
	Damage Tolerance	N.C.	N.C.		N.C.	N.C.		N.C.	N.C.		
INTERIOR SPAR (6-4 $\beta$ MA) (Sheet)	Static Tension	N.C.	N.C.		N.C.	N.C.		N.C.	N.C.		
	Safe Life	113	133(4)		130	144(4)		137	152(4)		
	Damage Tolerance	(5)	108*	3,4,5	(5)	124*		(5)	131*		

- (1) Gross area allowable stress with allowance for net section. Conservative for 3A.  
 (2) Using spectra at W.S. 30, 73, and 93 with  $K_t = 3.65$ . Not applicable to Concept 3A.  
 (3) 10% forging reduction assumed from values listed for 6-5 MA plate  
 (4) Increase allowing for spar operating at 85% of skin stress at 30 and 90% at 73 and 93  
 (5) Interior spars are not critical damage tolerant structure and may not have a slow crack growth life of 8000 hrs with a .05 thru flaw at a hole in the flange. Actual flange life plus added stresses and load transfer in skin after spar flange failure require skin design stresses indicated thus, \*.

CHORDWISE LAND AT RIBS

The following thicknesses are minimum required to provide 16,000 hr safe life and 8000 hr slow crack growth considering transfer of spanwise load in skin into and out of lower flanges of ribs. Not applicable to Concept 3A. Net section and fastener head requirements are additional.

	W.S. 30	W.S. 73	W.S. 93
t @ 15% spar	.125	.115	static critical
t @ 44% spar	.374	.290	static critical

TABLE VIII - SUMMARY OF ALLOWABLE ULTIMATE DESIGN STRESSES (KSI)  
FOR ALUMINUM LOWER STRUCTURE (CONCEPTS 1A, 8, 8A)

SPANWISE STRUCTURE BETWEEN RIBS

Member	Failure Mode	W.S. 30			W.S. 73			W.S. 93		
		Allow. In Member	Corres. Skin Allow.	Crit. F/ Concept	Allow. In Member	Corres. Skin Allow.	Crit. F/ Concept	Allow. In Member	Corres. Skin Allow.	Crit. F/ Concept
SKIN (7475-T7651) (Plate)	Static Tension		62 (1)			62 (1)			62 (1)	1A, 8
	Safe Life		57 (2)			63 (2)			74 (2)	
	Damage Tolerance		N.C.			N.C.			N.C.	
SKIN (2048-T851) (Plate)	Static Tension		59 (1)	8A		59 (1)	8A		59 (1)	8A
	Safe Life		65 (3)			65 (2)			65 (2)	
	Damage Tolerance		65 (4)			N.C.			N.C.	
EDGE SPAR (7050-T736) (Precision Forging)	Static Tension	61 (1)	78 (5)		61 (1)	76 (5)		61 (1)	76 (5)	
	Safe Life	44 (2)	54 (5)	1A	48 (2)	60 (5)	1A, 8	N.C.	N.C.	
	Damage Tolerance	N.C.	N.C.		N.C.	N.C.		N.C.	N.C.	
INTERIOR SPAR (7050-T736) (Precision Forging)	Static Tension	61 (1)	78 (5)		61 (1)	76 (5)		61 (1)	76 (5)	
	Safe Life	43 (2)	55 (5)		48 (2)	60 (5)		N.C.	N.C.	
	Damage Tolerance	(6)	54*	8	(6)	60*		(6)	70*	

- (1) Gross area allowable stress with allowance for net section  
(2) Using spectra at W.S. 30, 73, and 93 with  $K_t = 3.65$   
(3) Using spectrum at W.S. 30 with  $K_t = 2.0$   
(4) Part Thru flaw  
(5) Increase allowing for spars operating at 82% of skin stress at 30 and 80% at 73 and 93  
(6) Allowable skin stress considering interior spar flange failures indicated thus, \*. See Section III-4.

CHORDWISE LANDS AT RIBS

The following thicknesses are minimum required to provide 16,000 hr safe life and 8000 hr slow crack growth considering transfer of spanwise load in skin into and out of lower flanges of ribs. Net section and fastener head requirements are additional.

	W.S. 30	W.S. 73	W.S. 93
t @ 15% spar	.212	.195	static critical
t @ 44% spar	.632	.490	static critical



and intra-cell dimpling, with most of the material concentrated in the outer skin. With this configuration, there is much less reduction in centroidal depth, inserts for fasteners are not required, and load transfer to the inner face sheet is minimized.

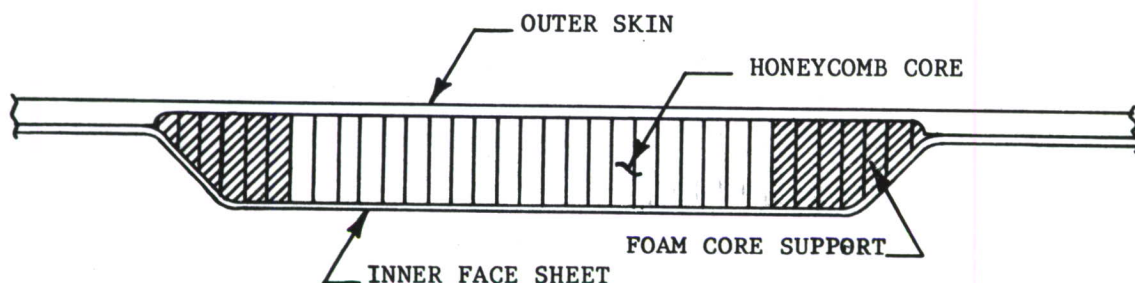


FIGURE 31. TYPICAL HONEYCOMB PANEL

Ti-6-22-22 STA titanium is used for both the inner face sheet and outer skin for the wing upper surface and Ti-6Al-4V  $\beta$  mill annealed for both faces of the lower surface. These faces are adhesively bonded to a 5056-H39 aluminum honeycomb core. The ribbon direction of the core is parallel to the long side. Potting foam is provided along the panel edges to transfer load to the inner skin, and to stabilize any crushed cells.

The upper and lower panels were analyzed for the following failure modes in combined compression and shear: general instability, MIL-HDBK-23A<sup>(1)</sup>; face wrinkling and intra-cell dimpling, Bruhn<sup>(2)</sup>; and shear crimping, NASA CR 1457<sup>(3)</sup>. The specific method chosen for each failure mode considered is based on previous comparisons with test data. These methods are considered satisfactory for preliminary design. However, in view of the large difference in thickness between the inner and outer face sheets and the relatively small core thickness, panel tests are recommended in the follow-on program.

- (1) Anon, Structural Sandwich Composites, MIL-HDBK-23A, Dept. of Defense, Washington, D. C., 20005, 30 December 1968.
- (2) E. F. Bruhn, Analysis and Design of Flight Vehicle Structures, Tri-State Offset Co., Cincinnati, Ohio, 1965.
- (3) R. T. Sullins, C. W. Smith, E. E. Spier, Manual for Structural Stability, Analysis of Sandwich Plates and Shells, CR 1457 NASA, Washington, D. C., December, 1969.

The maximum compression stress in the outer skin and inner face sheet of the upper surface was limited to approximately 90% of the compressive yield (140 KSI) to avoid excessive plasticity effects. For the lower surface, only the outer skin was assumed effective in tension, due to the eccentricity of the inner face sheet at the ribs. However, both the inner face sheet and outer skin are effective in shear.

Concept 1 consists of a Ti-6-22-22 STA titanium upper skin and a Ti-6Al-4V  $\beta$  mill annealed lower skin adhesively bonded to a full depth 5056-H39 aluminum core. No interior spars are used. The critical failure mode for the upper surface and the extreme outboard region of the lower surface was face wrinkling in combined compression and shear. The maximum allowable compression stresses are the same as for the honeycomb panels. The balance of the lower surface was designed by tension.

Concept 1A is a full depth core design similar to Concept 1. The upper skin is 7050-T7651 and the lower skin is 7475-T7651 aluminum alloy. The critical failure modes are the same as for Concept 1. The maximum compression stress in the upper skin was limited to approximately 90% of compressive yield (67 KSI) to avoid excessive plasticity effects.

Concept 8 is a six spar configuration with machined aluminum skins. The upper skin is 7050-T7651 and the lower is 7475-T7651. The upper skin was designed by buckling in combined compression and shear, with compression stresses limited to a maximum of 70 KSI for strain compatibility with the 7050-T736 forged spars. The lower skin was critical entirely in tension.

Concept 3 is a six spar configuration with a 7050-T7651 aluminum upper skin and a Ti-6Al-4V  $\beta$  mill annealed lower skin. The upper skin is approximately the same as that of Concept 8. The lower skin was designed primarily by buckling in combined compression and shear for the negative bending conditions.

Concept 3A is similar to Concept 3 except the spar and rib webs are electron beam welded to the lower skin, with the skin lands acting as the lower flanges. Holes in the lower skin are eliminated. The lower skin is critical in combined compression and shear for negative bending conditions. The corresponding maximum ultimate tension stress is 97 KSI.

Concept 8A is also a six spar configuration. The upper skin is 7050-T7651 and is identical with that of Concept 8. The lower skin is designed

by tension. It is machined from thick X2048-T851 aluminum plate with integral legs to which the spar webs are attached. This construction effectively eliminates most of the holes in the lower surface and permits the use of higher tension allowables in the inboard regions.

## (2) Spars

Two basic spar web configurations were employed in the eight concepts analyzed. Plain web die forgings of Ti-6Al-4V  $\beta$  mill annealed titanium and 7050-T736 aluminum were used for the 15%, 44%, and 66% spars. Plain web 7050-T736 aluminum die forgings were also used for the interior spars of Concept 8A. The balance of the interior spars utilized a corrugated web. With the exception of 7050-T736 die forgings in Concept 8, these webs were formed from Ti-6Al-4V  $\beta$  mill annealed sheet.

The corrugated webs are loaded in shear and transverse compression due to crushing. Wing bending subjects the flanges of these spars to axial stress, but its effect on the spar webs is negligible due to their corrugated construction. These webs were analyzed for general instability in combined shear and transverse compression as a long orthotropic plate with simply supported edges. The orthotropic plate equations of Timoshenko and Gere<sup>(1)</sup> were used for this analysis. Local instability of the corrugated web was not critical.

The plain webs are loaded in shear, transverse compression, and in-plane bending. These webs were analyzed for general instability under the combined loading as long isotropic plates with simply supported edges. The conventional isotropic plate buckling equations were used from the Northrop Stress Manual.<sup>(2)</sup>

Shear strain compatibility between the spar webs and the honeycomb core is an additional consideration in the analysis of the full depth core designs. Local increases in the spar web gages were required to avoid induced shear failure of the core.

(1) S. P. Timoshenko and J. M. Gere, Theory of Elastic Stability, McGraw-Hill Book Co., New York, 1961.

(2) Anon., Structural Design Manual, Northrop Corp., Aircraft Division.



The spars must have sufficient stiffness to provide adequate support to the skins. Accordingly, the corrugated web spars were analyzed as line springs using the methodology of NASA TR 1202<sup>(1)</sup> modified to exclude the effect of bending stress in the webs. The details of this modification are shown in Appendix I. A WANG 600 computer program was used to determine the spar flange and web gages required. The plain web spar flange and web gages were sized for skin stability to provide the same spring stiffness as the equivalent spars in the F-5E.

The spar flanges were analyzed also for crippling. In some cases, this consideration was critical.

### (3) Ribs

The root ribs are die forgings of Ti-6-22-22 STA titanium or 7050-T736 aluminum depending on the specific design concept. Similarly, the inboard pylon ribs are either Ti-6Al-4V annealed castings or machined from aluminum 7175-T736 hand forged billets. The landing gear ribs are Ti-6-22-22 STA die forgings, and the tip ribs are Ti-6Al-4V annealed castings for all concepts.

These ribs were analyzed for the F-5E rib shears and bending moments shown in the baseline F-5E stress analysis<sup>(2)</sup> with minor modifications to reflect the different number of spars in the various design concepts. The required web and flange gages were determined using the chordwise skin lands as part of the flange material. The local effects of the numerous holes in the rib webs were analyzed using the same methodology as in the F-5E stress analysis. Where lugs and fittings are an integral part of these ribs, a corresponding local analysis was made.

For the full depth core concepts an analysis was made of shear strain compatibility between the rib webs and the honeycomb core similar to that for the spar webs. Local increases in the rib webs were required in some cases to avoid induced shear failure of the core.

- 
- (1) R. A. Anderson and J. W. Semonian, Charts Relating the Compressive Buckling Stress of Longitudinally Supported Plates to the Effective Deflectional and Rotational Stiffness of the Supports, NACA TR 1202, 1954.
  - (2) V. Betz, et al, F-5E Wing Stress Analysis, NOR 71-173, Northrop Corp., Aircraft Div., March, 1972.

#### d. Analysis of the Warren Truss Spar Concept (Concept 2)

Analytical work on the truss spar arrangement (Concept 2) involved two major areas:

- A possible increased torsional rigidity inherent in a truss spar design was investigated versus a conventional design with vertically oriented spars.
- A preliminary analysis of the wing root area was made to determine if the chordwise load carrying capability of this design could be used to eliminate a significant portion of the root rib.

Two NASTRAN finite element models of titanium wing box structures were run to determine the relative torsional rigidity of a truss spar vs. a conventional vertical spar design. Figures 32 and 33 show the gridwork of these two models. Both models were made representative of that portion of the F-5E wing between the root rib and the landing gear rib, but simplified by eliminating taper and by providing as many common nodal points as possible. Overall dimensions were 45 inch span, 30 inch chord, and 5 inch thickness. Upper and lower skins were a .136 inches thick, forward and aft spars were .128 and end ribs were .184. The six interior truss spars in Figure 32 were .025 corrugated webs. The five interior vertical spars in Figure 33 were .035 corrugated webs. An additional run was made with plain webs for the truss spar design. Torques were applied both as vertical couples at the four corners and also as T/2A shear flows along the outboard edge. Ribs at both ends were free to warp. There was no increased torsional rigidity evident in the truss spar design. The torsional stiffnesses were virtually identical between the two designs and essentially equal to that predicted by classical multi-cell two dimensional analyses. The truss spar design, however, did exhibit variations in the shear flows in the interior spars particularly near the end ribs. This indicates that the "continuous rib" action is indeed present, but the relatively thin gages of these spars apparently minimized this effect.

The second investigation of the truss spar design concentrated on the chordwise structure between the forward and aft wing to fuselage attach

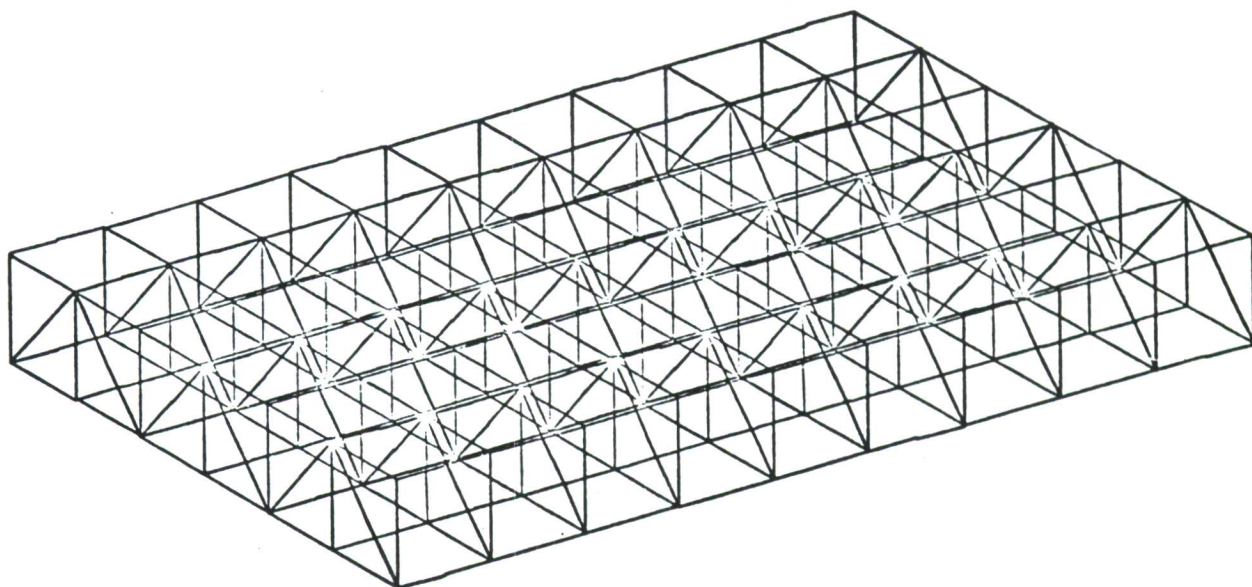


FIGURE 32. TRUSS SPAR GRIDWORK WITH 6 DIAGONAL SPARS

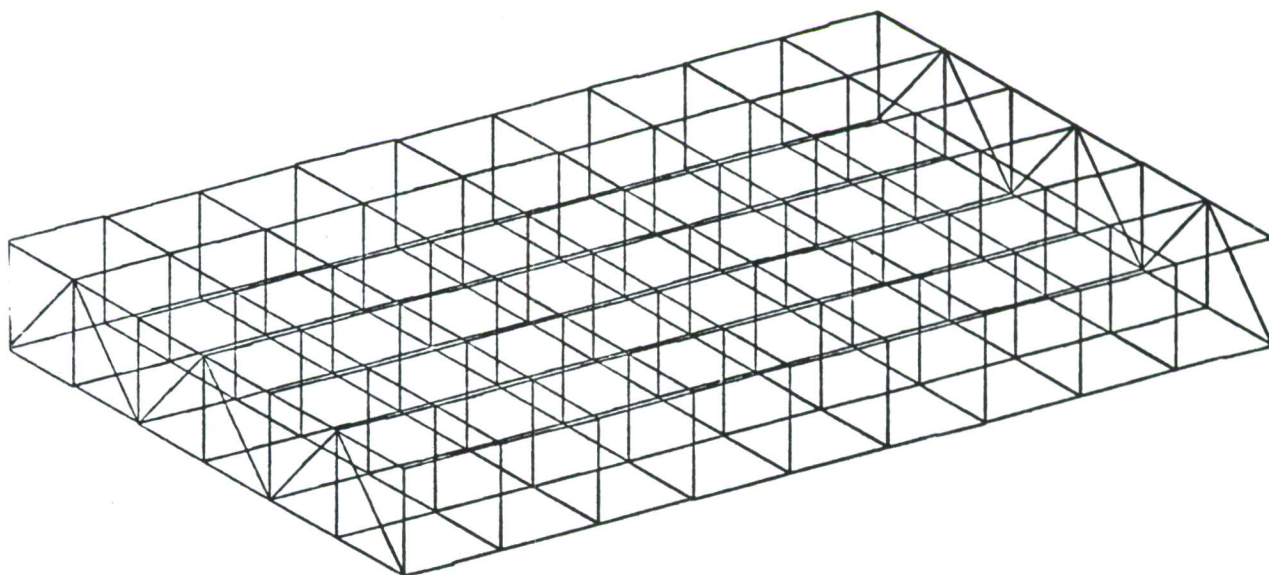


FIGURE 33. CONVENTIONAL SPAR GRIDWORK WITH 5 INTERIOR SPARS



trunnions. In a conventional design, this is the root rib area. The purpose of this investigation was to determine if any weight savings could be achieved by deleting the center portion of the root rib since the truss spar design is capable of carrying chordwise shears as well as spanwise shears.

Primarily, the root area is loaded by a torque generated both by basic wing torque and by the wing bending moments acting at the wing sweep point. This torque is fed into the chordwise structure in a rather uniform manner by shear flows in the upper and lower wing skins (i.e., by the basic bending material) and reacted by the fuselage attachment trunnions. Wing shear is also distributed rather uniformly into this structure because of the multi-spar configuration. As a result, there are no concentrated loads applied to this root area structure.

With a conventional root rib, the wing skin shear flows are reacted continuously by the root rib web which produces a minimum net bending moment in the rib (i.e., the chordwise load build-up in the skins/rib cap is held to a minimum).

In the truss spar design the function of the root rib web is provided instead by an effective spanwise width of the truss structure. This is a discontinuous load path as compared to the conventional rib web. The result is a "sawtooth" distribution of chordwise axial loads from torque that are built up in the wing skins between each spar vertex and reacted at each of these points by the loads in the spars acting as truss diagonals for the trunnion reactions. This effect has been studied for the specific situation at the F-5E root area. The results show that the peak chordwise loads in the wing skin reach 55,000 pounds (about three to four times higher than the comparable loads in the conventional root rib structure) and that the axial tension and compression loads in the truss spars themselves reach 60,000 pounds (nil in conventional structure). Under these conditions the skins are critical as wide beam-columns which require additional chordwise stiffening, and the truss spar structure also requires considerable beef-up. The net result is heavier than a conventional rib. The conclusion is that the truss spar design also requires a conventional root rib and that no weight savings can be achieved by deleting a portion of the rib.

e. Analysis of the Ti-Borsic Upper Skin Concept

Ti-Borsic is presently a high risk material--there is only a very limited amount of materials test data available and virtually no fatigue or fracture mechanics information. Ti-Borsic was explored in this program for upper skin applications (primarily compression loading) because its very high specific modulus could provide needed panel stability for 4 or 5 spar designs. Also, its specific modulus might be utilized in providing additional wing bending or torsional stiffness in selected areas if required for aeroelastic reasons (flutter or aileron effectiveness).

Preliminary estimates of the elastic and strength properties for unidirectional Ti-Borsic (6Al-4V) composite at room temperature were based on the very limited test data available in References (1), (2), (3), and (4). These estimates as of 11/6/72 are given in Table IX.

For the (0, 90,  $\pm 45$ ) laminates, the values of elastic modulus were generated with the use of SABUL computer program<sup>(5)</sup>. These curves are presented in Figure 34.

From the strength point of view, the laminate orientation and thickness is governed by the magnitude of the longitudinal and shear loads. However, in the 4-spar and 5-spar configurations, the panel buckling is also a critical factor. Therefore, selection of laminate orientation and thickness was governed by both the strength and buckling considerations. A survey

- 
- (1) I.J. Toth, W.D. Brentnall, and G.D. Menke, "A Survey of Aluminum Matrix Composites," presented at the Composites: State of the Art Conference, AIME Fall Meeting, 20 October 1971.
  - (2) W.D. Brentnall and I.J. Toth, High Temperature Titanium Composites, IR-7351-(1), Metal and Ceramics Division, AFML, 1 July 1971 to 1 Jan. 1972.
  - (3) W.D. Brentnall and I.J. Toth, High Temperature Titanium Composites, IR-7351-(2), Metals and Ceramics Division, AFML, 1 January 1972 to 1 July 1972.
  - (4) Telecon, R. Wells (Northrop) to I. J. Toth (TRW), 24 October 1972.
  - (5) Northrop Report NOR 71-134, Strength Allowable and Buckling Load Analysis of Laminated Composites Including the Effect of Normal Shear Stiffness, September 1971.

TABLE IX  
ESTIMATED ELASTIC AND STRENGTH PROPERTIES  
OF UNIDIRECTIONAL TI-BORSIC

Fiber Diameter	.0057 inches
Fiber Volume	50%
Average Ply Thickness	.0067 inches
Density	.125 lb/in <sup>3</sup>
$E_{11}^T$ and $E_{11}^C$	36 MSI
$E_{22}^T$ and $E_{22}^C$	30 MSI
$G_{12}$	11 MSI
$\gamma_{12}$	.28
$F_1^T/F_2^T$	205/75 KSI
$F_{12}$	28 KSI
$\epsilon_1^T/\epsilon_2^T$	6500/5700 $\mu$ in/in
$\gamma_{12}$	6000 $\mu$ in/in

of the F-5E design loads indicated that the (0, +45) family of laminates would be most suitable. Figures 35 and 36 show the estimated allowable tension and shear strength. These curves are based on 80% of the unidirectional failure strength as a best estimate of a realistic design allowable for a large laminated structure in a production situation.

The above properties and strengths were used to estimate the potential for a Ti-Borsic skin in a 4-spar concept for the F-5E wing. For comparative purposes, separate skin panel weight ratios (for idealized applications) were determined to give equal stiffness, buckling load per inch, and static strength relative to the baseline F-5E design. The ratios are summarized in Table X. The results show that the plain Ti/Borsic panel is a potentially advantageous upper skin concept, particularly when stiffness is a significant factor or if a 5-spar design may be contemplated.



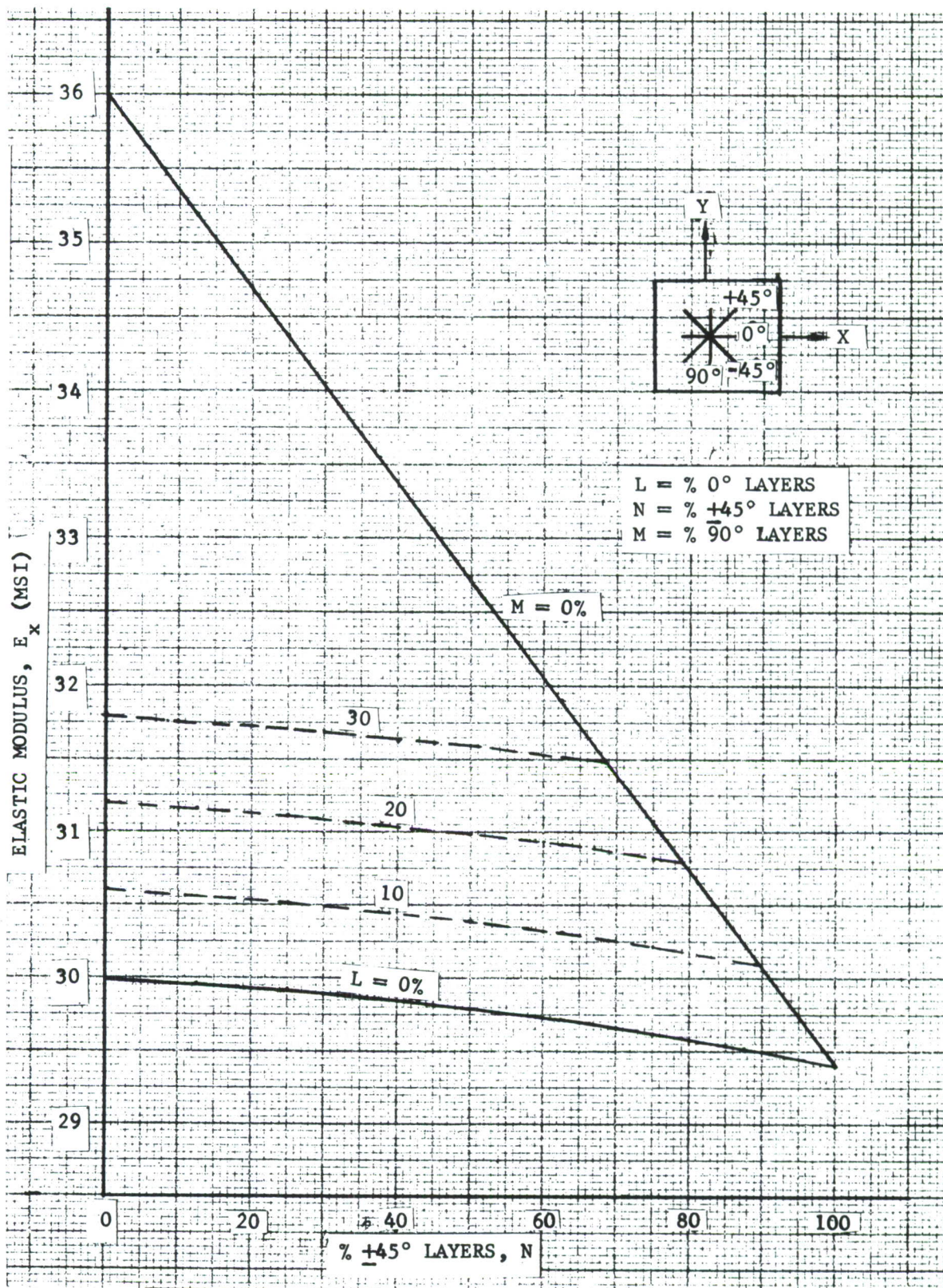


FIGURE 34. ELASTIC TENSION AND COMPRESSION MODULUS OF TI-BORSIC LAMINATES AT R.T.



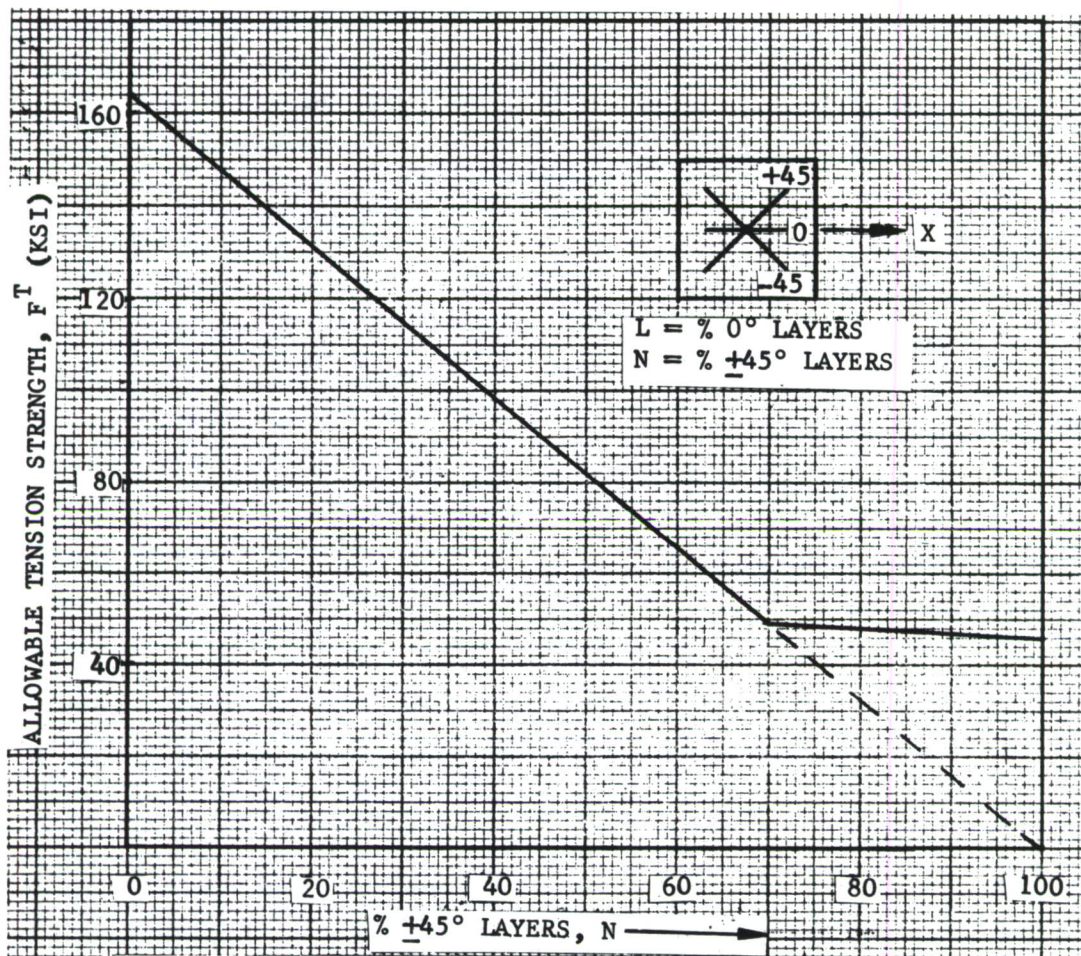


FIGURE 35. ESTIMATED ALLOWABLE TENSION STRENGTH OF TI-BORSIC LAMINATES AT R.T.

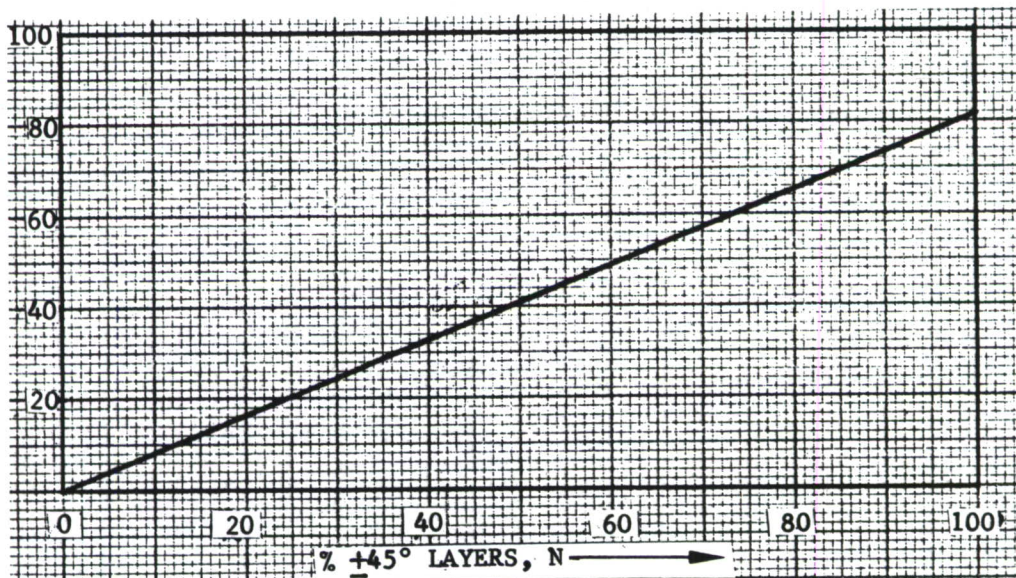




FIGURE 36. ESTIMATED ALLOWABLE IN-PLANE SHEAR STRENGTH OF TI-BORSIC LAMINATES AT R.T.



TABLE X

SKIN WEIGHT RATIOS FOR A TI-BORSIC 4-SPAR UPPER WING SKIN RELATIVE TO THE BASELINE F-5E 6-SPAR ALUMINUM WING, FOR EQUAL STIFFNESS, BUCKLING LOAD, AND STATIC STRENGTH

SKIN CONFIG.	SKIN WEIGHT RATIOS FOR EQUAL			
	STIFFNESS		BUCKLING LOAD 	STATIC STRENGTH
	AXIAL	SHEAR		
Plain	.39	.39	1.20	.71

 For buckling, the panel width ratio for a 4-spar relative to a 6-spar wing is 5/3.

To complete the study, a plain Ti-Borsic upper skin was sized for the 4-spar wing concept from the centerline to W.S. 123.5. For this study, the compression loads under positive bending, tension loads under negative bending and shear loads were computed by taking into consideration the relative stiffness of the Ti/Borsic skin and the Ti spar flanges. The optimum laminate orientation, based on strength under compression and shear loads, consists of approximately 50 percent 0-degree plies and 50 percent +45-degree plies. The skin thickness, however, was governed by buckling considerations.

In addition, a separate study was undertaken wherein local Ti-Borsic panels were sized on a strength basis as a substitute for selected titanium upper panels on Concepts 1, 4 and 5 to provide additional wing stiffness between W.S. 73 and 109.5. In these applications, the upper panels are stabilized by honeycomb core (full depth or panel construction) such that the strength of the basic laminate under combined loads established the minimum thicknesses.



f. Analysis of the Geodesic Titanium Lower Skin Concept

The geodesic wing skin design concept consists of a plate skin with a longitudinal and diagonal structural grid and triangular cutouts as shown in Figure 37. The covering skins may be either non-structural or may be relatively thin sheets adhesively bonded to the interior geodesic construction. This concept aims at providing a highly redundant multiple load path fail-safe structure in a "one piece" design as opposed to the conventional planked approach.

The sizing of the grid members of a geodesic structure is dictated by the applied axial and shear loads and the angle of orientation of the diagonal members. The optimum angle of orientation was found to be  $45^\circ$  to the longitudinal direction for minimum weight of the skin. To show this, a typical repeating section of the geodesic skin shown shaded in Figure 37 was considered.

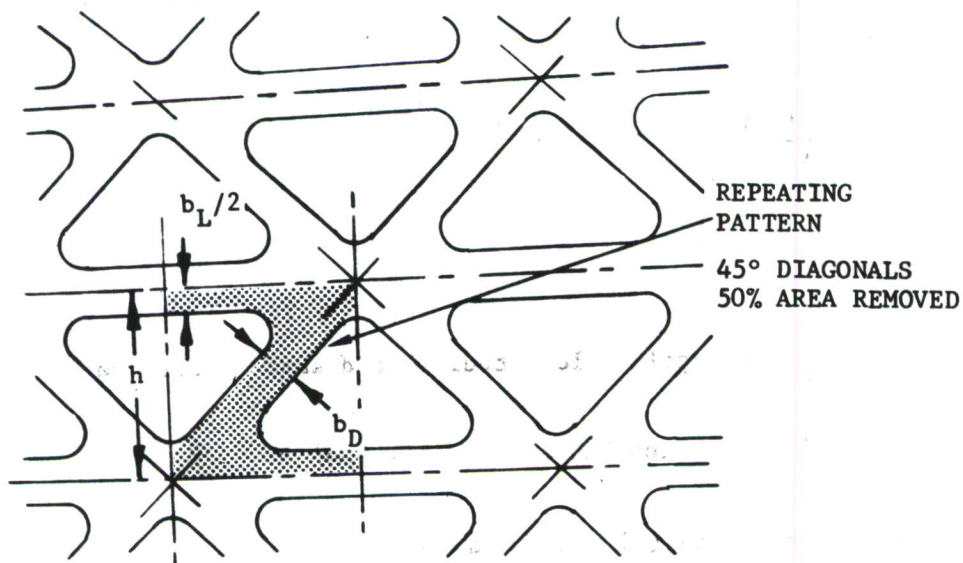


FIGURE 37.

GEODESIC SKIN WITH  $45^\circ$  DIAGONAL MEMBERS

The weight per unit area is approximately given by the equation,

$$W = \rho t \left[ (b_L/h) + \left( \frac{b_D}{h} \right) (1 - b_L/h) / \cos \theta \right] \quad (1)$$

where  $W$  = weight of the geodesic skin per unit area.  
 $\rho, t$  = material density and thickness of the skin, respectively.  
 $h$  = distance between longitudinal members.  
 $b_L, b_D$  = width of longitudinal and diagonal members, respectively.  
 $\theta$  = angle of orientation of the diagonal members with respect to the longitudinal members.

For concepts with non-structural covers, it can be assumed that all of the longitudinal load is in the longitudinal members and all of the shear load is in the diagonal members. This is a reasonable assumption based on the results of the finite-element analysis described later in this section. The optimum widths of the longitudinal and diagonal members are then given by the relations

$$b_L = \left( \frac{N_x}{\sigma_a} \right) \frac{h}{t} \quad \text{and} \quad b_D = \left( \frac{N_{xy}}{\sigma_a} \right) \frac{h}{t \sin \theta} \quad (2)$$

where

$N_x$  and  $N_{xy}$  = applied longitudinal and shear loads, respectively

$\sigma_a$  = allowable tension strength

Substituting Equations (2) into Equation (1), gives

$$W = \rho \left( \frac{N_x}{\sigma_a} \right) \left[ 1 + 2 \left( \frac{N_{xy}}{N_x} \right) \frac{(1 - b_L/h)}{\sin 2\theta} \right] \quad (3)$$

This equation shows that minimum weight under combined axial and shear loads occurs at  $\theta = 45^\circ$  and Equation (3) becomes

$$W = \rho \left( \frac{N_x}{\sigma_a} \right) \left[ 1 + 2 \left( \frac{N_{xy}}{N_x} \right) \left( 1 - \frac{b_L}{h} \right) \right] \quad (4)$$

In view of the above result, the remaining studies of the stiffness properties and stress distributions in geodesic structures concentrated on configurations with 45° diagonal members.

The influence of the relative sizes of the longitudinal and diagonal members on the member stresses in the geodesic skin design was analyzed and the results are presented below. The ratio R of the geodesic skin area over the gross surface area for a typical skin, shown in Figure 37 with 45° diagonal members, is given by

$$R = \left(\frac{b_L}{h}\right) \left[ 1 + \sqrt{2} \left(\frac{b_D}{b_L}\right) \left(1 - \frac{b_L}{h}\right) \right] \quad \text{for } \left(\frac{b_D}{b_L}\right) \leq \frac{1}{\sqrt{2}} \quad (5a)$$

and

$$R = \left(\frac{b_L}{h}\right) \left(1 + \sqrt{2} \frac{b_D}{b_L}\right) \left[ 1 - \frac{1}{4} \left(\frac{b_L}{h}\right) \left(1 + \sqrt{2} \frac{b_D}{b_L}\right) \right] \quad \text{for } \frac{1}{\sqrt{2}} \leq \left(\frac{b_D}{b_L}\right) \leq \frac{1}{\sqrt{2}} \left[ \frac{2}{\left(\frac{b_L}{h}\right)} - 1 \right] \quad (5b)$$

For the same weight of geodesic and plain skins, the ratio of skin thickness is

$$\left(\frac{t}{t_o}\right) = \frac{1}{R} \quad (6)$$

It is again assumed that all of the longitudinal load is in the longitudinal members and all of the shear load is in the diagonal members. Then, for the same longitudinal and shear loads in geodesic and plain skins, the stress ratios for the longitudinal and diagonal members become,

$$\left(\frac{\sigma_L}{\sigma_{LO}}\right) = \frac{R}{(b_L/h)} \quad \text{and} \quad \left(\frac{\sigma_D}{\tau_{xy}}\right) = \frac{\sqrt{2}}{(b_D/b_L)} \times \frac{R}{(b_L/h)} \quad (7)$$

The values of R and the stress ratios are obtained from Equations (5a), (5b), and (7) for specified values of  $(b_L/h)$  and  $(b_D/b_L)$ . The above equations are the basis for the design curves shown in Figures 38 and 39, which show the percentage of area removed and longitudinal stress ratios as functions of  $(b_L/h)$  and  $(b_D/b_L)$ .



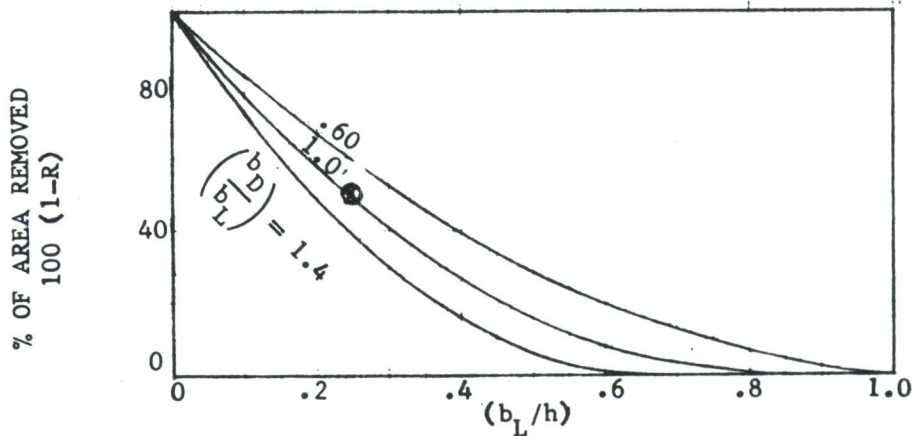


FIGURE 38. PERCENT OF AREA REMOVED VERSUS  $(b_L/h)$  FOR THE GEODESIC SKIN DESIGN (Computed from Finite Element Model with  $b_L/h = 0.25$ ,  $b_D/b_L = 0.8$ )

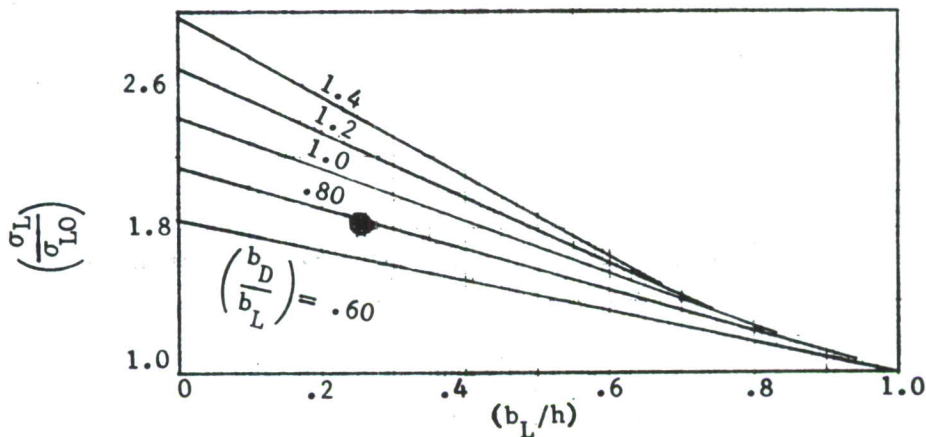


FIGURE 39. RATIO OF LONGITUDINAL MEMBER STRESS IN GEODESIC SKIN OVER STRESS IN PLAIN SKIN OF SAME WEIGHT (Computed from Finite Element Model with  $b_L/h = 0.25$ ,  $b_D/b_L = 0.8$ )

To check these equations, the geodesic skin design shown in Figure 37 with  $45^\circ$  oriented diagonal members and  $(b_L/h) = 0.25$ ,  $(b_D/b_L) = 0.8$  was concurrently analyzed by the finite element method. To minimize computing time, the analysis was restricted to the repeating stress and deformation pattern of the geodesic area shown shaded in Figure 37. This repeating pattern with its boundary constraints was based on the analytical methods described in Appendix II. For this pattern, the finite element model shown in Figure 40 was developed and analyzed using the SAAS-4 computer program.<sup>(1)</sup> This computer

(1) Northrop Report NOR 70-203, User's Manual for Northrop Version of Finite Element Program "SAAS-4" dated March, 1972.

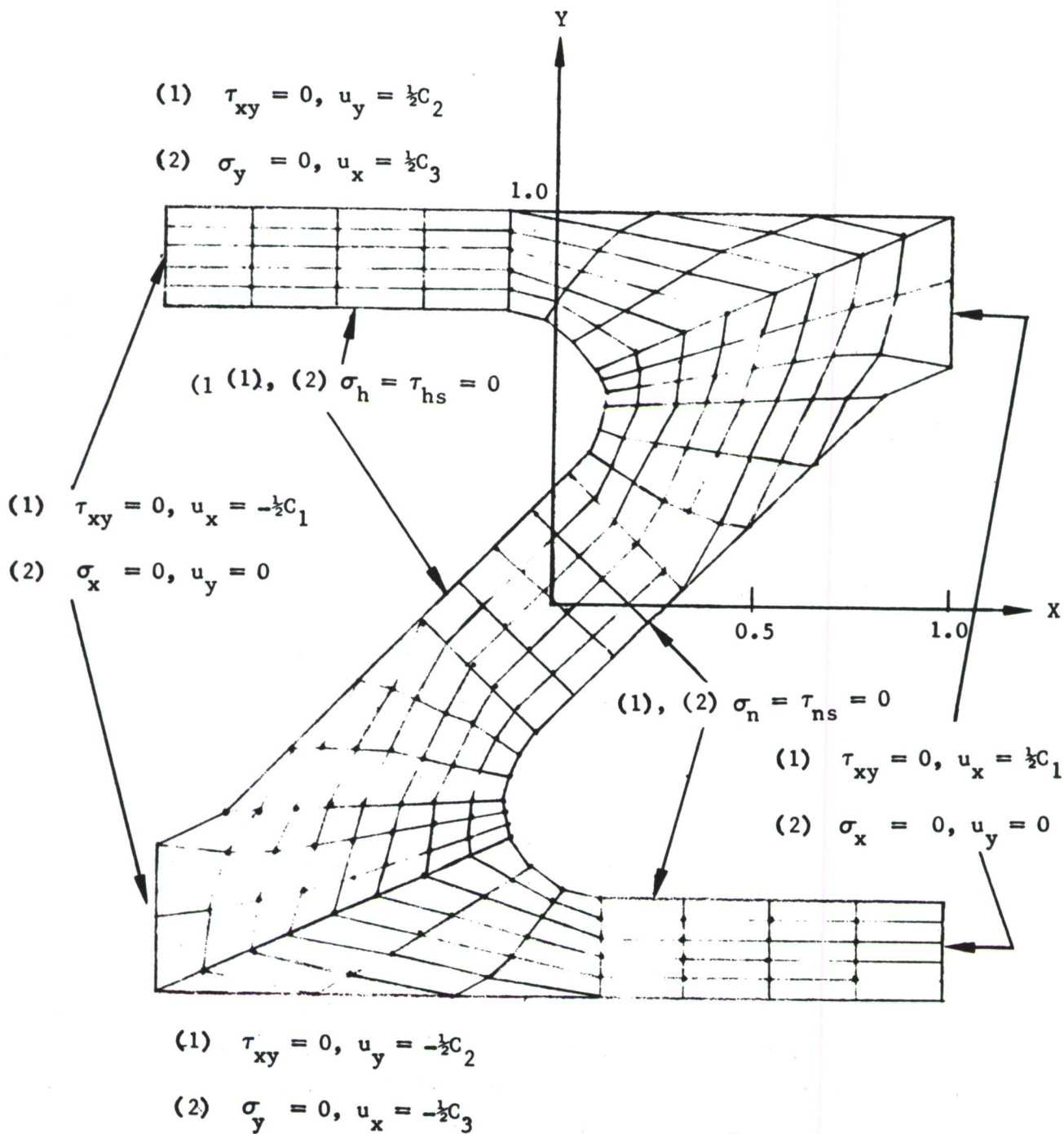


FIGURE 40. FINITE-ELEMENT MODEL OF THE REPEATING GEODESIC PATTERN UNDER (1) AXIAL LOADS & (2) SHEAR LOADS

program was used because of its mesh generation feature which reduces considerably the required input data. The mesh and boundary conditions are shown in Figure 40 for both the bi-axial normal load case and for the shear load case. Stress distributions were obtained under applied boundary displacements. These results were used to calculate the average elastic properties, member stresses and peak stresses per unit load using the methods presented in Appendix II. The analysis showed that, for this particular case, 94 percent of longitudinal load was in the longitudinal members, and 90 percent of shear load was in the diagonal members. The actual computed values from this finite-element analysis for the geometry ( $b_L/h = 0.25$  and  $(b_D/b_L) = 0.8$ ), are superimposed on Figures 38 and 39 for comparison. The computed values show very good agreement with the design curves.

The results of this particular finite-element analysis are summarized in Table XI. The stiffness properties and stresses for this design are compared with a plain titanium skin and with the F-5E baseline aluminum skin of equal weights. The last column shows that this design is considerably less stiff and has high member stresses as compared to the plain aluminum skin of same weight. Therefore, this particular geodesic Ti skin design is not practical.

The curves of Figure 39 show that a considerable improvement is possible by increasing the  $(b_L/h)$  ratio and by decreasing the  $(b_D/b_L)$  ratio within the limits dictated by the F-5E wing skin loading. Also, structural cover skins bonded to the main geodesic construction would aid in reducing stresses and increasing stiffnesses. Accordingly a revised design with 20 percent of the total weight in the cover skins and with geodesic parameters of  $(b_L/h) = 0.5$  and  $(b_D/b_L) = 0.7$  was analyzed both in the basic intact configuration and with failures presumed at various locations. These latter evaluations were conducted to assess the load redistribution characteristics of the basic design under representative fail-safe situations.

A course finite-element model of this redesigned geodesic Titanium skin was formulated which included 165 node points and 160 elements as shown in Figure 41. It was analyzed with the use of the SAAS-4 finite-element computer program. The results of the analysis indicated that the most



TABLE XI. COMPARISON OF EQUAL WEIGHT PLAIN ALUMINUM,  
PLAIN TITANIUM AND GEODESIC TITANIUM SKINS

The geodesic Ti skin design has  $(b_L/h) = .25$ ,  $(b_D/b_L) = .8$  and  $R = .5$

Stiffness & Stress Values for:	Plain Alum.	Plain Ti	Geodesic Ti	Ratios for Same Wt. Skin		
				Plain Ti Plain Al	Geod Ti Plain Ti	Geod Ti Plain Al
Skin Thickness	$t_o$	$t_1$	$t_2$	$\frac{t_1}{t_o} = \frac{1}{1.6}$	$\frac{t_2}{t_1} = 2.0$	$\frac{t_2}{t_o} = 25$
$(E_x t) \times 10^{-6}$ psi	$10 t_o$	$16 t_1$	$5 t_2$	1.0	.624	.624
$(E_y t) \times 10^{-6}$ psi	$10 t_o$	$16 t_1$	$3.5 t_2$	1.0	.438	.438
$(Gt) \times 10^{-6}$ psi	$3.76 t_o$	$6.2 t_1$	$1.17 t_2$	1.03	.378	.390
$\nu_{xy}$	.33	.31	.41			
$b_{cr}$ (same buckling load, lbs/in)	$b_o$	$b_1$	$b_2$	.625	1.45	.904
For Applied Axial Load, $N_x$ , lb/in						
Gross Stress $\bar{\sigma}_x$	$N_x/t_o$	$N_x/t_1$	$N_x/t_2$	1.6	.5	.8
Longit. Member $\sigma_L$	$N_x/t_o$	$N_x/t_1$	$3.7(N_x/t_2)$	1.6	1.85	2.96
Longit. Member Peak Stress (at radius) $\sigma_{peak}$	$3 N_x/t_o$	$3 N_x/t_1$	$5.6 (N_x/t_2)$	1.6	.93	1.49
Longit. Member Peak Stress at hole $\sigma_{peak}$	$3 N_x/t_o$	$3 N_x/t_1$	$11.1(N_x/t_2)$	1.6	1.85	2.96
For Applied Shear Load, $N_{xy}$ , lb/in						
Gross Stress $\bar{\tau}_{xy}$	$N_{xy}/t_o$	$N_{xy}/t_1$	$N_{xy}/t_2$	1.6	.5	.8
Diagonal Member $\sigma_D$	$N_{xy}/t_o$	$N_{xy}/t_1$	$6.3 (N_{xy}/t_2)$	1.6	3.15	5.04
Diagonal Member Peak Stress (at radius) $\sigma_{peak}$	$4 N_{xy}/t_o$	$4 N_{xy}/t_1$	$10.4(N_{xy}/t_2)$	1.6	1.30	2.08

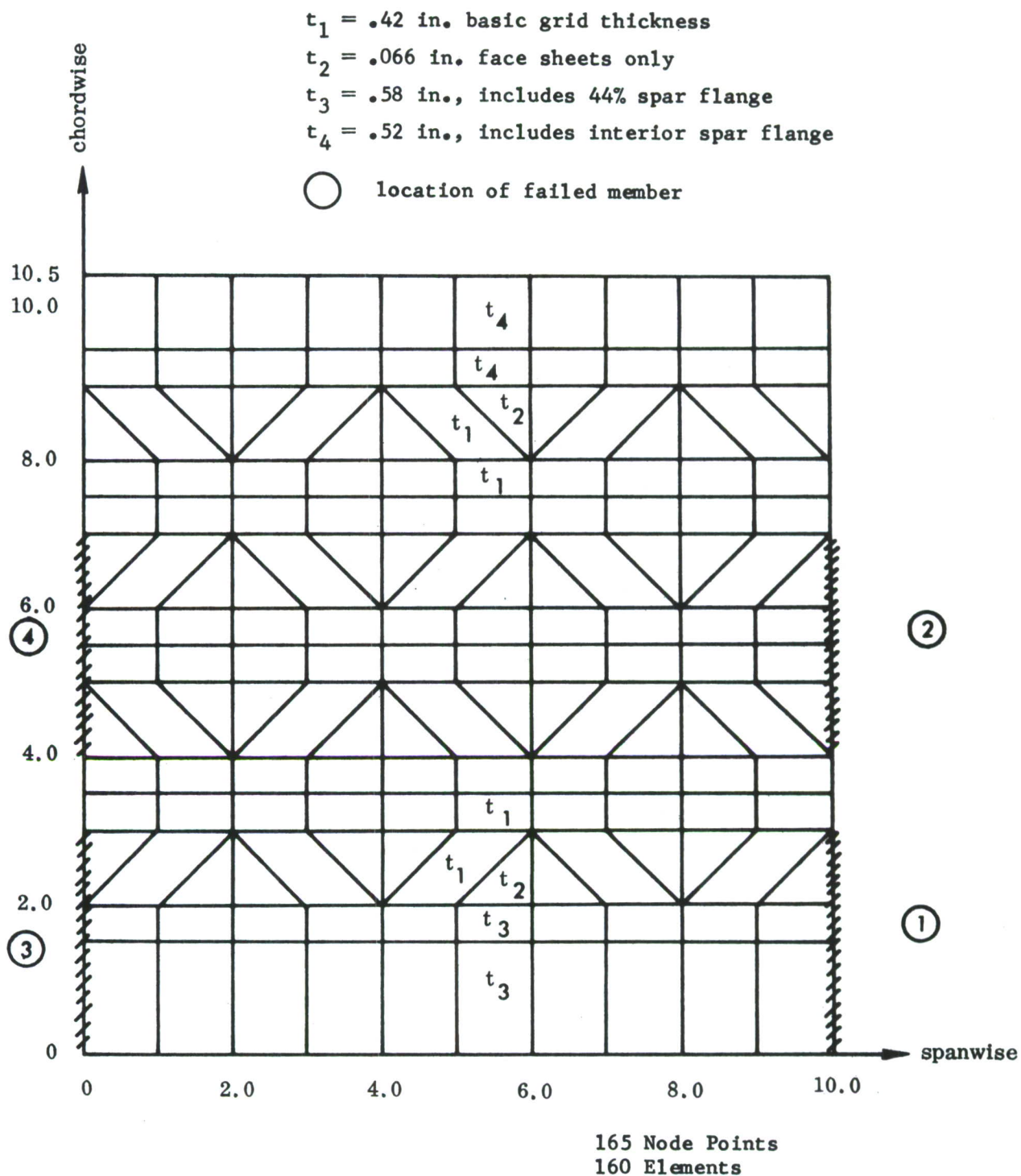


FIGURE 41. FINITE-ELEMENT MODEL FOR LOWER GEODESIC SKIN  
REPRESENTATIVE OF W.S. 73

severe failure location was at the juncture of the longitudinal and diagonal members at the peripheral 44-percent spar (failure area 3 in Figure 41). The stress increase in the highest stressed unfailed element was 140 percent. To reduce this stress level, the design was locally reconfigured along the peripheral spar into a 3-member arrangement (i.e., the geodesic skin, spar flange, and a spanwise strap) of the same total area. This design shifted the critical failure point to an intermediate member (area 4 in Figure 41) and reduced the stress increase in an unfailed element to 50 percent. Based on these studies the indications are that the resulting design could be particularly effective in containing damage--both from flaws and from unforeseen fatigue problems. The structure redistributes failed member loads over a relatively large area of adjacent structure with moderate stress increases. The adjacent structure is largely independent structure without common hole patterns or common flaws and the adhesively bonded cover skins are relatively light compared to the primary longitudinal and diagonal members.

For application to the baseline F-5E airplane, the unfailed characteristics of this final geodesic design (20 percent cover skins,  $b_L/h = 0.5$  and  $b_D/b_L = 0.7$ ) were determined and are summarized in Table XII. Fundamentally, it has 90 percent of the extensional stiffness of an equal weight aluminum or titanium skin, 69 percent of the shear stiffness and about a 40 percent increase in stress level over an equal weight plain titanium skin. Relative to the gross stress (i.e.,  $w_T/t_2$ ) the cover skins show a 77 percent increase in stress level. Compressive stability is reduced, however, and this can be critical in negative bending conditions.

Using this information, a geodesic titanium lower skin for the 4-spar wing concept was sized for application between the centerline and W.S. 93.5 taking advantage of the improved stiffness and safe-life properties as compared to the earlier design. For the redesign, the skin tension, compression under negative bending, and shear loads were recomputed by taking into consideration the relative stiffness of the skin and spar flanges. The skin thickness was governed by buckling consideration under negative bending load.



TABLE XII  
COMPARISON OF EQUAL WEIGHT PLAIN ALUMINUM, PLAIN  
TITANIUM, AND GEODESIC TITANIUM WITH 20% COVER SKINS

The Geodesic Ti skin design has  $(b_L/h) = 0.5$ ,  $(b_D/b_L) = 0.7$ , and  $R = 0.75$

Stiffness & Stress Values For	Plain Alum.	Plain Ti	Geodesic Ti With 20% Cover	Ratios for equal Wt. Skins		
				Plain Ti Plain Al.	Geod Ti Plain Ti	Geod Ti Plain Al.
Skin Thickness	$t_o$	$t_1$	$t_2$	$\frac{t_1}{t_o} = \frac{1}{1.6}$	$\frac{t_2}{t_1} = 1.27$	$\frac{t_2}{t_o} = .79$
$(E_x t) \times 10^{-6}$ psi	$10 t_o$	$16 t_1$	$11.3 t_2$	1.0	.90	.90
$(E_y t) \times 10^{-6}$ psi	$10 t_o$	$16 t_1$	$8.0 t_2$	1.0	.63	.63
$(Gt) \times 10^{-6}$ psi	$3.76 t_o$	$6.2 t_1$	$3.25 t_2$	1.03	.67	.69
$\nu_{xy}$	.33	.31	.31			
$b_{cr}$ (same buckling Load) Lbs/in	$b_o$	$b_1$	$b_2$	.625	1.10	.70
For Applied Axial Load, $N_x$ , lb/in						
Applied Stress $\bar{\sigma}_x$	$\left(\frac{N_x}{t_o}\right)$	$\left(\frac{N_x}{t_1}\right)$	$\left(\frac{N_x}{t_2}\right)$	1.6	.79	1.27
Longit. Member $\sigma_L$	Same	Same	$1.71 (N_x/t_2)$	1.6	1.35	2.16
Diagonal Member $\sigma_D$	Same	Same	$1.15 (N_x/t_2)$	1.6	.91	1.45
Cover skin stress $\sigma$	Same	Same	$1.77 (N_x/t_2)$	1.6	1.40	2.24
For Applied Shear Load, $N_{xy}$ , lb/in						
Applied Stress $\bar{\tau}_{xy}$	$\left(\frac{N_{xy}}{t_o}\right)$	$\left(\frac{N_{xy}}{t_1}\right)$	$\left(\frac{N_{xy}}{t_2}\right)$	1.6	.79	1.27
Diagonal Member $\sigma_D$	Same	Same	$3.3 (N_{xy}/t_2)$	1.6	2.6	4.2
Longit. Member $\sigma_L$	Same	Same	$2.0 (N_{xy}/t_2)$	1.6	1.6	2.5
Cover skin stress $\sigma$	Same	Same	$4.4 (N_{xy}/t_2)$	1.6	3.5	5.6

g. Analysis of Beaded Stiffening for Titanium Panels

The concept of using beaded stiffening to provide compression and shear stability to titanium skins on a multi-spar substructure was examined in detail. The major potential advantage over the honeycomb panel approach would be in eliminating much of the cost and fit-up penalties associated with honeycomb construction.

The concept is illustrated in Figure 42. The external compression panel is stabilized by a thin internal beaded panel with beads running parallel to the direction of loading. The inner panel could consist of individual segments between the spars and ribs or it could be continuous, but unbeaded, over the substructure. The inner panel would be attached to the external skin with adhesives supplemented with mechanical fasteners as required. The inner panel is virtually fully effective in shear which contributes to the overall wing torsional stiffness, GJ.

General instability of the panels in compression and shear was analyzed using the methodology for plates with longitudinal stiffeners given in NACA TN 3782. <sup>(1)</sup> With this method, it was determined that for physically feasible stiffening of this type, a beaded titanium upper skin would not be competitive with the weight of the baseline aluminum upper skin.

A brief analysis was also made of the beaded titanium concept in a lower skin application wherein the reverse bending stability requirements are less severe. Here the beaded panel was compared to a plain titanium panel in a 6-spar design. As an orthotropic panel, the beaded panel was slightly heavier than the isotropic plain panel.

As a result of these investigations, the beaded panel concept was abandoned in favor of the honeycomb panel and full depth core concepts.

(1) Becker, H., Handbook of Structural Stability, Part II - Buckling of Composite Elements, NACA TN-3782, July 1957.

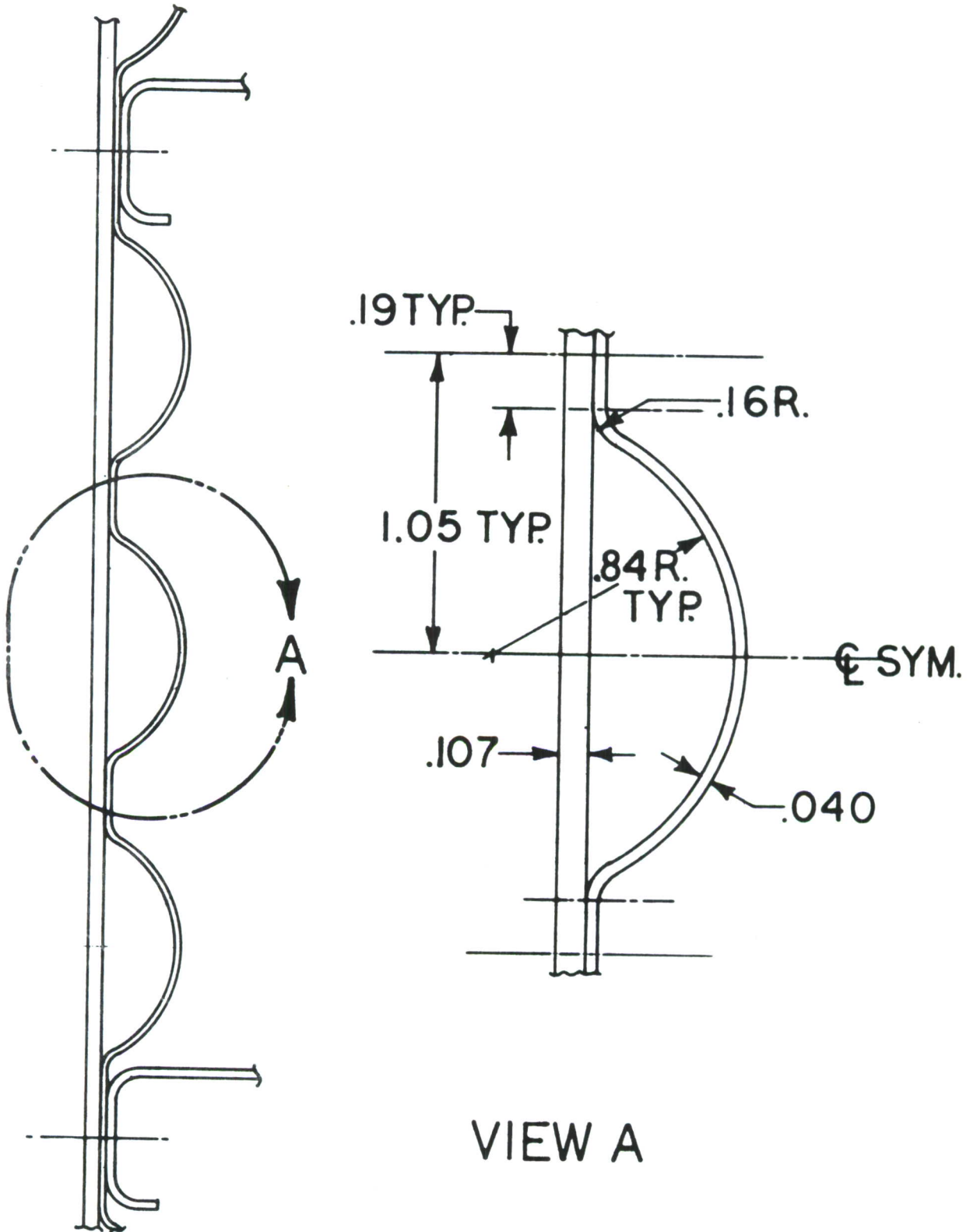


FIGURE 42. TYPICAL BEADED COMPRESSION PANEL



### 3. AEROELASTIC ANALYSIS

Aileron effectiveness and wing flutter studies were conducted to gain insight into what effect potential mass and stiffness changes of the advanced designs would have on these characteristics and to provide design guidance for the advanced design concepts.

#### a. Aileron Effectiveness Studies

The "Quick Look" program<sup>(1)</sup> indicated that aileron effectiveness (or reversal) could be a major design consideration if significant wing stiffness changes occurred in the advanced concepts. Accordingly, a series of aeroelastic stability and control analyses were made to predict the quantitative impact of such changes.

Initially, a 20% cut in both the bending stiffness (EI) and torsional stiffness (GJ) from root to tip was selected as being representative of the advanced concepts. Concurrently, three other stiffness configurations were also explored for comparative purposes:

80% EI, 100% GJ root to tip

100% EI, 100% GJ root to mid span and

80% GJ mid span to tip

100% EI, 80% GJ root to mid span and

100% GJ mid span to tip.

The results of these preliminary studies are shown in Figure 43 as aileron reversal speeds vs. altitude. The corresponding predicted F-5E data are also shown for comparative purposes together with the lg level flight and  $q_{\max}$  curves for the F-5E. The following conclusions were drawn from these data:

---

(1) C. Rosenkranz, et al, Advanced Lightweight Fighter Structural Concept Study, AFFDL TR-72-98, dated July 1972

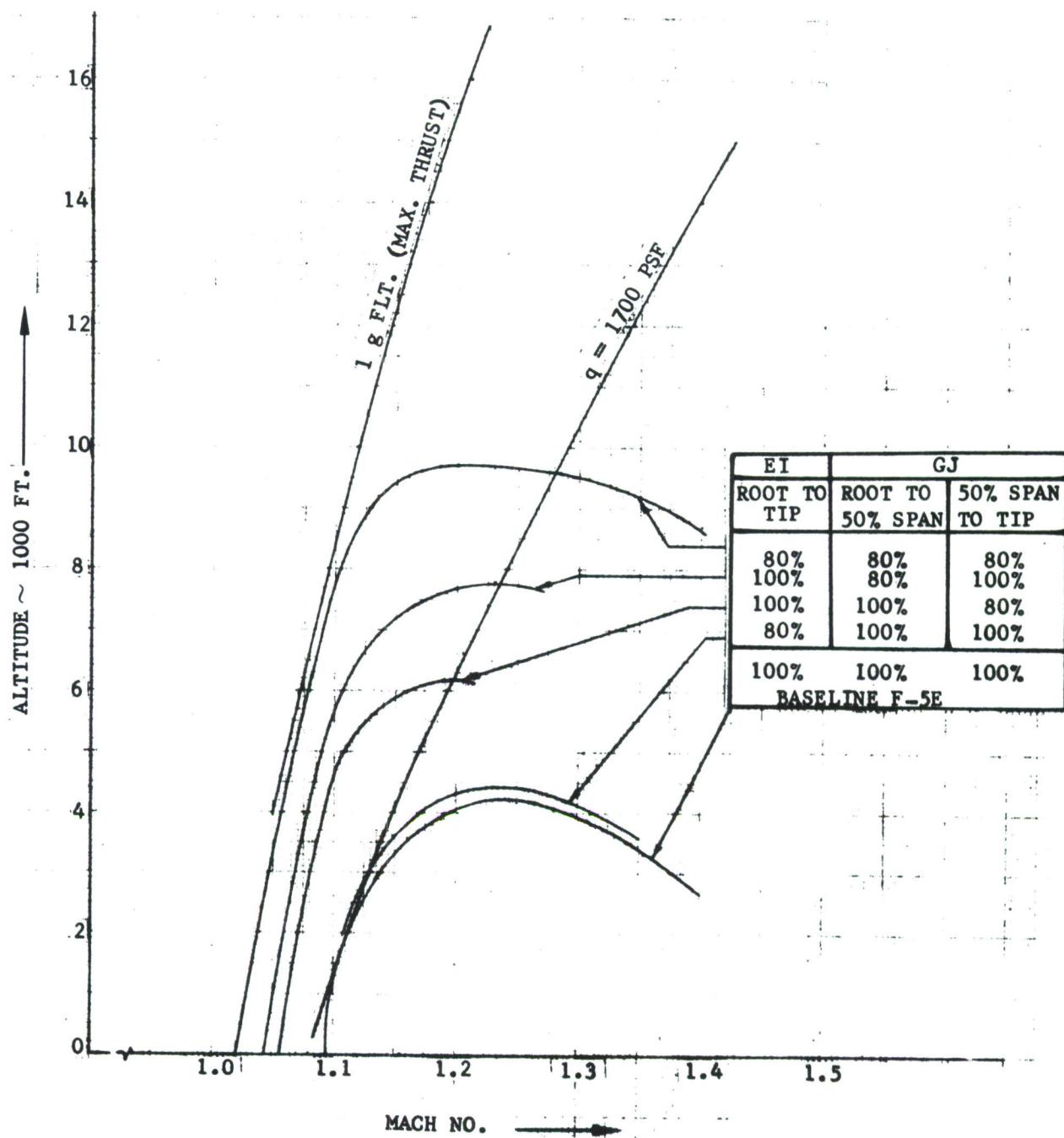


FIGURE 43. PREDICTED AILERON REVERSAL SPEEDS

1. Aileron effectiveness is a definite design consideration. Significant reductions in wing stiffness can have an unacceptable effect on aileron effectiveness or reversal speeds.
2. The wing is relatively insensitive to EI changes -- torsional stiffness changes (GJ) are the predominant consideration.
3. Reinstating torsional stiffnesses over either the inboard half or over the outboard half of the wing did not reinstate aileron effectiveness.

A second more detailed study was then undertaken to determine the best location to add torsional stiffness which would be more efficient than reinstating the F-5E stiffnesses root to tip. Figure 44 shows a plot of wing twist for the rolling maneuver at Mach 1.1,  $q = 1200$  psf and also the derivative of the curve,  $\Delta \alpha / \Delta s$ . This second curve shows that the most effective general location to add reinstating GJ is near the mid semi-span -- predominantly between 40% and 60%. In reality, after including design details and manufacturing considerations, such additional stiffness would generally be concentrated in the area between the landing gear rib (W.S. 73.3) and the inboard pylon rib (W.S. 93.5) and decrease to strength-critical values at the root rib (W.S. 30) and at the outboard pylon rib (W.S. 123).

Concurrently with this study, the F-5E flight tests demonstrated aileron effectiveness margins in the most critical speed-altitude operating range. As a result, the analytical concern depicted in Figure 43 was reduced and it was determined that a moderate reduction in wing torsional stiffness could be allowed for the advanced concepts. Broadly speaking, this reduction was found to be equivalent to a 5% reduction in F-5E torsional stiffness, root to tip.



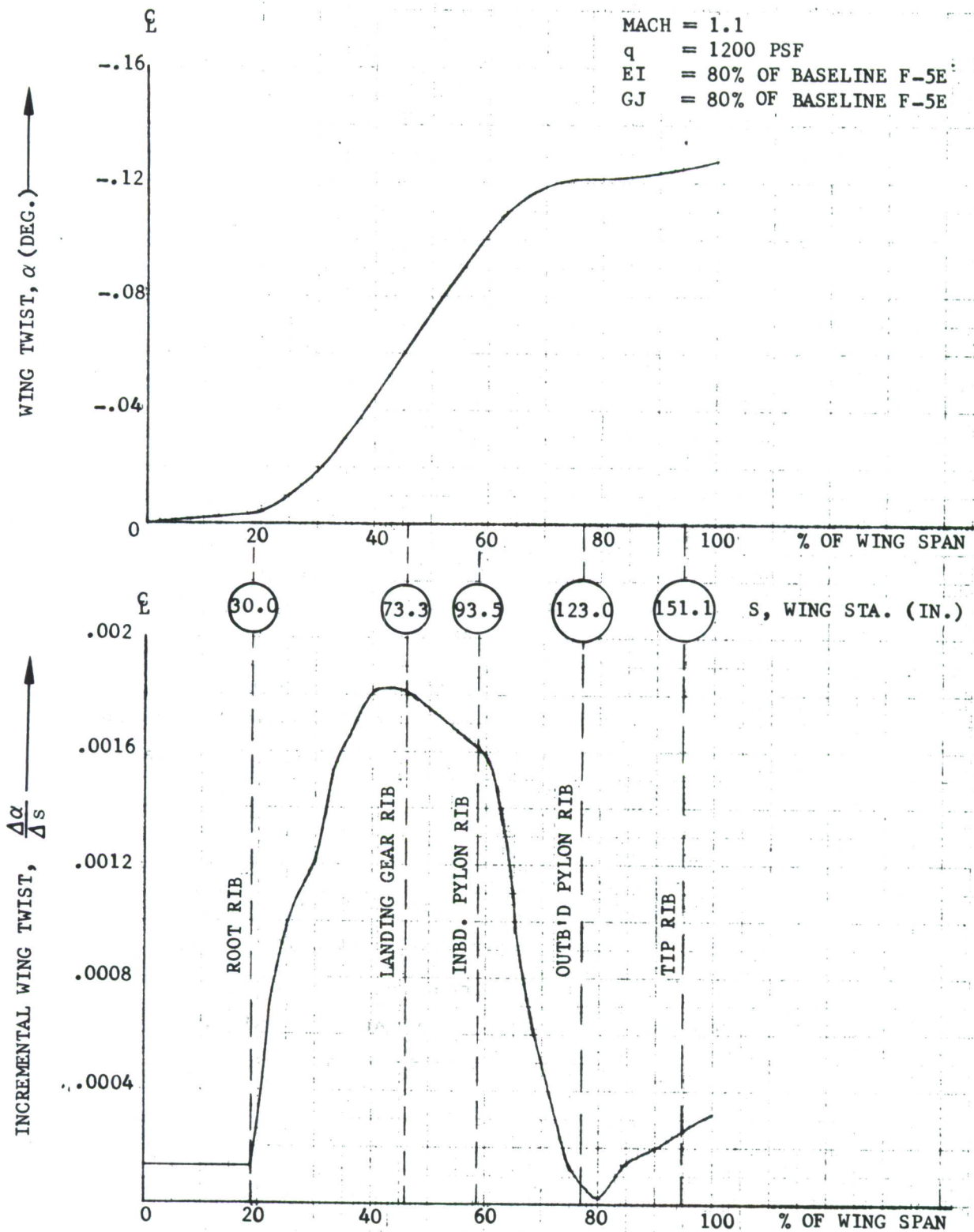


FIGURE 44.. WING TWIST PER DEGREE OF AILERON TRAVEL

A design method was formulated for determining the amount and location of additional wing torsional stiffness (GJ) which might be required of the advanced concepts to insure this degree of aileron effectiveness. A test case and an actual design (Concept 5) were evaluated and stiffened using this method, and were checked by the Aerodynamics Quasi-Stationary Aeroelastic Solution computer program. The aileron effectiveness and reversal speeds were virtually indistinguishable from the desired values.

Spanwise distributions of wing bending and torsional stiffnesses (EI and GJ) were determined for the advanced concepts as initially sized by safe life, damage tolerance, and static strength requirements. The actual stiffnesses versus the allowable 5 percent reduction mentioned above were:

Concept 1	5.4 percent too flexible
Concept 1A	O.K. as designed
Concept 3	O.K. as designed
Concept 3A	O.K. as designed
Concept 4	9.0 percent too flexible
Concept 5	8.0 percent too flexible
Concept 8	3.0 percent too flexible
Concept 8A	3.0 percent too flexible

Three different approaches were considered to supply the required additional stiffnesses. The first is limited to designs with titanium upper wing skins. Here, selected upper panels in the main structural box are replaced with metal matrix Ti-Borsic composite material. These are inserted between the basic titanium spar and rib lands and then electron beam welded to produce a one-piece upper wing skin. This is an effective approach weight-wise and utilizes the very high specific stiffness of this advanced material in non-tension critical areas of the primary structure. The second approach consists of replacing portions of both upper and lower skins of the secondary box structure (that structure aft of the 44% spar and outboard of the landing gear rib) with graphite or boron-epoxy

composite skins. These skins are step-tapered bonded within a narrow titanium frame which contains all panel to rib and spar fastener holes. There are two distinct advantages to this approach. First, much of the secondary structure is removable for aileron bay access, thus splicing penalties are held to a minimum. Secondly, advanced composites can be "tailored" to provide nearly any relationship between shear and extensional stiffness. This allows the secondary box structure to be designed highly effective in torsion (thus utilizing the available enclosed torque box area to best advantage) without also picking up high spanwise loads in the area of the landing gear cutout. The third method consists simply of proportionately increasing the thickness of both the main and secondary box structures. This increases torsional stiffness without adversely affecting the spanwise loads in the secondary structure outboard of the landing gear cutout. Estimated weight penalties for the first and third approaches are summarized in Subsection III-10. The second approach was not analyzed in detail because of the relatively small weight penalties involved with the first two approaches. However, it will certainly be lighter than the all metal solution.

The spanwise distributions of overall wing bending and torsional stiffness after reinstating to the desired rigidities are shown in Figures 45 and 46 together with the baseline F-5E stiffness. These figures show concepts 1, 5, and 8 which cover the range of structural arrangements investigated (i.e., full depth core and multi-spar configurations) and materials used (titanium and aluminum designs). Stiffnesses of other designs are within the range of these plots.

b. Flutter Analyses

The general flutter characteristics initially studied in the "Quick Look" program<sup>(1)</sup> for two store arrangements were expanded to include four more arrangements. The wing model was structurally representative of the advanced

---

(1) C. Rosenkranz, et al, Advanced Lightweight Fighter Structural Concept Study, AFFDL TR-72-98, dated July 1972 (pages 5-130).



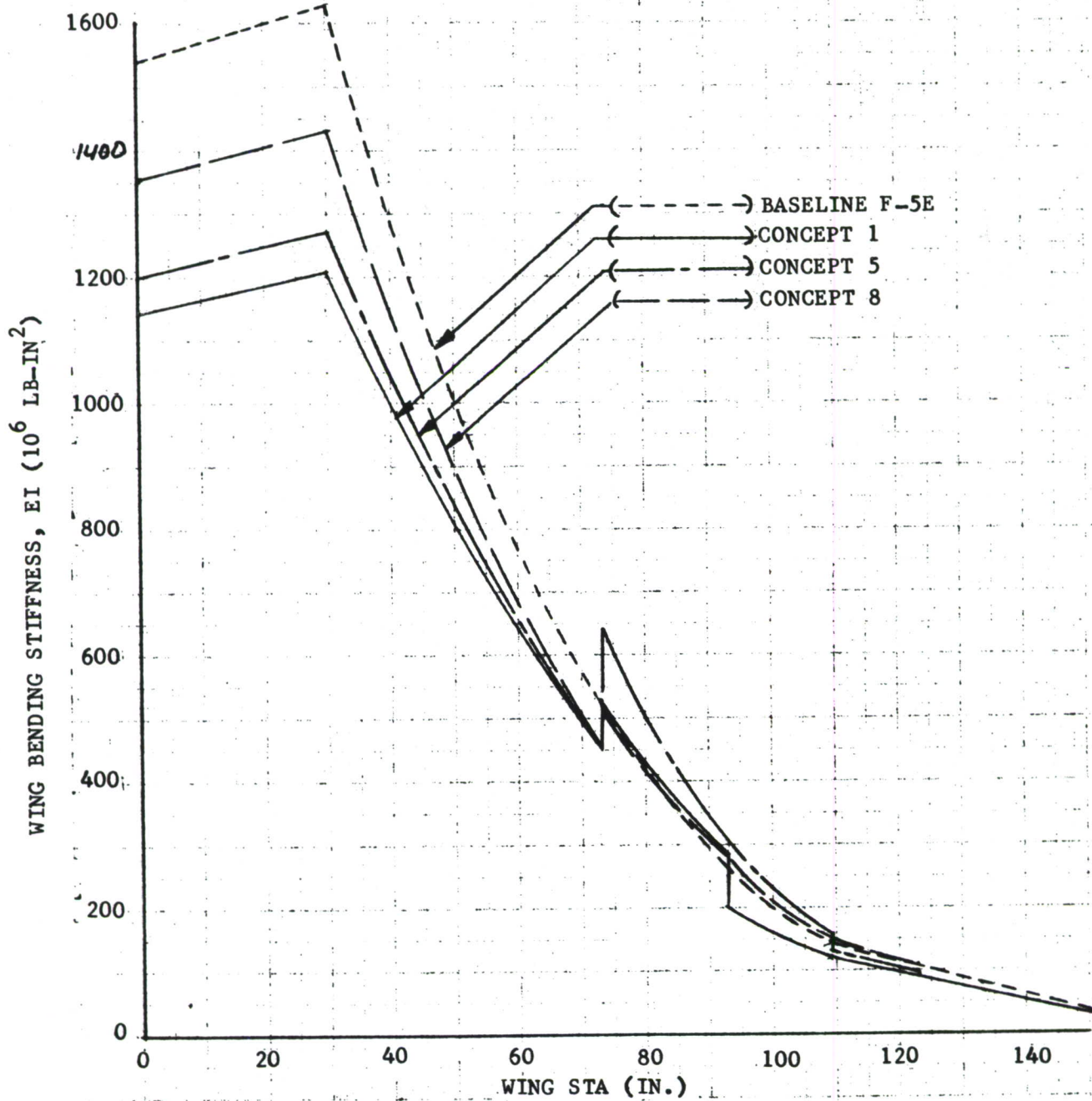


FIGURE 45. WING BENDING STIFFNESSES FOR BASELINE F-5E AND FOR CONCEPTS 1, 5, AND 8

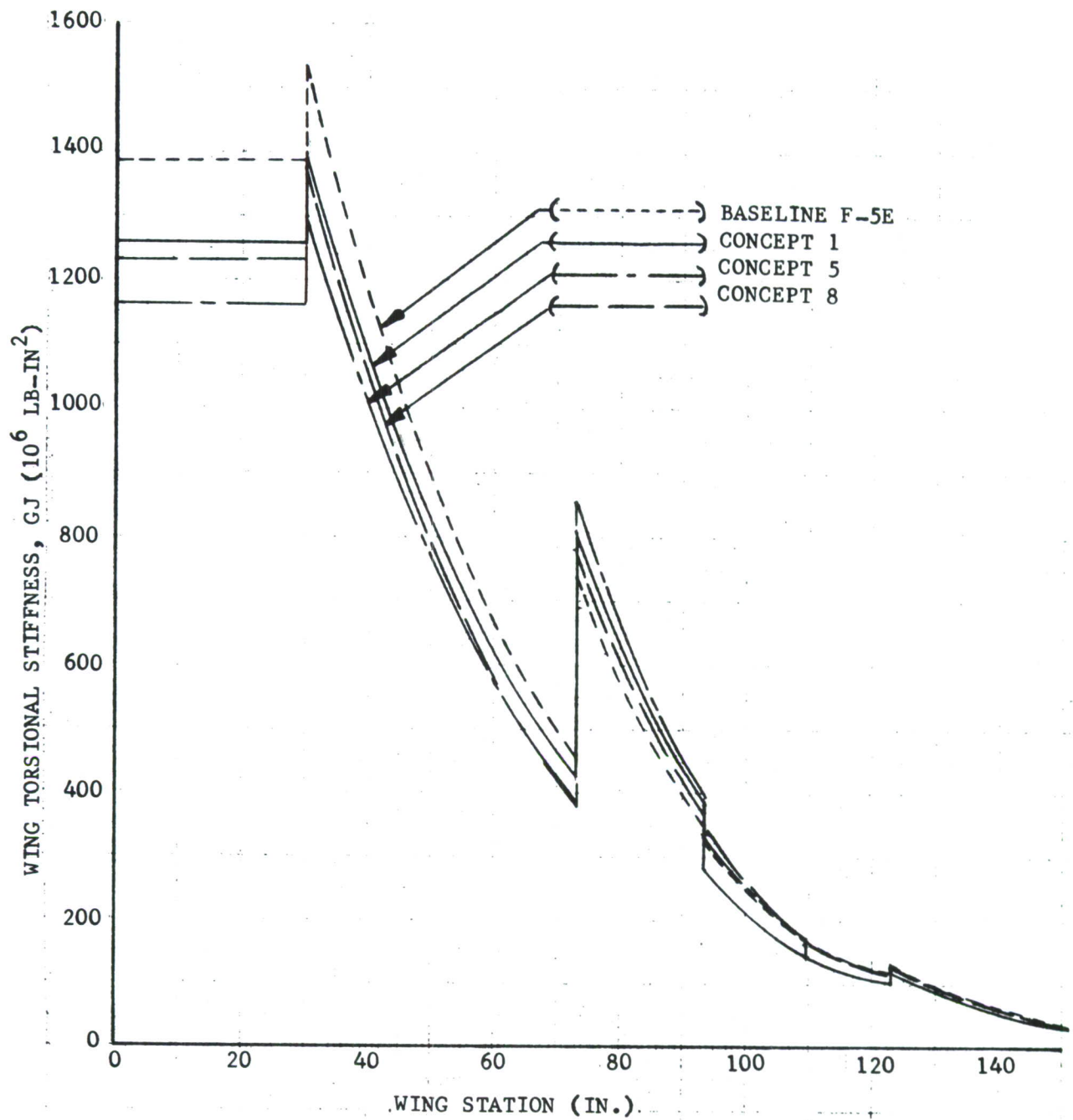


FIGURE 46. WING TORSIONAL STIFFNESSES FOR BASELINE F-5E, AND FOR CONCEPTS 1, 5, AND 8

concepts rather than a discrete model of any one concept. It consisted of an estimated 20 percent reduction of bending and torsional stiffness, root to tip, with attendant weight and mass moment of inertia changes relative to the F-5E baseline wing. Flutter data for this model were developed with the fore and aft position of the wing tip missile launcher as an independent parameter and compared with the corresponding data generated for the baseline F-5E wing. The table below shows the store configuration matrix for this investigation:

	TIP	OUTBOARD PYLON	INBOARD PYLON
Quick Look	AIM-9J	----	BLU-27B(F)
Quick Look	AIM-9J	----	----
Phase 1A	AIM-9J	CBU-24	CBU-24
Phase 1A	AIM 9J	CBU-24	----
Phase 1A	Launcher	----	BLU-27B(F)
Phase 1A	Launcher	----	----

No serious flutter problems were encountered with this model, although considerable shifting between critical symmetric and antisymmetric modes was evident relative to the production F-5E data. For one configuration, however, (tip launcher plus inboard BLU-27B(F)), a 50-knot degradation to 580 knots was indicated, but this would not be significant for operational usage.

These flutter studies did reveal that for most store configurations the ratio of the first bending frequency to the first torsion frequency is in the range of 1.18 to 1.32. This indicates that particular attention should be given to flutter considerations for those designs which have relatively greater torsional stiffnesses in relation to bending stiffnesses than the representative model investigated.



In this regard, the stiffness curves (EI and GJ) shown in Figures 45 and 46 reveal that Concept 8 can be considered flutter-free with a high degree of confidence. The full depth core titanium design (Concept 1), however, shows a proportionately greater reduction in bending stiffness than in torsional stiffness particularly over the inboard half of the wing. In this case, an in-depth flutter analysis of this particular concept for each suspected critical store combination would be necessary before flutter-free performance could be predicted with a similar high degree of confidence. The third recommended concept (Concept 3A), though not shown on the EI/GJ curves is a multi-spar configuration similar to Concepts 5 and 8, but with more inherent rigidity. As such, it will more closely approximate the desired EI/GJ relationship and can reasonably be expected to be a flutter-free design.

#### 4. DAMAGE TOLERANCE ANALYSIS

In this program advanced air superiority wing structure concepts have been designed to satisfy damage tolerant requirements as stated in MIL-STD-1530 and the "USAF Damage Tolerant Criteria" contained in the proposed revision to MIL-A-008866A (see Volume II, Appendix II). Application of this criteria has insured that major emphasis is given in the design phase to analysis of structure containing inadvertent or inherent flaws. Flaw sizes considered are those standing little chance of being detected by existing NDI techniques.

Damage tolerant analysis in support of the design concept studies consists of four main facets, 1) identifying critical damage tolerant structure, 2) establishing an acceptable method of analysis, 3) defining suitable material properties, and 4) development of a representative flight loading spectrum. Careful attention must be given to each of these facets to insure proper application of damage tolerant requirements.

The particular flight loading spectrum used throughout this analysis is a modified version of the basic F-5E design fatigue spectrum. The development of this spectrum is outlined in Volume II, Section III.5.

##### a. Damage Tolerant Critical Structure

Structural components of the advanced design wing concepts have been reviewed for the purpose of identifying damage tolerant critical structure.

The following criteria have been used for selecting critical structure. A structural component must be designed to damage tolerance requirements if:

1. An undetectable inflight failure would (1) cause catastrophic structural failure when operating up to the full required residual strength load for both flight and landing conditions, or (2) endanger safety of flight due to loss of control or by reduction of flutter speed.
2. A detectable inflight failure would preclude a safe return flight to base.

Using the above tests, the following main box structure must be designed to damage tolerance requirements. Refer to Figure 47.

- Lower wing skin inboard of W.S. 123
- Forward (15%) spar from the root rib to W.S. 123

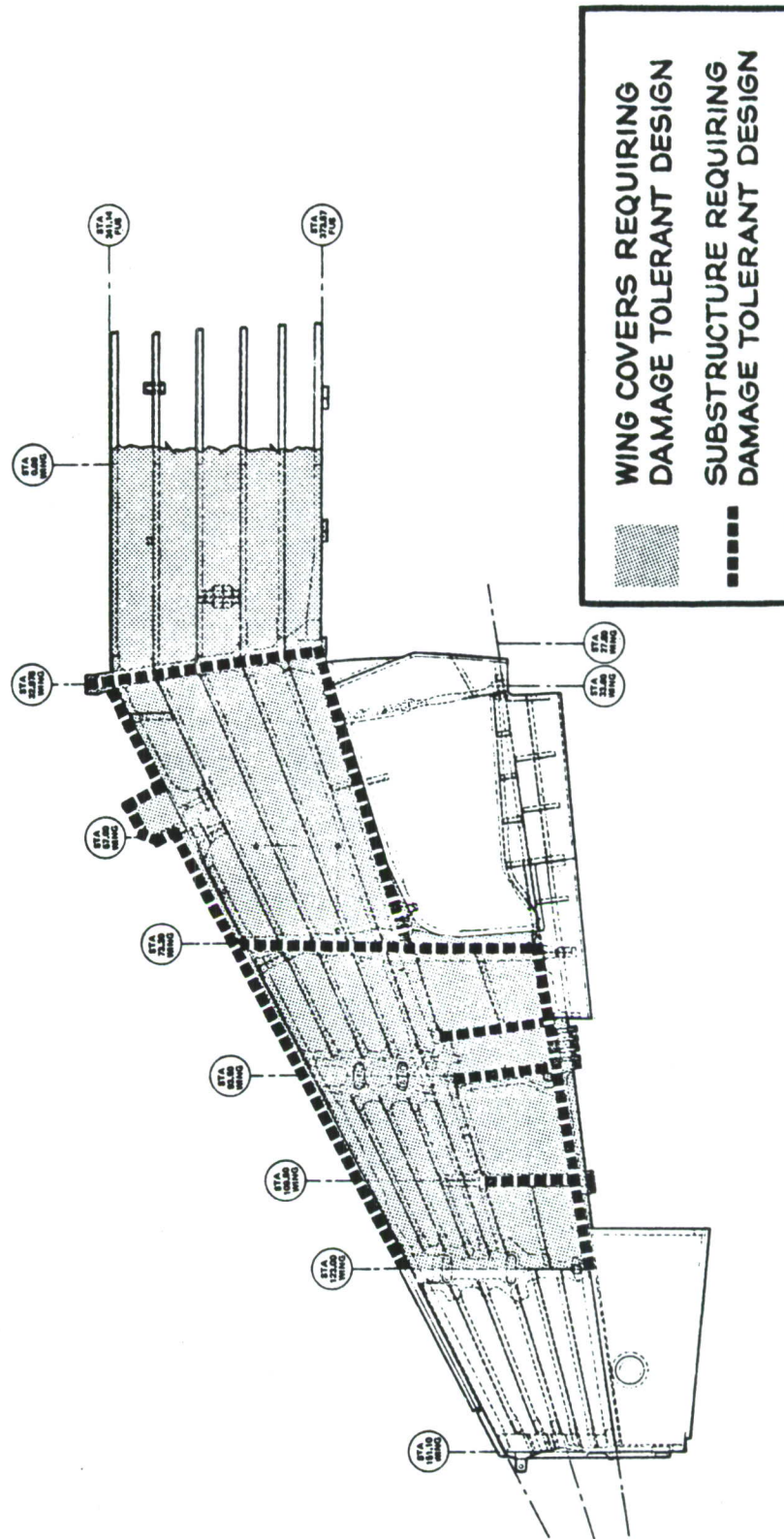


FIGURE 47. F-5E DAMAGE TOLERANT CRITICAL WING STRUCTURE



- 44% spar from the root rib to W.S. 73
- Aft (66%) spar from W.S. 73 to W.S. 123
- Root rib
- Landing gear rib (W.S. 73)
- Aileron back-up ribs at W.S. 84, 93, and 109.

The following main box structures are not required to satisfy the damage tolerance requirement tests listed above; consequently, damage tolerance need not be considered in the design of these structures (in concepts in which they occur):

- Main skins, all spars and ribs outboard of W.S. 123, and the fixed trailing edge structure outboard of W.S. 116.
- Landing gear bay upper panel, 66 percent spar inboard of W.S. 73, and associated trailing structure aft of the landing gear bay.
- Interior spars inboard of W.S. 123. The failure of an interior spar flange will not cause catastrophic failure or loss of control up to the maximum fatigue spectrum load.
- Forward and aft spars in center section between root ribs. The center wing section is not torsion critical because of the four bolt wing to fuselage attachment and the stiff fuselage structure. Consequently, these boundary spars fall in the same category as the interior spars described above.
- W.S. 93 pylon rib and W.S. 123 pylon rib. A failure of this structure may cause loss of the pylon. This would be detectable in flight and would not preclude a safe return flight to base.

In the structure listed as requiring damage tolerant design, the lower wing skin (inboard of W.S. 123) and the 44% spar to skin interface (root rib to W.S. 73) stand out as the most critical. Both of these structural items are subjected to the wing bending spectrum and as such are the most highly loaded tension members. The 15% spar operates at a slightly lower stress due to the decreased box depth, and the ribs will experience a less severe repeated load environment than the skin.

b. Analysis

Unlike the application of more familiar technologies to structural design, such as static strength analysis, damage tolerant analysis methods have yet to be standardized into universally acceptable procedures. Also lacking at this time is sufficient service experience to "test out" the accuracy of particular damage tolerant analytical approaches. The analysis approach defined herein is an attempt to fill this gap by combining engineering judgment with current damage tolerant analysis technology and design criteria. The end result is a crack growth life prediction that reflects some confidence in having accounted for all significant but elusive variables without compromising structural weight and cost.

Due to the variety of design concepts considered in this program, the major damage tolerant analysis emphasis was on a few typical structural details. These are the most critical details in each concept where crack growth in the presence of a flaw may limit the life of that concept. Ultimate damage tolerant design stresses may be determined from crack growth life analysis of these details using the appropriate combination of materials and local geometry for a given advanced concept. This design stress would then be compared to static and fatigue design stresses to determine the minimum requirement. With the exception of the geodesic skin concept, all lower skin arrangements are monolithic, designed to slow crack growth requirements. Three types of typical structural details must be considered, depending on the skin to spar attachment arrangement.

(1) Nonmechanically Fastened

Spar shear webs that are integral, bonded (such as full-depth honeycomb), or welded to the lower skin, are considered a typical detail for flaw analysis purposes. In this case the lower skin would be checked for crack growth from a surface flaw. Initial damage size is defined as  $a/q = 0.10$ . Flaw aspect ratio,  $a/2c$ , may be assumed from 0.10 to 0.50. For the thicknesses investigated in this program the shallower flaw ( $a/2c = 0.10$ ) was the more severe.

However, when compared to tensile ultimate design allowables, the surface flaw ultimate design stresses are always higher. Thus, for the combination

of materials Ti-6Al-4V  $\beta$ MA, 7475-T7651, and 2048-T851) and thickness (0.30 to 0.45 inches) considered in the nonmechanically fastened concepts, surface flaw requirements were not critical.

## (2) Mechanically Fastened

Spar flanges mechanically fastened to the lower skin panel must be evaluated considering multiple flaws (flaws in both flange and skin at common fastener holes), inspectability, flange failure effect on skin, and load transfer effects on crack growth. Possible crack growth retardation at fastener holes due to special fastener systems or hole preparation were ignored insofar as meeting the crack growth service life requirements is concerned.

As mentioned in the preceding discussion on damage critical structure, two typical structural details are the most critical, the 44% spar to skin interface, and the interior spar to skin interface.

### (a) 44 Percent Spar

The 44 percent spar was classified as non-inspectable in that a flaw in the spar flange is not inspectable by any of the techniques allowed under paragraph 1.1.1.5 of the damage tolerant criteria (Volume II, Appendix II). This indicates that the 44 percent spar must meet a slow crack growth requirement of 2 lifetimes (8000 hours) with a minimum assumed initial damage of an 0.05 through flaw at a hole. Subsequent crack growth analysis indicated that this flawed aft spar was less critical than the flawed interior spar to skin interface. This is due primarily to its greater flange width and reduced fastener load transfer at the flawed hole (aft spar to skin attachments are sized mostly by torsional induced shear requirements). Therefore the 44 percent spar damage tolerance is only a factor in the absence of interior spars.

### (b) Interior Spar to Skin

Defining a critical mode of failure for the interior spar to skin interface presented a problem since there is a question of how to account for damage in the interior spar flange. Remembering that the interior spar flange was classified as not critical to flight safety, service failure of



the flange may therefore be allowed. What must be determined is what impact this failure has on the skin panel, consistent with the damage tolerant criteria.

The necessary analysis assumptions are discussed in Volume II, Section III. In this Volume II discussion, two methods of analysis are considered:

1. Crack growth at the common flawed hole taking into consideration stress buildup in the skin due to the spar flange failure, and
2. Crack growth at the adjacent hole taking into account stress buildup as well as high load transfer into the skin resulting from a discontinuous spar flange.

High load transfer only occurs at the adjacent fastener since the spar flange is discontinuous at the common flawed hole and is unloading at the adjacent hole. In application of the above methods to design studies, method 2 produced somewhat shorter crack growth lives than the first method.

In the interest of a conservative design approach, method 2 was used in the design concept studies with interior spars. As pointed out in Volume II, Section 3.2, a 0.05 fatigue initiated flaw is assumed to exist at the skin fastener hole due to high load transfer from the failed spar flange. This flaw is present at the instant of spar flange failure.

All crack growth analysis has been based on curve fit to constant amplitude crack growth rate data using the Forman et al equation, <sup>(1)</sup>

$$da/dN = \frac{C (\Delta K)^n}{(1-R)K_{cf} - \Delta K}$$

in conjunction with the CRACKS computer program.  $K_{cf}$  is a "dummy" critical stress intensity value to facilitate curve fitting. Actual crack growth is terminated at  $K_c$ . C and n are materials constants and R is the stress intensity ratio  $K_{MIN}/K_{MAX}$ .

---

(1) Forman, R. G., Kearney, V. E., and Engle, Jr., R. M., "Numerical Analysis of Crack Propagation in Cyclic-Loaded Structures," Journal of Basic Engineering, Trans. ASME Series D, Vol. .89, No. 3, 1967.

Retardation predictions for variable amplitude loading have been determined by the Willenborg retardation model.<sup>(1)</sup> Plastic zone sizes were based on assumed plane strain conditions in the aluminum skin panels, plane stress in the titanium skin panels, and plane stress in the spar cap. The crack tip stress intensity,  $K_I$ , for a through crack emanating from a hole is,

$$K_I = \sigma \sqrt{\pi a} f(a/r) f(a/w) f(a/p)$$

where  $f(a/r)$  is the Bowie magnification factor for flawed hole analysis and  $f(a/w)$  is the finite width correction factor.<sup>(2)</sup> Residual strength limitation on crack growth life is determined from the maximum spectrum load, which is slightly greater than design limit.

The factor  $f(a/p)$  is a magnification factor to account for bearing load in the skin hole. This factor was approximated by an assumed linear relation between peak stresses (due to bearing loads) at the hole edge and gross stresses at the edge of the spar flange. The effects of interference fits, load transfer across the fastener head, etc., were ignored. This adjustment resulted in approximately a 35% increase in initial stress intensities, approaching the open hole value as the crack grew. Crack growth life prediction was based on the average of the computed variable load amplitude retarded and non-retarded lives. This was an attempt to account for possible time dependent retardation relaxation effects and variations in analysis parameters. The latter was in anticipation of the criteria sensitivity study results reported in Volume II.

The result of a typical analysis is shown in Figure 48 for Ti-6Al-4V  $\beta$  MA. A complete listing of pertinent damage tolerant design stresses for each concept is contained in Tables VII and VIII.

- 
- (1) Willenborg, J., Engle, R. M., and Wood, H. A., "A Crack Growth Retardation Model Using an Effective Stress Concept," AFFDL-TM-71-1-FBR, January 1971.
- (2) Wilhem, D. P., "Fracture Mechanics Guidelines for Aircraft Structure Application," AFFDL-TR-69-111, February 1970.

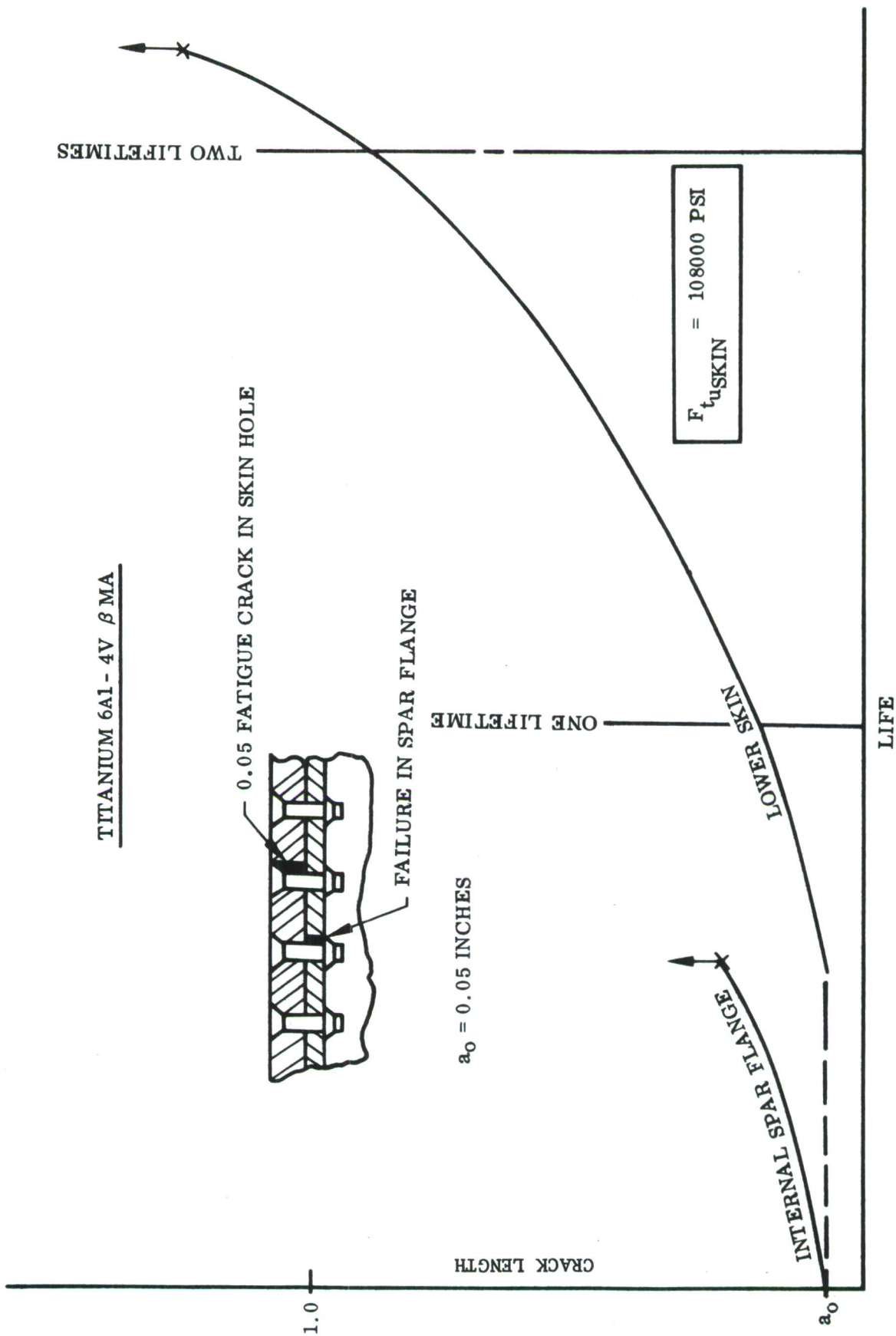


FIGURE 48. INTERNAL SPAR AND LOWER SKIN FAILURE ANALYSIS



### c. Material Properties

The method of damage tolerant analysis described in the preceding section requires the use of certain basic material properties. These basic properties are constant amplitude crack growth rate data and fracture toughness data for each damage critical material investigated.

The damage critical materials of interest here are those used in the primary tension application, the lower, inboard, wing skin, and lower spar flange:

#### Lower Inboard Skin Panel

2048-T851 Aluminum Plate

7475-T7651 Aluminum Plate

Ti-6Al-4V  $\beta$ MA Plate

#### Spars (Interior and 44%)

7050-T736 Precision Forging

Ti-6Al-4V  $\beta$ MA Precision Forging

Ti-6Al-4V  $\beta$ MA Sheet

While the interior spar flanges are not classified as damage critical structure, their failure does affect crack growth in the skin and therefore must be considered in the analysis.

In general, damage tolerant analysis in support of design concept studies was based on preliminary material properties obtained from a variety of literature sources. These properties were checked against test data developed in this program as it became available. Preliminary damage tolerant design stress levels were found to be fairly accurate in most cases and usually within the limits of expected variations in crack growth rate and fracture toughness data.

#### (1) Crack Growth Rate Data

Design curves for 7475-T76 and Ti-6Al-4V  $\beta$ MA are plotted in Figures 49 and 50, respectively. Also included are the appropriate data from the materials Test Program (Volume III), both dry air and 3.5% NaCl salt solution results.

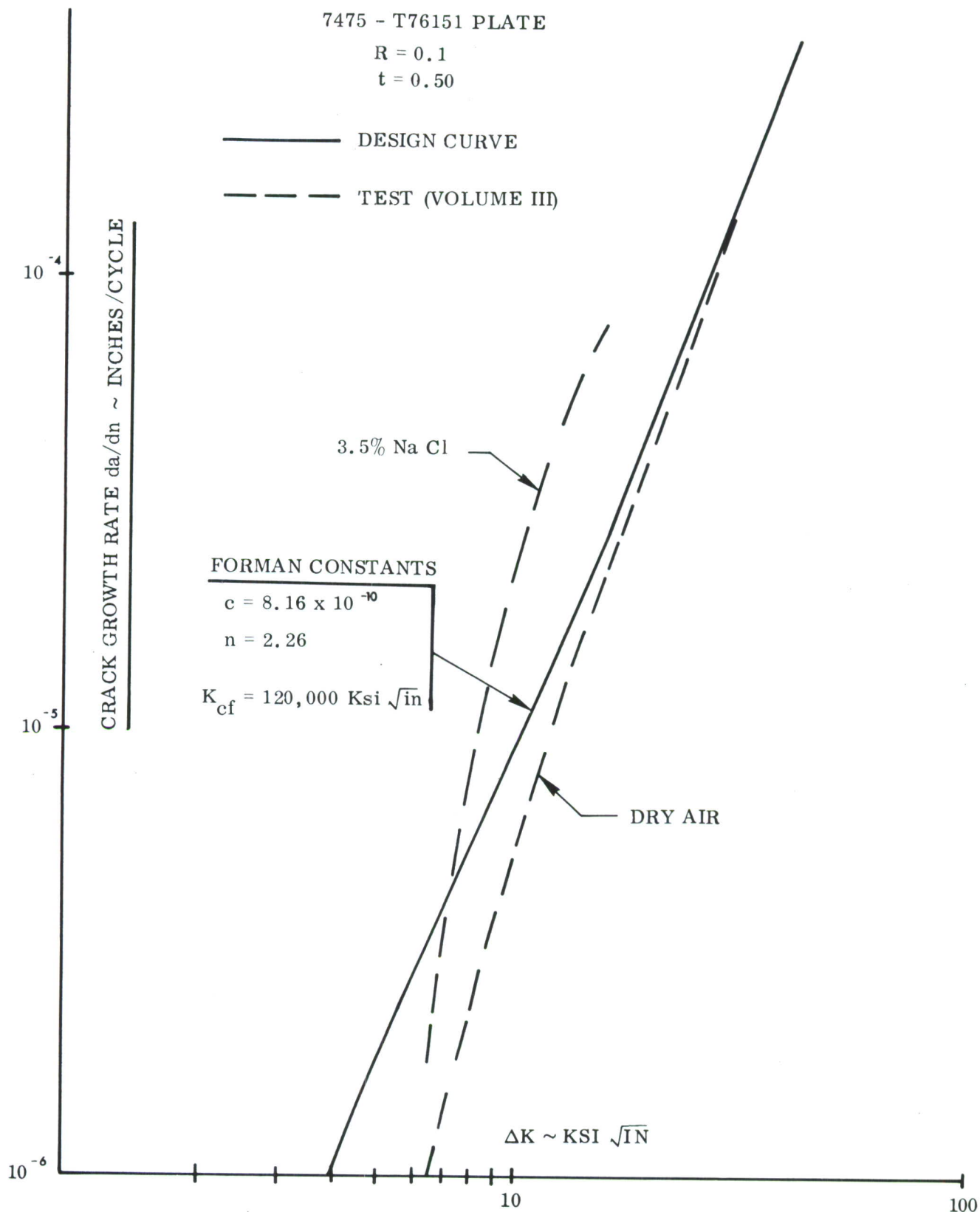


FIGURE 49. 7475-T76 PLATE CRACK GROWTH RATE COMPARISON, TEST VS. DESIGN.

Ti-6Al - 4V  $\beta$  MA PLATE

R = 0.1

t = 0.30

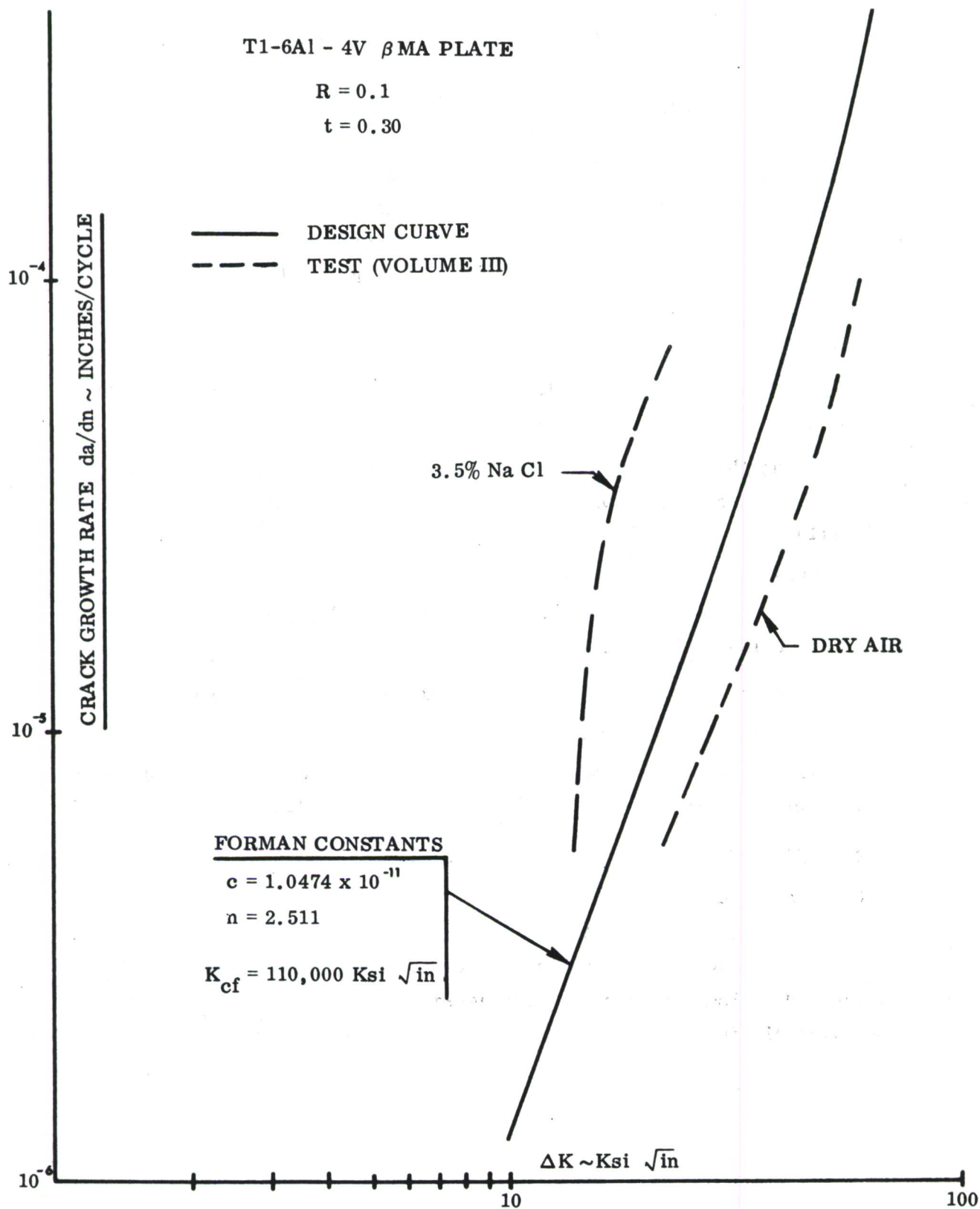


FIGURE 50. Ti-6Al-4V  $\beta$  MA PLATE CRACK GROWTH RATE COMPARISON, TEST VS. DESIGN



As can be seen from these curves, the design values appear fairly reasonable in comparison to the test data. In this case a "reasonable" environment is considered to be between the two extremes, salt solution and dry air, and somewhat closer to the dry air in terms of environmental effects on crack growth. The test data indicates faster growth rates above approximately  $\Delta K = 30 \text{ Ksi} \sqrt{\text{in.}}$  than used in analysis for the 7475-T76 material. However, this is not considered a problem since only 15% of the crack growth occurs at  $\Delta K$  values of  $30 \text{ Ksi} \sqrt{\text{in.}}$  or greater.

Materials test data for 7050-T73651 and vendor supplied data for 2048-T851 are compared in Figure 51 to the 7475-T76 design curve, assumed applicable in preliminary analysis of these alloys as well. On the basis of this comparison, it appears that this has been a conservative assumption.

Regarding the remaining damage critical materials, the following conclusions have been reached based on evaluation of the test data (see Volume III):

1. There is no significant difference between 7050-T7651 and 7050-T73651 plate crack growth rates in either dry air or 3.5% NaCl solution.
2. Crack growth rates are slower in 7050-T736 forging than in 7050-T73651 plate.

On the basis of this last conclusion, Ti-6Al-4V  $\beta$ MA precision forging crack growth rates are assumed no higher than those in the plate stock.

## (2) Fracture Toughness

Critical stress intensity ( $K_{IC}$ ) values essentially define the critical crack length under given spectrum stresses. For design purposes these values were selected as  $60 \text{ Ksi} \sqrt{\text{in.}}$  for the aluminum and  $110 \text{ Ksi} \sqrt{\text{in.}}$  for Ti-6Al-4V  $\beta$ MA. These values are considered sufficiently representative for these materials in the thickness ranges investigated.

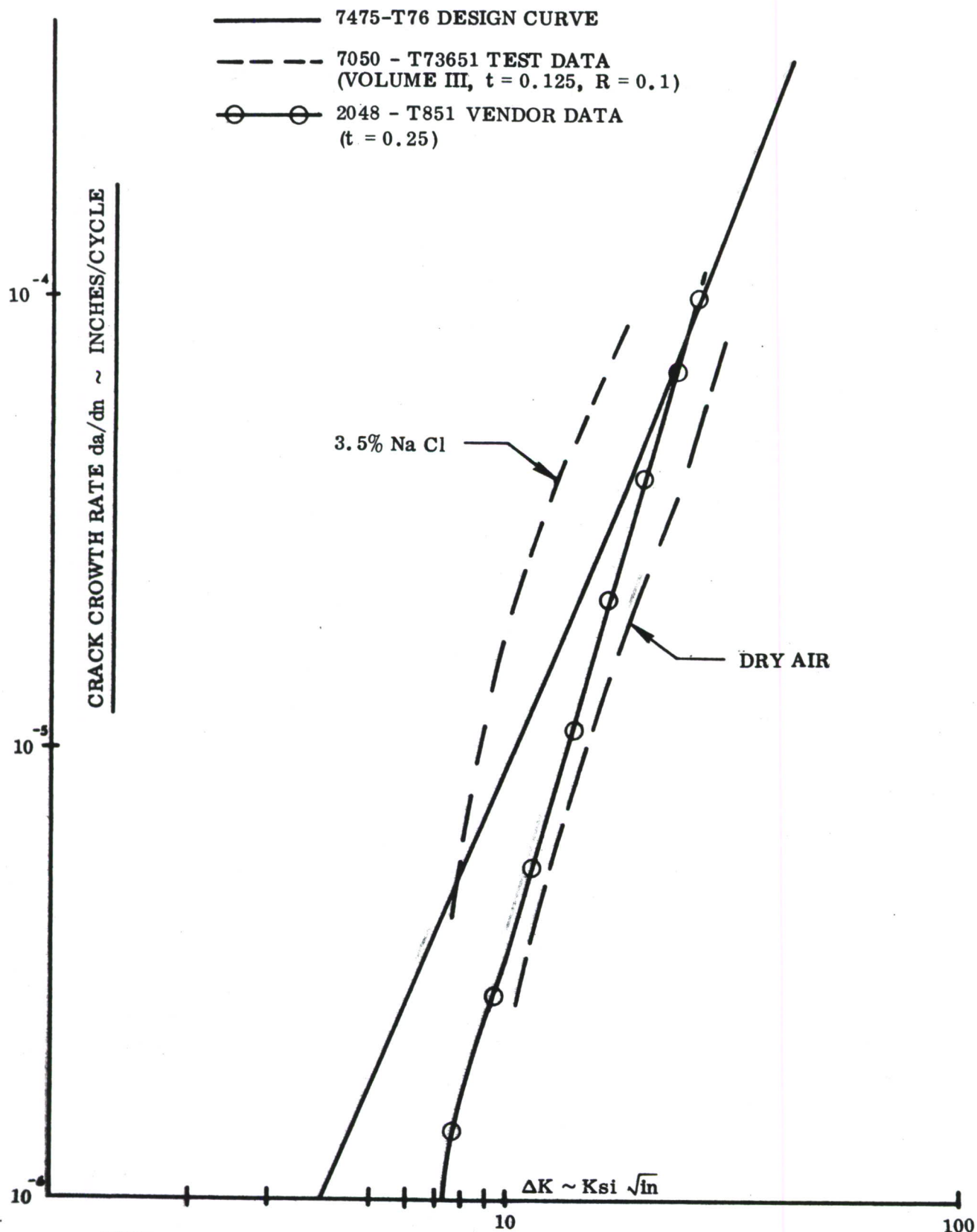


FIGURE 51. CRACK GROWTH RATE COMPARISON OF ALUMINUM ALLOYS.

## 5. FATIGUE ANALYSIS

Fatigue analysis has been used in this program for predicting and controlling crack initiation as a means of assuring adequate safe life in the advanced concepts. The fatigue life goal is identical with the F-5E baseline requirement, 4000 service hours, or 16,000 design service hours. This safe life requirement is considered a primary requirement for structure vital to the integrity of the vehicle or to personnel safety and is in addition to the damage tolerance requirements (see Section III.4). The lower wing skin is the most fatigue critical structural component, and the principal effort was in analysis of materials for this structure.

In general, the approach is preliminary design in nature in that spectrum usage and predicted fatigue quality is based on experience with the baseline or similar structural systems. This information is then combined with appropriate S-N fatigue data through cumulative damage analysis to determine fatigue design stresses. These stresses are compared with static and damage tolerant design stresses to determine the minimum design requirement for structural weight assessment.

### a. Spectrum Development

The fatigue loads spectrum for the F-5E baseline is fully developed and described.<sup>(1)</sup> This spectrum is a comprehensive service loads spectrum representing all external load variables which affect fatigue evaluation. The total spectrum encompasses thousands of possible combinations of weight, c.g. location, store configuration, flap position, maneuver, etc., and was intended for use in a rigorous computer analysis of F-5E details involving well defined materials.

The requirements of this program to develop advanced and innovative wing concepts indicated that a more streamlined and condensed spectrum would greatly facilitate material selection and design trade-off studies. Along with the need for a high confidence, simplified spectrum, was the practical requirement of restricting or limiting the number of wing stations

---

(1) Joyce, R. E., and Fortier, M., "F-5E Structural Fatigue Criteria Report," Northrop Corporation, Aircraft Division Report NOR 71-214, December, 1971.



to be evaluated, since each spanwise wing station has an individual spectrum due to the many load variables acting on the wing.

With these needs in mind, a careful evaluation of fatigue critical areas on the baseline F-5E wing was made. This evaluation indicated that the geometric constraints which led to critical areas on the baseline would be inherent in all new wing concepts, creating similar fatigue critical areas. These areas are shown as the shaded area in Figure 52 and are identified principally as the lower wing skin from the wing root to the inboard pylon, and the wing root ribs which extend from the wing fore and aft, attaching the wing to the fuselage.

On all new concepts, the root ribs have improved section properties, resulting in less operating stresses than on the baseline. Therefore, the root ribs on all new concepts will preserve at least the same fatigue life as the baseline, and do not require additional fatigue life substantiation.

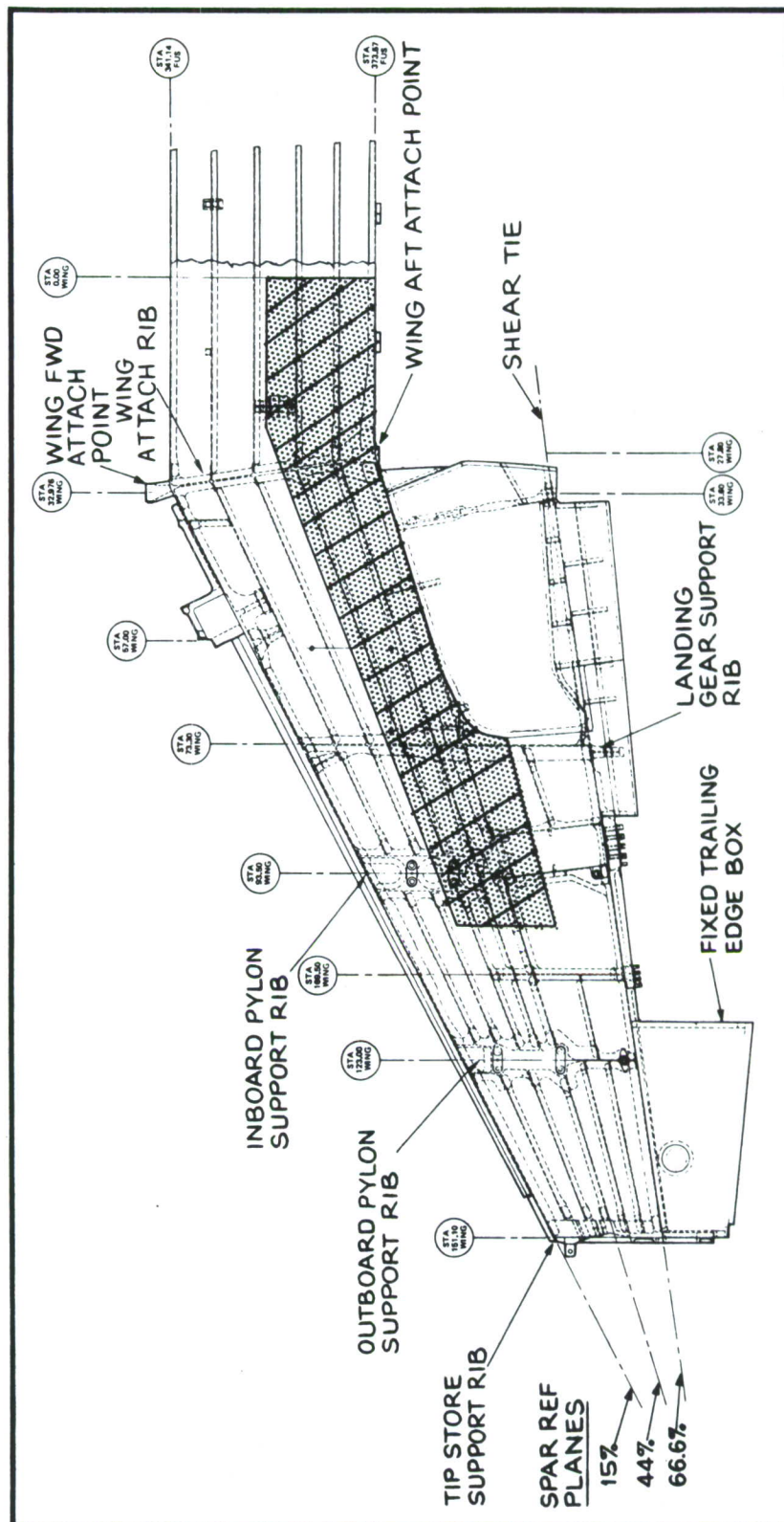
The most fatigue critical areas on the lower wing skin are at the root rib area around wing station 30, and at the landing gear rib area at wing station 73 where the wheel well cut out ends. Thus, stations 30 and 73, plus station 93 near the inboard pylon rib, were selected as the three locations where fatigue analysis would be made on all new concepts.

An individual fatigue spectrum was developed for each of these three wing stations. The object of this procedure was to condense the spectra in such a manner that damage predicted by using the condensed spectra would be equal to that predicted by using the full comprehensive spectra.

The procedure used to develop these condensed spectra will be briefly described using the wing root spectrum as a typical example.

A thorough evaluation of all contributing factors to fatigue loads indicated the following significant sources of load at the wing root area:

1. Symmetrical maneuvers
2. Roll maneuvers
3. Abrupt pitch maneuvers



4. Ground-air-ground, or peak to peak once per flight loads
5. Landing impact
6. Vertical gusts.

Through rational combining, lumping, and adjusting, using both statistical and empirical techniques, the spectrum generated by the above six sources was reduced to 205 load levels, each level occurring a certain number of cycles in the 4,000 hours total lifetime of the aircraft.

This 205 level spectrum was then used to establish an index  $K_t$  for all subsequent analysis. The specific objectives of the program require all new concepts to maintain the same life as the baseline. Original F-5E fatigue analysis showed projected component lives exceeding the design target of 16,000 hours by various amounts. Rather than compare each new concept detail to target lives variously exceeding 16,000 hours, a rationalized approach was taken which assumed that the baseline had a uniform life of 16,000 hours. The design  $K_t$  was then analytically determined which would give this 16,000 hour life. In the case of the baseline spectrum operating on baseline S-N curves, the derived  $K_t$  for 16,000 hours was 3.65. This  $K_t$  of 3.65 was then established as the index  $K_t$  for evaluating all new concepts using similar design methods and construction details as the baseline F-5E.

The 205 level spectrum was then further condensed and combined into a more useful 33 level spectrum which gave the same analytical fatigue damage as the 205 level spectrum at a  $K_t$  of 3.65. This streamlined spectrum then became the analytical spectrum used to evaluate new concept materials and designs. The spectrum for the wing root is shown in Table XIII.

The same procedure described above was used at wing stations 73 and 93 to develop condensed spectra which were equivalent in severity to the full F-5E spectra.

The basic condensed spectra are load level spectra, and as such, are applicable to all new concepts since wing loads will remain the same as on the baseline. The stresses which these moments generate in a given structure depend principally on the geometric properties of the wing cross section, or more specifically, on the thickness of the lower and upper wing skins.



TABLE XIII

CONDENSED BENDING MOMENT SPECTRUM - WING STA 29.50

LAYER	M <sub>Min</sub> (in/lb)	M <sub>Max</sub> (in/lb)	M <sub>Mean</sub> (in/lb)	M <sub>Alt</sub> (in/lb)	OCCURRENCES PER 4,000 HRS.
1	0	246000	123000	123000	1774
2	↑	367000	184000	184000	22622
3	↑	446000	223000	223000	6584
4	↑	574000	287000	287000	506
5	↑	713000	356000	356000	135
6	↓	908000	454000	454000	30
7	0	1109000	554000	554000	3247
8	107000	1615000	861000	754000	52
9	107000	1747000	927000	820000	14
10	107000	1903000	1005000	898000	12
11	141000	380000	261000	120000	14618
12	↑	467000	304000	163000	12444
13	↑	563000	352000	211000	12976
14	↑	675000	408000	267000	10496
15	↑	789000	465000	324000	6741
16	↑	916000	529000	388000	5143
17	↑	1040000	591000	450000	1641
18	↓	1153000	647000	506000	572
19	↓	1299000	720000	579000	319
20	141000	1481000	810000	670000	102
21	222000	420000	321000	99000	29348
22	↑	535000	378000	156000	19894
23	↑	634000	428000	206000	18649
24	↑	741000	482000	260000	12982
25	↑	850000	536000	314000	5954
26	↑	949000	586000	364000	4462
27	↓	1029000	626000	404000	2220
28	↓	1158000	690000	468000	1553
29	222000	1414000	818000	596000	115
30	307000	618000	463000	156000	4230
31	↑	904000	605000	298000	976
32	↓	1178000	743000	436000	178
33	307000	1515000	911000	604000	13

This relationship can be expressed as follows:

$$\frac{f_{\text{operating}}}{M_{\text{operating}}} = \frac{F_{\text{ult.}}}{M_{\text{ult.}}} = \text{constant}$$

Once the loads and the design of any aircraft wing are established, the above relationship, stress divided by moment, for a particular location, is a constant ratio. If S-N data is available for the new material, the stress spectrum can be adjusted by varying this constant until a value is determined which results in a 16,000 hour fatigue life at a  $K_t$  of 3.65. The ultimate design stress allowable is then readily found by multiplying this derived constant by the ultimate wing moment at the section being investigated.

In the case of the concept involving the use of X2048-T851 thick plate machined with integral spar webs, the skin areas between ribs from wing stations 30 to 73 and from 73 to 93 have a significantly reduced  $K_t$  factor due to the absence of bolts or joints of any type along the skin surface. In these areas, a  $K_t$  of 2.0 was judged reasonable for analysis since unknown residual stresses and material handling nicks and scratches prevent the elimination of stress concentrations.

#### b. Material Properties

The materials selected for the three final design concepts are summarized as follows:

##### Lower Wing Skin

7475-T7651 Plate

2048-T851 Thick Plate

Ti-6Al-4V Beta Annealed Plate

##### Spars

7050-T736 Precision Forging

Ti-6Al-4V Beta Annealed Formed Sheet

Ti-6Al-4V Beta Annealed Precision Forging.

S-N curves for the selected aluminum alloys are presented in Figure 53 and the titanium alloys in Figure 54. Curves shown for 7475-T7651 and

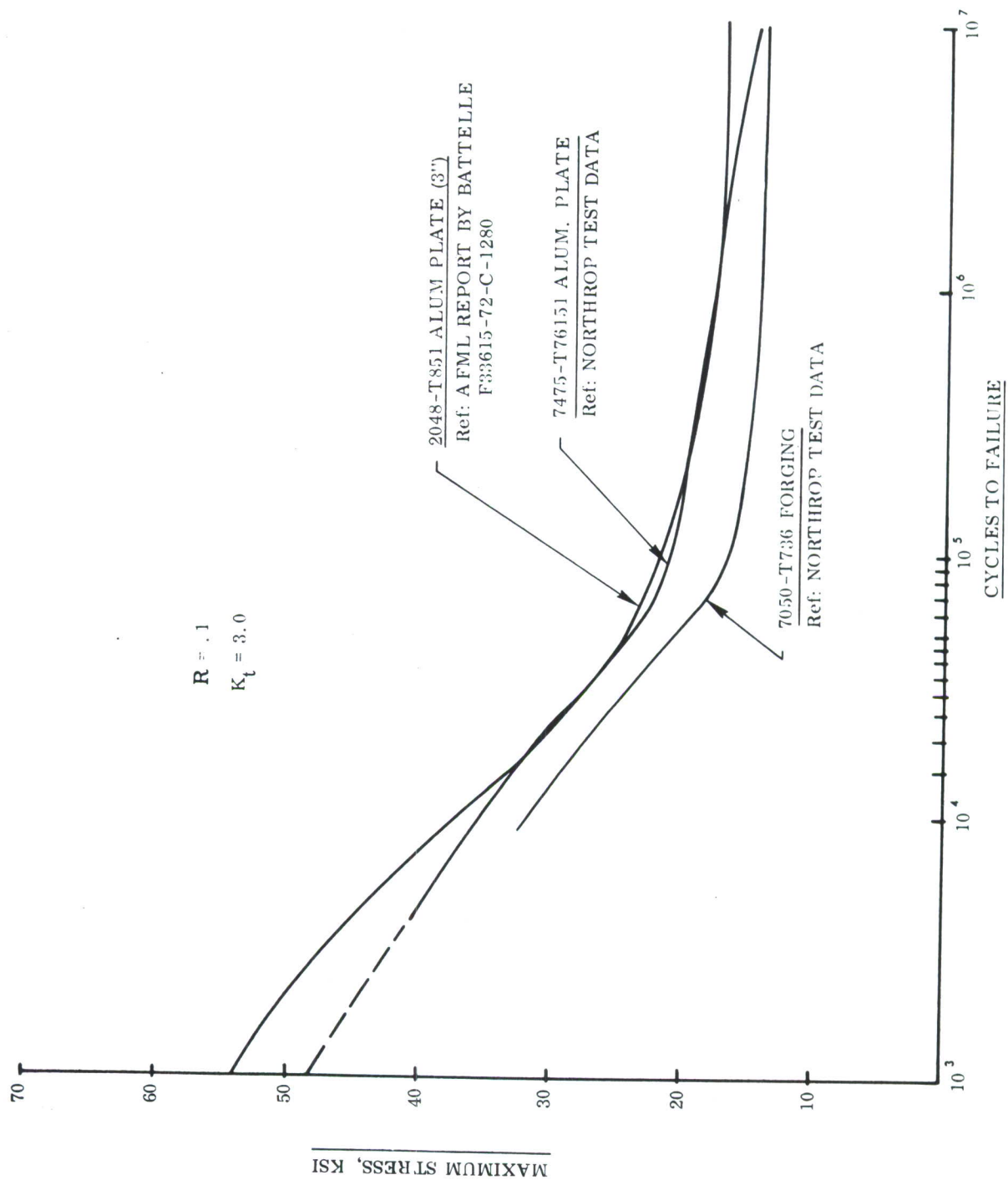
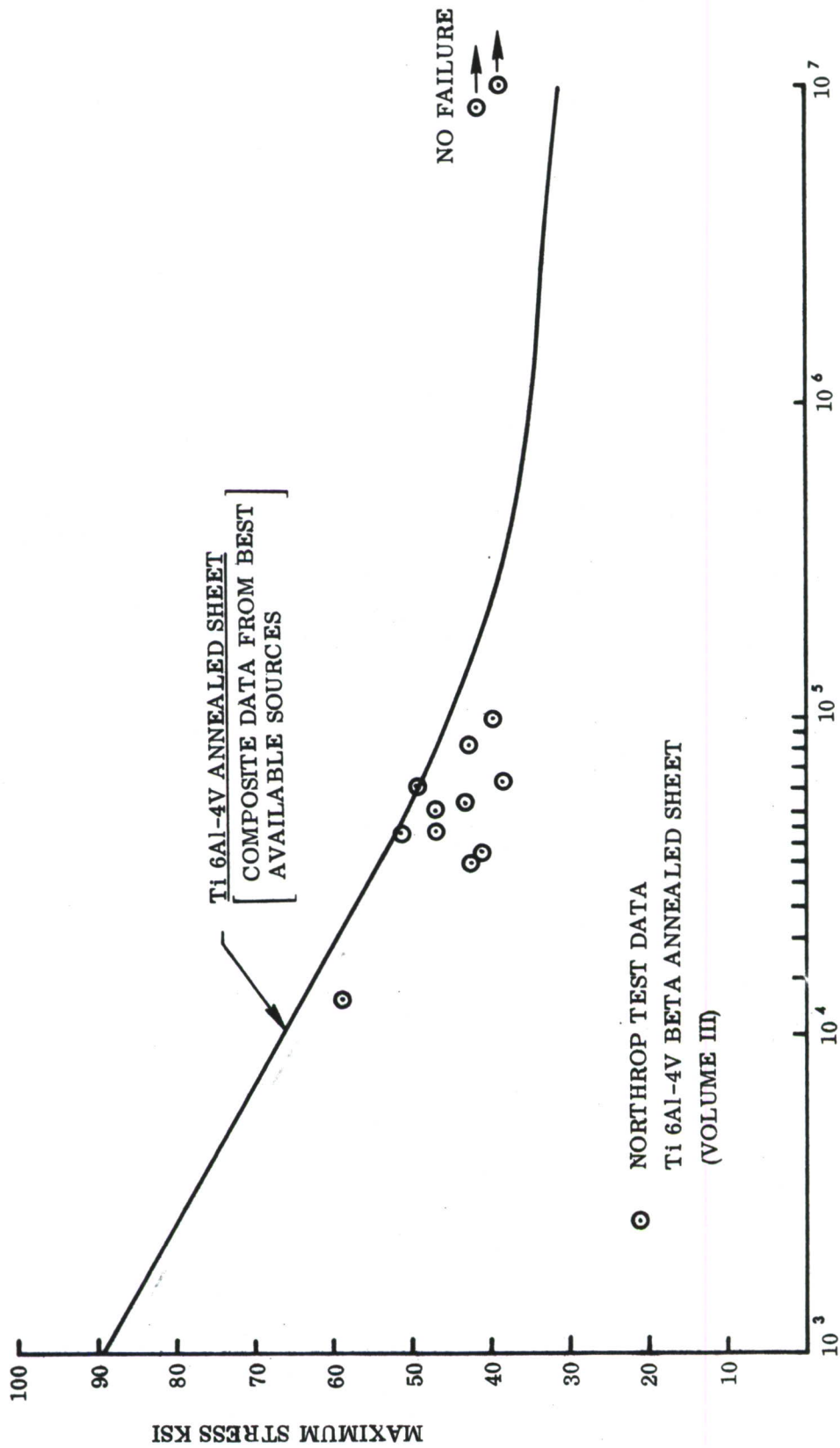


FIGURE 53. AXIAL LOAD FATIGUE BEHAVIOR OF SELECTED ALUMINUM ALLOYS



$R = .1$   
 $K_t = 3.0$



CYCLES TO FAILURE  
 FIGURE 54. AXIAL LOAD FATIGUE BEHAVIOR OF Ti-6Al-4V ANNEALED SHEET

7050-T736 were derived from data obtained in the material test program (Volume III). The X2048-T851 was a relatively recent selection for the thick plate concept. Northrop test data for 7050-T7651 thick plate demonstrated an unexpectedly poor fatigue performance. Although the 7050-T7651 had admirable crack growth characteristics and superior static strength, it was felt after reviewing the AFML report on X2048-T851<sup>(1)</sup> that the X2048 alloy offered a superior combination of properties for the needs of this program.

Preliminary design on the Ti-6Al-4V concepts was accomplished before the material test program could furnish data on Ti-6Al-4V Beta annealed sheet. Material properties used to support this preliminary design were obtained from a combination of best available sources, primarily representing Ti-6Al-4V annealed sheet. A derived S-N curve at  $K_t = 3$  obtained from these sources is shown in Figure 54. Early in the program, it was felt that the beta processed Ti-6-4 could offer an attractive weight saving potential. However, to avoid the possibility of error, Ti-6-4 annealed data was conservatively used. Data subsequently obtained on the Beta processed alloy is shown in Figure 54. It can be seen in the figure that an unexplained scatter occurred in the data points. It was concluded that without further test verification, modification of the preliminary curve shown was not justified.

### c. Method of Analysis

The fatigue analysis objective is to determine an ultimate design stress for static analysis purposes based on fatigue design stress requirements. The basic analysis procedure for each material and design concept is as follows:

1. A Palmgren-Miner cumulative damage analysis is completed for a range of reference spectrum stress levels and theoretical stress concentration factors,  $K_T$ .
2. The reference spectrum stress levels are then converted to ultimate design stresses using the relationship:

$$F_{ult.} = f_{oper.} \left( \frac{M_{ult.}}{M_{oper.}} \right) \quad (\text{See paragraph "a".})$$

---

(1) Mechanical-Property Data, X2048-T851 Aluminum Alloy, issued by AFML, October, 1972, prepared by Battelle Memorial Institute under contract F33615-72-C-1280.

3. Design stress level vs.  $K_T$  plots are constructed for the specified life requirement (16,000 hours).
4. Ultimate design stress based on fatigue requirements may now be determined for the appropriate structural fatigue quality index ( $K_{Te}$ ).

An example of a fatigue design stress vs.  $K_{Te}$  plot developed in this program is shown in Figure 55 for Ti-6Al-4V  $\beta$ MA plate. At a fatigue quality index of 3.65, the fatigue design stress in this case is 113,000 PSI. Fatigue design stresses for other materials and concepts are tabulated in Tables V through VIII.



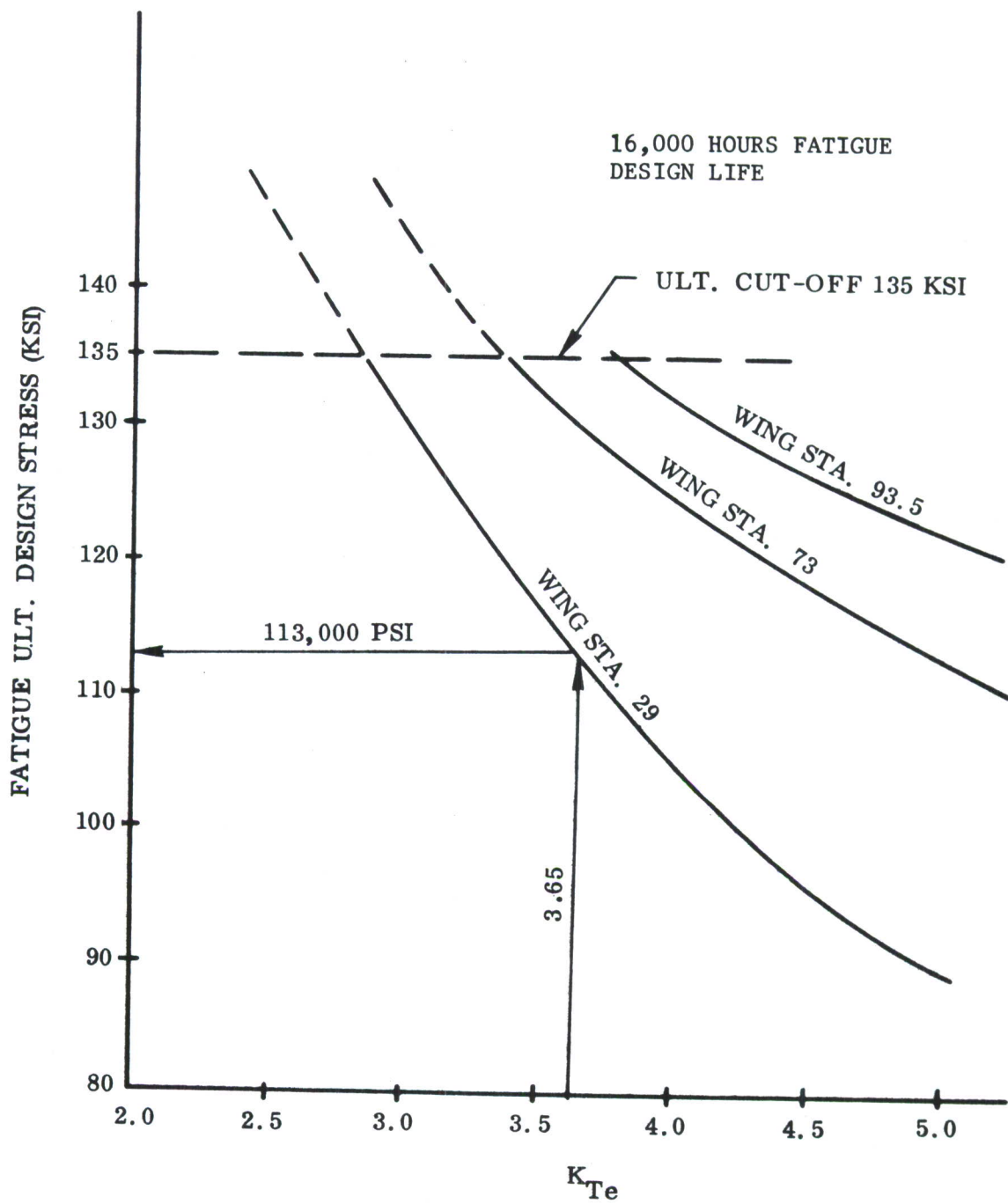


FIGURE 55. FATIGUE DESIGN STRESS FOR Ti-6Al-4V  $\beta$ MA PLATE

## 6. MATERIALS ENGINEERING

The portion of this contract dealing with the Materials Test Program is detailed in Volume III and summarized in this section. Table XIV presents a summary of typical test results on the advanced materials (approximate average values) as compared to the current F-5E materials 7075-T7351 and 7075-T651 plate and T73 forgings. In addition, literature data on the commonly used titanium alloys Ti-6-4 and Ti-6-6-2 are included for comparison with the titanium test data. This table is also presented as Table LV of Volume III, Section 1.

For aircraft design use, the typical values listed in Table XIV for tension and compression need to be reduced to "A" values. Normal statistical techniques penalized the new alloys and heat treatments so severely, due to the limited number of specimens, that none of them were as good as the presently available materials. Therefore, an analysis of typical literature data and "A" values was made to establish a rule-of-thumb for estimating the design values. Modulus values remained at 100 percent of the average test values, fracture toughness values were normally 95 percent to 100 percent of the lowest test value, depending on the amount of scatter, and strength values were taken as 93 percent of the average test values. These values were further modified when other sources of data were available. The largest modification occurred for the 1/8-inch Ti-6-4  $\beta$ MA sheet which was of an unacceptable microstructure. (See Volume III,) The Northrop data for this sheet was substantially above all other reported values. Therefore, the values were reduced substantially to those given in Table XV. Table XVI contains the design values computed for the aluminum alloys.

Table XIV has the test results grouped with comparable alloys and heat treatments, which will be discussed as application groups, the main applications being:

- a. lower wing skin (damage tolerant critical)
- b. upper wing skin (compression strength critical)

- c. ribs and spars (formed, forged or cast parts which must match the lower and upper wing skin properties).

The 7050-T73651 alloy plate has the highest strength of the lower wing skin group. However, 7475-T7651 was superior in S-N fatigue, fatigue-crack growth resistance and fracture toughness. For this reason, the 7475-T7651 was selected for use in the fatigue toughness critical lower wing skin application when an aluminum skin was desired. Note that the design of the lower wing skin is primarily based upon fatigue crack growth rates and S-N fatigue strength.

In fact,  $da/dn$  data, although not generally obtained, is perhaps one of the most significant parameters upon which to base material comparison and selection.

The second grouping represents upper wing skin candidates. Of these, both the 7475-T651 and the 7050-T7651 appear to be equal to or better than the 7075-T651 alloy in all properties listed, and the 7050-T7651 had the best stress corrosion resistance. Therefore, for both normal skin and integrally stiffened skin applications, the 7050-T7651 was selected as the best aluminum upper wing skin material.

For forged components, the 7050-T73 material appears to be equal to or better than the 7075-T73 in all cases. Thus, it was selected for the forged aluminum spars and ribs.

The new generation of titanium alloys has been developed for high fracture toughness characteristics. Thus, while Ti-6-4A and Ti-6-6-2A have good static strength and S-N fatigue strength, they are limited in applications for lower wing skins due to their poor fracture toughness and fatigue crack growth rates. The newer materials sacrifice some static strength and S-N fatigue strength but offer improved fatigue crack growth characteristics and fracture toughness. The Ti-6-4  $\beta$ MA material appears to have an excellent balance of strength and fracture properties. Therefore, based upon these test data and published data on beta forgings, Ti-6-4  $\beta$ MA was selected for use in lower wing skins as well as formed and forged spars.

The Ti-6-4 castings were either annealed or given an STA treatment. The annealing treatment produced more uniform test results with reasonably good properties. The STA material is apparently quite sensitive to various casting defects. Thus, many of the STA casting tests exhibit a lot of scattering. Until this problem is corrected the STA castings cannot be



TABLE XIV. MATERIALS COMPARISON

MATERIAL ALLOY	FORM	STATIC PROPERTIES										S-N FATIGUE				FATIGUE CRACK GROWTH (DRY AIR)				FATIGUE CRACK GROWTH 3.5% NaCl				FRACTURE TOUGHNESS		STRESS CORROSION		
		F <sub>tu</sub> KSI	F <sub>ty</sub> KSI	E <sub>t</sub> 10 <sup>6</sup> PSI	%	F <sub>cpl</sub> KSI	F <sub>cy</sub> KSI	E <sub>c</sub> 10 <sup>6</sup> PSI	F <sub>bu</sub> KSI WET PIN	F <sub>by</sub> KSI WET PIN	MAXIMUM FATIGUE STRESS KSI			CRACK GROWTH		CRACK GROWTH		CRACK GROWTH		K <sub>Ic</sub> KSI √IN LW	K <sub>scc</sub> KSI √IN	K <sub>scc</sub> KSI √IN	K <sub>scc</sub> KSI √IN					
											CYCLES/ 10 <sup>4</sup>	10 <sup>5</sup>	10 <sup>6</sup>	K <sub>t</sub>	R	RATE/10 <sup>-6</sup> IN/CYCLE	K KSI √IN	RATE/10 <sup>-6</sup> IN/CYCLE	K KSI √IN					CRACK GROWTH RATE/10 <sup>-6</sup> IN/CYCLE	K KSI √IN	CRACK GROWTH RATE/10 <sup>-6</sup> IN/CYCLE	K KSI √IN	CRACK GROWTH RATE/10 <sup>-6</sup> IN/CYCLE
ALUMINUM 7075-T7351* 7475-T7651 7050-T73651	1/2"-1/2" Plate 1" Plate 1" Plate	78	63	10.3	7	--	62	10.6	--	--	30	18	14	3.0	0.1	5	10	20	--	--	--	--	35	24 TL	3.5% NaCl			
		78	68	10.2	10	60	72	10.6	145	107	38	20	18	3.0	0.2	5.5	10	25	5.5	7	15	40	25 TL					
		82	73	10.2	10	62	74	10.7	150	110	30	14	11	3.0	0.2	5	10	25	5	7.5	18	33	33	25 TL				
		7075-T651* 7475-T651 7050-T7651	85	76	10.3	8	--	75	10.5	--	--	33	21	15.5	3.0	0.1	5	9	18	--	--	--	--	26	7 TL			
7075-T651* 7475-T651 7050-T7651	1" Plate 1" Plate 1" Plate	86	75	10.3	12	67	79	10.6	156	115	--	--	15.3	--	--	--	--	--	--	--	--	--	35	7 TL				
		84	77	10.0	9	69	83	10.6	158	115	34	17	6	3.0	0.2	6	10	25	5.5	7	16	31	<20 TL					
		7075-T73* 7050-T73	71	60	10.3	7	--	60	10.5	--	--	--	--	--	--	--	4	10	22	--	--	--	--	34	23 TL			
		1 1/2" Forging	73	64	10.1	9	61	68	10.6	140	106	34	18	15	3.0	0.2	11	16	27	--	8	19	35					
TITANIUM Ti-6-4A** Ti-6-6-2A** Ti-6-2-1-1A Ti-6-4 βMA 0.3" Plate Ti-6-4 βMA 1/8" Sheet Ti-6-4A	0.18"-4" Plate 0.18"-2" Plate 1/2" Plate 1/2" Plate 0.3" Plate 1/8" Sheet 1/8" & 1/2" Casting	137	126	16.0	10	--	132	16.4	245	198	80	60	54	3.0	0.1	10	19	37	--	--	--	55	35					
		158	147	17.0	10	--	158	17.5	--	--	82	50	35	3.0	--	8	19	35	--	--	--	40	30					
		130	115	16.5	13	90	130	17.5	255	196	52	39	34	3.0	0.1	12	22	48	12	20	29	Reported* to be 90	>93 LW					
		137	126	16.0	13	--	--	--	--	--	=55	37	33	3.0	0.1	13	25	48	13	20	28	Reported to be >95	34 LW					
Ti-6-4 βMA Ti-6-4 βMA Ti-6-4A	0.3" Plate 1/8" Sheet 1/8" & 1/2" Casting	145	136	16.5	11	--	--	--	295	225	--	--	--	--	--	15	28	60	--	15	26	Reported to be >95	38 LW					
		159	153	17.5	15	--	--	--	302	234	60	40	39	3.0	0.1	15	28	65	--	23	26	66 LW						
		140	136	16.0	2.0	117	148	16.4	290	235	<43	31	28	3.0	0.1	15	24	50	--	20	--	75	>30 LW					
		168	152	16.0	8	--	162	16.4	--	--	87	50	40	3.0	0.1	--	--	--	--	--	--	--	41	28				
Ti-6-4 STA** Ti-6-6-2 STA** Ti-6-22-22 STA Ti-6-22-22 STA Ti-6-22-22 STA Ti-6-4 STA	0.18"-75" Plate 0.18"-1.5" Plate 1/2" Plate 1 1/2" Forging 1/8" & 1/2" Casting	178	168	17.0	8	--	168	17.5	--	--	72	48	39	3.0	0.1	11	22	37	--	--	--	34	--					
		173	159	17.2	13	145	177	18.1	315	260	--	--	--	--	--	--	--	--	--	--	--	50	36 LW					
		161	151	16.0	13	128	162	17.3	--	--	47	39	37	3.0	0.1	15	26	60	15	24	--	42	--					
		128	~128	17.1	1.5	122	155	17.8	295	240	<38	23	21	3.0	0.1	13	22	47	10	15	30	70	>44 LW					

\* C. Rosenkranz, et al, Advanced Lightweight Fighter Structural Concept Study, AFFDL-TR-72-98, July 1972

\*\* C. Rosenkranz, et al, Advanced Lightweight Fighter Structural Concept Study, AFFDL-TR-72-98, July 1972 and MIL-5 Handbook, S values

TABLE XV. TITANIUM DESIGN VALUES BASED ON LIMITED TEST PROGRAM

MATERIAL FORM	Ti-6-4A		Ti-6-6-2 A		Ti-6-2- 1-1 A		Ti-6-4 $\beta$ MA		Ti-6-4 A		Ti-6-4 STA		Ti-6-6-2 STA		Ti-6Al-2Sn-2Zr 2Cr-2Mo-.25Si STA		Ti-6Al- 4V STA	
	PLATE	0.18-4	PLATE	0.18-2	PLATE	0.5	PLATE	0.5	CASTING	1.0	PLATE	0.18-.75	PLATE	0.18-1.5	PLATE	0.5	CASTING	0.5
THICKNESS/IN																		
PROPERTY																		
$F_{tu}$ , ksi	130		150		117		128	149(134)*	130		160		170		161		123	
$F_{ty}$ , ksi	120		140		107		116	142(126)	120		145		160		148		122	
$E_c$ , $10^3$ ksi	16.0		17.0		16.5		16.0	17.5(16.0)	16.0		16.0		17.0		17.2		17.1	
$F_{cy}$ , ksi	126		150		106		121	142(132)	126		154		160		160		144	
$F_{cpl}$ , ksi	-		-		70		104	121	108		-		-		137		116	
$E_c$ , $10^3$ ksi	16.4		17.5		17.5		16.4	17(16.4)	16.4		16.4		17.5		18.1		17.8	
$K_{Ic}$ , ksi $\sqrt{in}$	55		40		90		95		75		41		34		50		70	

\* As the Ti-6-4  $\beta$ MA sheet values were much higher than any other reported values, the values were lowered to those in parenthesis.

TABLE XVI. ALUMINUM DESIGN VALUES BASED ON LIMITED TEST PROGRAM

MATERIAL	7075	7475	7050	7075	7475	7050	7075	7050
	T7351	T7651	T73651	T651	T651	T7651	T73	T736
FORM	PLATE	PLATE	PLATE	PLATE	PLATE	PLATE	FORGING	FORGING
THICKNESS/IN	$\frac{1}{4}$ "- $\frac{1}{2}$ "	1.0	1.0	$\frac{1}{4}$ "- $\frac{1}{2}$ "	1.0	1.0	3"	1.5
PROPERTY								
$F_{tu}$ , ksi	69	69	75	77	77	78	66	68
$F_{ty}$ , ksi	57	59	67	69	68	72	56	61
$E_t$ , $10^3$ ksi	10.3	10.2	10.2	10.3	10.2	10.0	10.3	10.1
$F_{cy}$ , ksi	56	58	66	68	67	74	56	63
$F_{pl}$ , ksi	-	47	56	-	58	63	-	56
$E_c$ , $10^3$ ksi	10.6	10.6	10.7	10.5	10.6	10.6	10.5	10.6
$K_{Ic}$ , ksi $\sqrt{\text{in}}$	35	37	34	26	36	29	34	34
$K_{Isc}$ , ksi $\sqrt{\text{in}}$	-	25	34	7	7	17	-	22



considered for wing structures. Therefore, the annealed castings were selected for several rib applications, i.e. specific designs.

The Ti-6-22-22 STA plate and forgings were the other new STA materials which were evaluated. As stated in Volume III, the strength levels of these test samples were lower than expected, probably due to poor cooling rates during the solution treating. Even so, the Ti-6-22-22 STA was nearly equal to Ti-6-4 STA in strength and S-N fatigue and better than both Ti-6-4 STA and Ti-6-6-2 STA in fracture toughness and fatigue crack growth rates. The Ti-6-22-22 STA has higher strength than Ti-6-4A with better fatigue crack growth characteristics and slightly poorer fracture toughness. For applications requiring high strength and good damage tolerance the Ti-6-22-22 STA appears to be a promising new alloy and was selected for use as forged ribs and as an upper wing skin material. Further evaluation of the heat treatment, i.e. forced air cooling, and the resultant properties should be evaluated to fully realize the potential of this new alloy.

## 7. MANUFACTURING RESEARCH AND DEVELOPMENT

Manufacturing Research and Development engineers have worked with the Program Team from the start of the project. Manufacturing support and effort was centered in the following:

- Consultation on manufacturability of engineering designs.
- Analysis of the impact on manufacturing methods and processing requirements for the newly-developed alloys of aluminum and titanium.
- Analyzing the impact on manufacturing of the newer design concepts of precision forgings and net castings from some of the newly-developed aluminum and titanium alloys.
- Creating manufacturing plans for the various wing concepts.
- Participating in concept merit ratings.
- Manufacturing has taken a positive approach on some of the concepts in the fact that new emerging manufacturing techniques do not have a clearly defined path for accomplishing some of the tasks.

Engineering designs of the various proposed wing design concepts were reviewed for producibility capabilities within Northrop and industry specialists in the associated fields. Process development requirements have been identified. Specific development areas for the three primary wing concepts are described below and also identified in **Figure 56 (Full Depth Honeycomb)**, **Figure 57 (Aluminum/Titanium Welded)**, and **58 (Aluminum, 6 Spar)**.

### a. Machining

The machining of skins from 6Al-4V, 6-22-22 Titanium in the  $\beta$ MA and STA conditions will require development programs to establish cutter geometry, speed and feed rates to eliminate warpage. The newly-developed aluminum alloys should **require** very little change from current machining techniques but need to be verified.

### b. Forming

Vacuum creep forming of 6Al-4V and 6-22-22 titanium skins in the  $\beta$ MA and STA conditions will require the development of time, temperature and pressure cycles that will form the skins and maintain physical and mechanical properties.

Current forming techniques should be satisfactory, with minor changes, to form the skins made from the newly-developed aluminum alloys. However, verification of manufacturing techniques is required.

c. Castings

Net casting of titanium will require development and testing programs to establish data to provide criteria for establishing porosity acceptance levels, acceptable dimensional tolerances, surface finish and straightening techniques.

d. Precision Forging

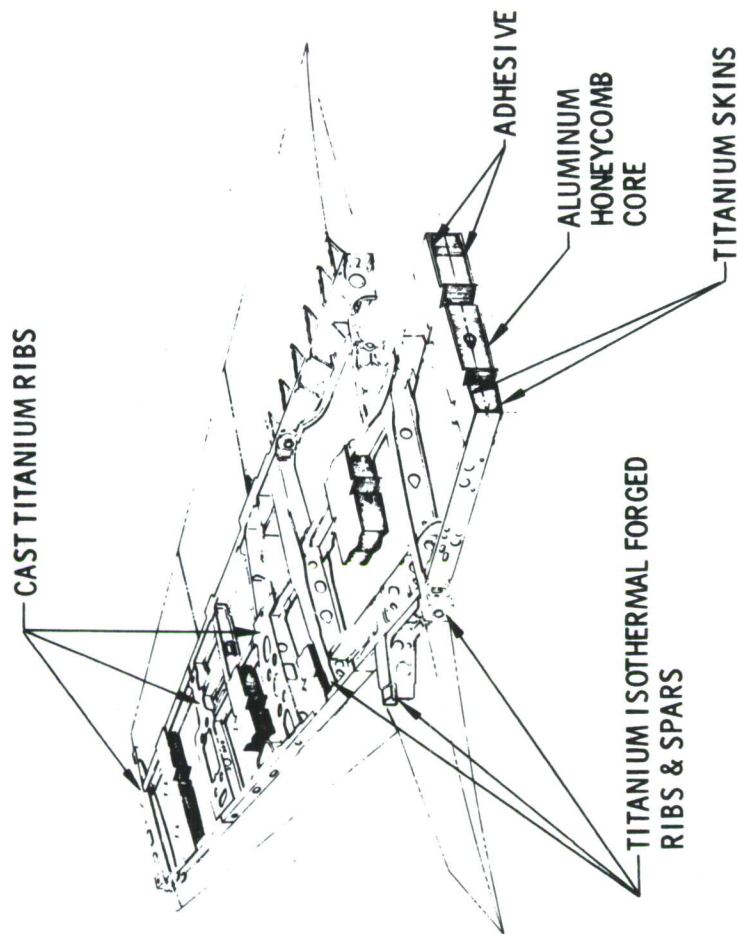
The isothermal precision forging for titanium parts of the complexity and size considered will require the development of facilities and equipment to maintain constant precise die temperatures to maintain size and shape of the finished articles.

Precision forging of aluminum is an established process for currently-used alloys. The newly-developed aluminum alloys will require verification of the manufacturing technique.

e. Adhesive Bonding

Adhesive bonding of aluminum core to titanium skins will require further development of adhesive and surface preparation systems to assure durability of the bonded assembly to be compatible with increased life expectancy. Pressure application and cure cycle time and temperature requirements will be established during the further development of the adhesive system.





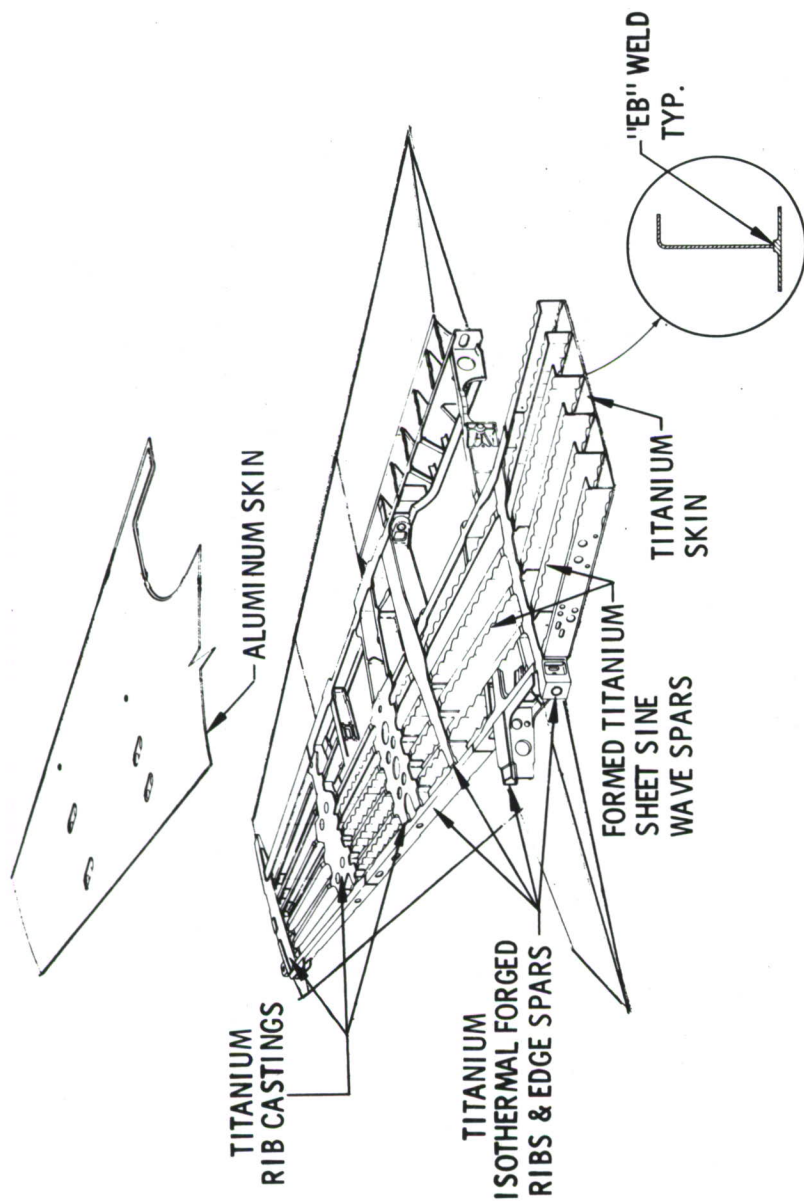
#### MANUFACTURING PROCESSES

Machining  
Forming  
Casting  
Forging  
Adhesive Bonding

#### TECHNOLOGICAL ADVANCEMENT AREAS

Maintaining skin flatness in titanium STA &  $\beta$ MA condition.  
Forming of titanium in the  $\beta$ MA & STA condition.  
Net casting of titanium.  
Isothermal precision forging of titanium  
Adhesive development & surface preparation.  
Pressure application - cure cycles

FIGURE 56. FULL DEPTH HONEYCOMB



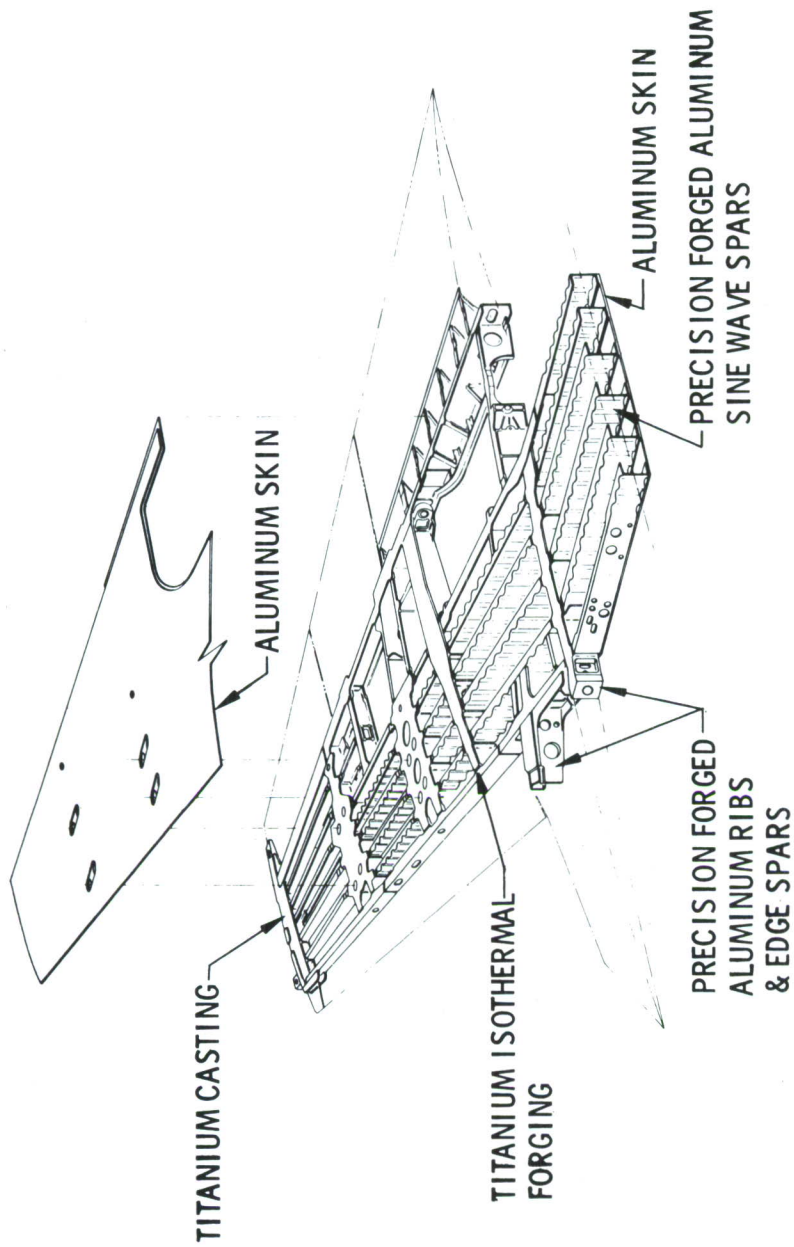
#### MANUFACTURING PROCESSES

Machining  
Forming  
Casting  
Forging  
Welding

#### TECHNOLOGICAL ADVANCEMENT AREAS

Maintaining flatness in  $\beta$  MA condition plate  
Forming titanium plate in  $\beta$  MA condition  
Net casting of titanium  
Isothermal precision forging of titanium  
Welding techniques  
Associated tooling  
Facilities requirements  
Establishing time, temperature and pressure requirements  
Associated tooling

FIGURE 57. PRECISION FORGED SUBSTRUCTURE WING



#### MANUFACTURING PROCESSES

Machining

Forming

Casting

Forging

#### TECHNOLOGICAL ADVANCEMENT AREAS

New aluminum alloys - minor development

New aluminum alloys - minor development

Net casting of titanium

Isothermal precision forging of titanium

Precision forging of aluminum

FIGURE 58. WELDED 6 SPAR WING



## 8. QUALITY CONTROL AND NDI

An important factor relating to the design and manufacture of aircraft structures of high integrity and reliability, is the development of a Quality Assurance Program encompassing the entire product cycle from raw materials through operational service. This comprehensive quality control plan must be implemented for all fabrication, and must include all operations from production of raw material through the final assembly. Critical operations and process variables would be defined, characterized and documented for inclusion into the process controls and detailed manufacturing plans.

The role of NDI in this inclusive quality control plan, includes receiving inspections performed on incoming raw materials (precision castings, forgings, etc.) to assure that quality of materials for manufacturing processes meet all defect acceptance standards, in-process NDI to assure that no defects or flaws are introduced during the manufacturing sequence of operations, in-service NDI to assure that structural degradation has not been introduced during in-service operations and that flaw growth can be monitored. NDI must consider evaluating or monitoring the product at almost any stage of manufacture and/or service operation to confirm integrity.

Investigation of NDI techniques and limitations has considered the defects applicable to various wing design concepts. Feasibility studies were formulated as an integral portion of the preliminary engineering and manufacturing development programs to obtain pertinent data in a timely manner. These data consisted of engineering requirements, critical levels, material types and configurations.

Quality Control's investigation of NDI method capability and techniques must consider several types of defects: (1) detection of defects in adhesive bonded components; (2) detection of cracks and crack propagation in details such as spars, ribs and other supporting structures.

Evaluation studies were also conducted on in-house NDI equipment to determine capability or requirements for modification. It was intended that the in-house ultrasonic equipment be utilized as a method of measuring fatigue crack growth. Ultrasonic techniques, whereby a change in crack length of .005" can be detected, have been reported in technical literature.

A section of an F-5 wing was obtained to prepare NDI test specimens. Included in the test methods were eddy current, ultrasonics and eddy sonics for the detection of the simulated cracks in fastener holes. Radiography and eddy current were used for crack detection capability in the ribs and spars. Other tests consisted of an evaluation of a conductive material applied to the spars. It is anticipated that this technique may be useful for crack detection.

The use of radiographic image enhancement was investigated. The increase in crack detection sensitivity as compared to the normal X-ray film is quite large; however, additional studies are required for justification of this costly process.

A test panel, consisting of titanium skins bonded to honeycomb core with a 3-ply graphite prepreg bonded to the exterior surface of one face skin, was submitted for high resolution ultrasonic tests. These tests were conducted to establish the best useable frequency ranges for this type of construction. Results were not conclusive.

Ultrasonic pulse echo tests were conducted on diffusion bonded titanium honeycomb sandwich panels. The honeycomb core contained known defects such as removal of one cell wall, and a .125 inch gap machined across the panel and various other size defects. The titanium skin was 0.016 inches thick. Other tests with a panel having a skin thickness of 0.040 inches resulted in comparable definition of core defects. High resolution pulse echo techniques were very successful.

The establishment of inspectability guidelines and constraints, including accessibility requirements, and the influence of material selection has been a major effort of Quality Control. As an active member of the Program Team, coordination with the Design Group has been very close. Inspectability of each design concept was assessed and an approach was developed which will assure that NDI techniques capable of realizing the greatest possible sensitivity would be available for the selected configurations. The necessity of developing new NDI techniques is not anticipated. Existing techniques can be adapted for application.

Based upon literature surveys, related industry visitations and Northrop's in-house research, a tabulation of NDI methods that are currently applicable and others with potential applicability for NDI of the wing structure are as follows:

TABLE XVII. NDI METHODS

<u>Bonded Structures</u>		
<u>In-Process</u>	<u>Methods</u>	<u>In-Service</u>
Yes	Eddy Sonics	Yes
Yes	Resonant Frequency	Yes
Yes	Through Transmission	No
Yes	Neutron Radiography	P
P	Thermal	P
P	Sonics	P
P	Low KV X-Ray	P
Yes	Optical Holography	P
<u>Forgings and Castings</u>		
Yes	High Resolution Ultrasonics	
Yes	High Resolution Penetrants	
Yes	Acoustic Holography	P
Yes	Fastress	
P	Eddy Current	P
	Magnetic Rubber	P
	Fixed Permanent Transducers	P
	Conductive Paints	P
	Crack Wires	P
	Fatigue Gage	P
	Fiber Optics	P
P	Acoustic Emission	P

Legend: P Potential Application



A brief study has been accomplished of the requirements for demonstrating the quantitative limitations of the various NDI methods for production use. Examination of magnetic particle, penetrant, ultrasonic and radiographic inspection emphasized the need for using actual structural parts in the demonstration in order to simulate as closely as possible the production environment. It has been further recommended that a rating system be established that recognizes the variability of the ease of detection of defects of the same size. Location, orientation and alloy differences must be taken into account by the statistical ratings.

NDI survey visits were made to various aircraft companies, commercial airline maintenance depots and military installations for the purpose of reviewing and discussing NDI methods and techniques that could be applicable to the Advanced Air Superiority Fighter Wing Structures Program.

With the exception of techniques utilizing a magnetic rubber material and an automated eddy current method for crack detection in fastener holes, no other applicable new NDI methods or techniques were observed in use. However, most survey areas were investigating new NDI methods which were still in the development laboratory stage. Methods indicating future potential included: Acoustic Emission, Video Processing by Data Suppression, and Ultrasonic Spectroscopy.

## 9. COST ANALYSIS

The cost analysis for this program is an integral part in the design decision process for recommending designs to be developed in the follow-on program. As such, the cost estimates were developed from preliminary manufacturing plans and engineering drawings. Close coordination was maintained among the cost analysis, engineering and manufacturing disciplines throughout the study. Cost estimates were developed and iterated as design improvements were made or as new information about manufacturing technology became available. The three basic estimating specialties called on in this study were: Factory, which supplied standard factory labor hours; tooling, which estimated the nonrecurring tooling hours; and materiel, which estimated production material costs. All these specialists coordinated with design engineering, weights, cost estimating, and manufacturing engineering, and were in frequent contact with each other.

As a result of the combined effort of these disciplines, cost estimates were developed for eight wing structural concepts and the baseline. The discussion of the cost data is in five parts:

1. Methodology of cost determination
2. Ground rules for the cost estimates and cost projections
3. Cost comparison of interior spar designs
4. Cost comparisons between various design concepts
5. Sensitivity analysis

### a. Methodology of Cost Determination

To perform the cost comparison of the advanced composite structure designs with the conventional baseline, a uniform cost structure was developed. It forms the framework for the detailed plan by which each and every factor contributing to the cost of a structure will be estimated.

#### (1) Uniform Cost Structure

The cost element structure provides a rational breakdown for the collection and presentation of cost data. It standardizes cost elements for estimation, validation, and comparison. A standard set of cost element

definitions eliminates the need to redefine terms or explain common factors when analyzing costs. It also serves as a checklist to assure that significant cost elements have not been overlooked.

The cost element structure is shown in Figure 59. A brief description of each of the cost elements follows.

(a) Recurring Costs

Costs incurred by all departments for their repetitive and sustaining effort associated with and in support of the delivery of the product.

(b) Recurring Labor-Factory

The costs associated with factory labor include the manufacturing hours for operations such as machining, processing, bonding, assembly, and final fabrication. These basic factory operations make up the initial cost elements for any hardware items manufactured in a production environment. Direct factory labor estimates are developed from total detail time standards basic data for set-up and run. Set-up time is the time required to prepare to do work. It is prorated over lot size. Run time is the recurring time per unit.

(c) Recurring Labor-Support Functions

The cost elements that make up support functions include sustaining engineering, manufacturing engineering, graphic services, tooling maintenance, and quality control. The costs associated with these elements are derived as percentages of factory labor. The percentage relationships have been developed from the substantial historical data collected on T-38/F-5 aircraft by correlating support function costs with the factory labor.

(d) Recurring Costs - Material

There are three basic recurring material costs. They are (1) raw material, (2) allocated material, and (3) those materials that are purchased off-site such as castings, forgings, specific machined parts, and any other specialized part fabrication not available at Northrop.

The raw material is defined as the material that is purchased specifically against each individual detailed drawing that is used to make up



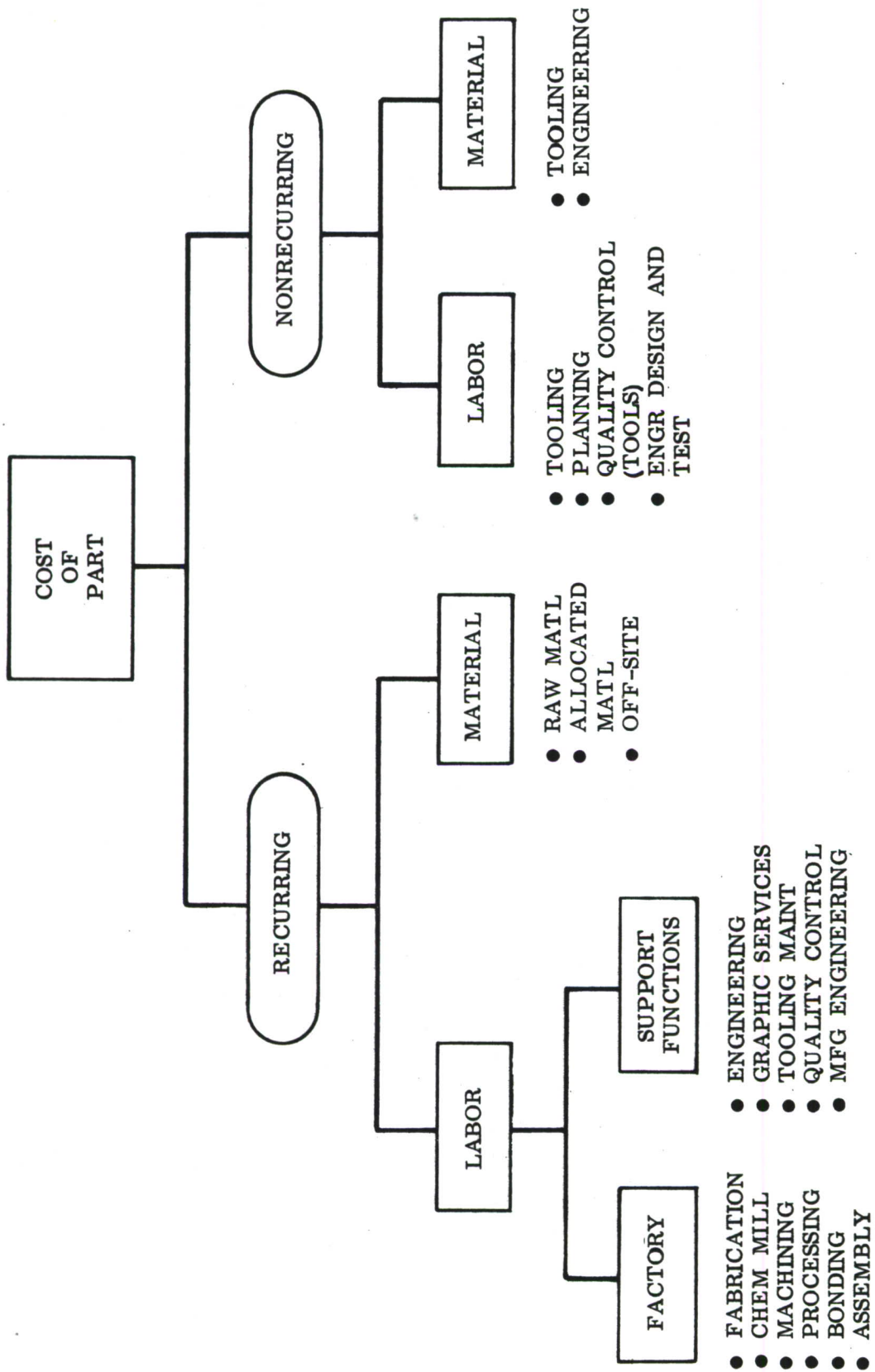


FIGURE 59. COST ELEMENT STRUCTURE FOR PART COST ESTIMATION IN A PRODUCTION ENVIRONMENT

a complete assembly. The allocated material costs expressed as a percentage of factory labor dollars, account for items such as rivets, nuts, bolts, adhesives, etc.

Additionally, in developing the total recurring material cost estimates, costs of recurring material for tooling and engineering must be considered. These are expressed as a percent of recurring tooling labor dollars and engineering labor dollars respectively.

(e) Non-Recurring Labor

Non-recurring labor cost elements consist primarily of tooling, planning, quality control of tools, engineering design and test. The bulk of non-recurring factory labor is used to produce tooling. The number of tools required for each configuration was determined by an examination of the manufacturing statement of work and the engineering drawings.

(f) Non-Recurring Material

The non-recurring material costs incurred are related to the manufacture of tools and non-production manufacturing and engineering test materials. The tooling material is estimated as a percentage of non-recurring tooling labor dollars, based on historical data. Special detail estimates may be necessary if the tool is untypical or has special requirements.

(2) Estimating Methodology

The three basic methods used for cost estimating are the parametric, analog and industrial engineering standards approaches. The first, parametric, is defined as using a statistically valid sample size and statistical techniques to develop a model of cost estimating relationships based on physical parameters of the product as the independent variables and cost as the dependent variable.

Analog estimating requires a judgment that certain aircraft parts, or manufacturing times to perform certain operations, are like others in a direct or proportionate relationship. Thus, the time to drill a hole in aluminum is proportionate to the time to drill one in titanium and

historical data (time standards) on drilling holes in one titanium part can be used directly in estimating the time to drill holes in other titanium parts.

The basic steps in cost estimating with these approaches are as follows:

1. Determination of the basic assumptions and constraints pertaining to the part or process to be estimated. This is fundamental to the accuracy and reliability of the estimate. If all pertinent data is not available to the estimator, parts of the estimate may be distorted or certain costs may be omitted entirely.
2. Selection of the estimating approach - parametric or analog. This will depend on the data available and the degree of detail design available in the part or component being estimated.
3. Application of the estimating approach and improvement curves theory. Improvement curve theory in general use in the aerospace industry states that as total quantity of units produced doubles, unit cost declines by some constant percentage.
4. Application of labor rates and burden factors typical of industry experience.
5. Summarization of the estimate with the cost structure described above.

At Northrop, in estimating new technologically advanced components, detailed part cost estimates are developed using Industrial Engineering Time Standards. These standards represent the time required to perform an operation under ideal conditions. They are developed by industrial engineering methods and do not allow for fatigue, worn tools, and other time-consuming factors. The standards on an operation-by-operation basis are the foundation of the labor hours estimate to which a variance is applied. This adjusts the standards (ideal conditions) to realistic conditions. The variances reflect actual history for the fabrication and assembly of various types of end items and include provisions for learning, methods improvement, fatigue and other considerations.



b. Ground Rules for Cost Estimates and Cost Projections

For Concepts 1, 3, 4, 5 and 8, detail cost estimates were developed using the industrial engineering time standards approach. In order to compare the relative costs of the baseline and each of the new concepts on a one-to-one basis, the following set of ground rules were applied:

1. Quantity of 300 units in production with a full complement of production tools.
2. Set-up time prorated over 25 units.
3. A typical industry composite improvement curve of 79 percent with a variance factor of 1.45 at  $T_{1000}$ .
4. Material costs based on a parametric estimate derived from the titanium quotes supplied by vendors. Those specific parts, quoted on by vendors, were estimated at the price specified by the potential supplier. All material costs are based on a 100 shipset buy.
5. Both labor and material escalated to 1977 dollars
6. Labor and burden rates typical of industry as follows (in 1977):

Engineering Labor	\$8.82 per hour
Graphic Services	\$6.30 per hour
Tool Design & Fabrication	\$6.93 per hour
Manufacturing Engineering	\$7.56 per hour
Factory fabrication	\$6.30 per hour
Quality Control	\$7.56 per hour
Engineering Burden	130%
Factory Burden & Fringe	150%
Material Burden	20%
G & A	20%

7. Recurring Support labor hours are directly related to recurring factory labor hours in the following ratios:

Engineering Liaison	20% of factory labor hours
Graphic Services	4% of factory labor hours
Tooling Maintenance	15% of factory labor hours
Manufacturing Engineering	15% of factory labor hours
Quality Control	15% of factory labor hours

8. The non-recurring costs are for tooling only and are amortized over 300 units. The aforementioned ground rules are applied to both the baseline and each of the new concepts to compare the relative costs on a one-to-one basis.
9. In preparing the cost estimates, consideration was given to the expected advancement in the state-of-the-art in titanium technology by 1977. For estimating purposes, the following assumptions were made for technological progress:
  - a. The titanium cleaning procedures, bonding procedures, and materials, would have been fully tested (under other development programs).
  - b. All titanium forgings (pressings) and castings will require machining only on the mold line surfaces and other areas where attachment to adjacent structure occurs.
  - c. All titanium forgings are net and machining is only required where necessary to remove material which has been added to eliminate die lock.
  - d. All plate stock for skins will have a minimum of 0.125" material removed on each surface.
  - e. Production techniques and precision castings, forgings, not currently available will be obtainable in 1977, at the prices quoted by the vendors.

To project the costs for the time standards basic data using these ground rules, a simple computer program was developed. A sample computer printed cost sheet showing labor hours, labor rates and dollar figures is displayed in TABLE XVIII which is the cost data for Concept No. 1 - Ribs.

TABLE XVIII. COMPUTER PRINTED COST SHEET FOR CONCEPT NO. 1 - RIBS

## CONCEPT NO. 1 - RIBS

CATEGORY -----	HOURS -----	RATE -----	TOTAL \$ -----
ENGINEERING	48.80	8.82	430.42
GRAPHIC SERVICES	9.76	6.30	61.49
SUBTOTAL ENGINEERING			491.90
ENGRG. OVERHEAD-130%			639.48
TOTAL ENGINEERING			1131.38
TOOL DESIGN AND FAB.	36.60	7.56	276.70
MFG. ENGINEERING	36.60	6.93	253.64
FACTORY	244.00	6.30	1537.20
QUALITY CONTROL	36.60	7.56	276.70
SUBTOTAL FACTORY			2344.23
FACTORY OVERHEAD-150%			3516.34
TOTAL FACTORY			5860.57
ENGINEERING MATERIAL			0.43
TOOLING MATERIAL			41.50
PRODUCTION MATERIAL			11846.00
ALLOCATED MATERIAL			153.72
SUBTOTAL MATERIAL			12041.65
MATERIAL OVERHEAD-20%			2408.33
TOTAL MATERIAL			14449.99
ADMIN. OVERHEAD-20%			4288.39
TOTAL COST			25730.33



### c. Cost Comparison of Interior Spar Designs

A cost comparison of sixteen interior spar designs was conducted previously to choosing the interior spar design used in Concepts 3, 3A, 4 and 5. The spar design chosen was the titanium sine wave formed spar which is twice as costly as the baseline on a cost per unit basis for 300 units. This particular spar design (#1Ti as shown on Figure 8 ) was chosen primarily because of its comparatively low cost-quantity relationship to the baseline.

The cost analysis which contributed to the selection of the titanium sine wave formed spar design was conducted using the same ground rules discussed in the previous section. Detailed cost estimates were developed on all sixteen proposed interior spar designs. The cost of each design was then compared with the cost of a typical interior spar (27% spar for this comparison) currently used in the F-5E wing box.

To establish a cost-quantity relationship, the cost per unit was projected for 1, 25, 50, 100, and 300 units. A group of normalized cost curves are presented in Figures 60 through 63 to clearly display the variations in cost-quantity relationships of the spar designs.

Only four curves were included per figure to facilitate clarity of the presentation. The normalized cost curve for each spar design is determined by dividing each spar cost by the baseline for quantities of 1, 25, 50, 100, and 300 units. Thus, the baseline normalized cost curve is 1 for all quantities and the behavior of the cost of the various designs can readily be compared.

Typically with increasing quantity, the normalized cost curves either diverge from or converge on the baseline. Labor and tooling costs diminish with increasing quantities of production causing total costs to decline. The impact of the improvement curve and tooling amortization is shown in Figure 64. The production (recurring) material cost remains relatively constant for each unit and proportionately dominates the cost of a spar design at larger quantities. Those spar designs with normalized cost curves that diverge from the baseline (see Figure 8 , spar design #3Ti) exhibit production material costs approximately 16 times the baseline production material cost; and the spar designs with normalized cost curves which

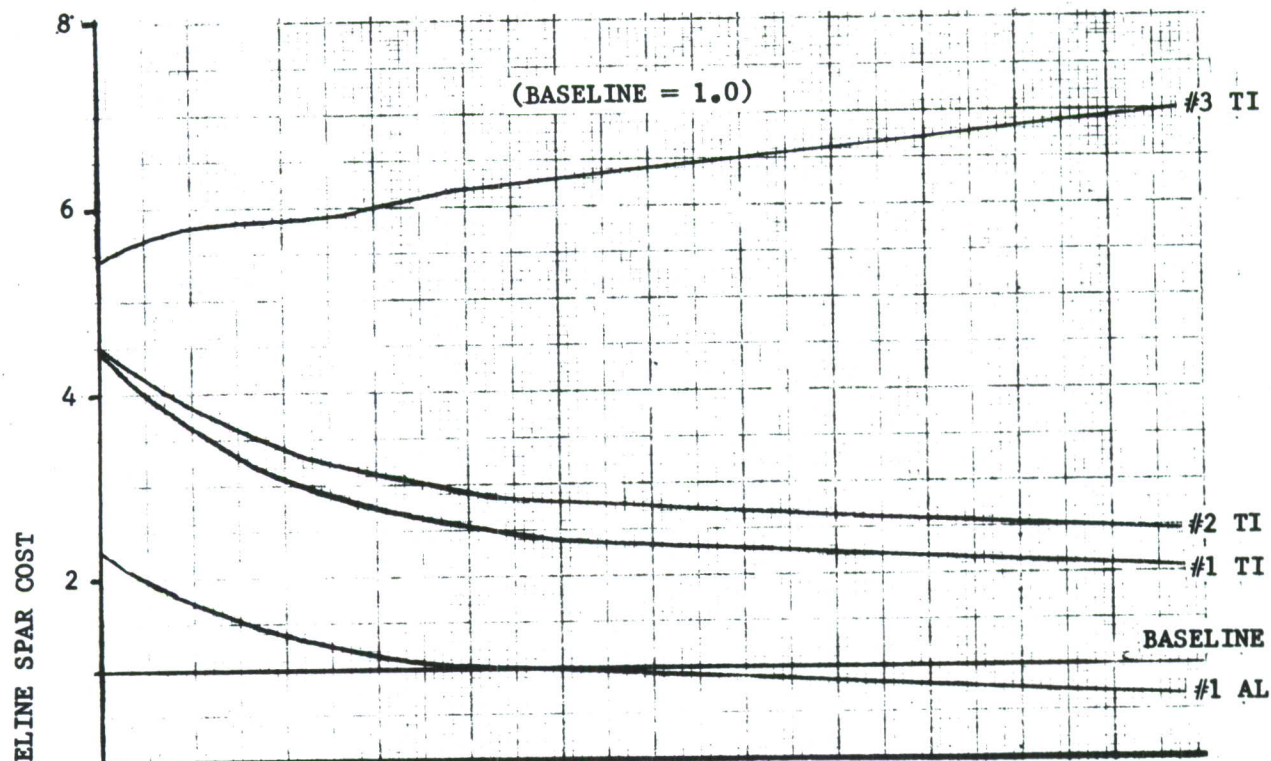


FIGURE 60. NORMALIZED COSTS FOR SPAR DESIGNS

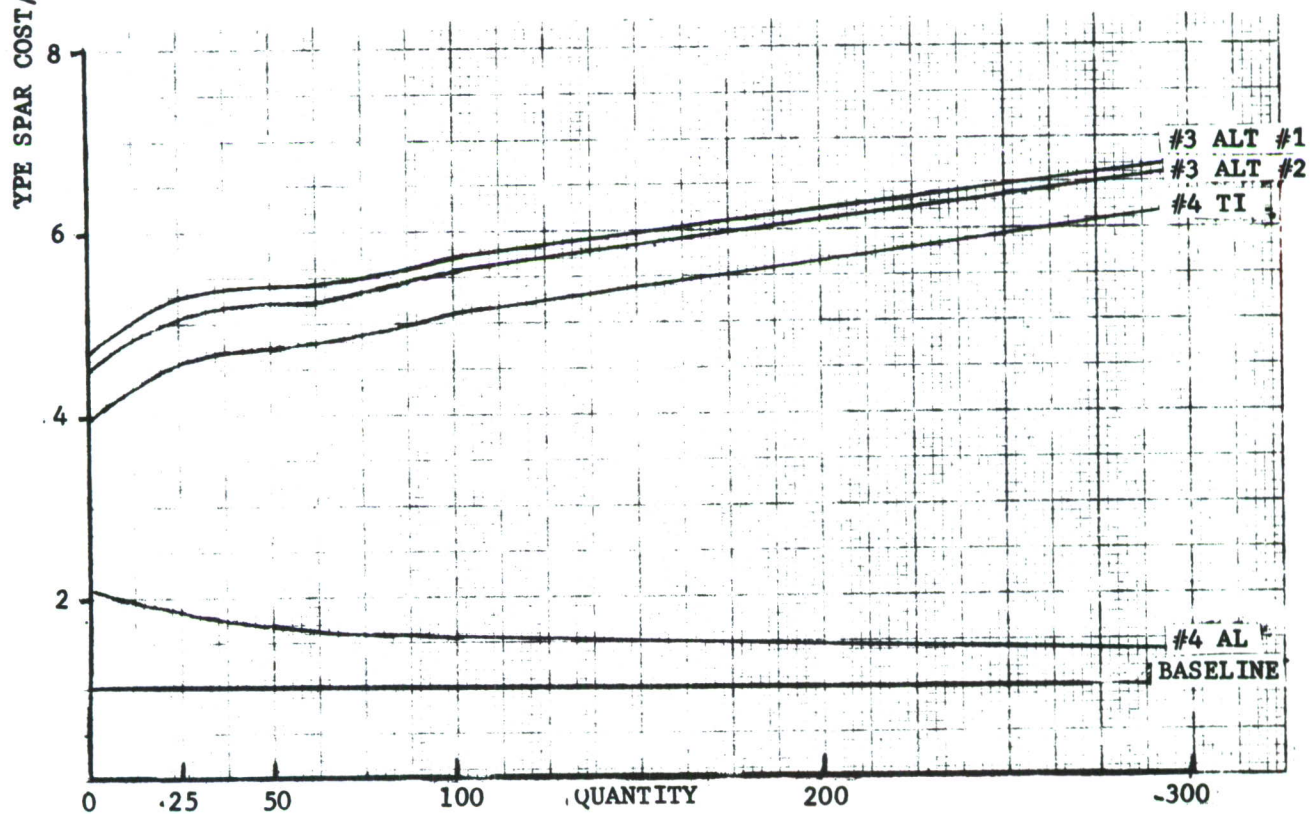


FIGURE 61. NORMALIZED COSTS FOR SPAR DESIGNS (Continued)

(BASELINE = 1.0)

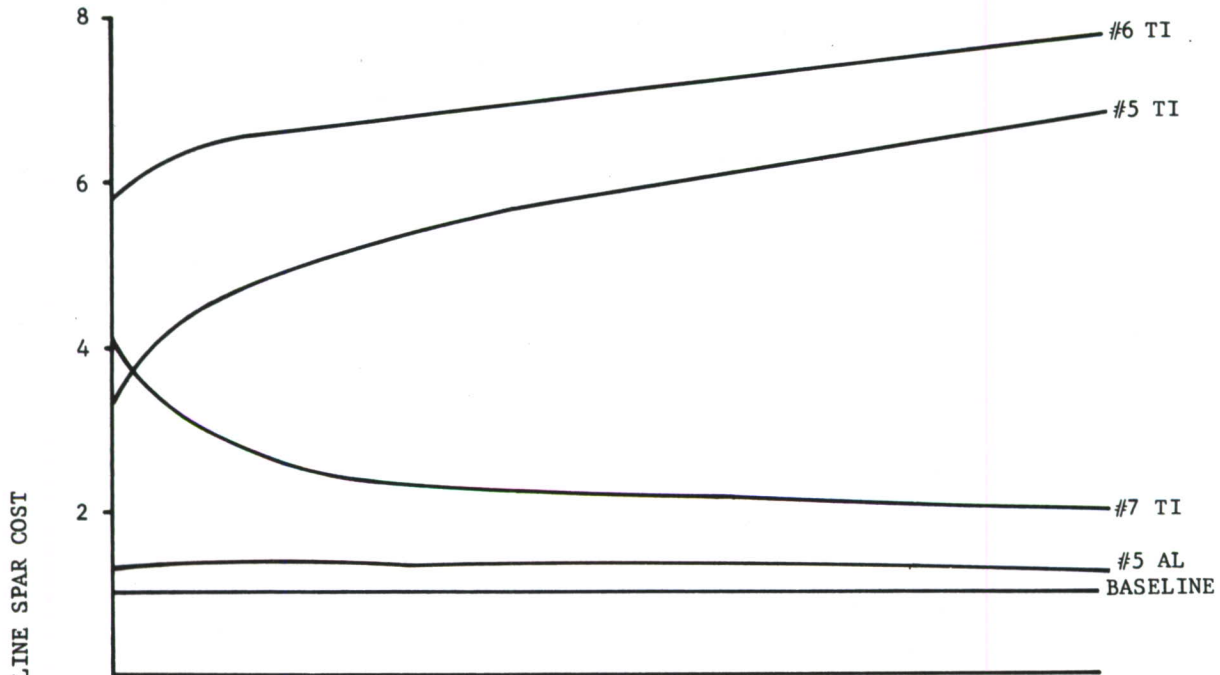


FIGURE 62. NORMALIZED COSTS FOR SPAR DESIGNS (Continued)

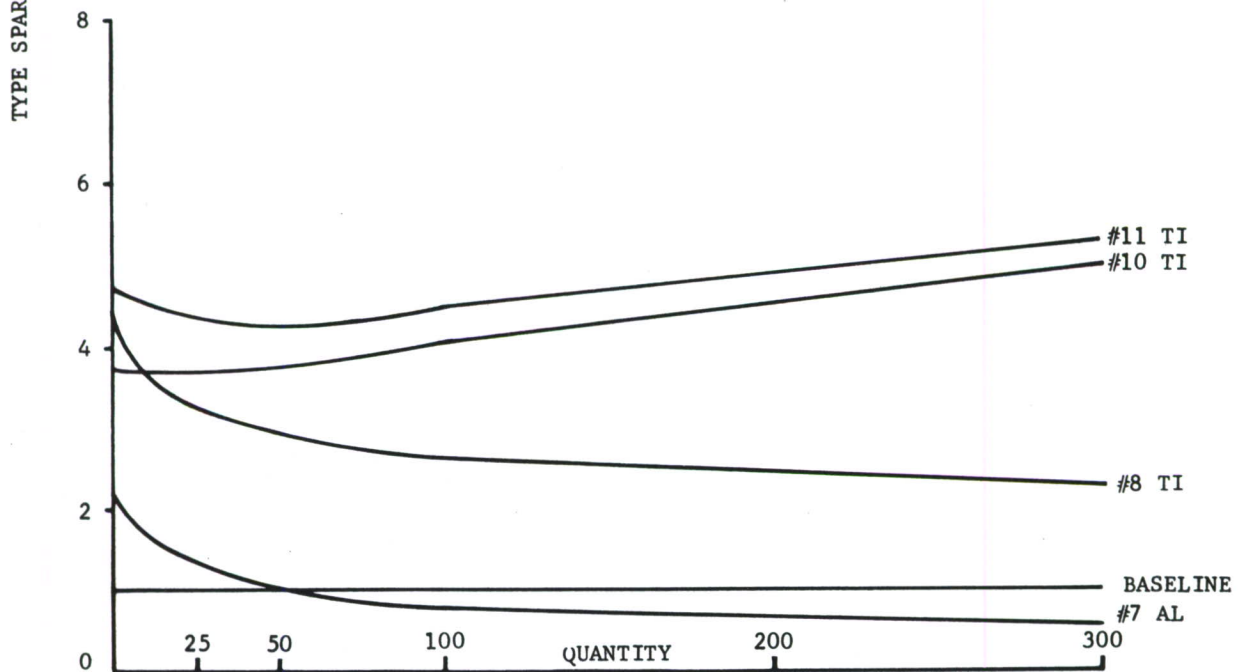


FIGURE 63. NORMALIZED COSTS FOR SPAR DESIGNS (Concluded)



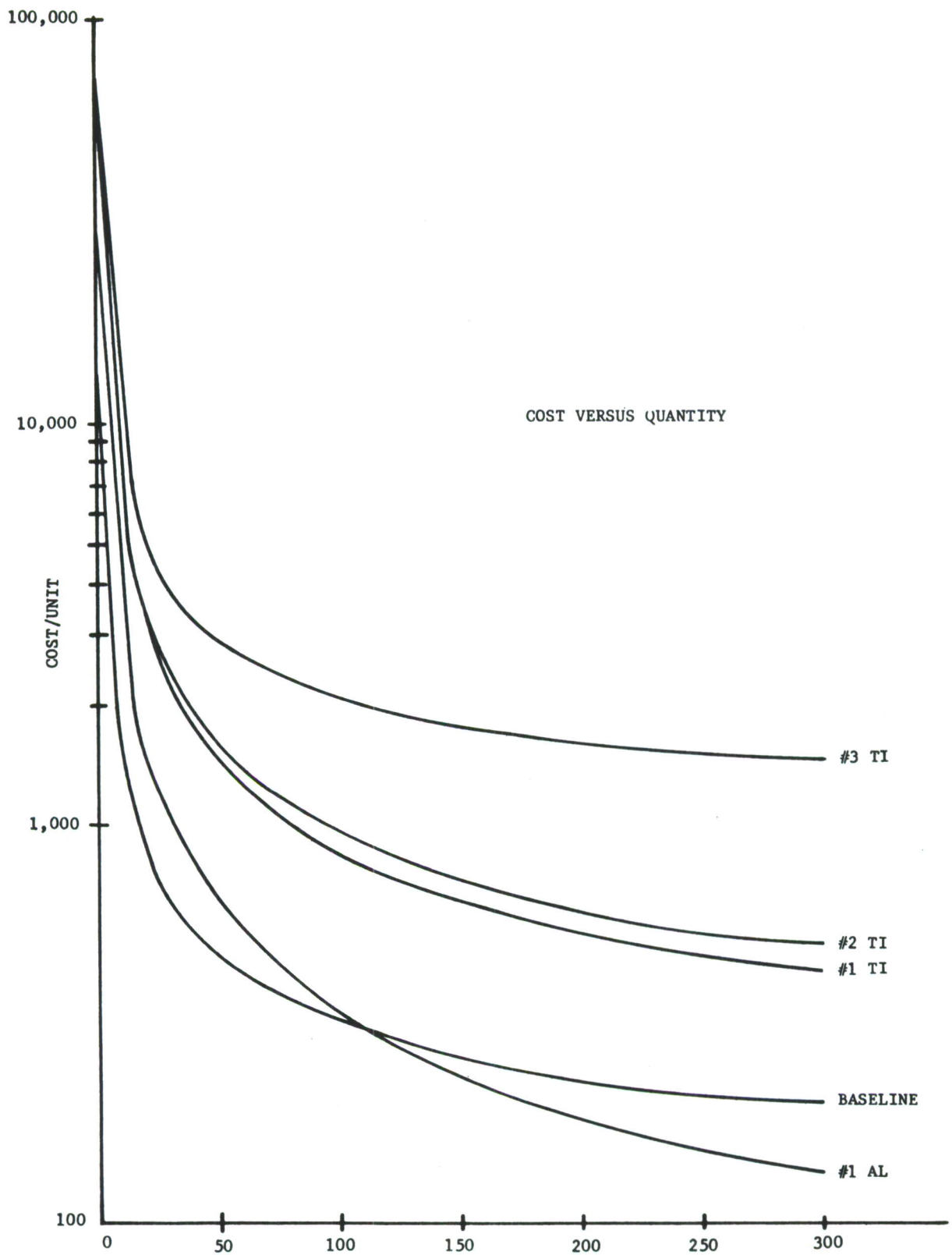


FIGURE 64. COST-QUANTITY RELATIONSHIP AND COMPARISON BETWEEN VARIOUS SPAR DESIGNS

converge on the baseline (see Figure 60, spar designs #1Ti) have production material costs of approximately 2 times the baseline production material costs.

The total cost of those spar designs with high production material costs (see Figure 60, spar design #3Ti) become dominated by the material costs at relatively low quantities of production. Therefore, the decline in total cost is much slower, flattens out at much higher per unit cost, as compared with those designs with low production material costs (see Figure 60, spar design #Ti and baseline); hence, the normalized cost curves of the two types of designs diverge (see Figure 61) with increasing quantity.

Those curves which cut beneath the baseline represent spar designs which become less expensive to produce than the baseline at and beyond the quantity where the normalized cost curve passes beneath the baseline (see Figure 64, spar design #1Al and Figure 63, spar design #7Al).

As compared to the baseline, eight titanium spar designs become more expensive to produce with increasing quantity and four titanium and four aluminum spar designs become less expensive to produce at greater quantities. The results indicate that titanium spar designs are more expensive than aluminum, but there are titanium designs that approach the baseline from a cost standpoint. When combined with the weight advantage of titanium, these designs may become competitive with those of aluminum.

#### d. Cost Comparisons Between Various Design Concepts

Using both the assumptions on the technological advances and the ground rules for cost projections, the cost/unit for 300 units was established for each of the new concepts. Since all concepts are being compared against the baseline, the costs of all other configurations utilized the baseline cost as the common denominator. Thus, each of the concepts could be expressed in relative terms when compared either to the baseline or to each other. The results of the relative cost comparisons are summarized in Figure 65. For example, the baseline concept is 1.00 by definition, while concept No. 1 is 1.28 or 28% higher than the baseline, concept 1A is .85 or 15% less than the baseline, etc. Table XIX is included to show the breakdown of cost for

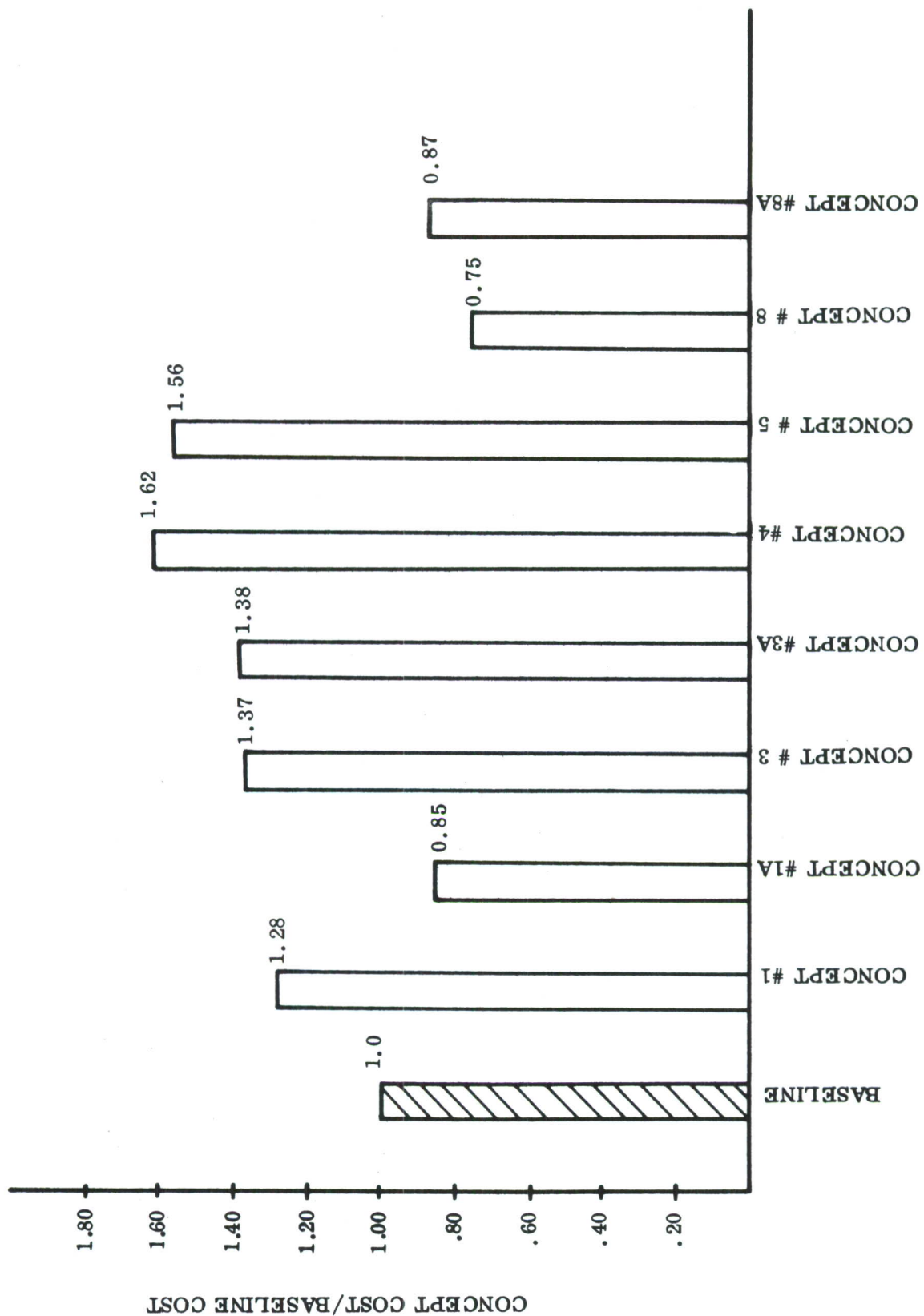


FIGURE 65. SUMMARY OF RELATIVE COST FOR VARIOUS WING BOX CONCEPTS



TABLE XIX. COST/UNIT FOR 300 UNITS (1977 DOLLARS)

CONCEPT	SPARS	RIBS	UPPER SKINS	LOWER SKINS	MISC	ASSEMBLY	NONREC. TOOLING	TOTAL
Baseline	30,103	31,062	3,036	3,457	8,594	6,104	7,059	89,415 (1.00)
# 1 F.D. Honeycomb	32,065	25,730	8,355	14,112	12,509	9,610	12,538	114,919 (1.28)
1A	20,880	16,684	3,475	4,206	8,594	9,610	12,538	75,987 (0.85)
# 3 A1/T1 6-Spar	43,247	32,349	3,473	15,071	10,227	6,688	11,414	122,469 (1.37)
# 3A	44,287	28,233	3,473	15,071	10,227	10,485	11,470	123,246 (1.38)
# 4	41,566	29,851	16,756	23,083	12,238	5,625	15,477	144,596 (1.62)
# 5	39,313	28,799	16,180	21,931	12,238	5,306	15,434	139,201 (1.56)
# 8	18,712	14,648	3,475	4,206	12,197	6,607	7,592	67,437 (0.75)
# 8A	18,712	14,648	3,475	12,618	12,197	8,809	7,592	78,051 (0.87)

the major components (spars, ribs, etc.) for each of the concepts considered in Figure 65. The data presented in Table XX represents detailed cost breakdowns for the baseline and the three selected concepts.

To more clearly delineate the underlying factors for the cost differences exhibited in Table XIX, a breakdown of the major components and the nature of the material comprising them is displayed in Table XXI. The factors causing the cost differences are discussed below:

Concept 1 is a full-depth honeycomb design, featuring titanium skins and aluminum core. Both the spars and ribs are slightly less expensive than the baseline because both are precision forgings and castings which reduce the machining labor costs of the ribs and spars dramatically (see Table XX ). The major cost differential is found in the skins which are titanium and are roughly four times as expensive as the aluminum skins. The miscellaneous items (panels, doors and hardware) are more expensive than the baseline because of a graphite composite aileron access door and precision cast titanium aileron hinge. (These two features are common to all of the concepts). Assembly costs are higher than the baseline, because both bonding and riveting are required. The total effect of these items is a 28% increase over the baseline.

Concept 1A is similar to concept 1 except that the spars and ribs are precision forged aluminum and both skins are aluminum. This change from titanium to aluminum results in a 15% reduction in cost over the baseline compared to a 28% increase for concept 1.

Concept 3 is a six spar concept with precision forged titanium exterior spars and titanium sine wave sheet spars, titanium root and gear ribs, and titanium lower skin. The assembly requires riveting as in the baseline and is slightly higher because of the increased difficulty in drilling titanium. The concept is 37% more costly than the baseline as a result of the titanium spars and lower skins.

Concept 3A is a design featuring an aluminum upper skin, a titanium lower skin and substructure. Welding is used extensively in attaching the

TABLE XX. DETAILED COST BREAKDOWN OF BASELINE AND CONCEPTS 1, 3A, 8

Component	BASELINE					CONCEPT NO. 1				
	Labor	Mat'l	Overhead	Tooling	Total	Labor	Mat'l	Overhead	Tooling	Total
Spars	7,148	6,220	16,735	1,684	31,787	1,458 1,174	16,437 440	10,075 2,492	1,672 208	29,642 4,314
Ribs	8,734	3,627	18,701	2,382	33,444	2,836	12,042	10,853	1,608	27,339
Upper Skins	531	1,017	1,488	195	3,231	848	4,059	3,447	2,865	11,219
Lower Skins	531	1,309	1,617	402	3,859	848	8,057	5,197	2,865	16,967
Misc.	2,545	740	5,309	1,009	9,603	3,010	2,502	6,996	873	13,381
Assembly	2,063		4,041	1,387	7,491	3,248		6,362	2,447	12,057
Total	21,552	12,913	47,891	7,059	89,415	13,422	43,537	45,422	12,538	114,919



TABLE XX (CONCLUDED)

Component	CONCEPT NO. 3A					CONCEPT NO. 8				
	Labor	Mat'l	Overhead	Tooling	Total	Labor	Mat'l	Overhead	Tooling	Total
Spars	2,650	25,311	16,326	3,996	48,283	1,995	8,911	7,813	3,228	21,947
Ribs	2,953	13,538	11,740	1,428	29,559	2,255	5,535	6,853	1,223	15,866
Upper Skins	838	693	1,944	255	3,730	838	691	1,944	255	3,728
Lower Skins	1,161	8,078	5,832	2,910	17,981	838	1,200	2,168	475	4,681
Misc.	3,053	822	6,352	873	11,100	3,053	2,199	6,945	873	13,070
Assembly	3,429		7,056	2,008	12,493	2,234		4,373	1,538	8,145
Total	14,084	48,442	49,250	11,470	123,246	11,213	18,536	30,096	7,592	67,437

TABLE XXI. MAJOR DIFFERENCES IN WING BOX CONCEPTS

CONCEPTS	SPARS	RIBS	UPPER SKINS	LOWER SKINS	MISCELLANEOUS	ASSEMBLY
Baseline	Exterior-Hogouts of Conventional Forgings (100% Machined) of Al and Steel Interior-Machined Extrusions	Hogouts of Conventional Forgings (100% Machined) of Al and Steel	Aluminum	Aluminum	All Aluminum	Riveting
#1 F.D. Honeycomb	Exterior-Precision Forged Ti Aluminum Honeycomb Core	Precision Forgings and Castings - Ti	Titanium	Titanium	Aileron Access Door Composed of Graphite Aileron Hinge-Precision Cast Titanium	Both Bonding and Riveting Required
#1A F.D. Honeycomb	Exterior Precision Forged-Al Aluminum Honeycomb Core	Precision Forged - Al Except: Gear Rib-Precision Forged Ti Tip Rib-Ti Casting	Aluminum	Aluminum	Aileron Access Door Composed of Graphite Aileron Hinge-Precision Cast Titanium	Both Bonding and Riveting Required
#3 Al/Ti 6-Spar	Exterior-Precision Forged Ti Interior Spars-Ti Sine Wave Sheet	Root & Gear Rib-Precision Forged Ti-Pylon Ribs Same as Baseline	Aluminum	Titanium	Aileron Access Door Composed of Graphite Aileron Hinge-Precision Cast Titanium	Riveting
#3A Al/Ti	Exterior-Precision Forged-Ti Interior-Ti Sine Wave Sheet	Precision Forgings and Castings - Ti	Aluminum	Titanium	Aileron Access Door Composed of Graphite Aileron Hinge-Precision Cast Titanium	Upper Skin Riveted Welding on Lower Skin and Structures
#4 5-Spar	Exterior-Precision Forged Ti Interior Spars-Ti Sine Wave Sheet	Root & Gear Rib-Precision Forged Ti - Pylon Ribs Same as Baseline	Titanium (Bonded Assembly)	Titanium (Bonded Assembly)	Aileron Access Door Composed of Graphite Aileron Hinge-Precision Cast Titanium	Both Bonding and Riveting Required
#5 4-Spar	Exterior-Precision Forged-Ti Interior Spars-Ti Sine Wave Sheet	Root & Gear Rib-Precision Forged Ti - Pylon Ribs Same as Baseline	Titanium (Bonded Assembly)	Titanium (Bonded Assembly)	Aileron Access Door Composed of Graphite Aileron Hinge-Precision Cast Titanium	Both Bonding and Riveting Required
#8 6-Spar	Exterior-Precision Forged-Al Interior-Precision Forged-Al	Precision Forged-Al Except: Gear Rib-Precision Forged Ti Tip Rib-Ti Casting	Aluminum	Aluminum	Aileron Access Door Composed of Graphite Aileron Hinge-Precision Cast Titanium	Riveting
#8A 6-Spar	Exterior-Precision Forged-Al Interior-Precision Forged-Al	Precision Forged-Al Except: Gear Rib-Precision Forged Ti Tip Rib-Ti Casting	Aluminum	Aluminum (thick)	Aileron Access Door Composed of Graphite Aileron Hinge-Precision Cast Titanium	Riveting

lower skin to the substructure. This characteristic makes Concept 3A the most expensive assembly of all the designs (see Table XIX). The major item resulting in the 38% increase in cost over the baseline is the material cost of the titanium lower skin and spars.

Concept 4 is a five-spar design which is 62% more expensive than the baseline primarily because of substantially higher material costs in both lower and upper titanium skins.

Concept 5 is a four-spar design very similar to concept 4. The reduction in the number of interior spars and in the number of pans and cores in the skins results in the cost being 56% higher than the baseline compared to a 62% increase in #4.

Concept 8 is an aluminum design, somewhat similar to the baseline, but featuring sine-wave interior spars and titanium tip and gear ribs. This concept is the least expensive of all the concepts, showing a 25% cost reduction below the baseline, as a result of the major cost savings realized in the spars and ribs. Both components are aluminum forged net (no final machining required), hence, labor costs are four times lower than the baseline. The baseline requires a considerable amount of machining time on the conventional aluminum forgings and extrusions.

Concept 8A is similar to concept 8 except for a much thicker lower aluminum skin. This results in only a 13% reduction in cost compared to a 25% reduction over the baseline for concept 8.

#### e. Sensitivity Analysis

Sensitivity analysis is a method of evaluating the impact of a change in one parameter on the total result while holding all other parameters constant. This approach can be iterated several times to develop a ranking of the most significant variables. This provides a tool used in decision making under conditions of uncertainty. The results of the cost analysis form the foundation for the application of sensitivity analysis.



Sensitivity analysis was performed to quantify the impact that changes in the value of significant cost elements have on total costs. Two analyses were conducted to ascertain the effects that significant alterations in labor hours and production material costs have on the cost rankings of the three designs chosen for further study in the follow-on program -- wing boxes 1, 3A and 8. Labor hours were varied within a range of -25% to +25% of the expected level and material costs were varied within a range of -40% to +40% of the original estimates.

The results of the analysis appear in Figures 66 and 67 which show a near-linear relationship between both changes in labor hours and production material cost to change in total cost. For example,  $\pm 25\%$  change in labor hours results in a  $\pm 10\%$  change in total cost for concept 1 and 3A and a  $\pm 14\%$  change in total cost for concept 8. Because labor has a greater impact on total cost of this concept than it has on any of the other concepts, concept 8 shows the highest sensitivity to labor.

The total cost of concepts 1 and 3A is affected proportionately much more by material cost than concept 8 because both of these concepts contain a higher percentage of titanium. As a result, a corresponding 25% change in production material causes only a  $\pm 11$  percent change in total cost for concept 8 and a  $\pm 15\%$  change in total cost for concepts 1 and 3A. Thus, concepts 1 and 3A are most sensitive with regard to material cost.

Future trends in the titanium industry indicate slowly rising prices in the foreseeable future. However, the possibility exists that advances in manufacturing techniques will materialize in addition to those enumerated earlier. Thus, the total cost of concepts 1 and 3A may possibly be reduced by lower labor costs through advanced technology.



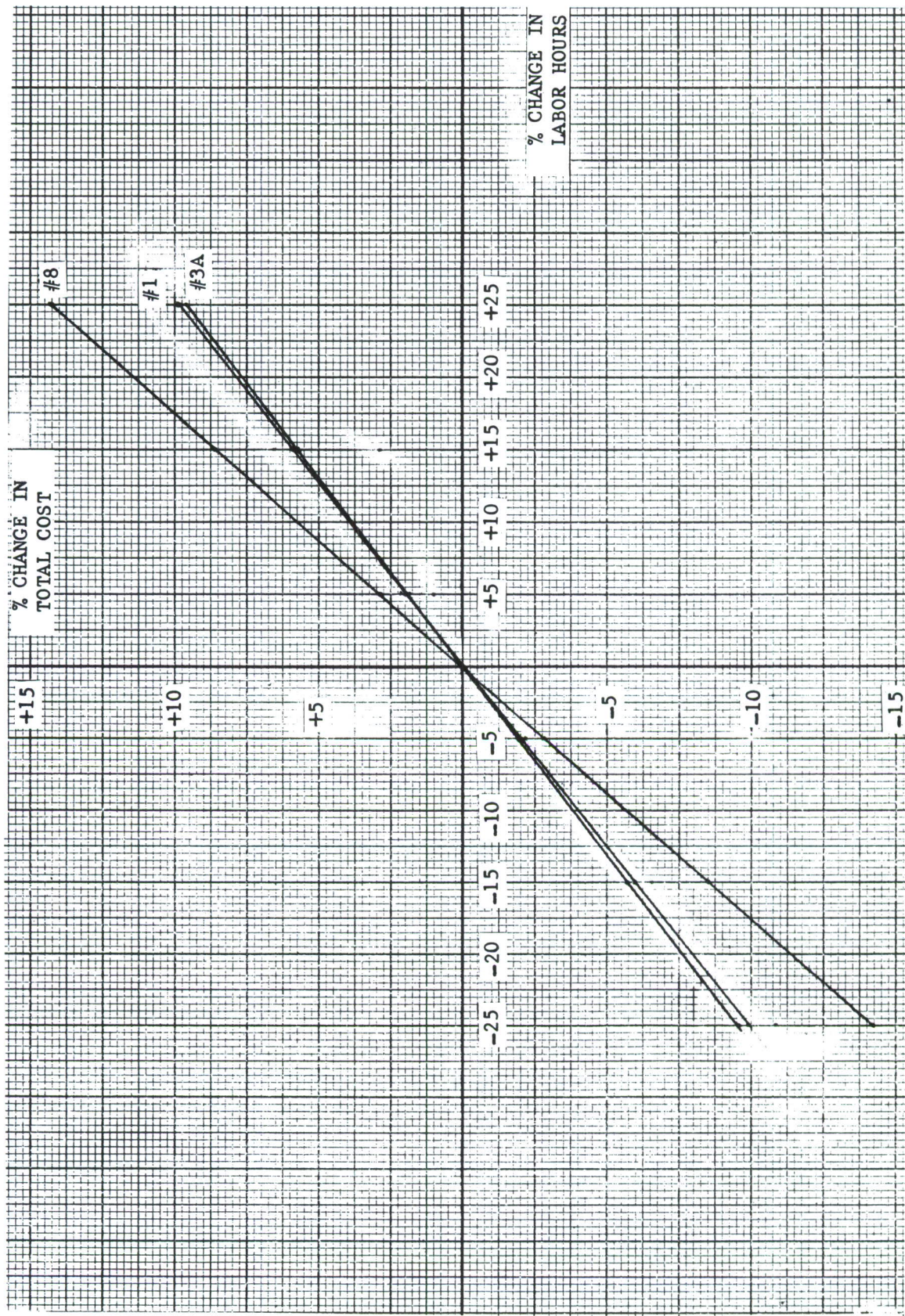


FIGURE 66. SENSITIVITY ANALYSIS ASSUMING CHANGE IN LABOR HOURS



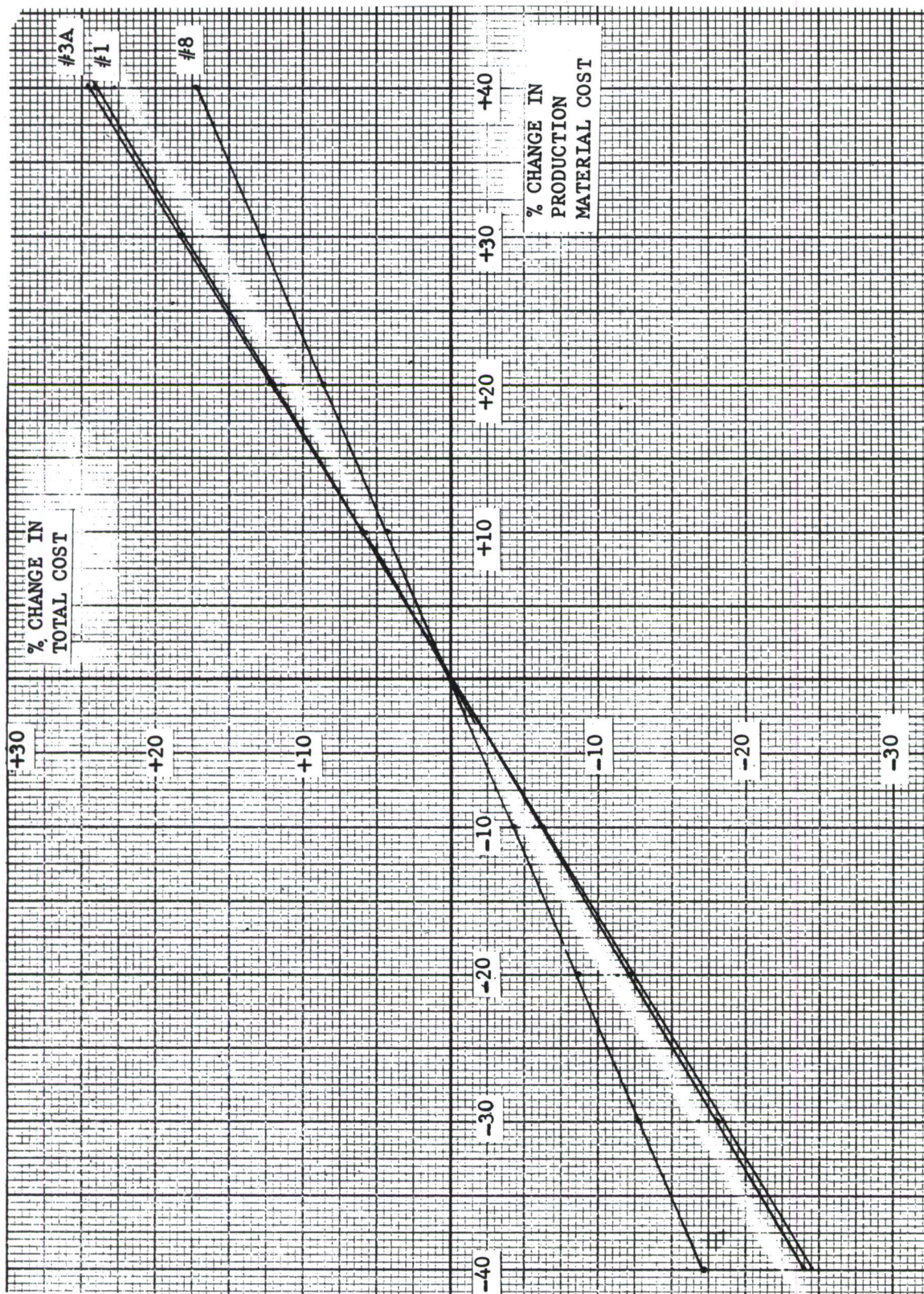


FIGURE 67. SENSITIVITY ANALYSIS ASSUMING CHANGE IN PRODUCTION MATERIAL COST



## 10. WEIGHTS ANALYSIS

Table XXII summarizes the structural weights for each of the eight advanced wing designs studied during this program. For comparison, the corresponding weights of the baseline production F-5E wing structure are included. Weight increments ( $\Delta$  weights) necessary to increase torsional stiffnesses to the levels required for aileron effectiveness (see Section III.3) are also shown. The lightest design based on strength, safe life and damage tolerance considerations only is Concept No. 5, a 4-spar design with titanium honeycomb panel wing skins. This design showed a 12.7 percent weight saving over the baseline. After aileron effectiveness considerations are included, Concept No. 1 is lightest with a 11.4 percent weight savings. This is the full depth honeycomb core design with titanium skins. A detailed part-by-part weight listing is presented in Table XXIII.

All weights were calculated consistent with the in-depth preliminary design study objective of the program. Particular care was taken to insure that all methods used were directly compatible with those used for the baseline F-5E, both in detail and in allowances for production tolerances.

Material volumes were determined using standard weight methods and desk computer programs. Material densities were used from the SAWE Weight Handbook<sup>(1)</sup>, and from materials data presented in Sub-section III.6. Fastener weight estimates took into account changes in grip length for each concept and unit weights were obtained from vendor handbooks and from Northrop's weights listings. Calculations were rounded off to the nearest tenth of a pound for weights greater than ten pounds and to the nearest hundredth for weights less than ten pounds. Totals were rounded to the nearest pound.

In addition to the total concept weights shown in Table XXII, the weights of two additional wing skin design concepts were also calculated and compared with baseline. These are (1) the Ti-Borsic upper skin design which investigated the compressive stability potential of this advanced, high specific modulus material and (2) the titanium geodesic lower skin

---

(1) Society of Aeronautical Weight Engineers, Inc., Weight Handbook, Volume 1, dated December 1968.

TABLE XXII. SUMMARY OF WING STRUCTURAL WEIGHTS FOR 8 CONCEPTS

CONCEPT	SPARS	RIBS	UPPER SKIN	LOWER SKIN	MISC	ASSY	TOTAL WT	% SAVING	Δ WEIGHT FOR WING (GJ)			TOTAL WEIGHT	% SAVING
									TI/ROBUSTIC	GRAPHITE EPOXY	METAL		
Baseline	166	211	203	250	85	66	981						
# 1	181 <sup>(1)</sup>	168	166	197	64	84 <sup>(8)</sup>	860	12.3	3	(< 10)	10	870	11.4
# 1A	151 <sup>(2)</sup>	171	206	238	64	92 <sup>(8)</sup>	922	6.0				922	6.0
# 3	203	169	198	250	64	49	933	4.9				933	4.9
# 3A	159	133	198	314	64	44	912	7.0				912	7.0
# 4	178 <sup>(3)</sup>	167	190 <sup>(4)</sup>	218 <sup>(6)</sup>	64	50	867	11.6	7	(< 18)	18	885	10.0
# 5	167 <sup>(3)</sup>	168	191 <sup>(5)</sup>	218 <sup>(7)</sup>	64	48 <sup>(9)</sup>	856	12.7	6	(< 15)	15	871	11.3
# 8	149	171	201	231	64	57	873	11.1				878	10.5
# 8A	155	171	201	229	64	52	872	11.2				877	10.6

(1) Fittings, doors, nonstructural panels, stop and seal panels, etc.

(2) Fasteners, adhesives, core splice foam

(3) Based on damage tolerance, safe life, and static requirements

(4) Including additional weight (metal option) to increase wing stiffness (GJ) to meet aileron effectiveness requirements

SEE TABLE III FOR CONCEPT DESCRIPTION.

- (1) Includes 46.6 lbs of core material, tip to tip  
(2) Includes 43.6 lbs of core material, tip to tip  
(3) Includes 2.8 lbs of core material, 123→TIP  
(4) Includes 6.0 lbs of core material and 12.0 lbs of adhesive and foam  
(5) Includes 8.0 lbs of core material and 12.0 lbs of adhesive and foam  
(6) Includes 5.0 lbs of core material and 10.0 lbs of adhesive and foam  
(7) Includes 3.0 lbs of core material and 9.0 lbs of adhesive and foam  
(8) Includes 42.8 lbs of adhesive and foam, tip to tip  
(9) Includes 5.2 lbs of adhesive and foam, 123→TIP

TABLE XXIII. DETAILED STRUCTURAL WEIGHT BREAKDOWN FOR 8 CONCEPTS

	F-5E Base- line	No. 1 F.D. Ti H/C	No. 1A F.D. Al H/C	No. 3 Al-Ti 6-Spar	No. 3A Al-Ti 6-Spar Welded	No. 4 5-Spar Ti	No. 5 4-Spar Ti	No. 8 Al-Al 6-Spar	No. 8A Al-Al 6-Spar Int. Fl.
SPARS									
Centerline to Root									
15%	3.9	5.4	3.9	4.9	3.5	4.9	4.9	3.3	3.1
No. 2	3.6			4.6	3.4	4.6	5.2	2.6	3.2
No. 3	3.6			4.7	3.5	4.8	5.2	2.0	3.2
No. 4	3.5			4.8	3.6	4.8		1.9	3.2
No. 5	5.0			4.9	3.7			3.1	4.7
Core		17.4	16.3						
44%	6.0	7.0	6.4	4.5	2.7	4.5	4.5	4.1	5.4
Root to Tip									
15%	41.5	49.9	42.3	49.9	40.2	49.9	49.9	41.5	41.5
66%	15.2	20.9	15.2	20.9	19.8	20.9	20.9	15.2	15.2
Root to MLG									
No. 2	4.7	6.8	4.7	6.3	4.6	6.8	8.6	3.9	4.0
No. 3	5.3			6.8	5.0	7.6	9.6	4.0	4.3
No. 4	6.1			7.4	5.5	8.2		4.4	4.9
No. 5	6.6			7.9	5.9			4.8	5.2
Core		16.6	15.5						
44%	23.5	31.8	25.8	30.4	25.0	30.4	30.4	23.5	22.2



TABLE XXIII. (Continued)

	F-5E Base- line	No. 1 F.D. Ti H/C	No. 1A F.D. Al H/C	No. 3 Al-Ti 6-Spar	No. 3A Al-Ti 6-Spar Welded	No. 4 5-Spar Ti	No. 5 4-Spar Ti	No. 8 Al-Al 6-Spar	No. 8A Al-Al 6-Spar Int. Fl.
SPARS (Continued)									
MLG to I.B. Pylon									
No. 2	1.9			2.4	1.4	2.4	2.6	1.7	1.7
No. 3	1.5			2.4	1.4	2.6	2.6	1.7	1.7
No. 4	2.8			2.6	1.8	2.6		1.6	1.6
No. 5	4.0			2.6	1.8			1.8	1.8
Core		4.6	4.3						
44%	4.0	4.6	4.0	4.6	3.4	4.6	4.6	4.0	4.0
Auxiliary	1.8	1.8	1.8	1.8	1.8	1.8	1.8	1.8	1.8
I.B. Pylon to O.B. Pylon									
No. 2	1.9			3.2	2.2	3.2	3.2	1.9	1.9
No. 3	2.0			3.2	2.2	3.2	3.2	1.9	1.9
No. 4	2.0			3.2	2.2			2.0	2.0
No. 5	1.6			3.2	2.2			2.2	2.2
Core		5.2	4.9						
44%	3.6	5.8	3.6	5.8	4.8	5.8	5.8	3.6	3.6
Auxiliary	1.3			1.5	1.5	1.5	1.5	1.3	1.3

TABLE XXXIII. (Continued)

	F-5E Base- line	No. 1 F.D. Ti H/C	No. 1A F.D. Al H/C	No. 3 Al-Ti 6-Spar	No. 3A Al-Ti 6-Spar Welded	No. 4 5-Spar Ti	No. 5 4-Spar Ti	No. 8 Al-Al 6-Spar	No. 8A Al-Al 6-Spar Int. Fl.
SPARS (Continued)									
O.B. Pylon to Tip									
No. 2	1.9			1.9	1.4			1.9	1.9
No. 3	1.4			1.4	.9			1.4	1.4
No. 4	1.4			1.4	.9			1.4	1.4
No. 5	2.1			2.1	1.5			2.1	2.1
No. 6	2.1			2.1	1.5			2.1	2.1
Core		2.8	2.6			2.8	2.8		
SPARS TOTALS	(166)	(181)	(151)	(203)	(159)	(178)	(167)	(149)	(155)

TABLE XXXIII. (Continued)

	F-5E Base- line	No. 1 F.D. Ti H/C	No. 1A F.D. Al H/C	No. 3 Al-Ti 6-Spar	No. 3A Al-Ti 6-Spar Welded	No. 4 5-Spar Ti	No. 5 4-Spar Ti	No. 8 Al-Al 6-Spar	No. 8A Al-Al 6-Spar Int. Fl.
RIBS									
Root	38.4	33.6	36.2	35.5	28.6	33.2	32.8	37.0	37.0
Landing Gear	64.6	43.4	39.4	40.0	28.0	40.0	39.8	40.2	40.2
Inboard Pylon	31.4	28.6	30.8	31.0	24.0	31.2	31.0	31.0	31.0
Outboard Pylon	28.1	26.4	29.4	27.0	19.6	26.4	26.3	28.1	28.1
Tip	28.0	15.4	15.4	15.7	14.2	15.4	15.4	15.7	15.7
Speed Brake Actuator	2.3	3.2	3.2	2.3	1.3	3.2	3.7	2.3	2.3
Landing Gear Uplock	6.4	6.4	6.4	6.4	6.4	6.4	6.4	6.4	6.4
W.S. 38.16 Cant	1.1	1.4	1.1	1.1	1.1	1.4	1.8	1.1	1.1
L.E. Flap Hinge, W.S. 57.0	2.0	1.8	2.0	2.0	2.1	1.7	2.2	2.0	2.0
L.E. Flap Hinge, W.S. 73.0	0.5								
Landing Gear Side Brace	0.7			0.7	0.7	0.9	1.2	0.7	0.7
Aileron Actuator 85.2 Cant	2.6	3.1	2.6	2.6	2.6	2.6	2.6	2.6	2.6
Aileron Actuator W.S. 91.7	1.6	1.9	1.6	1.6	1.6	1.6	1.6	1.6	1.6
Aileron Hinge	3.8	3.2	2.7	2.7	2.7	2.7	2.7	2.7	2.7
RIBS TOTALS	(211)	(168)	(171)	(169)	(133)	(167)	(168)	(171)	(171)
<div> <div>1</div> Includes the ail- eron actuator sup- port rib between 39 and 44% </div>									



TABLE XXIII. (Continued)

	F-5E Base- line	No. 1 F.D. Ti H/C	No. 1A F.D. Al H/C	No. 3 Al-Ti 6-Spar	No. 3A Al-Ti 6-Spar Welded	No. 4 5-Spar Ti	No. 5 4-Spar Ti	No. 8 Al-Al 6-Spar	No. 8A Al-Al 6-Spar Int. Fl.
UPPER SKIN									
Outer Skin	203	166	206	198	198	155	155	201	201
Inner Skin		Negl.				16.4	16.4		
H/C Core		Negl.				6.4	7.6		
Adhesive		Negl.				7.8	8.0		
Foam		Negl.				4.2	3.6		
UPPER SKIN TOTALS	(203)	(166)	(206)	(198)	(198)	(190)	(191)	(201)	(201)
LOWER SKIN									
Outer Skin	250	197	238	250	314	191	193	231	229
Inner Skin						14.4	13.6		
H/C Core						3.1	3.1		
Adhesive						6.8	6.6		
Foam						2.3	1.6		
LOWER SKIN TOTALS	(250)	(197)	(238)	(250)	(314)	(218)	(218)	(231)	(229)

TABLE XXXIII. (Continued)

	F-5E Base- line	No. 1 F.D. Ti H/C	No. 1A F.D. Al H/C	No. 3 Al-Ti 6-Spar	No. 3A Al-Ti 6-Spar Welded	No. 4 5-Spar Ti	No. 5 4-Spar Ti	No. 8 Al-Al 6-Spar	No. 8A Al-Al 6-Spar Int. Fl.
MISCELLANEOUS									
Panels and Doors									
Upper MLG Bay Panel	22.4	12.3							12.3
Aileron Actuator	4.8								
Upper Bay Panel									
Lwr Nut Plate Panel	1.4	1.4							1.4
Lwr Ail Act Access Dr	12.6	10.1							10.1
Lwr Access Cover	0.8	0.8							0.8
Hydraulic -Trlng Inbd	0.5	0.5							0.5
T.E. Pnl Bonded Assy	11.6	11.6							11.6
Hardware									
Brkt, Wing Attach 66%	1.4	0.9							0.9
I.B. Fixed Ail Hinge	4.5	2.8							2.8
O.B. Fixed Ail Hinge	0.8	0.8							0.8
O.B. Fixed T.E. Hinge	2.8	2.8							2.8
T.E. Flap Hinge Supt	1.0	1.0							1.0
L.E. Flap Brkt LES 66	3.8	3.0							3.0
L.E. Flap Brkt LES 86	4.0	3.4							3.4
L.E. Flap Brkt LES 116	0.9	0.7							0.7

TABLE XXXIII. (Continued)



	F-5E Base- line	No. 1 F.D. Ti H/C	No. 1A F.D. Al H/C	No. 3 Al-Ti 6-Spar	No. 3A Al-Ti 6-Spar Welded	No. 4 5-Spar Ti	No. 5 4-Spar Ti	No. 8 Al-Al 6-Spar	No. 8A Al-Al 6-Spar Int. Fl.
Hardware (Continued)									
L.E. Flap Brkt LES 141	0.6	0.5							0.5
L.E. Flap Brkt LES 158	0.5	0.4							0.4
Stop/Seal Assy	11.0	11.0							11.0
MISCELLANEOUS TOTALS	(85)	(64)	(64)	(64)	(64)	(64)	(64)	(64)	(64)
ASSEMBLY									
Rib Fasteners									
Root	3.3	2.5	3.5	2.3	1.9	1.9	1.9	2.8	2.5
MLG	4.5	4.3	4.7	3.6	3.0	3.5	3.5	3.8	3.3
I.B. Pylon	4.7	4.1	4.7	3.5	3.4	3.8	3.8	3.9	3.9
O.B. Pylon	2.6	2.0	2.8	1.9	1.6	2.0	2.0	2.0	1.7
Tip	1.4	1.3	1.4	1.4	1.1	1.3	1.3	1.4	1.3
Others	3.4	2.1	3.5	2.6	2.3	2.1	2.1	2.9	2.6
Peripheral Spar									
Fasteners 									
15%	8.8	8.0	9.1	7.1	5.7	6.6	6.6	8.2	6.3
44%	9.0	7.1	9.2	6.1	4.7	5.6	5.6	7.7	6.4
66%	3.2	2.9	3.3	2.6	2.5	2.9	2.9	2.8	2.6
 includes spar to rib fasteners									



TABLE XXXIII. (Concluded)

	F-SE Base- line	No. 1 F.D. Ti H/C	No. 1A F.D. Al H/C	No. 3 Al-Ti 6-Spar	No. 3A Al-Ti 6-Spar Welded	No. 4 5-Spar Ti	No. 5 4-Spar Ti	No. 8 Al-Al 6-Spar	No. 8A Al-Al 6-Spar Int. Fl.
Int. Spar Fasteners									
W.S. 0-30	4.2			2.8	2.4	2.3	1.5	3.5	3.0
30-73	4.5			2.9	2.6	2.3	1.6	3.6	3.4
73-93.5	3.8	0.3	0.4	2.5	2.5	2.5	1.9	3.5	3.8
93.5-123	4.0	0.9	1.2	2.4	2.5	2.0	2.0	2.8	3.2
123-151	2.7			1.5	1.7			1.8	2.2
Adhesives									
Core to Skins		9.2	9.2			1.6	1.6		
Core to Spars (Foam)		9.0	9.0			1.2	1.2		
Core to Ribs (Foam)		6.6	6.6			0.4	0.4		
Core Splices (Foam)		3.0	3.0			0.2	0.2		
Elec/Fuel Lines (Foam)		15.0	15.0			1.8	1.8		
Panels, Drs and Hardware Fasteners	6.3	5.8	5.8	5.8	5.8	5.8	5.8	5.8	5.8
ASSEMBLY TOTALS	(66)	(84)	(92)	(49)	(44)	(50)	(48)	(57)	(52)
includes spar to rib fasteners									

which is a highly redundant, multiple load path fail-safe concept. Both designs were sized for a 4-spar substructure. The Ti-Borsic upper skin weighed 224 pounds compared to the F-5E baseline upper skin weight of 203 pounds. Ti-Borsic was used from the centerline to wing station 123. Outboard of this station, the all titanium full depth tip similar to Concept No. 1 was used. This design was largely stability critical on the 4-spar substructure. A very brief study into the possible weights using a 6-spar substructure indicated that the minimum weight could possibly approach that of the present F-5E upper skin.

The geodesic titanium fail-safe lower skin design was studied from the centerline to W.S. 93 where safe-life becomes the pacing design consideration. Outboard, the monolithic titanium design from Concept 5 was used. This lower wing skin design weighed 300 pounds versus the baseline lower skin weight of 250. It too, was compressive and shear stability critical for reverse bending conditions due primarily to the low net modulus of elasticity inherent in the geodesic concept. A brief study indicated that the weight of this design inboard of W.S. 93 could also approach the present baseline weight if a 6-spar substructure were used. In this case, safe life rather than reverse bending stability is the pacing factor.

## SECTION IV

### RANKING OF CONCEPTS

Upon the completion of the weights and cost analyses, a concept ranking exercise was held. The weighting factors are as shown in Table XXIV and the definition of terms are as indicated on page 211.

All terms were graded on a scale of 1.0 to 10.0. For example, with respect to weight, the lightest scores 10.0 and the heaviest scores 1.0, irrespective of whether or not it is heavier or lighter than the baseline design.

A concept, designated as 6/7, comprised a Ti-Borsic upper skin, a geodesic lower skin and a four-spar titanium substructure. Although this concept scored very well (4.70) in the areas of "technology development," "integrity" and "ilities," it was eliminated from further consideration because a preliminary analysis showed that it weighed more and was costlier than the baseline.

The three chosen concepts were:

No. 1 - Full depth honeycomb with titanium skins

(This scored the highest on the rating chart)

No. 3A - Aluminum/titanium 6-spar wing with extensive use of welding on the bottom skin (This scored the second highest on the rating chart)

No. 8 - Aluminum 6-spar wing (This scored third highest on the rating chart)

Although Concept No. 1A (Full depth honeycomb with aluminum skins) scored a tie with Concept No. 8, No. 1A was eliminated because it is a variation from No. 1, and does not offer the cost and weight savings represented by No. 8.





## Merit Rating System

### Definitions

1. Cost - The cheapest scores 10, the most expensive scores 1.
2. Weight - The lightest scores 10, the heaviest scores 1.
3. Concepts - The extent to which a new concept differs from the baseline.  
The most radically different concept will score 10, the baseline will score 1, and the balance will lie in between these two.
4. Manufacturing - The extent to which new manufacturing techniques are used relative to the baseline. The concept incorporating the highest percentage of new techniques will score 10, whereas the baseline will score 1. The balance will lie in between.
5. Materials - The extent to which new materials are used with respect to the baseline. The scoring is as in (3) and (4) above.
6. Fracture - The extent to which fracture analysis has been used in the overall analysis of a new concept.
7. Static - A measure of the excess static strength over the minimum requirement.
8. Fatigue - A measure of the excess fatigue strength over the minimum requirement.
9. Safe crack - A measure of the excess damage tolerance strength over the minimum requirement for a safe crack design.
10. Fail safe - A measure of the excess damage tolerance strength over the minimum requirement for a fail safe design.
11. Inspectability - The degree to which a concept is judged to be inspectable under in-service conditions.
12. Manufacturability - The ease with which a particular concept can be manufactured.
13. Maintainability - The extent to which a particular concept is designed with a view for system support requirements.
14. Repairability - This is generally a part of "maintainability", but is shown separately in order to show the extent to which a particular design is repairable. One factor taken into account is: how much "down time" is involved?
15. Predictability - The extent to which confidence is held in the ability to assess the overall structural integrity of a particular concept.

## SECTION V

### CONCLUSIONS

The work performed under this contract shows that specific improvements in the cost and weight of a typical structural wing box for an air superiority fighter can indeed be obtained by combining advanced design concepts, materials, and manufacturing techniques.

The cost and weight summaries are shown elsewhere in this report for the concepts studied:

Table XIX - Costs

Table XXII - Weights

The maximum cost saving shown is 25 percent, and the maximum weight saving shown is 11 percent.



## SECTION VI

### PAYOFFS

The benefits can be shown primarily as a result of improvements in the two key parameters, cost and weight.

#### 1. COST

If one considers the two figures, 9-6 and 9-7, in the "Quick-Look" final report<sup>(1)</sup>, and replots them in a slightly different form, Figures 68 and 69 in this report are developed. Next, considering Concepts 1 (weight saving of 11%, cost increase of 28%) and 8 (weight saving of 11%, cost saving of 25%), the following is derived:

	Concept 1	Concept 8
Incremental Flyaway Cost	+ 1,000	- 38,000
Incremental Life Cycle Cost	- 4,000	- 108,000
Total per Aircraft	- 3,000	- 146,000

If a production lot of 300 aircraft is considered, the following savings are realized:

	Concept 1	Concept 8
	900,000	43,800,000

---

(1) C. Rosenkranz, et al, Advanced Lightweight Fighter Structural Concept Study, AFFDL TR-72-98, dated July 1972.

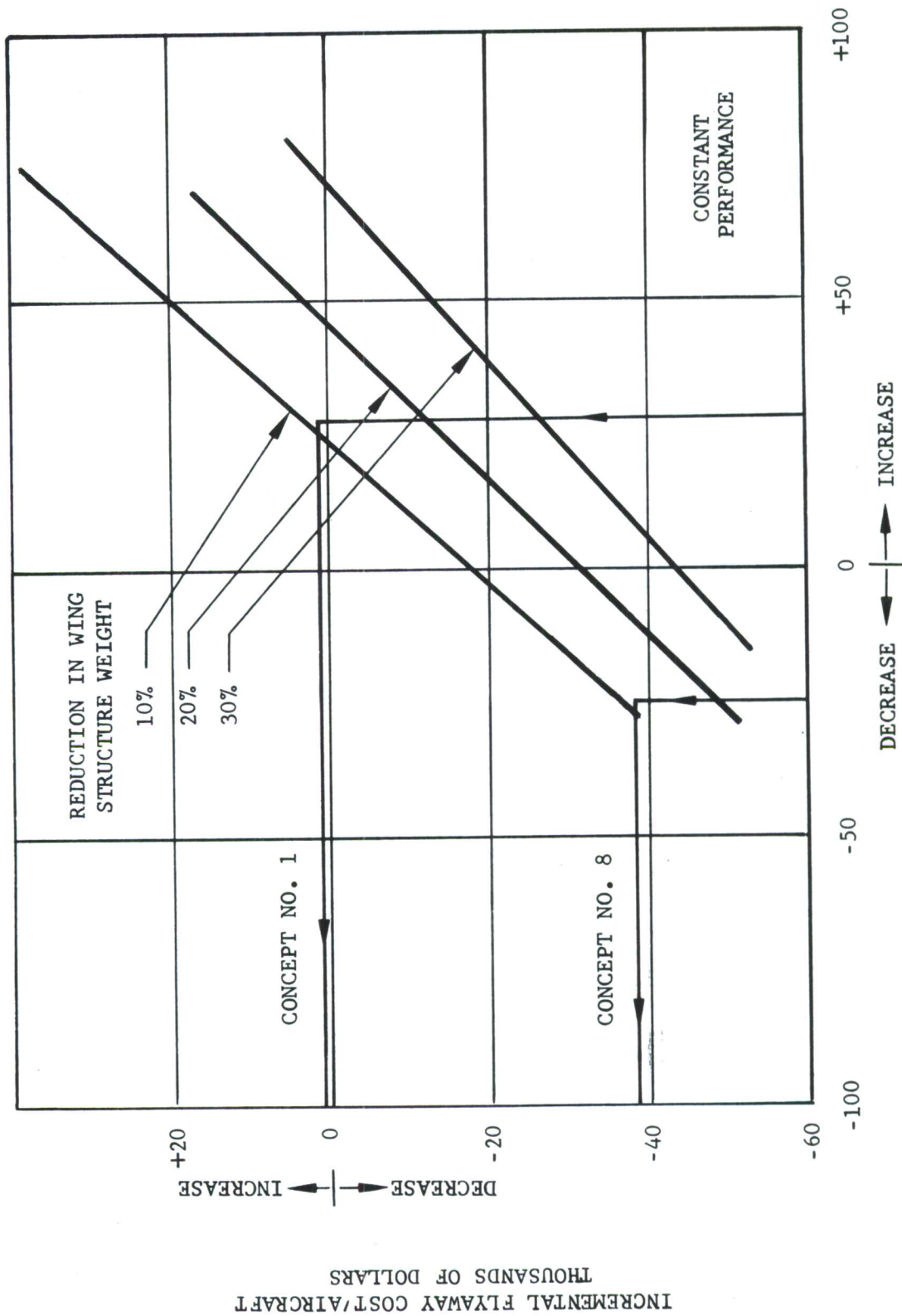


FIGURE 68. EFFECT OF WING STRUCTURE WEIGHT REDUCTION ON F-5E FLYAWAY COSTS

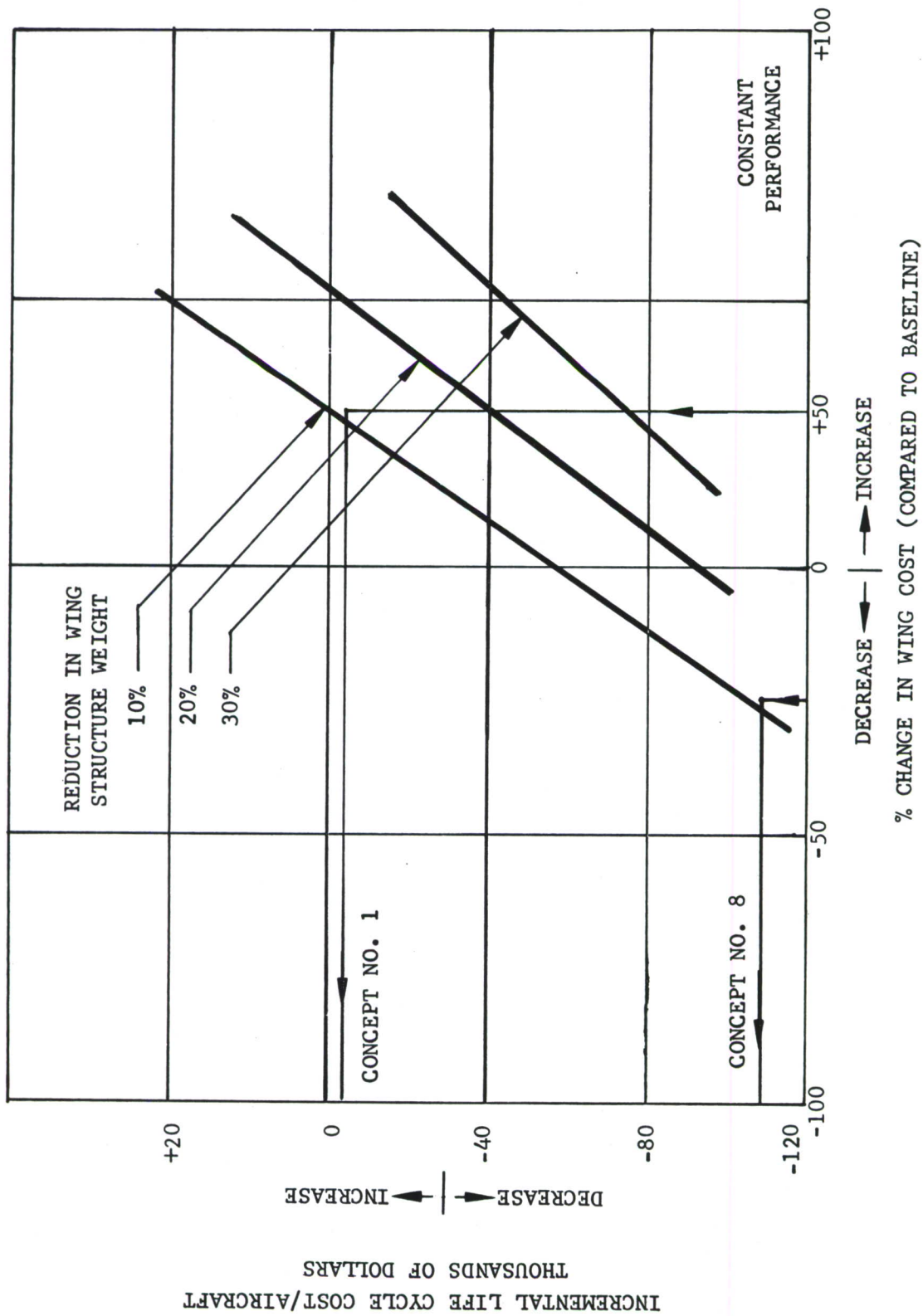


FIGURE 69. EFFECT OF WING STRUCTURE WEIGHT REDUCTION IN F-5E LIFE CYCLE COSTS



It can thus be seen that there is a large overall cost saving potential in the case where the wing box itself experiences a cost and weight saving. It is also of interest to note that an overall cost saving is possible, even though the cost of the wing box itself increases, as long as there is a sufficient decrease in the wing box weight, such as for Concept Number 1.

## 2. WEIGHT

If weight is the primary concern, then a weight saving can be transformed into a performance increase.

Figures 70 and 71 show two possible performance parameters, turn rate and maneuvering capability. The maximum realizable wing weight saving on the concepts considered can be transformed into an airplane weight saving approaching the smaller of the two shown on the two performance figures. Both weight savings curves are shown in order to permit the reader to extrapolate the weight payoff with a higher degree of certainty. Nevertheless, it is seen from both of these figures that a realistic weight saving in the wing can indeed have a measured performance payoff.

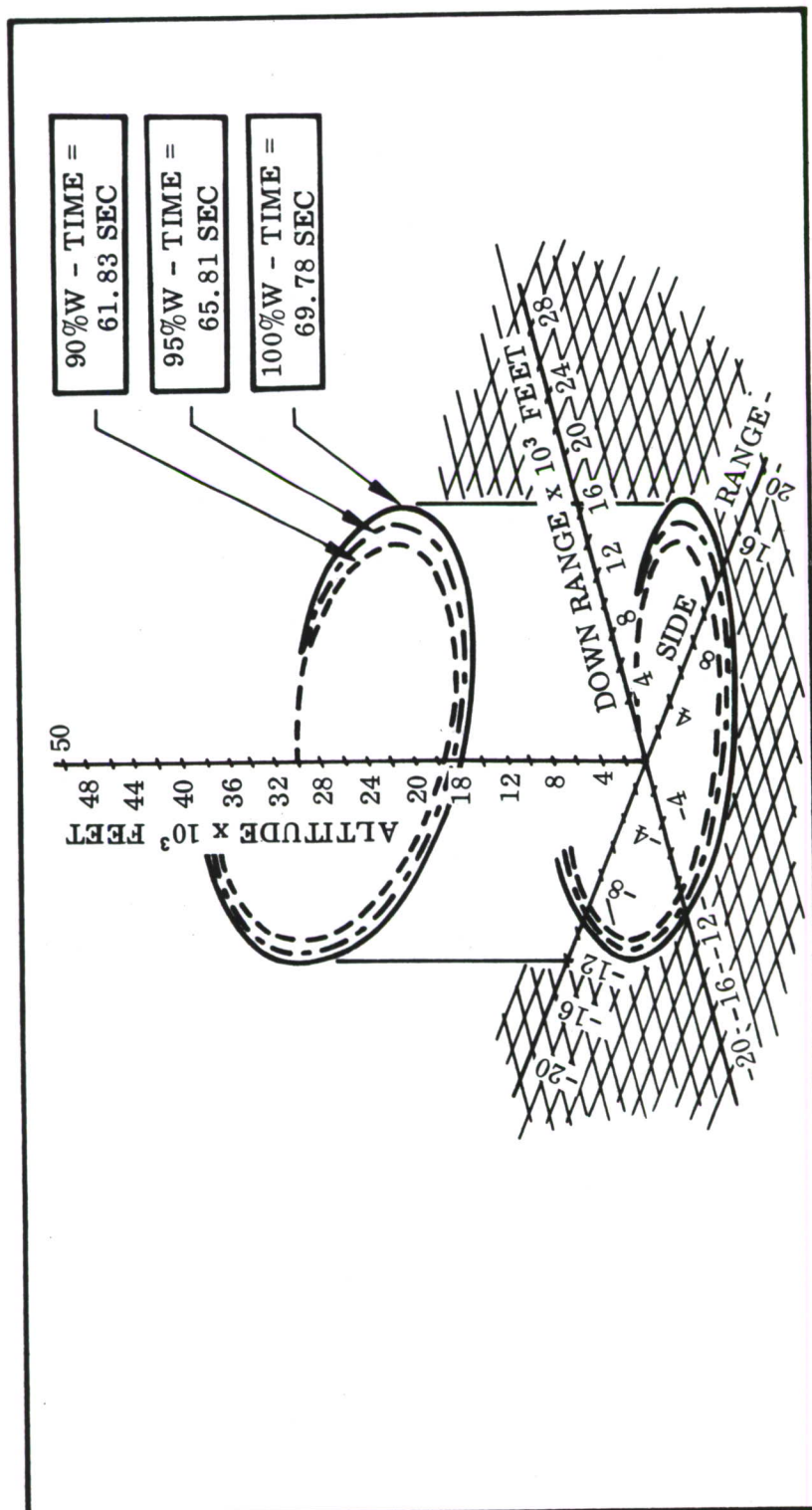


FIGURE 70. EFFECT OF WEIGHT REDUCTION ON F-5E TURN CAPABILITY

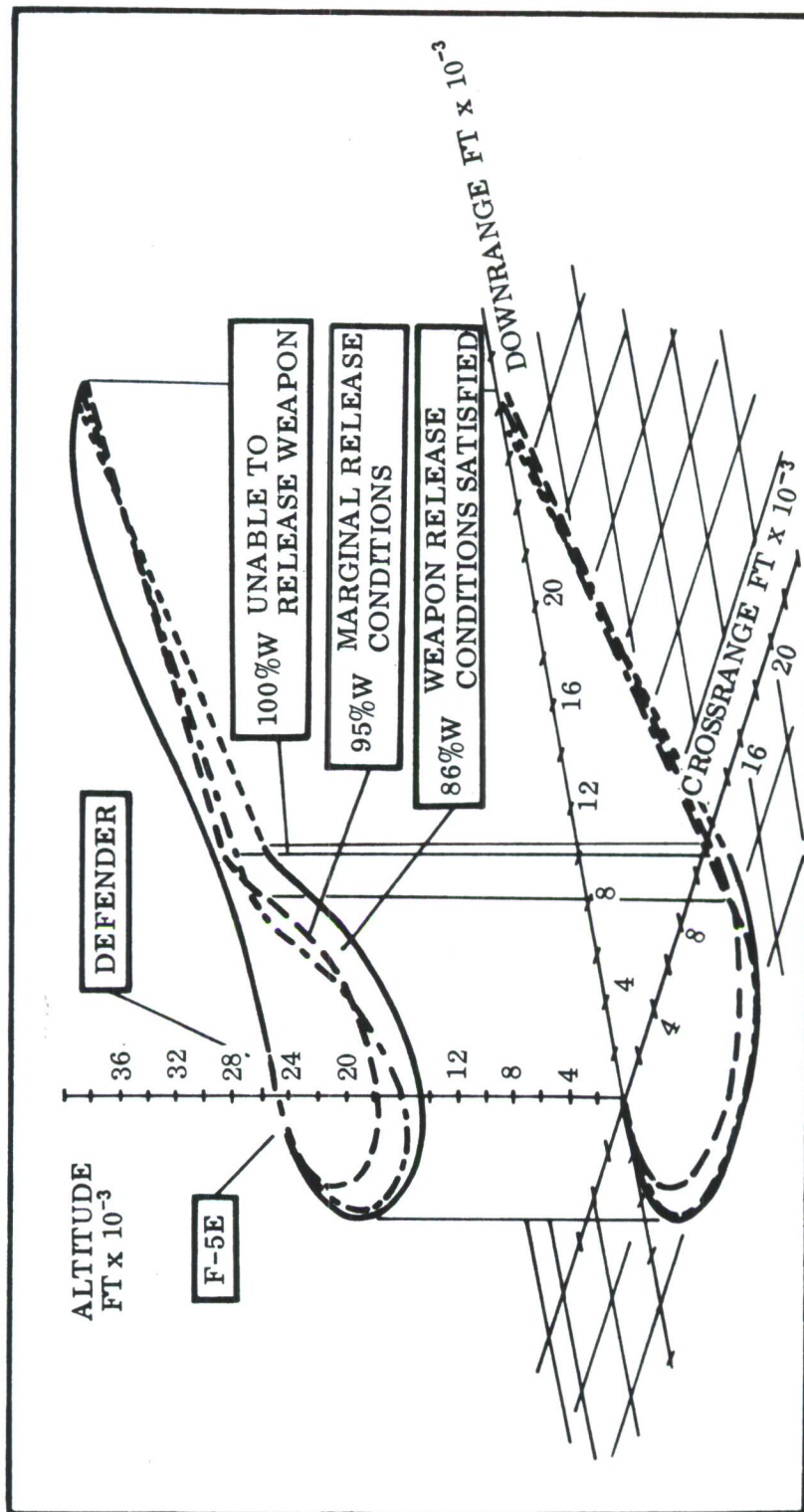


FIGURE 71. EFFECTS OF WEIGHT REDUCTION ON AIR-TO-AIR COMBAT MANEUVERING



## SECTION VII

### RECOMMENDATIONS FOR TECHNOLOGY DEVELOPMENT

The following is a summary of work activities, which should be investigated further, either as a part of the follow-on program, or as individual research contracts.

1. Ti-Borsic strength data, with particular emphasis on fracture data.
2. Manufacturing and design concept evaluation of Ti-Borsic.
3. A feasibility study on roll bonding a geodesic skin structure in order to reduce costs.
4. Analytical methods and experimental verification for reliably predicting the strength and stiffness requirements of honeycomb core to stabilize thick covers in full depth honeycomb structures in bending.
5. Analytical methods and experimental verification for reliably predicting the failure modes, and external support stiffness requirements for relatively thin honeycomb panels with thick outer face sheets and thin inner pan face sheets.
6. Experimental evaluation of the relative fatigue performance of channels with corrugated webs and heel angles with flat flanges mechanically fastened to heavy sheet or plate loaded in tension.
7. A program to establish cutter geometry, speed and feed rates to eliminate warpage for Ti 6-4 and Ti 6-22-22 skins in both the  $\beta$ MA and STA conditions.
8. A program for vacuum creep forming of the same skins as in 7. above.
9. A development and testing program on titanium net castings to provide criteria for establishing porosity acceptance levels, acceptable dimensional tolerances, surface finish and straightening techniques.

10. A development program on titanium isothermal precision forgings to investigate ways in which to control precise die temperatures to maintain size and shape of the finished articles.
11. A program to further investigate adhesive bonding of aluminum core to titanium skins in order to establish pressure application and cure cycle time and temperature requirements.
12. Further development of reliable NDI methods for multilayer bonded assemblies is required.
13. Development of criteria for high resolution ultrasonic inspection of titanium wrought products and welds for structural application is necessary.
14. Application of new X-ray technology to fatigue crack detection in aluminum and titanium structures.

## APPENDIX I

### CORRUGATED WEB SPAR STIFFNESS REQUIREMENTS

An analysis of the variation with buckle wave length of the buckling loads of panels on line elastic spring supports is presented in Reference (1). The results obtained there can be applied to the design of corrugated webs provided the proper stiffness parameter for the corrugated web is substituted for the support spring stiffness. In the present analysis, this stiffness parameter is derived and a method outlined for corrugated web analysis or design. The nomenclature for this analysis is presented on page 228.

In order to utilize the results of Reference (1), the corrugated web shown in Figure 72 is assumed to be idealized as a prismatic channel section (Figure 73) with two flanges having the same thickness  $t_f$  and width  $f$  equal to the average width of the corrugated web flange. The channel web is an effective flat plate having average flexural stiffness (References (2) and (3)).

$$D_1 = \frac{Et_w^3}{12(1-\mu)} \frac{\sin \phi}{\phi} \quad (1a)$$

$$D_2 = \frac{ER^2 t_w^2}{1-\mu^2} \left( \frac{1}{2} + \cos^2 \phi - \frac{3}{4} \frac{\sin 2\phi}{\phi} \right) \frac{\phi}{\sin \phi} \quad (1b)$$

$$D_3 = \frac{Et_w^3}{12(1+\mu)} \frac{\phi}{\sin \phi} \quad (1c)$$

- (1) R.A. Anderson and J.W. Semonian, Charts Relating the Compressive Buckling Stress of Longitudinally Supported Plates to the Effective Deflectional and Rotational Stiffness of the Supports, NACA TR 1202, 1954.
- (2) D.H. Emero and L. Spunt, "Optimization of Multirib and Multiweb Wing Box Structures Under Shear and Moment Loads," Proceedings Sixth AIAA Structures and Materials Conference, Palm Springs, Ca., Apr 1965, p 330.
- (3) S. Timoshenko and S. Woinowsky-Krieger, Theory of Plates and Shells, 2nd Ed. McGraw-Hill Book Co., Inc, 1959, pp 364-368.



NOMENCLATURE FOR APPENDIX I

$t_f$	flange thickness
$R$	radius of centerline of corrugation
$\phi$	maximum slope angle of corrugation
$\mu$	Poisson's ratio
$E$	Young's modulus
$D_f$	flange flexural stiffness
$D_1, D_2, D_3$	effective flexural stiffness of equivalent orthotropic plate
$f$	average flange width to edge of fastener
$b$	plate width between webs
$D_p$	panel flexural stiffness (isotropic panel)
$d$	web depth
$M_o$	amplitude of moment between flange and web
$\lambda$	buckle half-wave length
$A, B, C, D$	constants of integration
$\alpha'$	moment-rotation ratio for web
$t_w$	corrugated web thickness

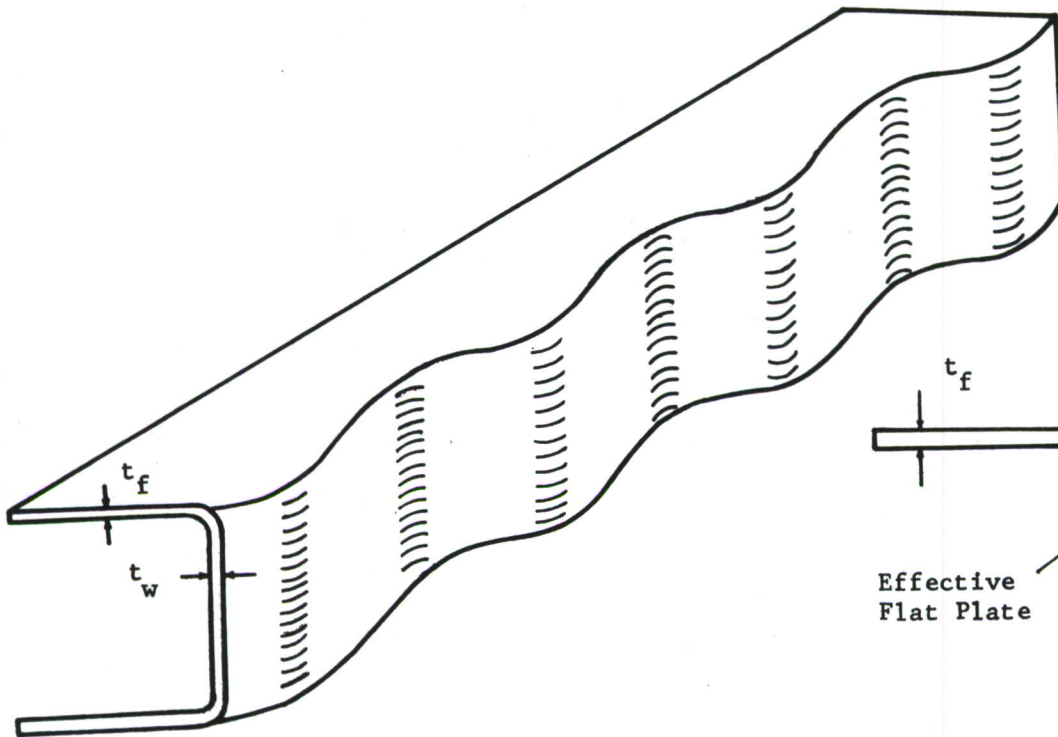


FIGURE 72. SCHEMATIC OF CORRUGATED WEB SPAR

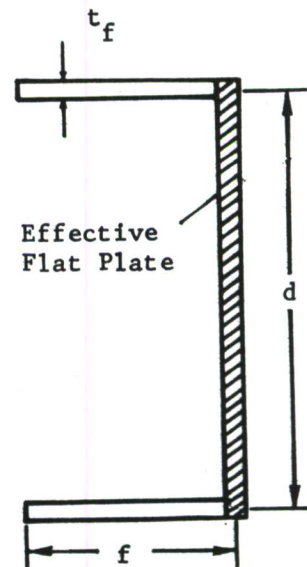


FIGURE 73. IDEALIZED PRISMATIC CHANNEL SECTION

Then the approximate analysis of Reference (1) yields the extensional stiffness parameter for the channel section as

$$\frac{\psi b^3}{\pi^4 D_p} = \frac{12}{\pi^4} \frac{D_f}{D_p} \left( \frac{b}{f} \right)^3 \frac{\frac{\alpha' f}{D_f} + 1}{\frac{\alpha' f}{D_f} + 4} \quad (2a)$$

$$D_f = \frac{Et^3 f}{12(1 - \mu^2)} \quad (2b)$$

- (1) R.A. Anderson and J.W. Semonian, Charts Relating the Compressive Buckling Stress of Longitudinally Supported Plates to the Effective Deflectional and Rotational Stiffness of the Supports, NACA TR 1202, 1954.

## 1. TORSIONAL RESTRAINT OF CORRUGATED WEB

The equation for the deflection of an orthotropic plate under edge loading is given by Reference (1)

$$D_1 \frac{\partial^4 w}{\partial x^4} + 2D_3 \frac{\partial^4 w}{\partial x^2 \partial y^2} + D_2 \frac{\partial^4 w}{\partial y^4} = 0 \quad (3)$$

The plate is assumed to be infinitely long and is prevented from deflecting along both long edges. At one edge a bending moment

$$M_y = M_0 \sin \frac{\pi x}{\lambda} \quad (4)$$

is applied; the other edge is either free to rotate or is completely prevented from rotating ( Figure 74).

Let the deformation pattern be described by

$$w = g(y) \sin \frac{\pi x}{\lambda} \quad (5)$$

where, from equations (3) and (5),  $g(y)$  satisfies the equation

$$D_2 \frac{d^4 g}{dy^4} - 2 \left( \frac{\pi}{\lambda} \right)^2 D_3 \frac{d^2 g}{dy^2} + \left( \frac{\pi}{\lambda} \right)^4 D_1 g = 0 \quad (6)$$

The value of  $\alpha'$  to be used in conjunction with equation (2a) is derived below under the assumption that axial forces in the corrugated web are negligible due to the axial extensional flexibility of the web.

- 
- (1) S. Timonshenko and S. Woinowsky-Krieger, Theory of Plates and Shells, 2nd Ed. McGraw-Hill Book Co., Inc, 1959, pp 364-368.



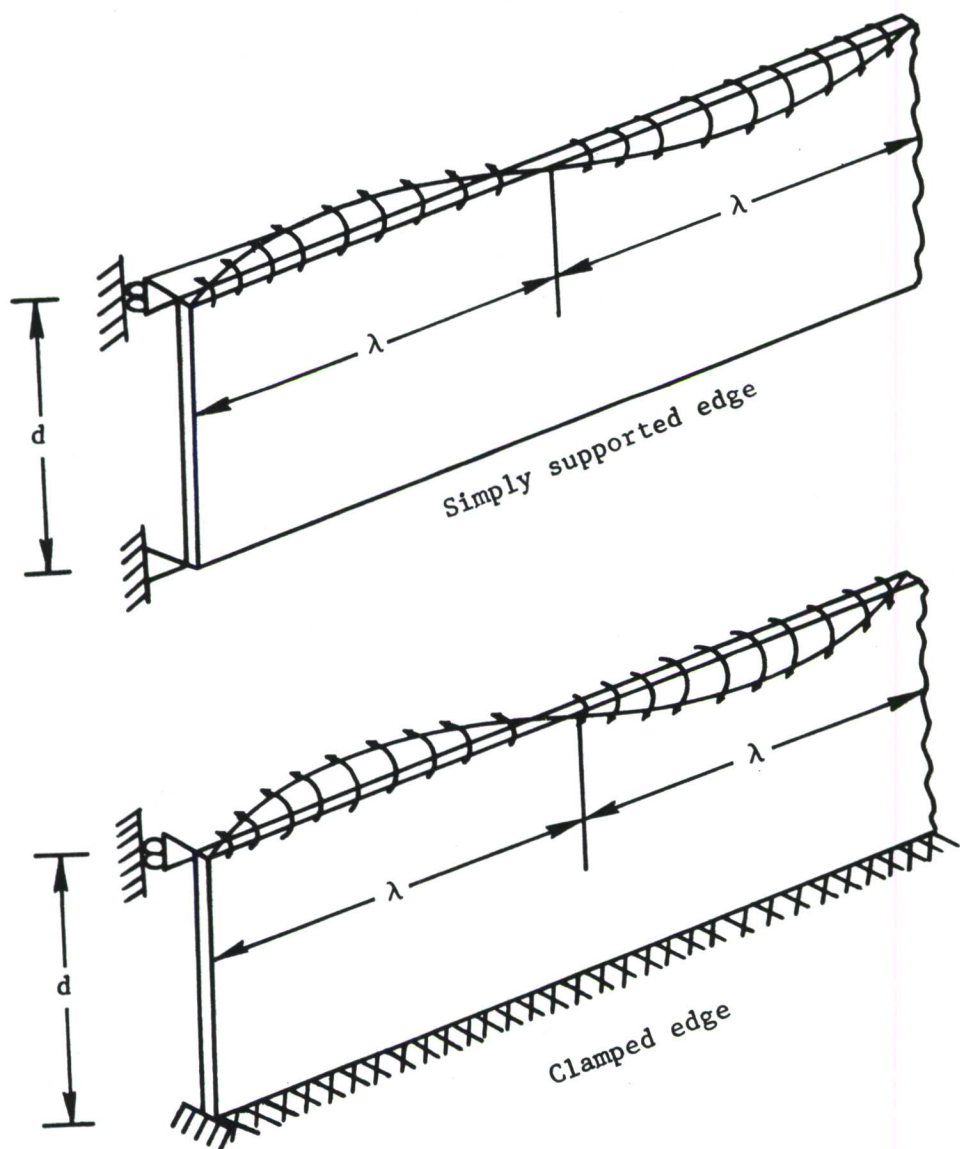


FIGURE 74. PLATE SUBJECTED TO HARMONICALLY VARYING EDGE MOMENT

The solution of equation (6) may be written as

$$g = e^{-\alpha \bar{y}} \left( A \cos \beta \bar{y} + B \sin \beta \bar{y} \right) + e^{\alpha \bar{y}} \left( C \cos \beta \bar{y} + D \sin \beta \bar{y} \right) \quad (7a)$$

with A, B, C, D constants of integration and

$$\left. \begin{matrix} \alpha \\ \beta \end{matrix} \right\} = \sqrt{\frac{1}{2} \left( \sqrt{\frac{D_1}{D_2}} \pm \frac{D_3}{D_2} \right)} \quad (7b)$$

$$\bar{y} = \frac{\pi y}{\lambda} \quad (7c)$$

The boundary conditions are

$$w = 0 \quad (8a)$$

$$\frac{\partial w}{\partial y^2} = - \frac{M_0}{D_2} \sin \frac{\pi x}{\lambda} \quad (8b)$$

at  $y = 0$ , and

$$w = \frac{\partial^2 w}{\partial y^2} = 0 \quad (8c)$$

or

$$w = \frac{\partial w}{\partial y} = 0 \quad (8d)$$

at  $y = d$ . Alternately these conditions may be written as

$$g = \frac{d^2 g}{dy^2} + \frac{M_o \lambda^2}{\pi^2 D_2} = 0 \quad (9a)$$

at  $\bar{y} = 0$  and

$$g = \frac{d^2 g}{d\bar{y}^2} = 0 \quad (9b)$$

or

$$g = \frac{dg}{d\bar{y}} = 0 \quad (9c)$$

$$\text{at } \bar{y} = \bar{d} = \frac{\pi d}{\lambda}$$

In the case of a simply supported edge, the conditions lead to the equations

$$A + C = 0 \quad (10a)$$

$$2\alpha\beta(D - B) + \frac{M_o \lambda^2}{\pi^2 D_2} = 0 \quad (10b)$$

$$e^{-\alpha\bar{d}}(A \cos \beta \bar{d} + B \sin \beta \bar{d}) + e^{\alpha\bar{d}}(C \cos \beta \bar{d} + D \sin \beta \bar{d}) = 0 \quad (10c)$$

$$e^{-\alpha\bar{d}}(A \sin \beta \bar{d} - B \cos \beta \bar{d}) + e^{\alpha\bar{d}}(C \sin \beta \bar{d} - D \cos \beta \bar{d}) = 0 \quad (10d)$$

In the case of a clamped edge, equation (10d) is replaced by

$$\begin{aligned} & e^{-\alpha\bar{d}} \left[ (\alpha \cos \beta \bar{d} + \beta \sin \beta \bar{d})A + (\alpha \sin \beta \bar{d} - \beta \cos \beta \bar{d})B \right] \\ & - e^{\alpha\bar{d}} \left[ (\alpha \cos \beta \bar{d} - \beta \sin \beta \bar{d})C + (\alpha \sin \beta \bar{d} + \beta \cos \beta \bar{d})D \right] = 0 \end{aligned} \quad (10e)$$

The solution of the two sets of equations may be readily obtained as



$$A = -C = \frac{\sin 2\beta \bar{d}}{\cosh 2\alpha \bar{d} - \cos 2\beta \bar{d}} \cdot \frac{M_o \lambda^2}{4\pi^2 \alpha \beta D_2} \quad (11a)$$

$$B = \frac{e^{2\alpha \bar{d}} - \cos 2\beta \bar{d}}{\cosh 2\alpha \bar{d} - \cos 2\beta \bar{d}} \cdot \frac{M_o \lambda^2}{4\pi^2 \alpha \beta D_2} \quad (11b)$$

$$D = \frac{\cos 2\beta \bar{d} - e^{-2\alpha \bar{d}}}{\cosh 2\alpha \bar{d} - \cos 2\beta \bar{d}} \cdot \frac{M_o \lambda^2}{4\pi^2 \alpha \beta D_2} \quad (11c)$$

for the simply supported edge, or

$$A = -C = \frac{\alpha (1 - \cos 2\beta \bar{d})}{\beta \sinh 2\alpha \bar{d} - \alpha \sin 2\beta \bar{d}} \cdot \frac{M_o \lambda^2}{4\pi^2 \alpha \beta D_2} \quad (12a)$$

$$B = \frac{\beta (e^{2\alpha \bar{d}} - 1) - \alpha \sin 2\beta \bar{d}}{\beta \sinh 2\alpha \bar{d} - \alpha \sin 2\beta \bar{d}} \cdot \frac{M_o \lambda^2}{4\pi^2 \alpha \beta D_2} \quad (12b)$$

$$D = \frac{\alpha \sin 2\beta \bar{d} - \beta (1 - e^{-2\alpha \bar{d}})}{\beta \sinh 2\alpha \bar{d} - \alpha \sin 2\beta \bar{d}} \cdot \frac{M_o \lambda^2}{4\pi^2 \alpha \beta D_2} \quad (12c)$$

for the clamped edge.

The quantity  $\alpha'$  is defined as

$$\alpha' = \frac{M_o}{\left( \frac{df}{dy} \right)_{y=0}} \quad (13)$$

The use of equation (7a) and either equations (11) or (12) in equation (11) then yields

$$\alpha' = \frac{D_2}{d} \cdot \frac{\frac{\cosh 2\alpha \bar{d}}{\sinh 2\alpha \bar{d}} - \frac{\cos 2\beta \bar{d}}{\sin 2\beta \bar{d}}}{2\alpha \bar{d} - 2\beta \bar{d}} \quad (14a)$$

for a simply supported edge, or

$$\alpha' = \frac{D_2}{d} \frac{\frac{\sinh 2\alpha \bar{d}}{2\alpha \bar{d}} - \frac{\sin 2\beta \bar{d}}{2\beta \bar{d}}}{\frac{\cosh 2\alpha \bar{d} - 1}{(2\alpha \bar{d})^2} - \frac{1 - \cos 2\beta \bar{d}}{(2\beta \bar{d})^2}} \quad (14b)$$

for a clamped edge.

For small values of  $\bar{d}$  ( $\lambda$  large), equations (14a) and (14b) become, respectively,

$$\alpha' \approx 3 D_2/d \quad (15a)$$

$$\alpha' \approx 4 D_2/d \quad (15b)$$

which are identical with the results for a supported beam subjected to a moment at one end and simply supported or clamped at the other end. For large values of  $\bar{d}$  ( $\lambda$  small), equations (14a) and (14b) both become

$$\alpha' \approx \frac{D_2}{d} \cdot 2\alpha \bar{d} = \frac{2\pi\alpha}{\lambda} D_2 \quad (16)$$

Values of  $\alpha'$  for both cases are shown in Figure 75 for the case when  $\sqrt{D_1 D_2} \gg D_3$  in which case  $\alpha \approx \beta = \sqrt[4]{\frac{D_1}{4 D_2}}$ .

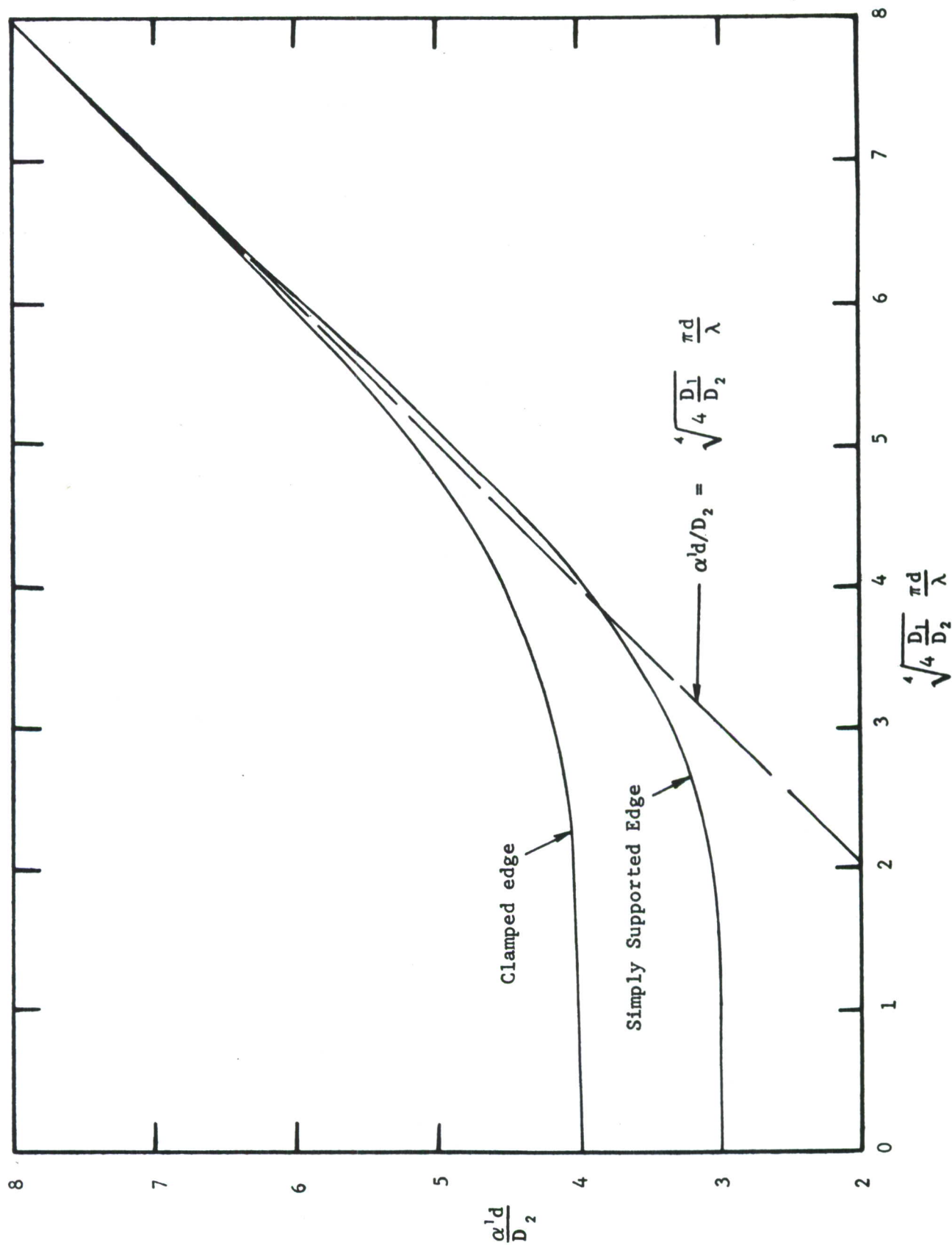


FIGURE 75. VARIATION OF WEB TORSIONAL RESTRAINT PARAMETER WITH WAVE LENGTH



## 2. CORRUGATED WEB ANALYSIS OR DESIGN

It is assumed that the effective torsional stiffness of the webs is negligible and that an optimum web is that which just produces plate buckling with nodes along the support lines. The plate is assumed to be long enough compared to its width that it can be considered infinite in length. Then the buckling coefficient for the plate is given by  $k = 4$  and the support spring stiffness parameter required to give this buckling load is shown in Figure 76 as a function of the wave length parameter  $\lambda/b$ . To determine whether or not the corrugated web has the required stiffness, it is necessary to compare the value of  $\psi b^3/\pi^4 D_p$  given by equation (2) with the values of Figure 76. To do this the following relation is plotted as a function of  $\lambda/b$

$$\frac{\psi b^3}{\pi^4 D_p} = \frac{12}{\pi^4} \frac{D_f}{D_p} \left(\frac{b}{f}\right)^3 \frac{\frac{\alpha^1 d}{D_2} + \frac{D_f}{D_2} \frac{d}{f}}{\frac{\alpha^1 d}{D_2} + 4 \frac{D_f}{D_2} \frac{d}{f}} \quad (17)$$

with  $\alpha^1 d/D$  a function of the parameter  $\sqrt[4]{4 \frac{D_1}{D_2}} \frac{\pi d}{b} \frac{b}{\lambda}$  given by equations (14) or by Figure 75. Then if the curve defined by equation (17) does not intersect the appropriate curve of Figure 76, the web has more than enough stiffness. If the two curves intersect, the web has insufficient stiffness. The optimum web stiffness is obtained when the two curves are tangent at only one point (Figure 77). The shape of the curves suggests that an approximation which may be adequate would be to assume that the point of tangency is near the maximum of the appropriate curve of Figure 76. Then, with  $\lambda/b$  taken as the value corresponding to the maximum value of  $\frac{\psi b^3}{\pi^4 D}$  in Figure 75 and with  $\frac{\psi b^3}{\pi^4 D}$  taken as the maximum value, equation (17) may be used to calculate one of the web parameters. The web dimensions would have to be varied to yield minimum weight.

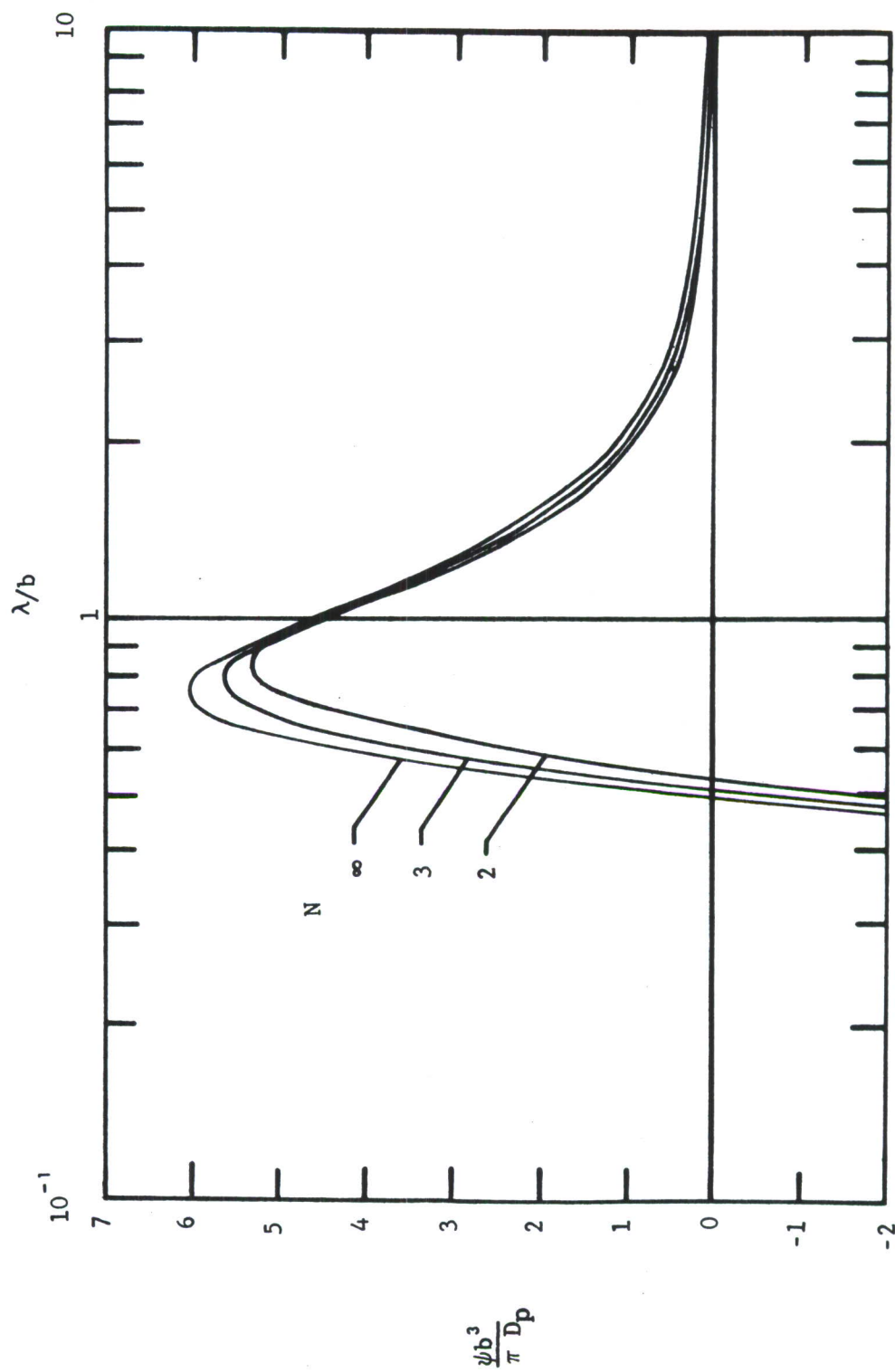


FIGURE 76. VARIATION WITH BUCKLE WAVE LENGTH OF MINIMUM EXTENSIONAL STIFFNESS PARAMETER REQUIRED TO PRODUCE NODES AT THE SUPPORTS FOR LONG PLATES. (ZERO TORSIONAL STIFFNESS.)

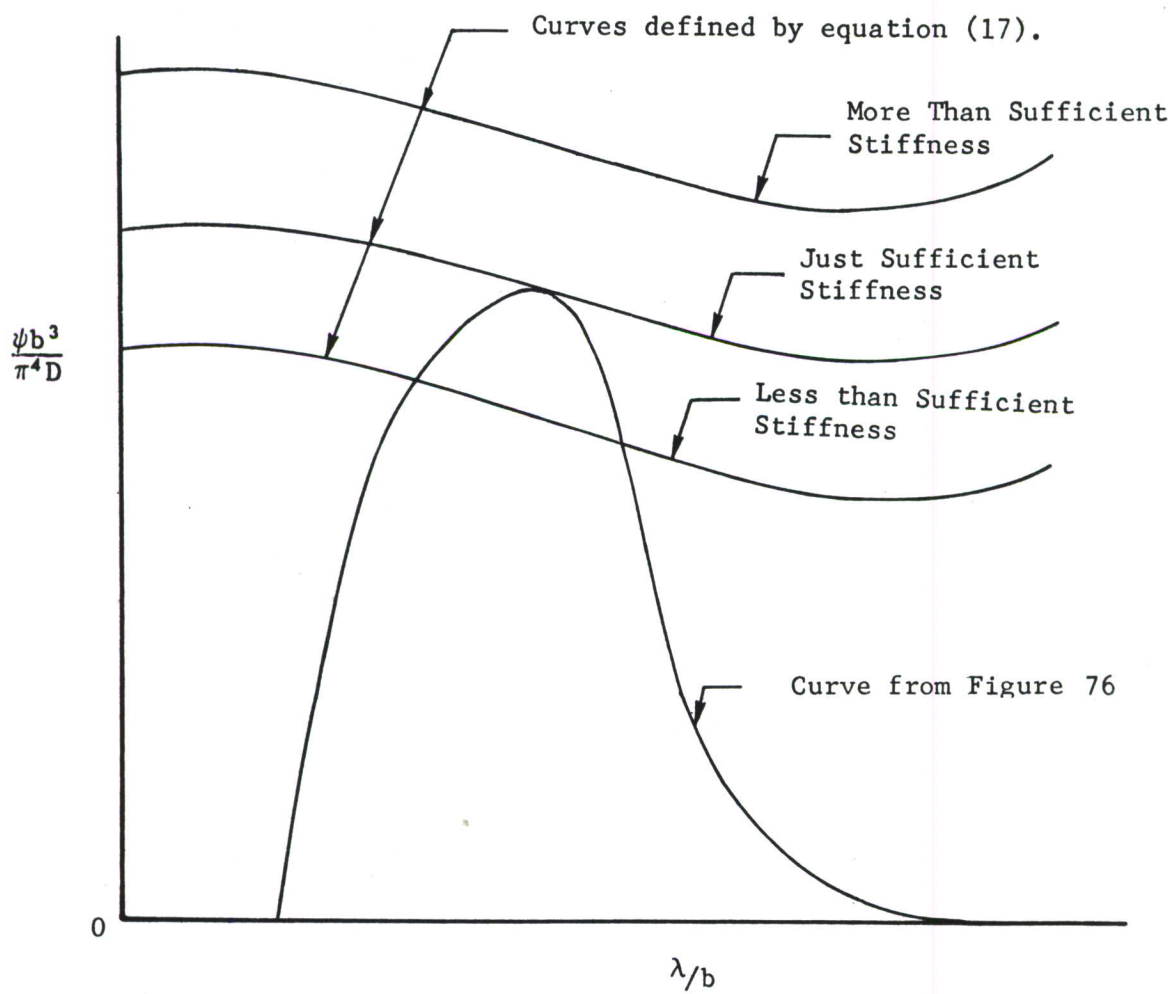


FIGURE 77. POSSIBLE STIFFNESS VARIATIONS



## APPENDIX II

### CALCULATION OF PERFORATED PLATE AVERAGE ELASTIC CONSTANTS AND STIFFNESSES

It is of interest in the analysis of perforated plates (Figure 78) to define a repeating stress and deformation pattern which can be used to determine average stiffnesses. Such a pattern is useful for two reasons: first, it represents a minimum problem to be analyzed by numerical means and thus requires the least amount of computer time; secondly, the stress and deformation distributions are those which would exist in the interior of a perforated plate under relatively uniform normal and shear edge forces. The required plate pattern and the associated boundary conditions are explained in the following sections. The nomenclature is presented on page 242.

#### 1. BIAXIAL NORMAL STRESS

Assume that the applied stress is parallel to the axes of symmetry of the pattern shown in Figure 79; i.e., axes AA and BB in the "x" direction and axes CC and DD in the "y" direction. A repeating stress pattern is expected to have these axes of symmetry as well. The implication of this requirement is that the shear stress  $\tau_{xy}$  vanishes along these lines. Conditions of symmetry also imply that these symmetry axes remain straight; this condition does not mean, however, that the normal displacement vanishes but that it is a constant along a line of symmetry, the exact value depending on the average stress that is applied. Thus, the problem to be analyzed is as shown in Figure 79.

## NOMENCLATURE FOR APPENDIX II

$C_1, C_2, C_3$	uniform biaxial extensions and shear of repeating element
$D_x, D_y, D_{xy}$	average bending and twisting stiffness of perforated plate
$E_x, E_y, G_{xy}$	average Young's moduli and shear modulus of perforated plate
$M_x, M_y, M_{xy}$	average bending and twisting moments per unit length
$t$	perforated plate thickness
$u_x, u_y, w$	in-plane and normal displacements of perforated plate
$\bar{\epsilon}_x, \bar{\epsilon}_y, \bar{\gamma}_{xy}$	average extensional and shearing strains of repeating element
$\nu_x, \nu_y$	average Poisson's ratios of perforated plate
$\sigma_x, \sigma_y, \tau_{xy}$	in-plane extensional and shearing stresses in perforated plate
$\sigma_n, \tau_{ns}$	normal and tangential edge stress
$\bar{\sigma}_x, \bar{\sigma}_y, \bar{\tau}_{xy}$	average in-plane extensional and shearing stress acting on repeating element
$\bar{\sigma}_{x1}, \bar{\sigma}_{y1}$	average extensional stresses corresponding to strain state for which $C_1 = 1, C_2 = C_3 = 0$
$\bar{\sigma}_{x2}, \bar{\sigma}_{y2}$	average extensional stresses corresponding to strain state for which $C_2 = 1, C_1 = C_3 = 0$

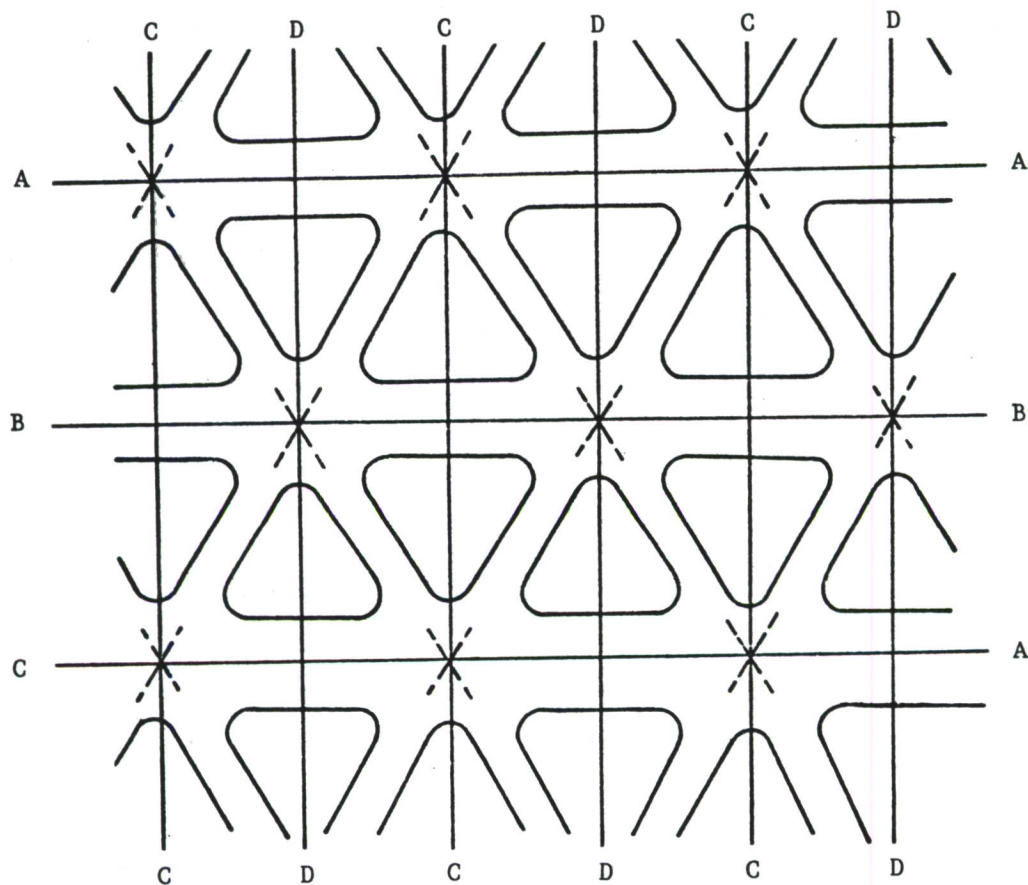


FIGURE 78. REPEATING TRIANGULAR HOLE PATTERN

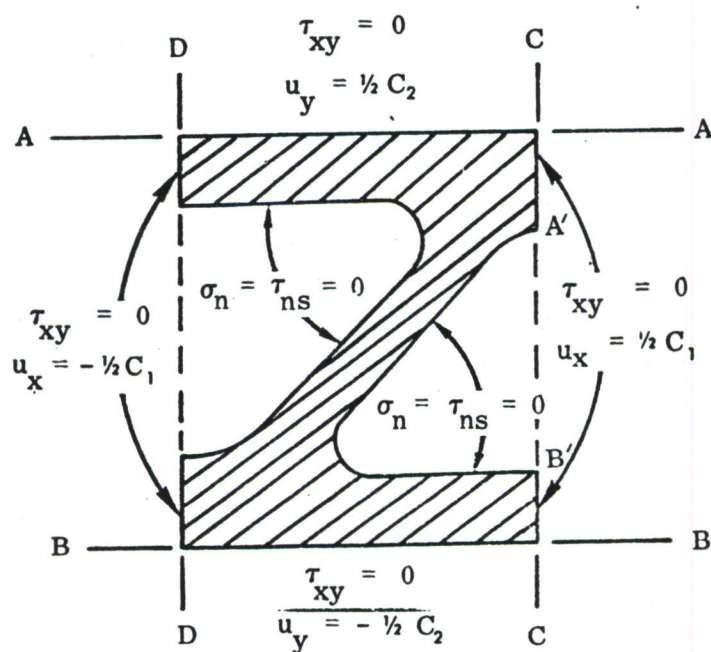


FIGURE 79. PROBLEM TO BE ANALYZED FOR BIAxIAL NORMAL STRESS DISTRIBUTION



Average elastic constants are defined through the overall average stress-average strain relationships

$$\bar{\epsilon}_x = \frac{1}{E_x} \bar{\sigma}_x - \frac{\nu_x}{E_y} \bar{\sigma}_y \quad (1a)$$

$$\bar{\epsilon}_y = -\frac{\nu_y}{E_x} \bar{\sigma}_x + \frac{1}{E_y} \bar{\sigma}_y \quad (1b)$$

with

$$\bar{\epsilon}_x = \frac{C_1}{|CD|} \quad (2a)$$

$$\bar{\epsilon}_y = \frac{C_2}{|AB|} \quad (2b)$$

$$\bar{\sigma}_x = \frac{\int_B^{B'} \sigma_x dy + \int_{A'}^A \sigma_x dy}{|AB|} \quad (2c)$$

$$\bar{\sigma}_y = \frac{\int_D^C \sigma_y dx}{|CD|} \quad (2d)$$

It would appear that to define these constants it is necessary to solve two problems, one for which  $C_1$  is equal to unity and  $C_2$  is equal to zero, another for which  $C_2$  is equal to unity and  $C_1$  is equal to zero. The value of  $\bar{\sigma}_x$  and  $\bar{\sigma}_y$  obtained from the first problem can be denoted by  $\bar{\sigma}_{x1}$  and  $\bar{\sigma}_{y1}$  and from the second problem by  $\bar{\sigma}_{x2}$  and  $\bar{\sigma}_{y2}$ . Then since  $E_x$  and  $\nu_y$  are associated with a stress state for which  $\bar{\sigma}_y$  vanishes,

$$C_1 \bar{\sigma}_{y1} + C_2 \bar{\sigma}_{y2} = 0 \quad (3a)$$

or

$$C_2/C_1 = - \frac{\bar{\sigma}_{y1}}{\bar{\sigma}_{y2}} \quad (3b)$$

The value of  $\bar{\sigma}_x$  to be used to determine  $E_x$  is then

$$\bar{\sigma}_x = C_1 \left( \bar{\sigma}_{x1} - \frac{\bar{\sigma}_{y1}}{\bar{\sigma}_{y2}} \bar{\sigma}_{x2} \right) \quad (3c)$$

which yields

$$E_x = \frac{\bar{\sigma}_x}{\bar{\epsilon}_x} = |CD| \left( \bar{\sigma}_{x1} - \frac{\bar{\sigma}_{y1}}{\bar{\sigma}_{y2}} \bar{\sigma}_{x2} \right) \quad (4a)$$

The following is also obtained

$$\nu_y = - \frac{\bar{\epsilon}_y}{\bar{\epsilon}_x} = - \frac{C_2/|AB|}{C_1/|CD|} = \frac{|CD|}{|AB|} \frac{\bar{\sigma}_{y1}}{\bar{\sigma}_{y2}} \quad (4b)$$

Similarly,  $E_y$  and  $\nu_x$  are associated with a stress state for which  $\bar{\sigma}_x$  vanishes, in which case

$$C_1 \bar{\sigma}_{x1} + C_2 \bar{\sigma}_{x2} = 0 \quad (5a)$$

or

$$C_1/C_2 = - \frac{\bar{\sigma}_{x2}}{\bar{\sigma}_{x1}} \quad (5b)$$

and

$$E_y = |AB| \left( \bar{\sigma}_{y2} - \frac{\bar{\sigma}_{x2}}{\bar{\sigma}_{x1}} \bar{\sigma}_{y1} \right) \quad (6a)$$

$$\nu_x = \frac{|AB|}{|CD|} \frac{\bar{\sigma}_{x2}}{\bar{\sigma}_{x1}} \quad (6b)$$

Note that since

$$\nu_x/E_y = \nu_y/E_x \quad (7a)$$

the stress states should verify the relationship

$$\bar{\sigma}_{y1} |CD| = \bar{\sigma}_{x2} |AB| \quad (7b)$$

## 2. SHEAR STRESS

The determination of the proper repeating pattern and boundary conditions for a state of shearing stress is somewhat more difficult. Assume shear applied parallel to axes AA and BB. These axes would be expected to be axes of antisymmetry of the stress distribution. Thus consider the region between axes AA and BB as shown in Figure 80 to be subjected to shear and normal stresses as shown. If the picture is rotated about axis BB the stress picture is as shown in Figure 81. Continuity and equilibrium of the shear stress

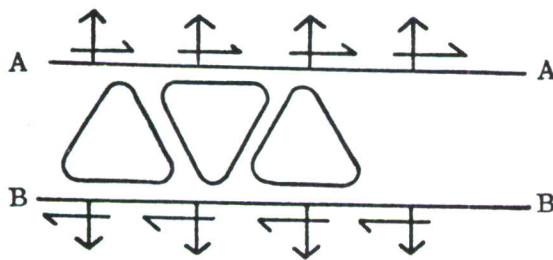


FIGURE 80. SHEAR & NORMAL STRESS DISTRIBUTION

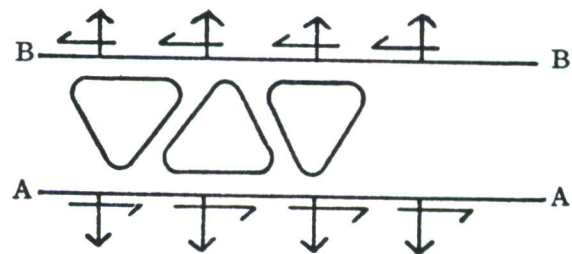


FIGURE 81. ROTATED STRESS DISTRIBUTION



along axis BB may be obtained by reversing the sign of the stresses in Figure 81.. But then, the normal stresses will not be in equilibrium unless they vanish. Since a similar argument can be made by rotating about axis AA, the conditions  $\sigma_y = 0$  must be imposed along axes AA and BB. By considering displacements it would appear that reversing the sign of the stresses in Figure 81 will bring about a discontinuity of the tangential displacement along axis BB unless it is equal to zero or a constant. Similarly the tangential displacements along axis AA must be zero or a constant. (A constant is permissible since a rigid body motion of the adjacent bay will make the tangential displacements continuous). Considerations of antisymmetry about axes CC and DD likewise imply that the normal stress vanishes and that the tangential displacement must be constant along these axes.

A solution of the problem shown in Figure 82 is thus found.

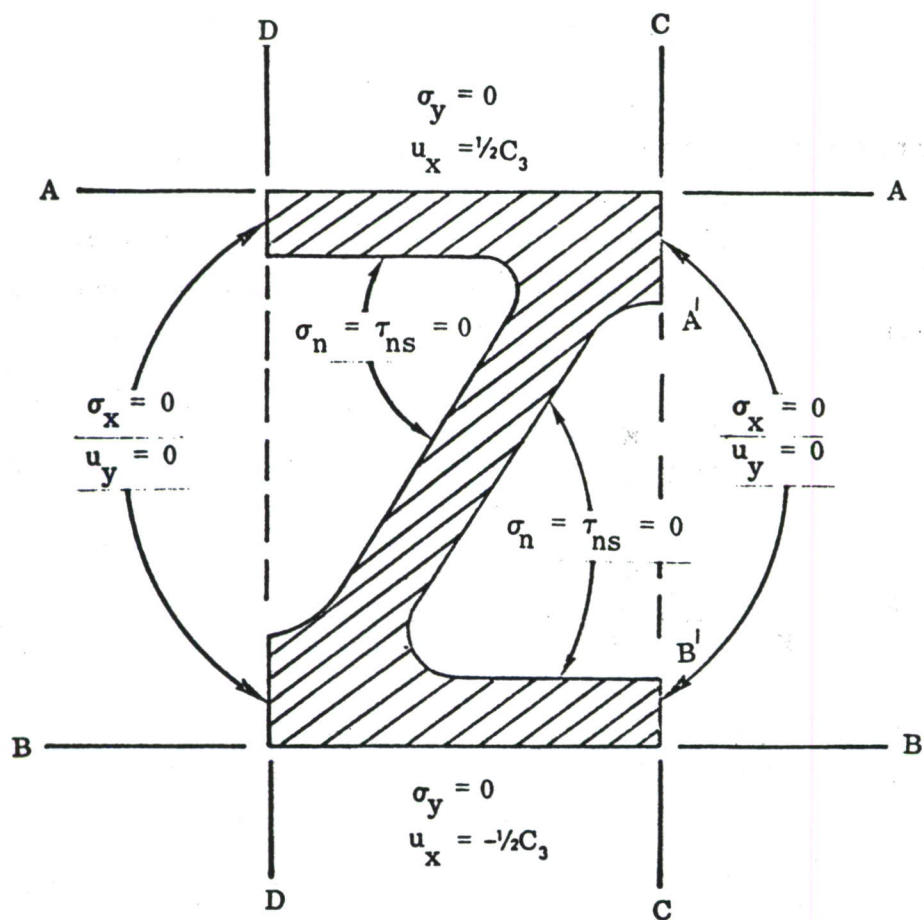


FIGURE 82. PROBLEM TO BE ANALYZED FOR SHEAR STIFFNESS

The elastic constant associated with this problem is given by

$$G_{xy} = \frac{\bar{\tau}_{xy}}{\bar{\gamma}_{xy}} \quad (8a)$$

with

$$\bar{\gamma}_{xy} = \frac{C_3}{|AB|} \quad (8b)$$

$$\bar{\tau}_{xy} = \frac{\int_D^C \tau_{xy} dx}{|CD|} = \frac{\int_B^{B'} \tau_{xy} dy + \int_{A'}^A \tau_{xy} dy}{|AB|} \quad (8c)$$

### 3. PLATE BENDING STIFFNESSES

With the effective elastic constants known the bending stiffness of thin perforated plates are readily obtained to yield the moment-curvature relations

$$\frac{\partial^2 w}{\partial x^2} = \frac{M_x}{D_x} - \nu_x \frac{M_y}{D_y} \quad (9a)$$

$$\frac{\partial^2 w}{\partial y^2} = \frac{M_y}{D_y} - \nu_y \frac{M_x}{D_x} \quad (9b)$$

$$\frac{\partial^2 w}{\partial x \partial y} = \frac{M_{xy}}{D_{xy}} \quad (9c)$$

with

$$D_x = \frac{E t^3}{12} \quad (10a)$$

$$D_y = \frac{E y t^3}{12} \quad (10b)$$

$$D_{xy} = \frac{G_{xy} t^3}{12} \quad (10c)$$

and  $\nu_x$  and  $\nu_y$  are given by equations (4b) and (6b).



### APPENDIX III

#### WEIGHT AND COST SAVINGS IN CONCEPTS

The following is a brief explanation of the bases by which the principal weight and cost savings shown in Tables XXV and XXVI, respectively, were achieved for the various concepts in this study. It should be emphasized that the stress levels shown are examples at a particular wing station only, and that ratioing these stresses will not necessarily produce the indicated weight savings. A significant portion of the weight saving in all the concepts is attributed to using titanium in place of steel in the landing gear and tip ribs.

#### 1. CONCEPT NO. 1

##### a. Ribs

The 43 pound (4.4%) weight saving, which represents an actual reduction from 211 pounds of baseline rib weight to 168 pounds of rib weight, is achieved primarily by the substitution of titanium for steel in the gear (Ti-6-22-22 STA) and tip (Ti-6-4 A) ribs. While it may be argued that the baseline gear rib is overweight and the weight savings achieved are therefore invalid, this is not actually the case. The load levels in this rib at the 44 percent spar intersection and the main landing gear lugs are such as to allow the efficient use of steel. However, as the load level rapidly decreases in the forward portions of the rib, stability considerations, minimum practical manufacturing gages, and required flange widths for fasteners make steel a very inefficient material for this application. Titanium with its lower density and somewhat lower mechanical properties does not incur these minimum section difficulties in these areas and is consequently the more efficient material overall. Additionally, as the program is free of the commonality restrictions placed on the baseline design (i.e., high utilization of F-5A parts), a more efficient leading edge flap hinge support structure allowed additional weight saving.

The 4.4 percent weight saving was achieved with a cost reduction of 6 percent (\$5,300.00). This is achieved mainly through the reduced labor

and overhead incurred by the use of the precision forging and investment casting processes to effectively reduce the buy-fly ratio of these ribs.

b. Upper Skin

There is a 37 pound (3.8%) weight decrease from 203 pounds to 166 pounds chiefly as a result of substituting full depth honeycomb core for internal spars. The increased panel stability imparted by the honeycomb core allows the higher specific compressive stress of Ti 6-22-22 STA ( $F_{cy} = 160,000$  - Table V) vis-a-vis 7075-T651 aluminum ( $F_{cy} = 67,000$ )<sup>(1)</sup> to be more fully utilized.

c. Lower Skin

The 53 pound (5.4%) weight saving from 250 pounds to 197 pounds is realized by the same improved efficiencies in structural arrangement described in 1.b. above, i.e., Ti 6-4  $\beta$  MA ( $F_{DU_{Fat}} = 113,000$  - Table VII) vis-a-vis 7075-T7351 aluminum ( $F_{DU_{Fat}} = 44,600$ )<sup>(2)</sup>.

d. Miscellaneous

This includes fittings, doors, nonstructural panels, stop and seal panels. There is a 21 pound weight decrease, from 85 pounds to 64 pounds, resulting chiefly from the substitution of graphite/epoxy honeycomb panels for aluminum honeycomb panels in the strut well area and aileron access doors and the substitution of titanium castings for steel castings in the aileron hinges and 66.6% spar attach fitting.

2. CONCEPT NO. 1A

a. Spars

A 15 pound (1.5%) weight saving, from 166 to 151 pounds, is achieved mainly due to the decrease in honeycomb core weight over the internal spars

(1) NOR 71-173, "Wing Stress Analysis, F-5E", page A-1.0.

(2) NOR 71-172, "F-5E Wing Internal Loads," Vol. II, page L-328.

it replaces. There are no directly comparative stress levels for honeycomb core and channel spars from which meaningful conclusions may be derived, because of the widely differing failure modes of the two designs under comparison. The 10 percent cost saving (\$9,223) results from the substitution of honeycomb core for the interior spars and the reduced labor and overhead in producing the precision forged exterior spars.

b. Ribs

The 40 pound weight decrease, from 211 to 171 pounds, is mainly the result of substituting titanium for steel in the gear and tip ribs (see 1.a. for complete description). This weight saving is accomplished with a concurrent 16 percent cost reduction (\$14,400). This cost reduction is the direct result of the reduced labor overhead and tooling expenditures required when utilizing precision forged and investment cast parts in lieu of hogouts. The 10 percent cost saving increase of this concept over Concept 1 is the result of limiting the use of titanium to the gear and tip ribs only. (The use of aluminum ribs was precluded in Concept 1 because of a lack of strain compatibility with the titanium cover skins.)

c. Lower Skin

A 12 pound weight saving from 250 to 238 pounds is realized through the substitution of a 7475-T7651 aluminum alloy ( $F_{DU_{Fat}} = 54,000$  - Table VIII) for 7075-T7351 aluminum alloy ( $F_{DU_{Fat}} = 44,600$ )<sup>(1)</sup>.

d. Miscellaneous

The weight savings and their sources are the same as in 1.d.

3. CONCEPT NO. 3

a. Ribs

The weight savings and their sources are the same as in 1.a.

---

(1) NOR 71-172, Volume II, Page L-328



b. Miscellaneous

The weight savings and their sources are as in 1.d.

c. Assembly

A 17 pound weight reduction, from 66 to 49 pounds (1.7%), is a result of reduced fastener grip lengths in the lower skin and the substitution of Bi-Ti rivets for Hi-Loks in the upper skin.

4. CONCEPT NO. 3A

a. Ribs

A 40 pound (4%) weight reduction and its source is the same as in 1.a. The additional 38 pounds (4%) weight saving is a result of transferring the lower rib flanges to the lower wing skin and does not result in a saving in total wing weight. The 3 percent cost saving (\$2,800.00) is a result of reduced labor overhead and tooling expenditures when precision forgings and investment castings replace hogouts.

b. Miscellaneous

The weight savings and their sources are as in 1.d.

c. Assembly

The 22 pound weight saving (2.2%) from 66 to 44 pounds, is a result of the elimination of fasteners through the lower skin and the reduction of blind fastener grip length. The upper skin is now attached with blind fasteners. The thicker lower skin of the baseline was attached with blind fasteners.

5. CONCEPT NO. 4

a. Ribs

The weight saving and sources of same are as in 1.a. The sources of the 2 percent cost saving (\$1,211.00) are as in 1.a. also.

b. Upper Skin

A 13 pound (1.3%) weight reduction from 203 to 190 pounds is achieved by the application of honeycomb panel stiffening to the skin panels between

spars. Again, maximizing the utilization of the higher specific compressive stress of Ti 6-22-22 STA ( $F_{cy} = 160,000$  - Table V) vis-a-vis 7075-T651 ( $F_{cy} = 67,000$ )<sup>(1)</sup> accounts for this weight saving.

c. Lower Skin

A 32 pound (3.3%) weight saving from 250 to 218 pounds is achieved in the same manner as the upper wing skin weight saving previously described, i.e., Ti 6-4  $\beta$ MA ( $F_{DU}^{DT} = 108,000$  - Table VII) vis-a-vis 7075-T7351 aluminum ( $F_{DU}^{Fat} = 44,600$ )<sup>(2)</sup>.

d. Miscellaneous

The weight saving and sources of same are as in 1.d.

e. Assembly

The 16 pound (1.6%) weight reduction from 66 to 50 pounds is a result of fewer interior spars, shorter fasteners and the substitution of Bi-Ti rivets for Hi-Loks. The 0.5 percent cost reduction (\$479.00) is a result of the reduced labor and overhead of a reduced quantity of fasteners to be installed.

6. CONCEPT NO. 5

a. Ribs

The weight saving and sources of same are as in 1.a. The sources of the cost reduction of 3 percent (\$2,263.00) are also as in 1.a.

b. Upper Skin

A 12 pound weight reduction from 203 to 191 pounds is achieved in the same manner as described in 5.b.

---

(1) NOR 71-173, Page A-1.0.

(2) NOR 71-172, Volume II, Page L-328.

c. Lower Skin

The weight saving and sources of same are as in 5.c.

d. Miscellaneous

The weight saving and sources of same are as in 1.d.

e. Assembly

The sources of an 18 pound weight saving (1.8%) from 66 to 48 pounds is as in 5.e. The cost saving of 1.0 percent (\$798.00) is twice that of the savings in 5.e., reflecting the deletion of one more interior spar.

7. CONCEPT NO. 8

a. Spars

There is a 17 pound weight saving (1.7%) from 166 to 149 pounds resulting from the reduced web thicknesses made possible by corrugating these webs. The 13 percent (\$11,391.00) cost saving results from the reduced labor and overhead attendant with procuring net precision forged spars.

b. Ribs

A 40 pound (4.1%) weight saving from 211 to 171 pounds results from the same sources quoted in 1.a. The 18 percent (\$16,414.00) cost saving sources are the same as in 1.a. The increased cost saving over Concept 1 ribs reflects the reduced use of titanium in this design, which is essentially aluminum.

c. Lower Skin

A 19 pound (1.9%) weight saving from 250 to 231 pounds results from the use of 7475-T7651 aluminum alloy ( $F_{DU_{DT}} = 54,000$  - Table VIII) for 7075-T7351

( $F_{DU_{Fat}} = 44,600$ )<sup>(1)</sup>.

---

(1) NOR 71-172, Vol. II, page L-328.



d. Miscellaneous

The weight saving and sources of same are as in 1.d.

e. Assembly

The 9 pound weight saving results from the substitution of Bi-Ti rivets for Hi-Loks.

8. CONCEPT NO. 8A

a. Spars

The 11 pound weight saving from 166 to 155 pounds has the same source as 7.a. The cost saving and source of same is as in 7.a.

b. Ribs

The weight and cost savings and sources of same are as in 1.a.

c. Lower Skin

The 21 pound weight saving (2.1%) from 250 to 229 pounds results from the use of the X2048-T851 aluminum alloy and the increased static design allowable of 59,000 psi (Table VIII) (the fatigue design allowable is no longer critical). This results from the removal of fasteners from the lower skin mold line.

d. Miscellaneous

The weight saving and sources of same are as in 1.d.

e. Assembly

The source of the 14 pound weight saving from 66 to 52 pounds is the substitution of Bi-Ti rivets for Hi-Loks and the use of blind fasteners in the titanium upper skin.

9. WEIGHT AND COST SAVINGS TABULATION

Tables XXV and XXVI show the principal weight and cost savings, respectively, expressed as a percentage of total baseline weight and cost.

TABLE XXV. PRINCIPAL WEIGHT SAVINGS BY CONCEPT  
(IN PERCENT OF BASELINE TOTAL WEIGHT)

Concepts	Spar	Ribs	Upper Skin	Lower Skin	Misc.	Assy.
No. 1 - Ti. Full Depth Honeycomb Core		4.4	3.8	5.4	2.1	
No. 1A - Al. Full Depth Honeycomb Core	1.5	4.1		1.2	↑	
No. 3 - Al./Ti. 6-Spar		4.3				1.7
No. 3A - Al./Ti. Welded 6-Spar		8.0				2.2
No. 4 - Honeycomb Panel 5-Spar		4.5	1.3	3.3		1.6
No. 5 - Honeycomb Panel 4-Spar		4.4	1.2	3.3		1.8
No. 8 - Al. Precision Forged 6-Spar	1.7	4.1		1.9	↑	0.9
No. 8A - Al. Integral Web 6-Spar	1.1	4.1		2.1	2.1	1.4

TABLE XXVI. PRINCIPAL COST SAVINGS BY CONCEPT  
(IN PERCENT OF BASELINE TOTAL COST)

Concepts	Spars	Ribs	Upper Skin	Lower Skin	Misc.	Assy.
No. 1 - Ti. Full Depth Honeycomb Core		6				
No. 1A - Al. Full Depth Honeycomb Core	10	16				
No. 3 - Al./Ti. 6-Spar						
No. 3A - Al./Ti. Welded 6-Spar		3				
No. 4 - Honeycomb Panel 5-Spar		2				0.5
No. 5 - Honeycomb Panel 4-Spar		3				1
No. 8 - Al. Precision Forged 6-Spar	13	18				
No. 8A - Al. Integral Web 6-Spar	13	18				



NOTE: LIMITS OF EQUATIONS INDICATED THUS

T = THICKNESS OF TAPERED SKIN

#1  $T = 0.0036999 Y_{xx} + 0.092918$

$$\#2 \quad T = 0.0033442 X_w^w + 0.0031781 Y_w + 0.223096$$

#3  $T = 0.0023554 X_W^w + 0.41947$

LINE C-D  $Y_w = 1.05211057X_w - 22.98076192$   $TAN \phi = 0.9504704$

LINE A-B  $Y_w = -6.4084173X_w + 249.45498165$   $TAN \alpha = 0.156044766$

POINT	X <sub>w</sub>	Y <sub>w</sub>	T
A	32.976	38.131	0.234
B	27.915	70.564	0.354
C	82.282	63.589	0.150
D	114.406	97.387	0.150
E	114.406	110.800	0.150

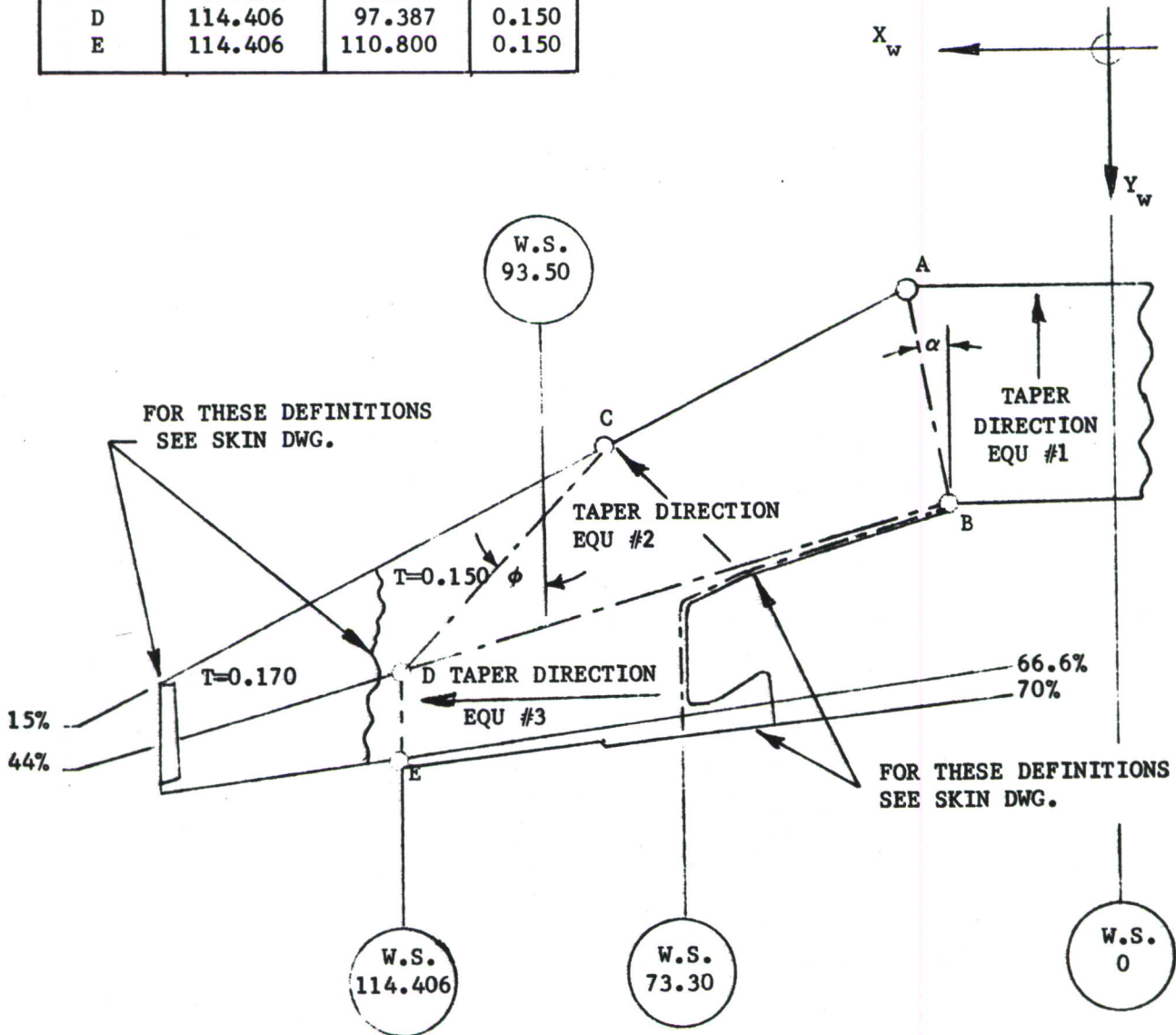
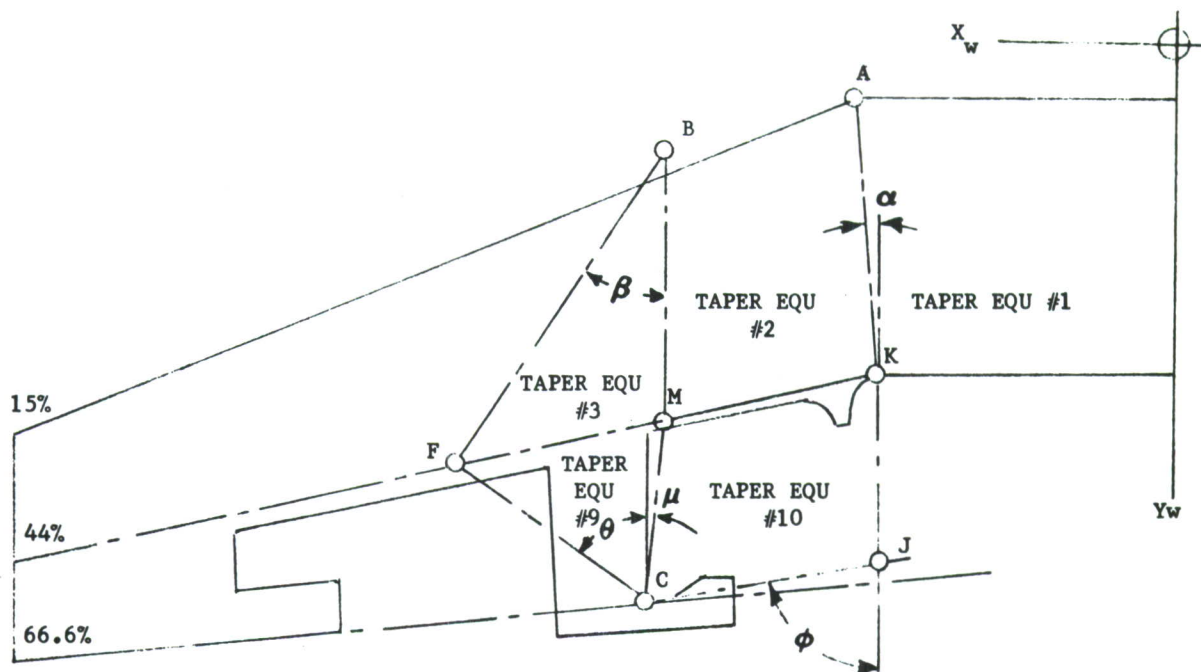


FIGURE 83. TAPERS - UPPER WING SKIN F-5E BASELINE



LINES:

A-K	$Y_w = -6.4084173 X_w + 249.45498165$	$TAN \alpha = 0.156044766$
B-F	$Y_w = 1.20184195 X_w - 27.4885747$	$TAN \beta = 0.83205615$
F-C	$Y_w = 0.43267411 X_w + 136.3730122$	$TAN \theta = 2.3112083$
M-C	$Y_w = 7.45964285 X_w - 442.13382092$	$TAN \mu = 0.13405467$
C-J	$Y_w = 0.1575851 X_w + 93.1070119$	$TAN \phi = 6.3457774$

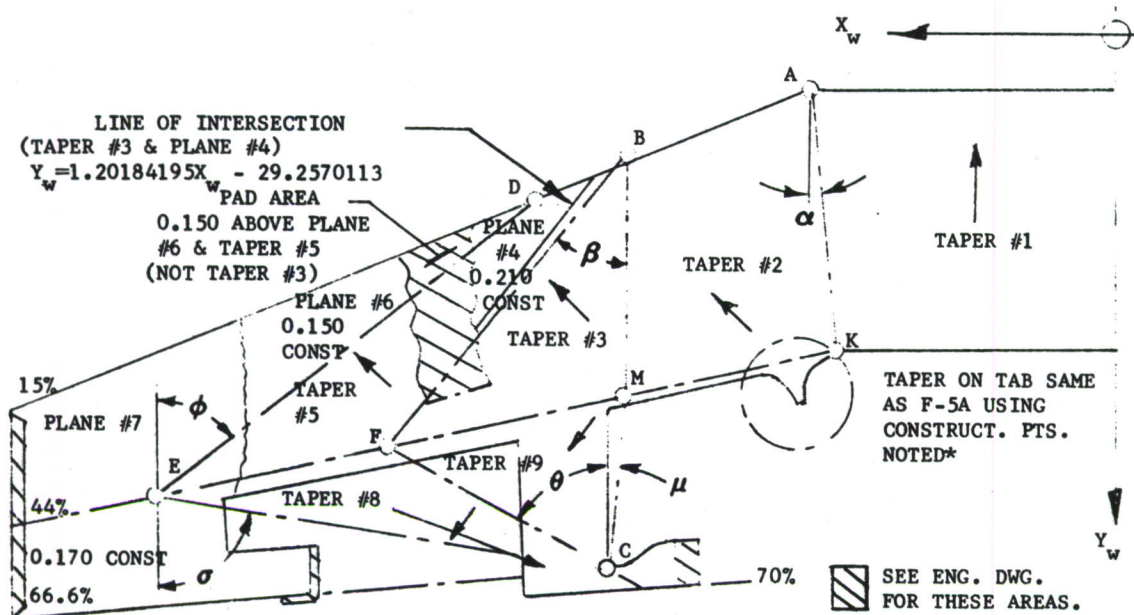
TAPER AREAS (ADDED THICKNESS FROM THEO. ML. TO ACTUAL ML.)

#1	$T = 0.0020349 Y_w - 0.0775927$
#2	$T = 0.0009603 X_w + 0.0018851 Y_w - 0.0402136$
#3	$T = 0.002265 X_w + 0.0018846 Y_w + 0.0518074$
#9	$T = 0.0009789 X_w - 0.0022625 Y_w + 0.3085449$
#10	$T = 0.0003830 X_w - 0.0024451 Y_w + 0.2278565$

	$X_w$	$Y_w$	$T^*$
PT. A	32.976	38.131	0
B	70.500	57.241	0
C	73.300	104.658	0
F	100.251	92.997	0
K	27.915	70.564	0.066
M	70.500	83.771	0.050
J Theo.	27.915	97.506	0

NOTE:  $T^*$  IS THE DISTANCE FROM THE THEO. W - 11 AIRFOIL TO THE ACTUAL OUTER SURFACE OF THE 14-23502 SKIN.

FIGURE 84. TAPER AREAS LOWER WING OUTER SURFACE F-5E BASELINE



#### LINES:

A-K	$Y_w = -6.4084173 X_w + 249.45498165$	$\tan \alpha = 0.156044766$
B-F	$Y_w = 1.20184195 X_w - 27.4885747$	$\tan \beta = 0.83205615$
D-E	$Y_w = 0.82611510 X_w - 4.27369676$	$\tan \phi = 1.21048507$
M-C	$Y_w = 7.45964285 X_w - 442.13382092$	$\tan \mu = 0.13405467$
F-C	$Y_w = -0.43267411 X_w + 136.3730122$	$\tan \theta = 2.3112083$
E-C	$Y_w = -0.5413126 X_w + 108.62582127$	$\tan \sigma = 18.47361344$

	$X_w$	$Y_w$	T
PT. A	32.976	38.131	0.233
B	70.500	57.241	0.230
C	73.300	104.658	0.230
D	81.918	63.400	0.150 THEO.
E	128.259	101.683	0.150 THEO.
F	100.251	92.997	0.230
K	27.915	70.564	0.630
M	70.500	83.771	0.531
POINTS USED	33.731	72.368	0.420
ONLY FOR TAB	73.300	84.639	0.307
TAPER*			

NOTE: T IS THE DISTANCE FROM THE THEO. W-11 AIRFOIL TO THE ACTUAL INNER SURFACE OF THE 14-23502 SKIN.

#### TAPER EQUATIONS:

#1T	$= 0.0122397 Y_w - 0.23372946$
#2T	$= -0.00583795 X_w + 0.01132864 Y_w - 0.00647907$
#3T	$= -0.135907 X_w + 0.011308 Y_w + 0.54085$
#9T	$= -0.00589273 X_w - 0.01361934 Y_w + 2.08728472$
#5T	$= -0.00457306 X_w + 0.00553562 Y_w + 0.173688$
#8T	$= -0.00166376 X_w - 0.00384531 Y_w + 0.75439403$
*TAB T	$= -0.00166291 X_w - 0.00384643 Y_w + 0.75444774$

FIGURE 85. TAPER AREAS WING INNER SURFACE F-5E BASELINE



# THICKNESS TAPERS FOR UPPER SKIN LANDS

- EQU # 1  $T = .001726375629 Y_w + .0591715709$   
 EQU # 2  $T = .00153436833 Y_w - .001230648792 X_w + .1070748757$   
 EQU # 3  $T = .0007932321435 Y_w - .0004095723456 X_w + .1082593228$   
 EQU # 4  $T = .0007932321434 Y_w - 1.000947417 X_w + .1529672781$   
 EQU # 5  $T = .26508842 - .0004392960747 X_w - .001017868685 Y_w$

NOTE :- SEE THICKNESS TAPERS FOR OUTER SURFACE 1891-105  
 $T = T_1 + T_2$

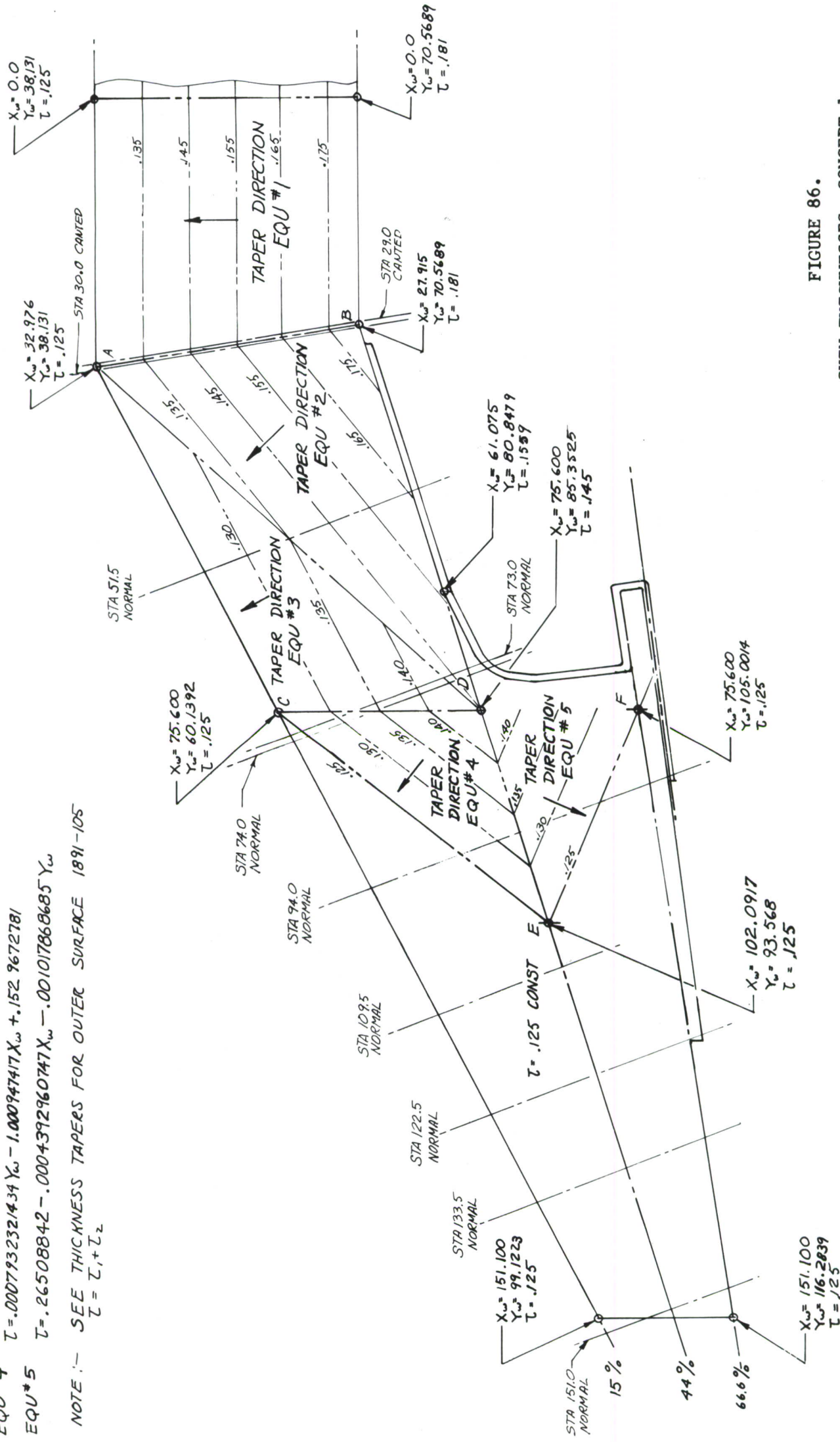


FIGURE 86.  
 SKIN THICKNESSES, CONCEPT 1

SKIN LANDS - INNER SURFACE UPPER SKIN  
 FULL DEPTH H'COMB WING  
 SCALE 1/10 J.C. MORPHER

1891-102

### THICKNESS TAPERS FOR UPPER SKIN POCKETS

NOTE :- THICKNESS SHOWN AT PLANE BOUNDARIES

1	A-D-INB'D	$T = .001479750539 \ Y_w + .0505756322$
2	A-B-N-P	$T = -.002000079594 \ X_w + .001167695726 \ Y_w + .1284292189$
3	B-C-M-N	$T = -.0004942248485 \ X_w + .001711627803 \ Y_w + .03$
4	C-D-L-M	$T = -.0005784981284 \ X_w + .000976844112 \ Y_w + .0498563071$
5	D-E-K-L	$T = -.0005229473594 \ X_w + .0003985265569 \ Y_w + .0735698226$
6	E-F-J-K	$T = .0005600860656 \ X_w + .0007864504964 \ Y_w + .0801989876$
7	F-G-H-I	$T = .0009608540925 \ X_w + .0681850533$

## EQUATION OF LINES

1	A-P	$Y_w = -6.409385497 X_w + 249.48688\%$
2	B-N	$Y_w = -2.672887142 X_w + 206.1650549$
3	E-K	$Y_w = -2.67293281 X_w + 382.8933519$
4	15%	$Y_w = .5163326 X_w + 21.1045$
5	44%	$Y_w = .3101313 X_w + 61.9066$
6	66.6%	$Y_w = .1494376 X_w + 93.7039$

POINT	$X_u$	$Y_u$
A	32.9760	38.1310
B	58.0269	51.0657
C	73.3000	58.9517
D	93.5000	69.3816
E	113.4906	79.6776
F	123.0000	84.6134
G	151.1000	99.1227
H	151.1000	116.2839
I	123.0000	112.0847
J	123.0000	100.0751
K	107.6041	95.2780
L	93.5000	90.9038
M	73.3000	84.6391
N	48.3599	76.9045
P	27.9150	70.5689

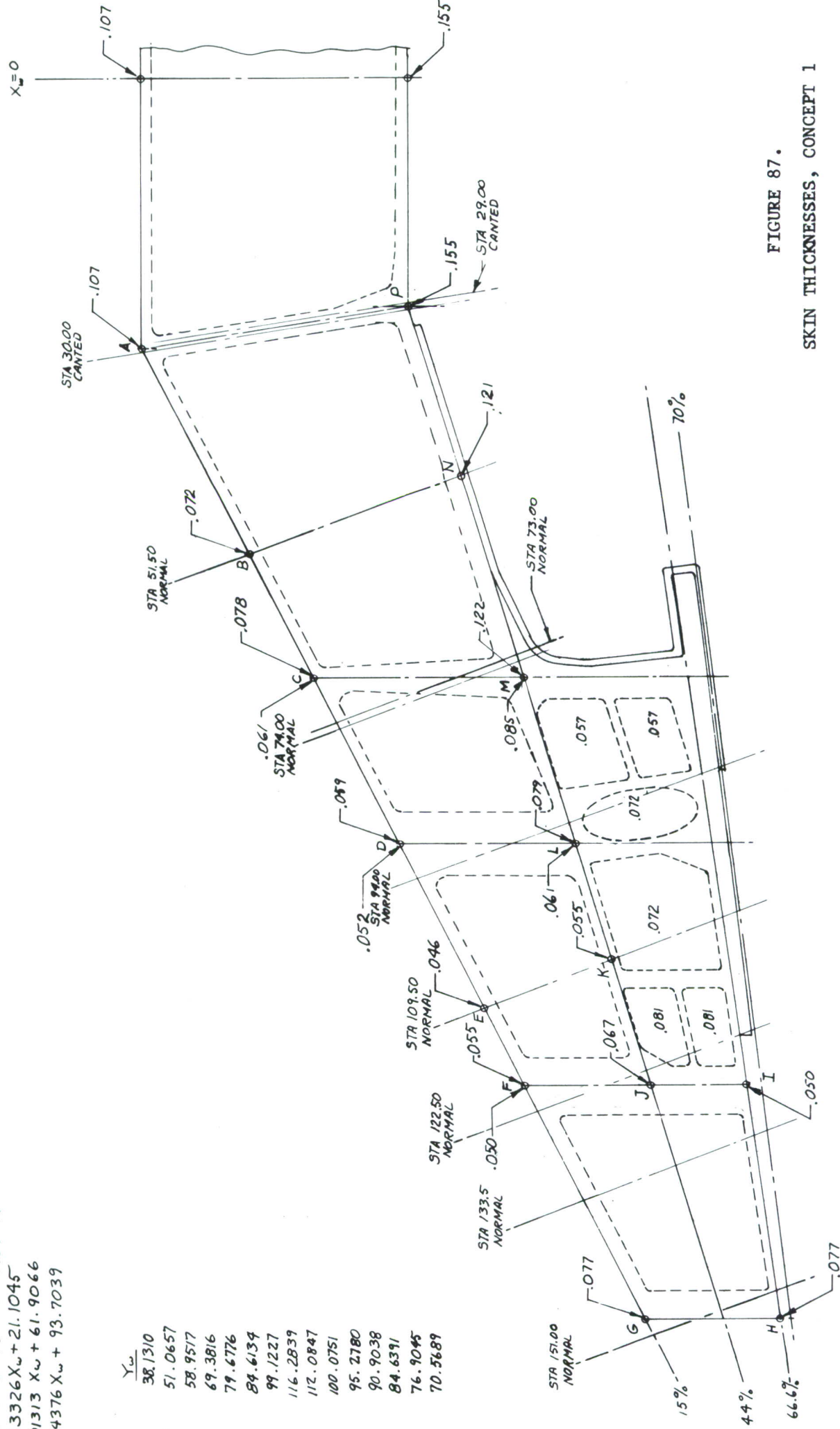


FIGURE 87.  
SKIN THICKNESSES, CONCEPT 1

"B" REV. 3-15-73  
"A" REV. 3-8-73

UPPER SKIN POCKETS- FULL DEPTH  
H'COMB WING SCALE 1/10 J.C. MOPPERT

1891-104



THICKNESS TAPERS FOR LOWER SKIN POCKETS	
1	A-P-INB'D $Z = .003884345166 Y_w - .0651139654$
2	A-B-N-P $Z = -.002262627494 X_w + .003531357497 Y_w + .022953329$
3	B-C-M-N $Z = -.201647671179 X_w + .002575682937 Y_w - .0242358708$
4	C-D-L-M $Z = -.00554216164 X_w + .002305321775 Y_w + .0307276065$
5	D-E-K-L $Z = -.0005851880438 X_w + .0008717853999 Y_w + .0529223144$
6	E-F-J-K $Z = .0007430434133 X_w + .001367706782 Y_w - .13726668845$
7	F-G-H-I $Z = .0009608540925 X_w - .0681850533$

EQUATION, OF LINES	
1	A-P $Y_w = -6.409385497 X_w + 249.4868961$
2	B-N $Y_w = -2.672887142 X_w + 206.1650549$
3	E-K $Y_w = -2.672903281 X_w + 382.8933519$
4	15% $Y_w = .5163326 X_w + 21.1045$
5	44% $Y_w = .3101313 X_w + 61.9066$
6	66.6% $Y_w = .1494376 X_w + 93.7039$

### EQUATION OF LINES

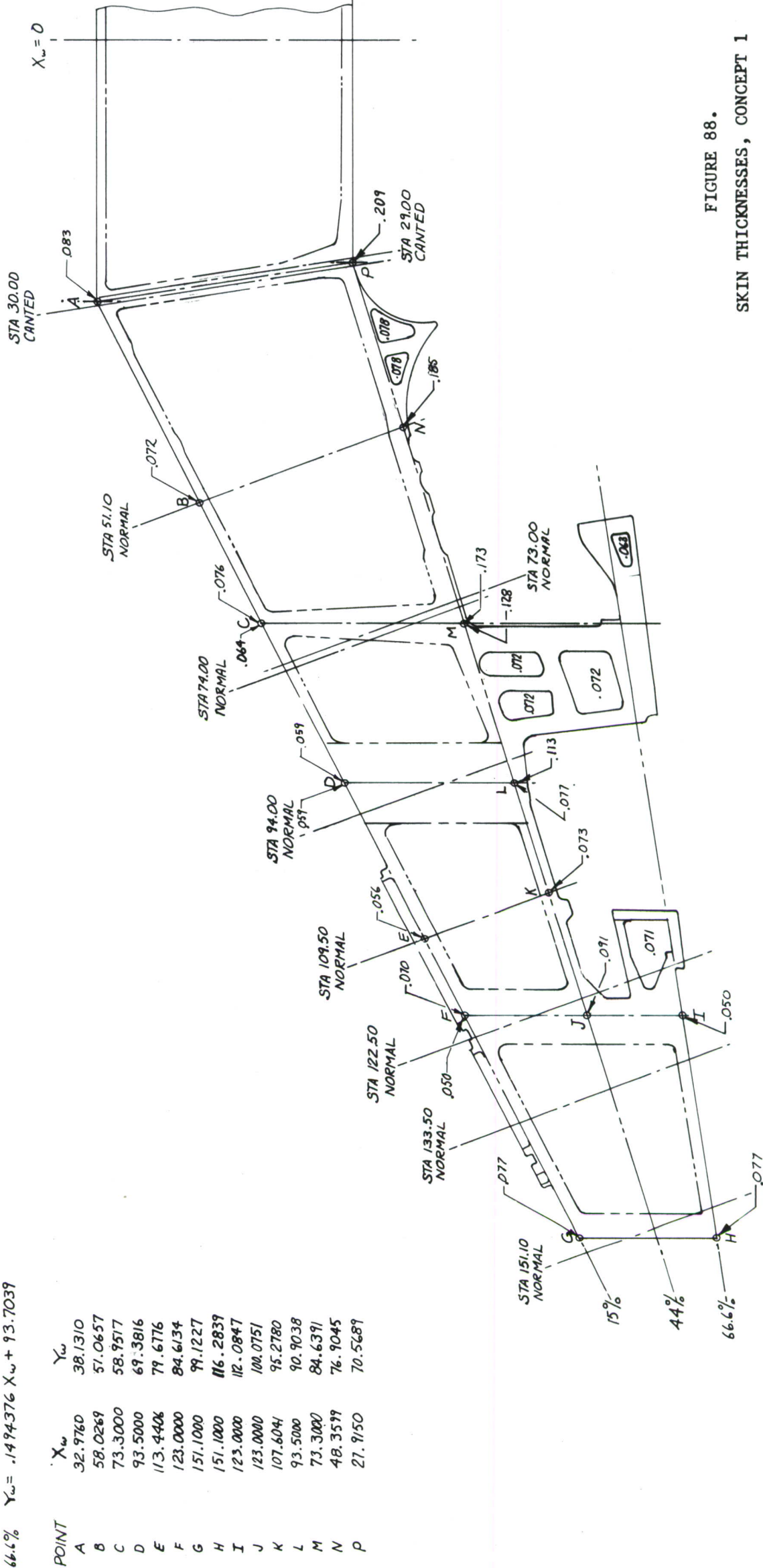


FIGURE 88.  
SKIN THICKNESSES, CONCEPT 1

"A" REV. 3-13-73  
LOWER SKIN POCKETS - FULL DEPTH H'COMB WING  
J.C. MOPPERT

1891-105



# THICKNESS TAPERS FOR LOWER SKIN LANDS (INNER SURFACE)

- EQU #1:  $T_1 = .005642401 X_w - .0901504$   
 EQU #2:  $T_2 = .003192213 X_w + .005144273 Y_w + .03411016$   
 EQU #3:  $T_3 = .002207558 X_w + .004334715 Y_w + .0325094$   
 EQU #4:  $T_4 = .005209643 X_w + .004334715 Y_w + .2441564$   
 EQU #5:  $T_5 = .002286534 X_w + .002767815 Y_w + .1618288$   
 EQU #6:  $T_6 = .125 \text{ CONST OUTLET OF B-F-C}$   
 EQU #7:  $T_7 = .002251626 X_w - .005203976 Y_w + .8346819$   
 EQU #8:  $T_8 = .001000607 X_w - .00071527 Y_w + .2634042$

THICKNESS TAPERS FROM THEORETICAL AIR FOIL TO THE ACTUAL OUTER SURFACE OF WING

- 1, A-K-180:  $T_1 = .0020349 Y_w - .0775927$   
 2, A-K-M-B:  $T_2 = .0009603 X_w + .0018851 Y_w - .0402136$   
 3, B-M-F:  $T_3 = .002265 X_w + .0018846 Y_w + .0518074$   
 4, B-F-C-G-E:  $T_4 = 0 \text{ CONST}$   
 5, M-F-C:  $T_5 = .0009789 X_w - .0022625 Y_w + .3085449$   
 6, K-M-C-J:  $T_6 = .000383 X_w - .0024451 Y_w + .2278565$

- LINE EQUATIONS  
 1, A-K:  $Y_w = -.640938597 X_w + 249.4868961$   
 2, 15%:  $Y_w = .51633226 X_w + 21.1045$   
 3, 44%:  $Y_w = .3101313 X_w + 61.9066$   
 4, A-M:  $Y_w = 1.2162882 X_w - 1.9773211$   
 5, B-F:  $Y_w = 1.2018419 X_w - 27.4885747$   
 6, F-C:  $Y_w = -.4326741 X_w + 136.3730122$   
 7 M-C:  $Y_w = 7.4596428 X_w - 442.1338209$   
 8 J-C:  $Y_w = .1575851 X_w + 93.1070119$

NOTE:- TOPOGRAPHY OF INNER SURFACE ONLY  
SEE 1891-107 FOR OUTER SURFACE

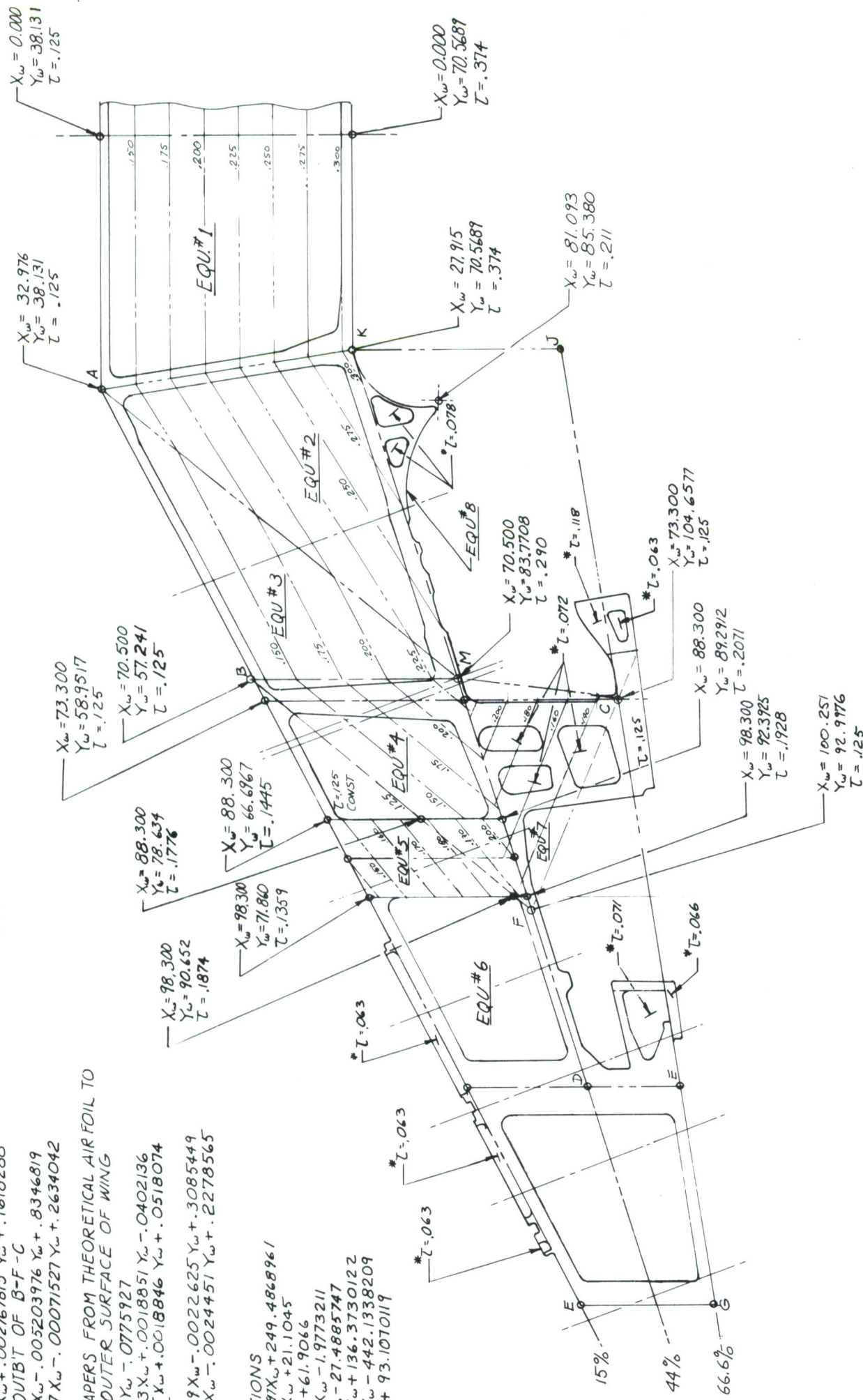


FIGURE 89.  
SKIN THICKNESSES, CONCEPT 1

$T_z$  = THICKNESS TAPERS FOR OUTER SURFACE

EQU #1

$T_z = .0020349 Y_w - .0775927$

EQU #2

$T_z = -.0009603 X_w + .0018851 Y_w - .0402136$

EQU #3

$T_z = -.002265 X_w + .0018846 Y_w + .0518074$

EQU #6

$T_z = -.0009789 X_w - .0022625 Y_w + .3085449$

NOTE :- SEE DWGS 1891-105, 1891-106

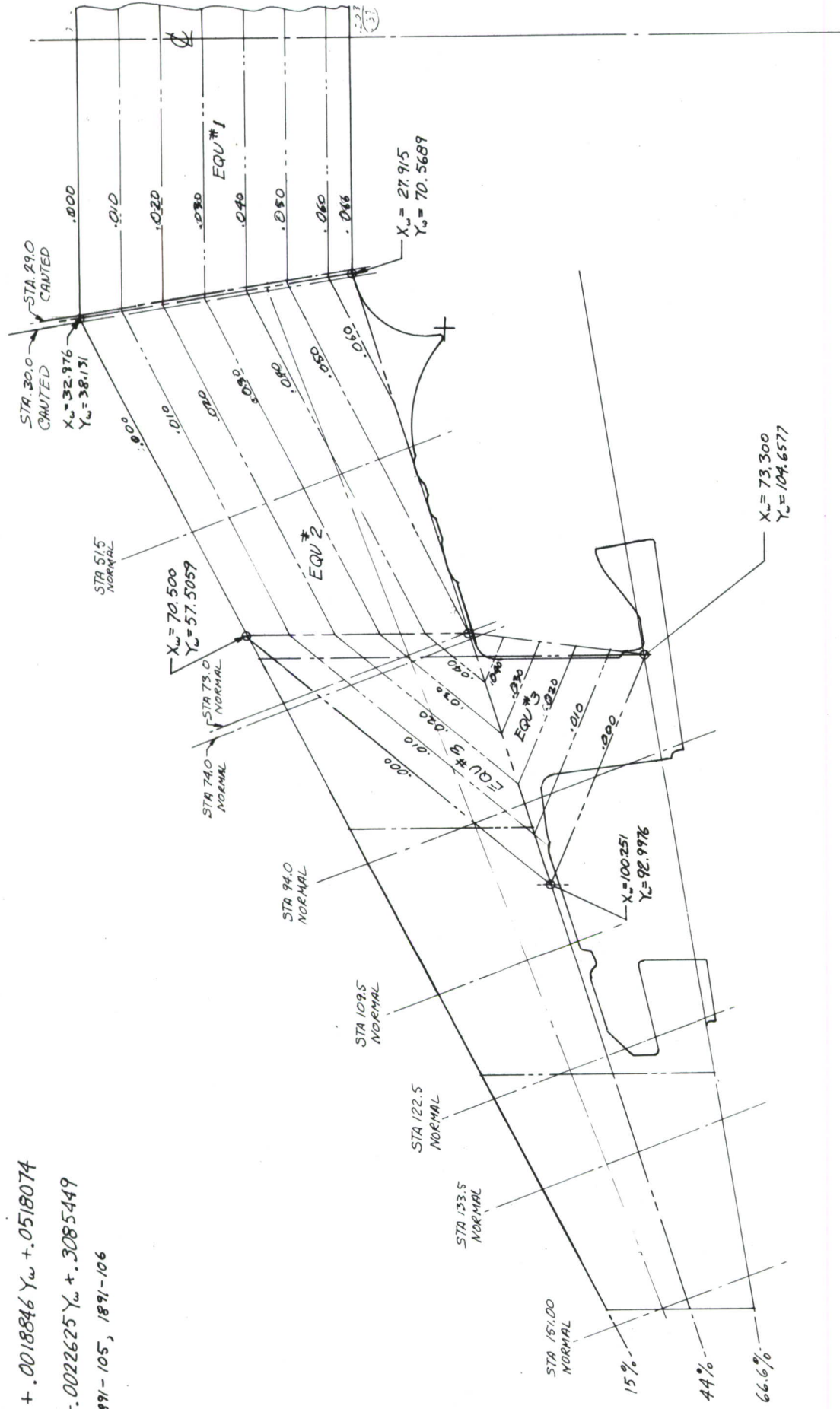


FIGURE 90.  
SKIN THICKNESSES, CONCEPT 1



THICKNESS TAPERS FOR POCKETS (ML TO INNER SURFACE)

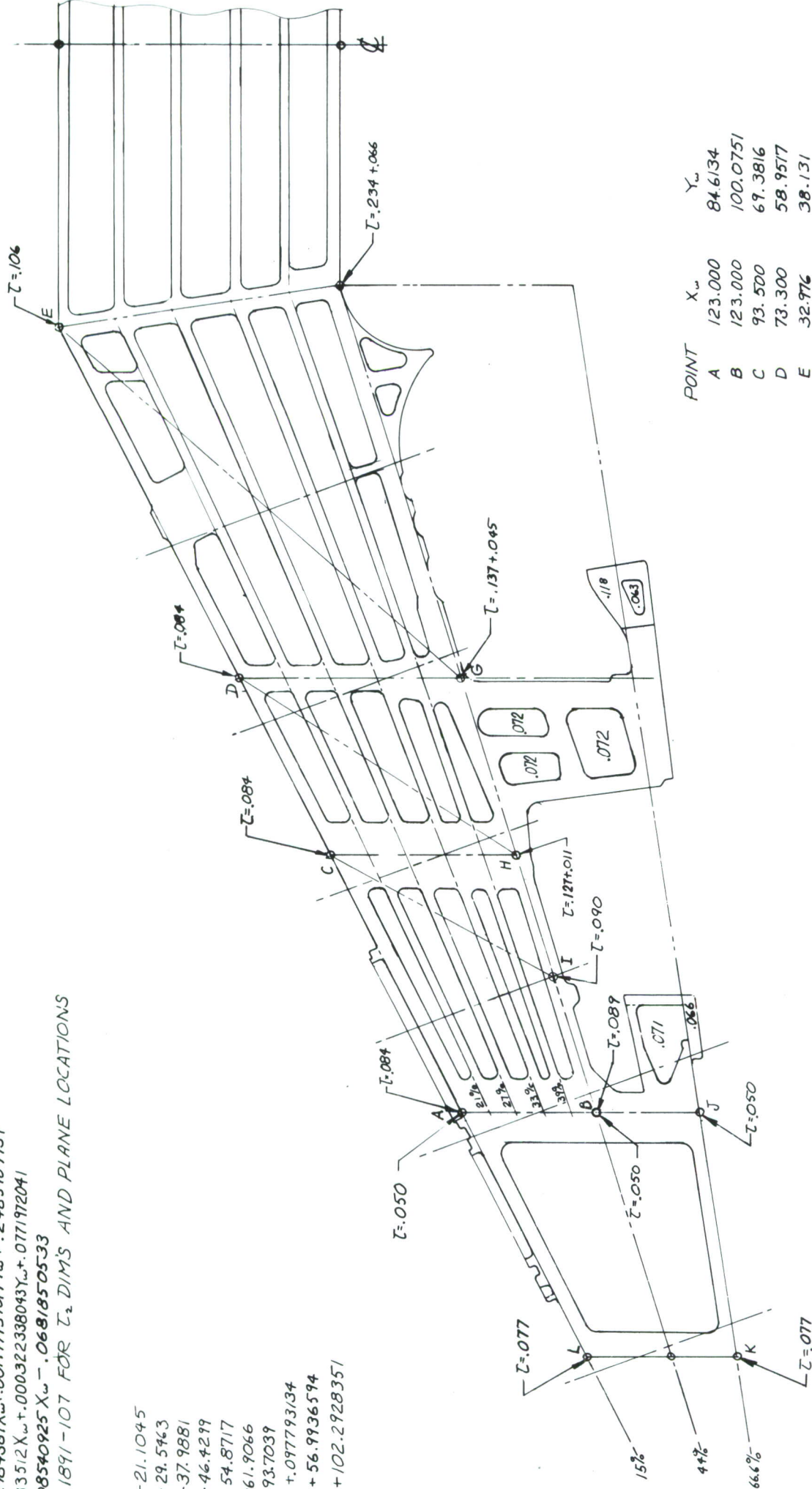
$$T = T_1 + T_2$$

1. E-F-INBD  $T_1 = .003946001438 Y_w - .0444649807$
2. E-G-F  $T_1 = -.00320553381 X_w + .003445867162 Y_w - .0803119675$
3. E-D-G  $T_1 = -.001610918853 X_w + .002063268374 Y_w + .0804471738$
4. D-H-G  $T_1 = -.001134938291 X_w + .002063268373 Y_w + .0455578127$
5. D-C-H  $T_1 = -.00103621183 X_w + .001997937014 Y_w + .0418343632$
6. C-I-H  $T_1 = -.003242984387 X_w + .001997937014 Y_w + .2485989734$
7. C-A-B-I  $T_1 = -.000166433512 X_w + .000322338043 Y_w + .0771972041$
8. A-L-K-J  $T_1 = .0009608540925 X_w - .0681850533$

NOTE: SEE DWG 1891-107 FOR  $T_2$  DIMS AND PLANE LOCATIONS

LINE EQUATIONS

- 15%  $Y_w = .5163326 X_w + 21.1045$   
 21%  $Y_w = .4736704 X_w + 29.5463$   
 27%  $Y_w = .4310079 X_w + 37.9881$   
 33%  $Y_w = .3883456 X_w + 46.4299$   
 39%  $Y_w = .3456833 X_w + 54.8717$   
 44%  $Y_w = .3101313 X_w + 61.9066$   
 66.6%  $Y_w = .1494376 X_w + 93.7039$   
 E-G  $Y_w = .153360282 X_w + .097793134$   
 D-H  $Y_w = .1581792079 X_w + .56.9936594$   
 C-I  $Y_w = .1836090215 X_w + 102.2928351$



POINT	$X_w$	$Y_w$
A	123.000	84.6134
B	123.000	100.0751
C	93.500	69.3816
D	73.300	58.9577
E	32.976	38.131
F	27.915	70.5689
G	73.300	84.6391
H	93.500	90.9039
I	107.604	95.2780
J	123.000	112.0847
K	151.100	116.2839
L	151.100	99.1223

FIGURE 91.

SKIN THICKNESSES, CONCEPT 3

"B" REV. 3-19-73

"A" REV. 3-6-73

LOWER SKIN POCKET PLANES

6 SPAR WING, TI-LOWER & AL UPPER

J.C. MOPPERT 3-5-73

SCALE 1/10

1891-302



## THICKNESS TAPERS FOR POCKETS

1. E-F-INBD :  $t = .001325809 Y_w + .03G44553$
2. E-F-G :  $t = -.00092995041 X_w + .001169843 Y_w + .075353573$
3. C-D-G :  $t = -.001850957 X_w + .0008512915 Y_w + .1618951$
4. A-C-H-J :  $t = -.000480217 X_w + .0007926235 Y_w + .0322032$
5. M-L-K-A :  $t = .0009608540925 X_w - .0681850553$

## THICKNESS TAPERS FOR LANDS

- |           |   |
|-----------|---|
| E-F-INBD  | $t' = .000647489 Y_w + .100310G$                  |
| E-F-G     | $t' = -.000663889 X_w + .00543892 Y_w + .1261532$ |
| E-G-OUTBD | $t' = .125 \text{ CONSTANT}$                      |

## LINE EQUATIONS

- |         |                                   |
|---------|-----------------------------------|
| 15%     | $Y_w = 516.3326 X_w + 21.1045$    |
| 22.25%  | $Y_w = 4647822 X_w + 31.3050$     |
| 24.667% | $Y_w = 4475253 X_w + 34.7057$     |
| 29.50%  | $Y_w = 4132319 X_w + 41.5055$     |
| 34.333% | $Y_w = 3788674 X_w + 48.3054$     |
| 36.75%  | $Y_w = 3616816 X_w + 51.7061$     |
| 44%     | $Y_w = 3101313 X_w + 61.9066$     |
| E-F     | $Y_w = -64084173 X_w + 249.4550$  |
| E-G     | $Y_w = 1.220626 X_w - 2.1204$     |
| D-G     | $Y_w = 2.6728925 X_w + 271.6761$  |
| D-H     | $Y_w = 2.3296092 X_w - 121.3614$  |
| C-H     | $Y_w = -2.6728894 X_w + 332.6162$ |
| C-J     | $Y_w = 1.2004298 X_w - 45.7169$   |
| A-J     | $Y_w = -2.6728950 X_w + 422.5038$ |

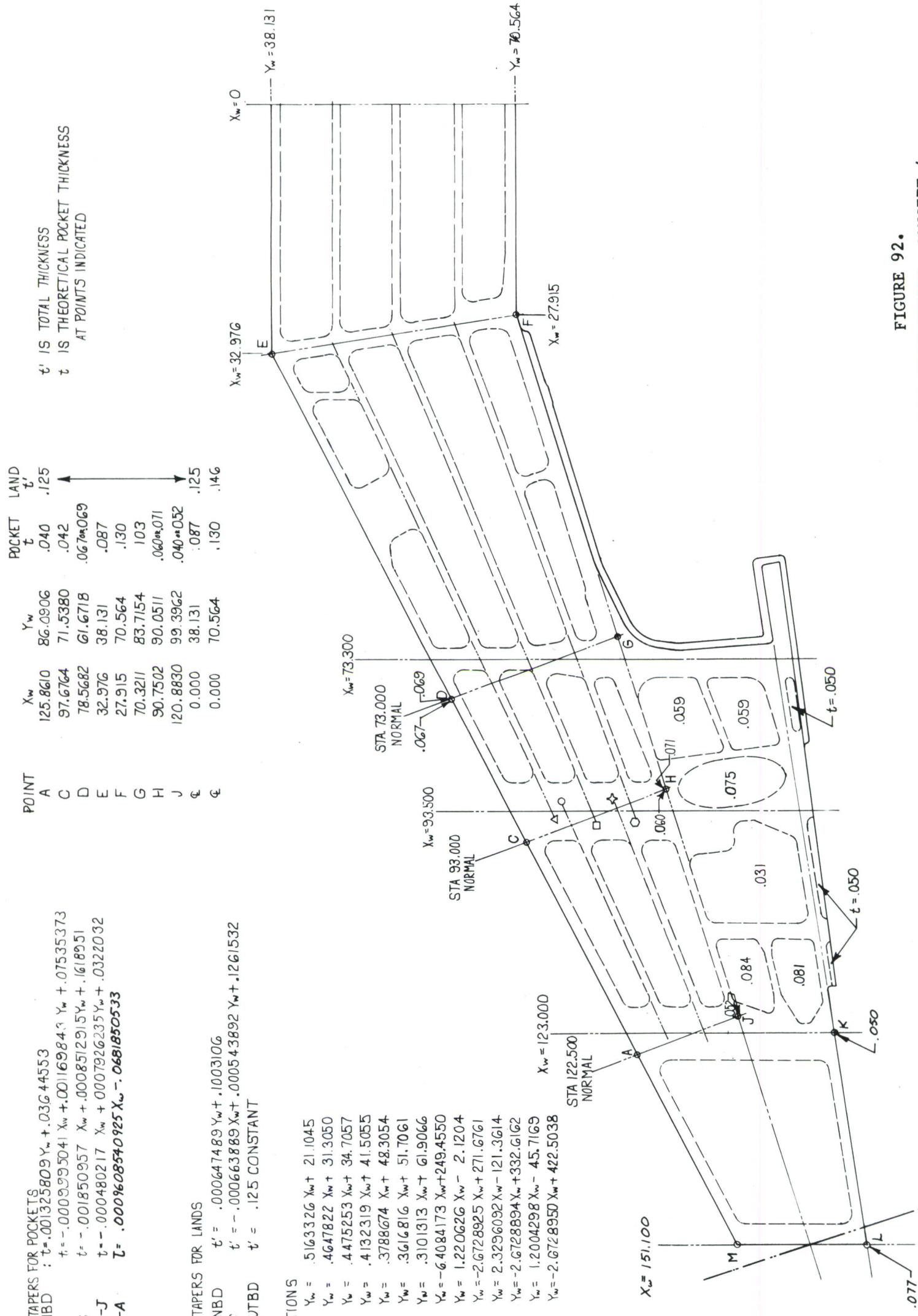


FIGURE 92.  
SKIN THICKNESSES, CONCEPT 4

UPPER SKIN POCKET & LAND PLANES  
5 SPAR WING HONEYCOMB STIFFENED  
SCALE : 1/10

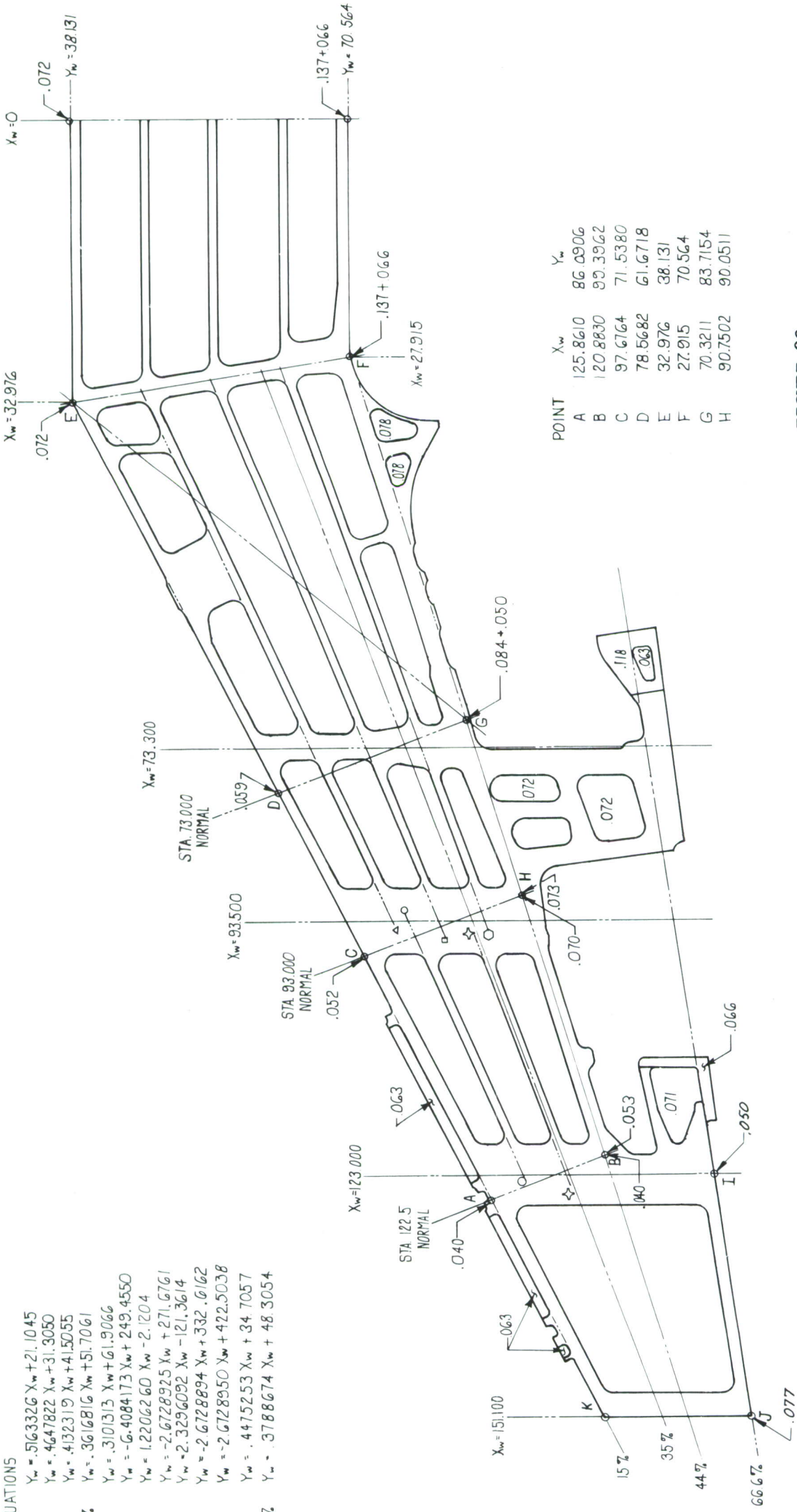
"B" REV 3-6-73  
"A" REV 2-27-73  
1891-402

# THICKNESS TAPERS FOR POCKETS (SEE NOTE 1.)

1. E-F-INBD  $t = +.00200413 Y_w - .00441954 Z$
2. E-F-G  $t = -.001784979 X_w + .001725595 Y_w + .06506280$
3. E-G-D  $t = -.000729750 X_w + .0008610970 Y_w + .06322975$
4. C-D-G  $t = -.000797802 X_w + .0008356369 Y_w + .0701466$
5. A-C-H-C  $t = -.000777579 X_w + .0006813733 Y_w + .07920703$
- 6 K-J-I-A  $t = .000960854925 X_w - .0681850533$

## LINE EQUATIONS

- 15%  $Y_w = .5163326 X_w + 21.1045$   
 $\Delta 22.25\% Y_w = .4647822 X_w + 31.3050$   
 $\Delta 29.50\% Y_w = .4132319 X_w + 41.5055$   
 $\Delta 36.75\% Y_w = .3616816 X_w + 51.7061$   
 $\Delta 44\% Y_w = .3101313 X_w + 61.9066$   
E-F  $Y_w = -.64084173 X_w + 249.4550$   
E-G  $Y_w = 1.2206260 X_w - 2.1204$   
D-G  $Y_w = -2.6728925 X_w + 271.6761$   
D-H  $Y_w = -2.3296092 X_w - 121.3614$   
C-H  $Y_w = -2.6728894 X_w + 332.6162$   
A-B  $Y_w = -2.6728950 X_w + 422.5038$   
O 24.667%  $Y_w = .4475253 X_w + 34.7057$   
 $\Delta 34.333\% Y_w = .3788674 X_w + 48.3054$



- NOTE: 1. TOTAL THICKNESS =  $t + T$  ( $T$  = LWR WING OUTER SURF)  
 SEE LOWER SKIN AND PLANES DWG FOR  $T$   
 2. THICKNESS SHOWN AT POINTS & POCKETS INCLUDES LWR WING OUTER SURF

FIGURE 93.  
SKIN THICKNESSES, CONCEPT 4

LOWER SKIN POCKET PLANES  
 5 SPAR WING H.C. STIFFENED  
 SCALE 1/10

"B" REV. 3-6-73  
 "A" REV. 2-26-73  
 1891-403



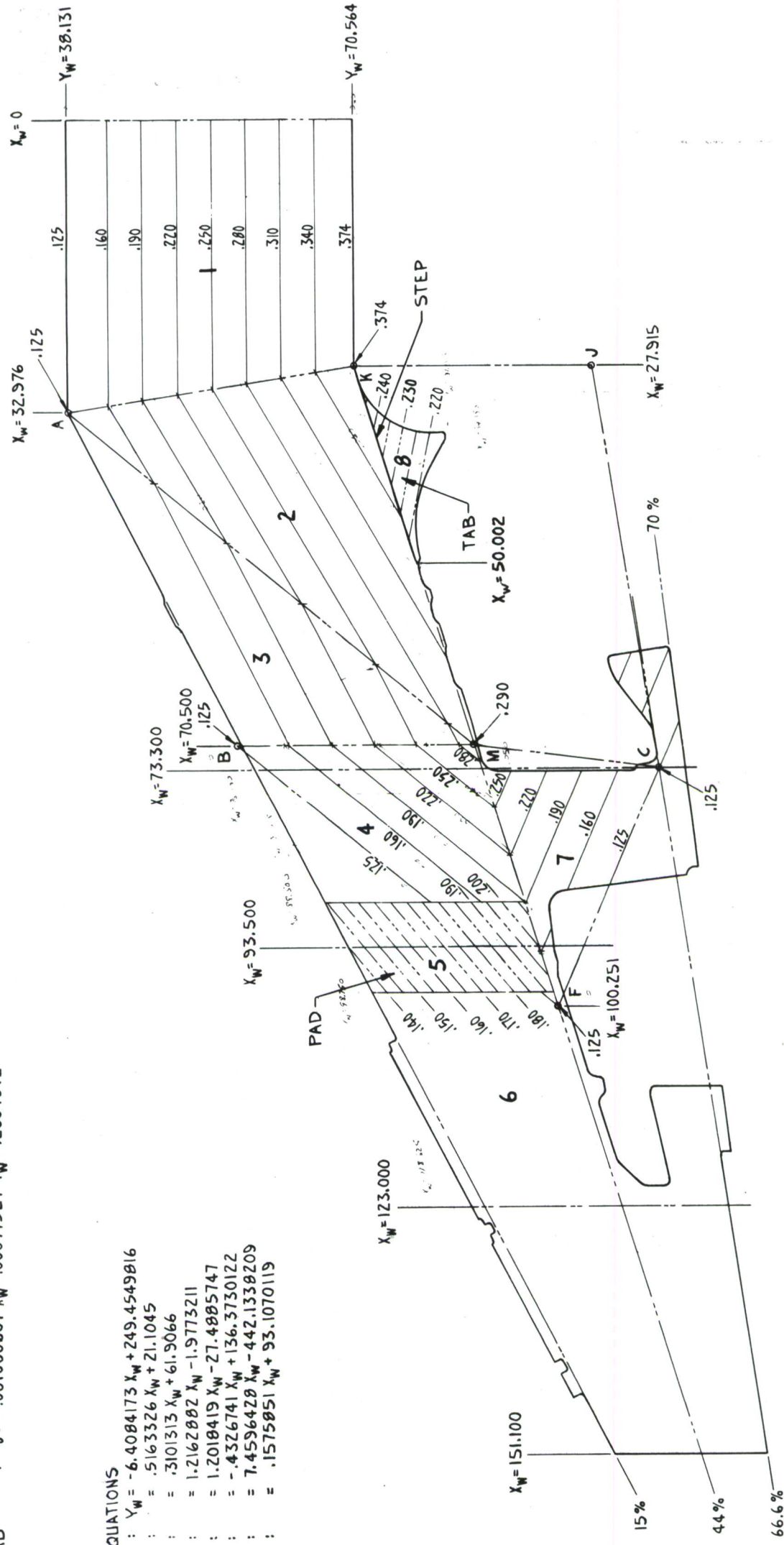
T IS DISTANCE FROM THEORETICAL AIRFOIL TO ACTUAL OUTER SURFACE OF WING SKIN

THICKNESS TAPERS LOWER WING OUTER SURFACE (SEE NOTE 1.)

- A-K-INBD :  $T = .0020349 Y_W - .0775927$   
A-K-M-B :  $T = -.0009603 X_W + .0018951 Y_W - .0402136$   
M-F-C :  $T = -.0009789 X_W - .0022625 Y_W + .3085449$   
K-M-C-U :  $T = .000383 X_W - .0024451 Y_W + .278565$   
B-M-F :  $T = -.002265 X_W + .0018946 Y_W + .0518074$   
B-F-C-OUTBD :  $T = 0$

## LINE EQUATIONS

- |     |                    |  |
|-----|--------------------|--|
| A-K | : Y <sub>W</sub> = | -6.4084173 X <sub>W</sub> + 249.4549816  |
| 15% | :                  | = 5.163326 X <sub>W</sub> + 21.1045      |
| 44% | :                  | = 3.101313 X <sub>W</sub> + 61.9066      |
| A-M | :                  | = 1.216282 X <sub>W</sub> - 1.9773211    |
| B-F | :                  | = 1.2018419 X <sub>W</sub> - 27.4885747  |
| F-C | :                  | = -4.326741 X <sub>W</sub> + 136.3731022 |
| M-C | :                  | = 7.4596428 X <sub>W</sub> - 442.1338209 |
| J-C | :                  | = .1575851 X <sub>W</sub> + 93.1070119   |



NOTE: 1. TOTAL LAND = t + T  
2. NO HONEYCOMB INBD OF STA 93.500 FOR 5 SPAR WING  
3. ALL THICKNESSES SHOWN INCLUDE LWR WING OUTER SURFACE

FIGURE 94.  
SKIN THICKNESSES, CONCEPTS 4 AND 5

LOWER SKIN LAND PLANES  
SPAR WING HONEYCOMB STIFFENED  
SCALE: 1/10



THICKNESS TAPERS FOR POCKETS

1. E-F-INBD  $t = .001356643Y_w + .03926985$
2. E-F-G-D  $t = -.001121090X_w + .001181703Y_w + .08290955$
3. C-D-G-H  $t = -.002127352X_w + .0008052331Y_w + .1851873$
4. A-C-J  $t = -.00001272289X_w + .0001127916Y_w + .05131161$
5. C-H-J  $t = -.0008649104X_w + .0006487006Y_w + .08007459$
6. M-L-K-A  $t = .0009608540925X_w - .0681850533$

THICKNESS TAPERS FOR LANDS

6. E-F-INBD  $t' = .0008324854Y_w + .0932565$
7. E F G  $t' = -.0008535716X_w + .00069929Y_w + .1264877$
8. E-G-OUTBD  $t' = .125 \text{ CONSTANT}$

LINE EQUATIONS

- 15%  $Y_w = .5163326X_w + 21.1045$
- 24.667%  $Y_w = .4475253X_w + 34.7057$
- 34.333%  $Y_w = .3788674X_w + 48.3054$
- 44%  $Y_w = .3101313X_w + 61.9066$
- E-F  $Y_w = -.64084173X_w + 248.4550$
- E-G  $Y_w = 1.220626X_w - 2.1204$
- D-G  $Y_w = -2.6728925X_w + 271.6761$
- D-H  $Y_w = 2.3296092X_w - 121.3614$
- C-H  $Y_w = -2.6728894X_w + 332.6162$
- C-J  $Y_w = 1.2004298X_w - 45.7169$
- A-J  $Y_w = -2.672895X_w + 422.5038$

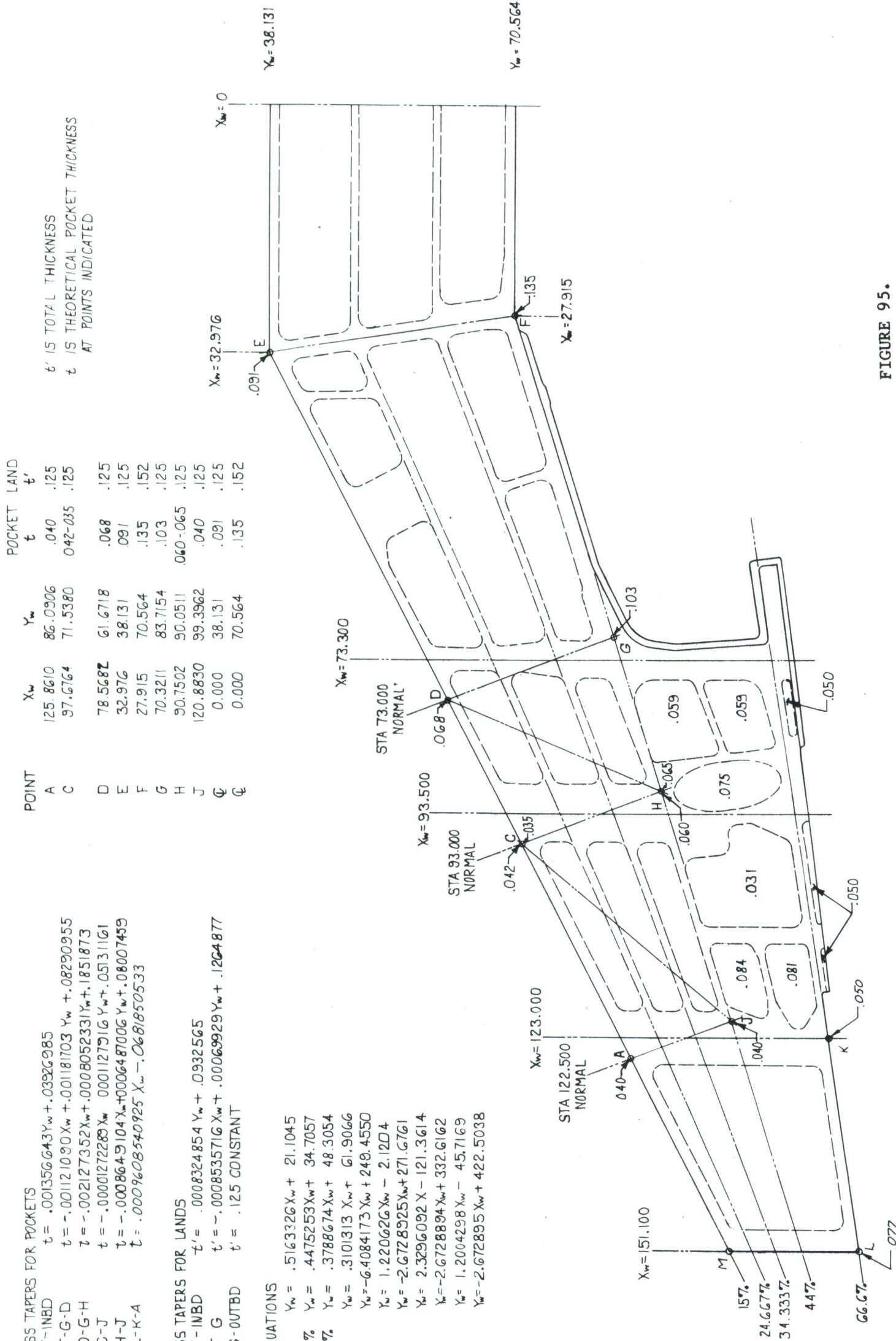


FIGURE 95.

SKIN THICKNESSES, CONCEPT 5

UPPER SKIN POCKET & LAND PLANES  
4 SPAR WING HONEYCOMB STIFFENED  
SCALE 1/10

THICKNESS TAPERS FOR POCKETS (SEE NOTE 1)

1. E-F-INBD  $t = .001973299 X_w - .005243857$
2. D-E-G  $t = -.000690488 X_w + .0007850568 X_w + .0628345$
3. E-F-G  $t = -.001798351 X_w + .001692676 X_w + .06475901$
4. D-G-H  $t = -.001425937 X_w + .0005099056 X_w + .1375865$
5. C-D-H  $t = .0002683912 X_w + .00001302152 X_w + .07728395$
6. A-C-H-J  $t = -.0000405921 X_w - .00003843168 X_w + .09439822$
7. M-L-K-A  $t = .009608540925 X_w - .0681850533$

LINE EQUATIONS

- 15%  $Y_w = .5163326 X_w + 21.1045$   
 24.667%  $Y_w = .4475253 X_w + 34.1057$   
 34.333%  $Y_w = .3788674 X_w + 48.3054$   
 44%  $Y_w = .3101313 X_w + 61.9066$   
 E-F  $Y_w = -.64084173 X_w + 2494550$   
 D-G  $Y_w = -2.6728925 X_w + 271.6761$   
 D-H  $Y_w = 2.3296092 X_w - 121.3614$   
 C-H  $Y_w = -2.6728894 X_w + 332.6162$   
 A-J  $Y_w = -2.6728950 X_w + 422.5038$

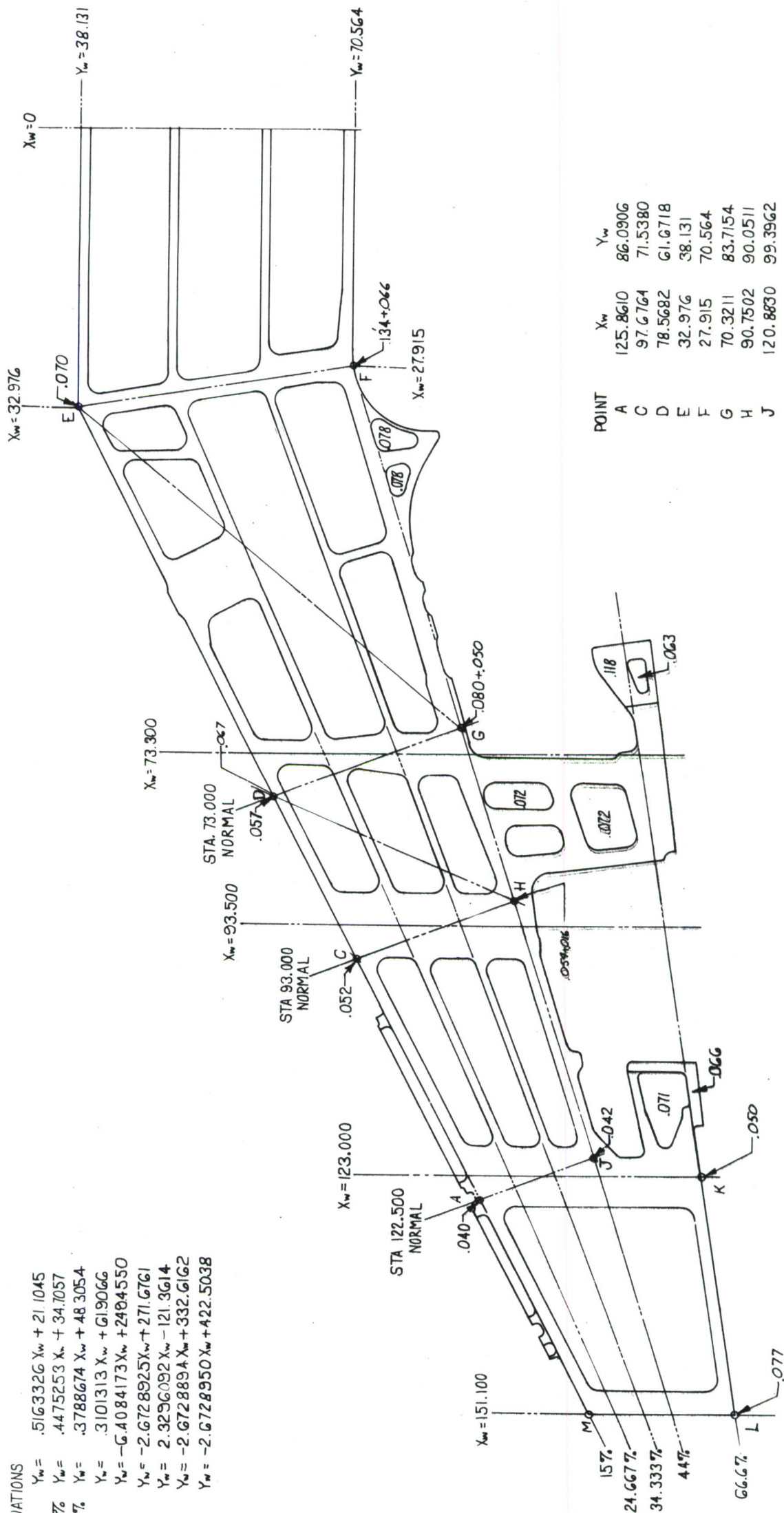


FIGURE 96.  
SKIN THICKNESSES, CONCEPT 5

NOTE: 1. TOTAL THICKNESS =  $t + T$  ( $T$  = LAR WING OUTER SURF)  
 (SEE LOWER SKIN LAND PLANE DWG FOR  $T$ )

2. THICKNESS SHOWN AT POINTS & POCKETS INCLUDES LOWER WING OUTER SURF

LOWER SKIN POCKET PLANES  
 4 SPAR WING HONEYCOMB STIFFENED  
 SCALE: 1/10

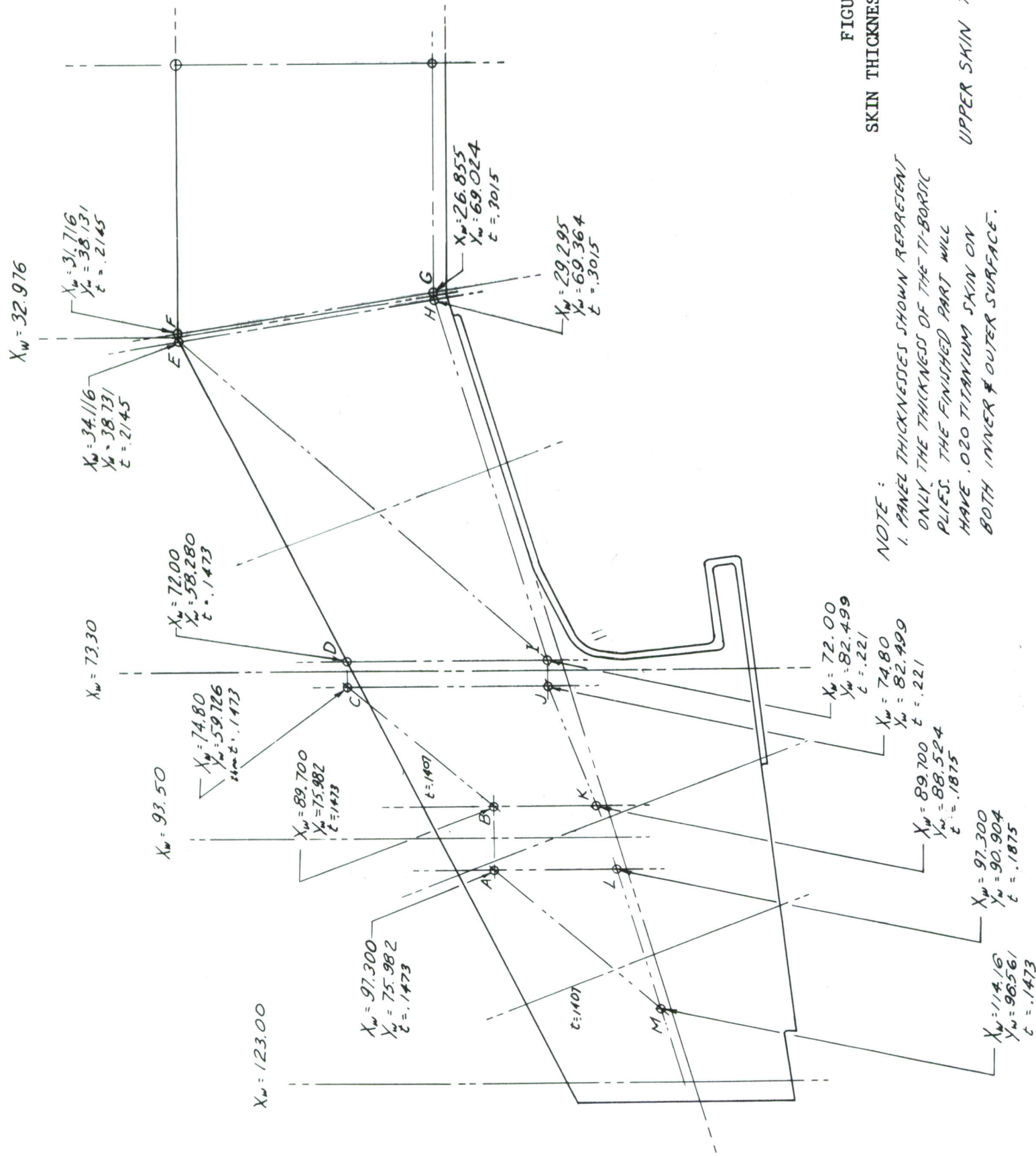


FIGURE 97.  
SKIN THICKNESSES, CONCEPT 6

NOTE:  
1. PANEL THICKNESSES SHOWN REPRESENT ONLY THE THICKNESS OF THE TI-BORONIC PLIES. THE FINISHED PART WILL HAVE .020 TITANIUM SKIN ON BOTH INNER & OUTER SURFACE.

UPPER SKIN TI-BORONIC AREA PLANES



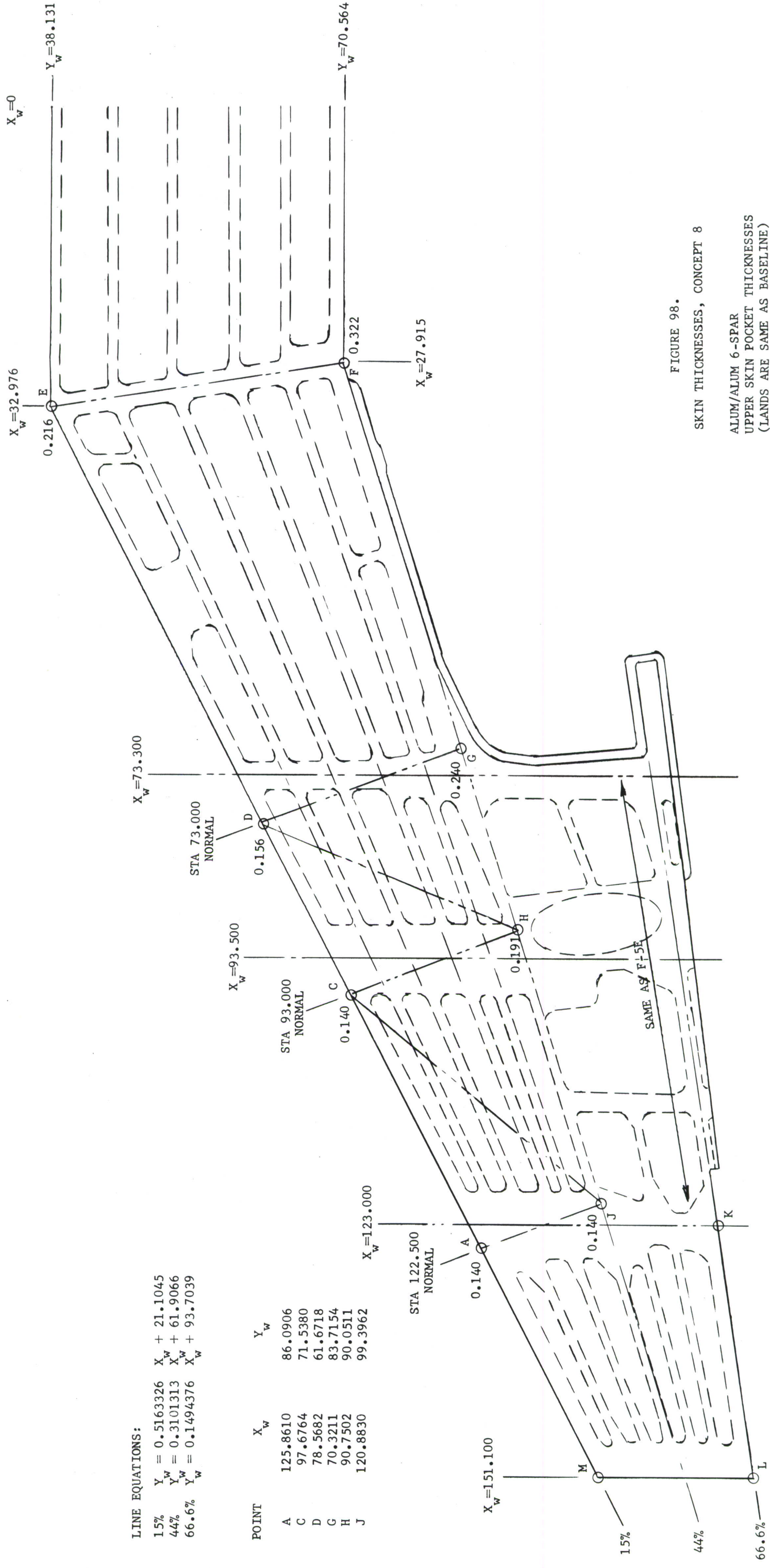


FIGURE 98.  
SKIN THICKNESSES, CONCEPT 8  
ALUM/ALUM 6-SPAR  
UPPER SKIN POCKET THICKNESSES  
(LANDS ARE SAME AS BASELINE)

LINE EQUATIONS:

15%  $Y = 0.5163326 X_w + 21.1045$   
 44%  $Y_w = 0.3101313 X_w + 61.9066$   
 66.6%  $Y_w = 0.1494376 X_w + 93.7039$

POINT	$X_w$	$Y_w$
A	125.8610	86.0906
B	120.8830	99.3962
C	97.6764	71.5380
D	78.5682	61.6718
G	70.3211	83.7154
H	90.7502	90.0511

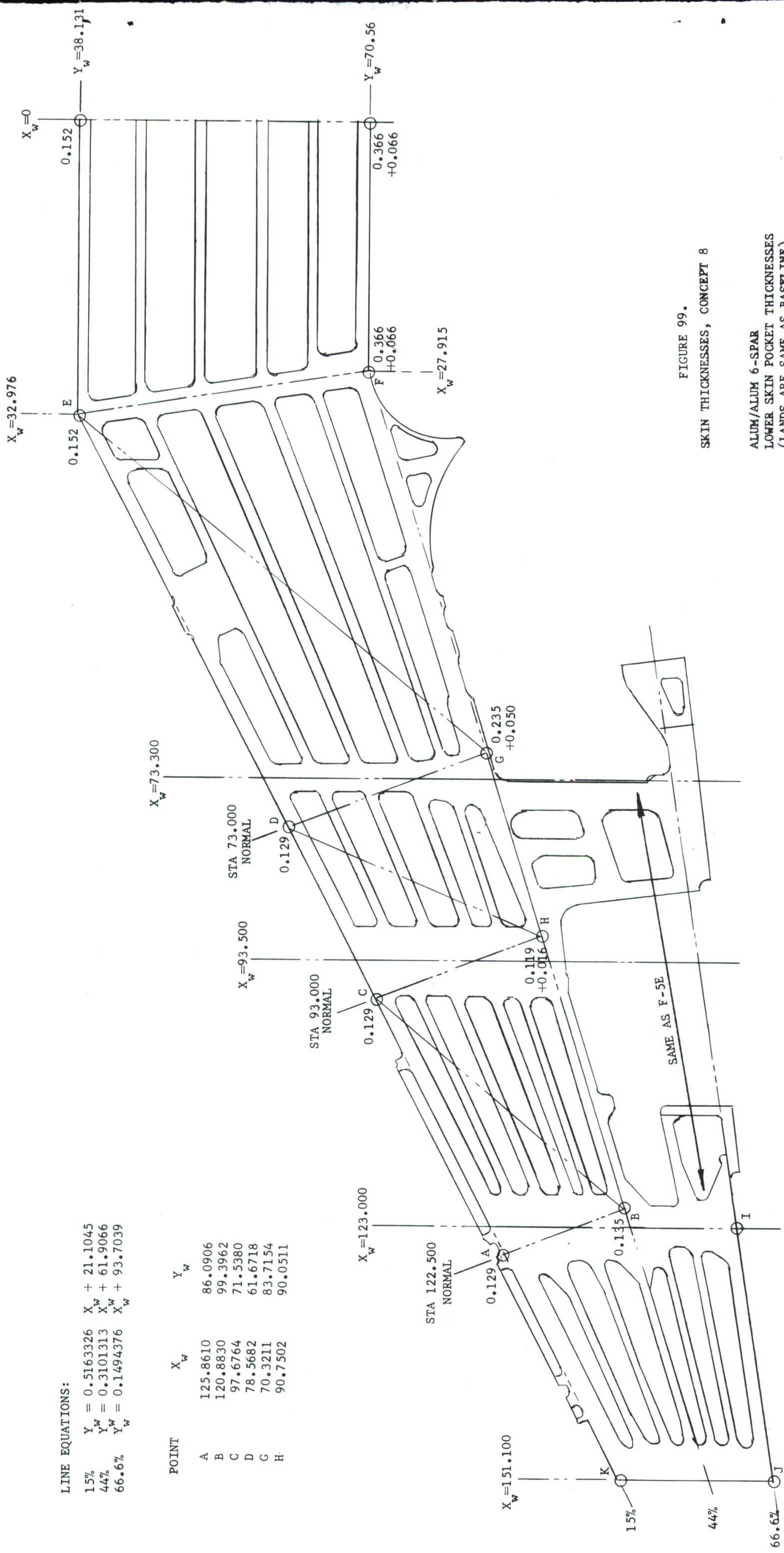


FIGURE 99.  
SKIN THICKNESSES, CONCEPT 8

ALUM/ALUM 6-SPAR  
 LOWER SKIN POCKET THICKNESSES  
 (LANDS ARE SAME AS BASELINE)



## REFERENCES

1. Willenborg, J., Engle, R. M., and Wood, H. A., "A Crack Growth Retardation Model Using an Effective Stress Concept," AFFDL-TM-71-1-FBR, January 1971.
2. C. Rosenkranz, et al, "Advanced Lightweight Fighter Structural Concept Study," AFFDL-TR-72-98, July 1972.
3. MIL-A-8860 (AGG) through -8870 (ASG), 18 May 1960.
4. Northrop Report NOR 69-35B, "Structural Design Criteria for the F-5E Aircraft," April 1971.
5. RFQ F33615-72-Q-1891, Attachment 1, "Service Life Requirements."
6. Proposed MIL-STD-1530 (USAF), September 1972.
7. "USAF Damage Tolerance Requirements," 18 August 1972.
8. Northrop Report NOR 71-118, "F-5E Structural Design Loads," February 1972.
9. Northrop Report NOR 62-89, "F-5 Structural Design Loads," Volume I, September 1965.
10. Northrop Report NOR 71-173, "F-5E Wing Stress Analysis," March 1972.
11. I. J. Toth, W. D. Brentnall, and G. D. Menke, "A Survey of Aluminum Matrix Composites," presented at the Composites: State of the Art Conference, AIME Fall Meeting, 20 October 1971.
12. W. D. Brentnall and I. J. Toth, "High Temperature Titanium Composites," IR-7351-(1), Metal and Ceramics Division, AFML, 1 July 1971 to 1 January 1972.
13. W. D. Brentnall and I. J. Toth, "High Temperature Titanium Composites," IR-7351-(2), Metal and Ceramics Division, AFML, 1 January 1972 to 1 July 1972.
14. Telecon, R. Wells (Northrop) to I. J. Toth (TRW), 24 October 1972.
15. Northrop Report NOR 71-134, "Strength Allowable and Buckling Load Analysis of Laminated Composites Including the Effect of Normal Shear Stiffness," September 1971.
16. Northrop Report NOR 70-203, "User's Manual for Northrop Version of Finite Element Program SAAS-4," March 1972.



17. Northrop Report NOR 71-172, "F-5E Wing Internal Loads," Volume II, May 1972.
18. Anon., "Structural Sandwich Composites," MIL-HDBK-23A, DOD, Washington, D.C., 20005, 30 December 1968.
19. E. F. Bruhn, "Analysis and Design of Flight Vehicle Structures," Tri-State Offset Co., Cincinnati, Ohio, 1965.
20. R. T. Sullins, C. W. Smith, E. E. Spier, Manual for Structural Stability, Analysis of Sandwich Plates and Shells, CR 1457 NASA, Washington, D. C., December, 1969.
21. S. P. Timoshenko and J. M. Gere, "Theory of Elastic Stability," McGraw-Hill Book Co., New York, 1961.
22. Anon., Structural Design Manual, Northrop Corp., Aircraft Division.
23. R. A. Anderson and J. W. Semonian, "Charts Relating the Compressive Buckling Stress of Longitudinally Supported Plates to the Effective Deflectional and Rotational Stiffness of the Supports," NACA TR 1202, 1954.
24. Becker, H., Handbook of Structural Stability, Part II - Buckling of Composite Elements, NACA TN-3782, July 1957.
25. Forman, R. G., Kearney, V. E., and Engle, Jr., R. M., "Numerical Analysis of Crack Propagation in Cyclic-Loaded Structures," Journal of Basic Engineering, Trans. ASME Series D, Vol. 89, No. 3, 1967.
26. Wilhem, D. P., "Fracture Mechanics Guidelines for Aircraft Structure Application," AFFDL-TR-69-111, February 1970.
27. Mechanical Property Data, X2048-T851 Aluminum Alloy, issued by AFML, October 1972.
28. Society of Aeronautical Weight Engineers, Inc., Weight Handbook, Volume 1, December 1968.
29. D. H. Emero and L. Spunt, "Optimization of Multi-rib and Multi-web Wing Box Structures under Shear and Moment Loads," Proceedings Sixth AIAA Structures and Materials Conference, Palm Springs, California, April 1965, page 330.
30. S. Timoshenko and S. Woinowsky-Krieger, "Theory of Plates and Shells," 2nd Ed., McGraw-Hill Book Company, 1959, pages 364-368.

UNCLASSIFIED

Security Classification

## DOCUMENT CONTROL DATA - R &amp; D

(Security classification of title, body of abstract and indexing annotation must be entered when the overall report is classified)

1. ORIGINATING ACTIVITY (Corporate author)		2a. REPORT SECURITY CLASSIFICATION	
Northrop Corporation, Aircraft Division 3901 West Broadway Hawthorne, Ca 90250		Unclassified	
3. REPORT TITLE		2b. GROUP	
ADVANCED METALLIC STRUCTURE: AIR SUPERIORITY FIGHTER WING DESIGN FOR IMPROVED COST, WEIGHT AND INTEGRITY		N/A	
4. DESCRIPTIVE NOTES (Type of report and inclusive dates) Final Report, Volume III (October 1972 through March 1973)			
5. AUTHOR(S) (First name, middle initial, last name)  Fred A. Figge, et al			
6. REPORT DATE June 1973		7a. TOTAL NO. OF PAGES 305	7b. NO. OF REFS 30
8a. CONTRACT OR GRANT NO. F33615-72-C-1891		9a. ORIGINATOR'S REPORT NUMBER(S)  AFFDL-TR-73-52	
b. PROJECT NO.  486U		9b. OTHER REPORT NO(S) (Any other numbers that may be assigned this report)	
c.		d.	
10. DISTRIBUTION STATEMENT Distribution limited to U.S. Government agencies only; test and evaluation; statement applied 18 April 1973. Other requests for this document must be referred to AFFDL (FBA), Wright-Patterson AFB, Ohio 45433.			
11. SUPPLEMENTARY NOTES		12. SPONSORING MILITARY ACTIVITY  Air Force Flight Dynamics Laboratory Wright Patterson Air Force Base, Ohio	
13. ABSTRACT The objective of this program was to reduce the weight of a fighter wing and carrythrough structure while maintaining its cost and life approximately equivalent to the baseline. Innovations in design concepts and application of new materials, manufacturing methods, and analysis techniques were to be expected. General tasks of the program were to provide for concept formulation, first iteration preliminary design, material property testing to support preliminary design, and preliminary planning and cost estimation of a separate follow-on program. An additional task, initiated several months after the basic go-ahead, was to consider the new Damage Tolerance criteria sensitivity and trade studies, utilizing the baseline structure materials and spectra, and by imposing "USAF Damage Tolerance Criteria," MIL-A-008866, dated 18 August 1972. The report is divided into three volumes: Volume I contains the basic report, Volume II contains the damage tolerance criteria sensitivity study, and Volume III contains the results of the materials test program. The structural wing box of the Northrop F-5E Air-Superiority Fighter was selected as the baseline structure to provide realistic structural and functional constraints and requirements for the study. It is a dry wing, all-aluminum, multi-spar design. It can carry a large variety of external stores and weighs approximately 1000 pounds. From a large variety of initial concepts, three designs emerged as having potential for further study and evaluation in a follow-on program. These are: (1) a full depth honeycomb design, featuring titanium skins and aluminum core, (2) a six-spar design featuring aluminum upper skin, titanium lower skin and substructure, with extensive			

(CONTINUED)

DD FORM 1 NOV 68 1473

Unclassified

Security Classification

Abstract (CONTINUED)

use of welding between the lower skin and substructure, and (3) a six-spar all-aluminum design, somewhat similar to the baseline, but utilizing sine-wave spars, titanium tip and landing gear ribs, and some newer aluminum alloys.



Unclassified

Security Classification

14. KEY WORDS	LINK A		LINK B		LINK C	
	ROLE	WT	ROLE	WT	ROLE	WT
Weight Reduction Fighter Wing Design Concepts New Materials New Manufacturing Methods Analysis Techniques Preliminary Design Materials Testing Follow-on Program Baseline Damage Tolerance Criteria Substructure Sine Wave Spars Precision Forgings Full Depth Honeycomb Titanium Castings Concept Ranking						

Unclassified

Security Classification